doi.org/10.26434/chemrxiv.14058332.v1

Iron-Catalyzed Halogen Exchange of Trifluoromethyl Arenes

Andreas Dorian, Emily Landgreen, Hayley Petras, James Shepherd, Florence Williams

Submitted date: 19/02/2021 • Posted date: 19/02/2021

Citation information: Dorian, Andreas; Landgreen, Emily; Petras, Hayley; Shepherd, James; Williams, Florence (2021): Iron-Catalyzed Halogen Exchange of Trifluoromethyl Arenes. ChemRxiv. Preprint. https://doi.org/10.26434/chemrxiv.14058332.v1

We report the facile production of $ArCF_2X$ and $ArCX_3$ from $ArCF_3$ using catalytic iron(III)halides, which constitutes the first iron-catalyzed halogen exchange for non-aromatic CF bonds. Theoretical calculations suggest direct activation of C–F bonds by iron coordination. $ArCX_3$ and $ArCF_2X$ products of the reaction are synthetically valuable due to their diversification potential. In particular, bromo-, chloro-, and iododifluoromethyl arenes ($ArCF_2Br$, $ArCF_2Cl$, $ArCF_2I$, respectively) provide access to a myriad of difluoromethyl arene derivatives ($ArCF_2R$). To optimize for mono-halogen exchange, a statistical method called Design of Experiments was used. Optimized parameters were successfully applied to electron rich and electron deficient aromatic substrates, and to the late stage diversification of flufenoxuron, a commercial insecticide.

File list (2)

Iron-Catalyzed Halogen Exchange of Trifluoromethyl Arenes

Andreas Dorian,[a] Emily J. Landgreen,[b] Hayley R. Petras,[b] James J. Shepherd,[b] Florence J. Williams*[b]

(a) University of Alberta. Edmonton, Alberta, Canada.
(b) University of Iowa. Iowa City, Iowa, USA. florence-williams@uiowa.edu

Supporting information (DOE designs, calculations, procedures, and characterization) provided in a separate supplementary document also available on ChemRxiv.

***Abstract**: We report the facile production of $ArCF_2X$ and $ArCX_3$ from $ArCF_3$ using catalytic iron(III)halides, which constitutes the first iron-catalyzed halogen exchange for non-aromatic C–F bonds. Theoretical calculations suggest this transformation likely involves direct activation of C–F bonds by iron coordination. $ArCX_3$ and $ArCF_2X$ products of the reaction are synthetically valuable due to their diversification potential. In particular, bromo-, chloro-, and iododifluoromethyl arenes ($ArCF_2Br$, $ArCF_2Cl$, $ArCF_2I$, respectively) provide access to a myriad of difluoromethyl arene derivatives ($ArCF_2R$). To optimize for mono-halogen exchange, a statistical method called Design of Experiment was used. Optimized parameters were successfully applied to electron rich and electron deficient aromatic substrates, and were applied to the late stage diversification of flufenoxuron, a commercial insecticide.*

C–F bonds impart desirable features to a molecule, such as chemical inertness and increased lipophilicity.[1] As such, fluorinated moieties continue to play a critical role in the modern pharmaceutical, agrochemical and materials chemistry fields, and are of longstanding synthetic interest to organic chemists.[2] A prominent example, the trifluoromethyl group (CF_3) is present in 24% of drugs globally approved in 2019.[3]

The selective conversion of C–F bonds to C–H or C–C bonds in polyfluorinated molecules has enjoyed increased focus as a strategy to access challenging fluorination patterns.[4] A related transformation is the conversion to higher halide C–X bonds (X = Cl, Br, I), through halogen-exchange (halex) reactions.[5] [6] These larger halides are versatile synthetic handles, with heightened reactivity over the parent fluoride.

Halex reactions on fluorinated substrates are typically performed with stoichiometric early valent metal halides (TiX_4, $MoCl_5$), or p-block metalloid halides (BX_3, AlX_3, R_3SiX).[7] These halide reagents provide the necessary thermodynamic drive through formation of a strong fluoride bond (e.g. SiF_4 166 kcal/mol, BF_3 170 kcal/mol).[8] However, additional catalysts are necessary in order to avoid high temperatures and long reaction times.

Iron, being a low-cost high abundance metal, has been surprisingly absent in catalytic defluorination development. The potential of iron catalysis in this field is nevertheless exemplified in enzymes such as Horseradish peroxidase (HRP), Methane monooxygenase (MMO) and Cytochrome P450s (CYPs), all employing iron-based catalytic motifs, which perform catalytic defluorination along with oxygenation.[9] In fact, to our knowledge only one precedent exists for iron-catalyzed halogen exchange of C–F bonds: Igumnov and coworkers observed chlorination of perfluorinated benzenes at high temperatures (120 °C) with yields up to 21%.[10] The following work constitutes the first example of iron-catalyzed halogen exchange of non-aromatic C–F bonds, and to our knowledge the first halogen exchange with mechanistic evidence for iron coordination and activation of the C–F bond directly. This method was applied and optimized for medicinally relevant $ArCF_3$ substrates.

We explored a variety of halophilic Lewis acidic transition metal complexes in the presence of boron tribromide and trifluoromethyl (*m*-fluoro)benzene **1a**. In the absence of a catalyst, the known background halex reaction between boron tribromide and trifluoromethyl arenes occurs slowly to provide compound **2a** at 7% conversion (Table 1, entry 1).[6b] While silver(I), copper(I), iron(0) and iron (II) showed no improvements on C–F exchange efficiencies (entries 2-5), iron(III) and gallium(III) compounds accelerated the halex process significantly (entries 6-10), generating tribrominated product **4a** in 83-91%. Interestingly, the identity of the halide on the iron(III) center did not affect the reaction significantly, aside from a small amount of chlorinated product formed when iron(III)chloride ($FeCl_3$) was used (entry 6), with bromination still predominant.

Ensuing investigations were performed with iron(III)fluoride. Solvent selection proved important (Table 1, entries 11-13), possibly due to solubility differences for the iron catalyst. In nitromethane, coordination of solvent with BBr_3 (confirmed by ^{11}B NMR) is suspected to mitigate reactivity.

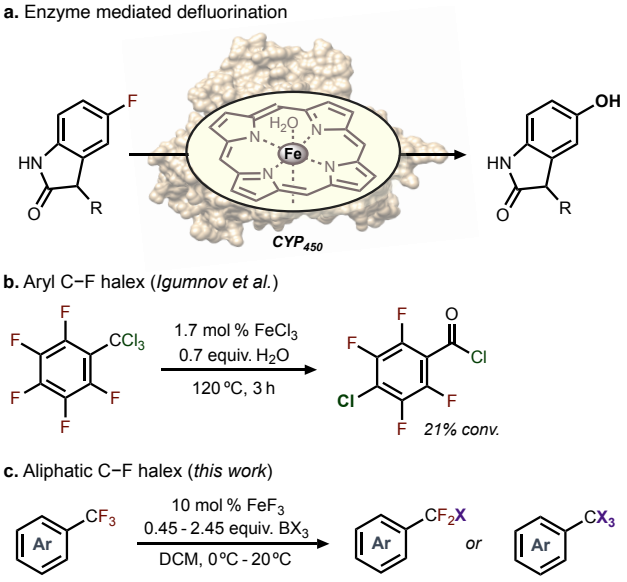

Figure 1. a) representative example of a CYP_{450} enzyme-catalyzed defluorination and concurrent hydroxylation.[9b] CYP_{450} contains an iron-porphyrin active site. b) prior iron-catalyzed aryl C–F halogen-exchange.[10] c) iron-catalyzed benzylic C–F halogen exchange described in this paper.

Table 1. Screening Investigations

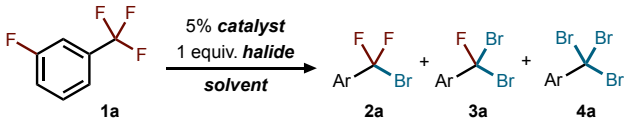

entry	*catalyst*	*halide*	*solvent*	2a (%)[a]	4a (%)[a]	C–F_{total} (%)[b]
1	–	BBr_3	DCM	7	*nd.*	7
2	AgBr	BBr_3	DCM	8	*nd.*	9
3	CuI	BBr_3	DCM	7	*nd.*	8
4	$Fe(CO)_5$	BBr_3	DCM	7	*nd.*	8
5	$FeCl_2$	BBr_3	DCM	6	*nd.*	7
6	$FeCl_3$	BBr_3	DCM	4	89	272
7	$FeBr_3$	BBr_3	DCM	5	83	256
8	FeF_3	BBr_3	DCM	5	83	255
9	$Fe(OTf)_3$	BBr_3	DCM	*tr.*	91	*273*
10	$Ga(OTf)_3$	BBr_3	DCM	*tr.*	83	*249*
11	FeF_3	BBr_3	heptane	*tr.*	*nd.*	*tr.*
12	FeF_3	BBr_3	PhCl	14	*tr.*	27
13	FeF_3	BBr_3	$MeNO_2$	*nd.*	*nd.*	*nd.*
14[c]	FeF_3	Me_2BBr	DCM	21	35	128
15[c]	FeF_3	(cat)BBr	DCM	*tr.*	*nd.*	*tr.*
16[d]	FeF_3	BCl_3	DCM	6	*nd.*	6
17[e]	FeF_3	BI_3	DCM	5	*nd.*	5
18[f]	FeF_3	BBr_3	DCM	*nd.*	*92*	277
19[g]	FeF_3	BBr_3	DCM	12	*nd.*	15

Reactions performed at 1.0 mmol scale, 20 °C, 5 hours, 0.2 M concentration. Compound **3a** was trace in all entries (< 3% conversion). *cat* = catechol. *nd.* = not detected. *tr.* = trace. [a] Conversions determined by ^{19}F NMR (relative to 4-fluorotoluene internal standard). [b] C–F_{total} refers to the molar percentage of C–F bonds converted to C–X bonds, relative to starting moles of $ArCF_3$. [c] 3 equiv. R_2BBr used. [d] $ArCF_2Cl$ formed instead of **2a**. [e] $ArCF_2I$ formed instead of **2a**. [f] 3 equiv. BBr_3 used, 12 h time. [g] Performed at –10°C.

To our satisfaction, alternative boryl halides were also competent in the halex reaction (entries 14-17), including boron trichloride (BCl_3) and boron triiodide (BI_3), which afforded $ArCF_2Cl$ or $ArCF_2I$, respectively (entries 16-17), although these reactions were slow relative to those with boron tribromide. Conversion to **4a** was optimized by using excess BBr_3 and extending the reaction time to 12 hours (entry 18). Tribromomethyl arenes can be used in a number of synthetic applications, including conversion to carboxylic acids/esters, alkynes and alkenes, and to generate heterocycles.[11] [6g] Accordingly, we envision this operationally-simple method using common reagents to be of significant utility, given the prevalence of trifluoromethyl groups in high profile compounds.

However, we were also intrigued by the potential to optimize the reaction for a single halogen-exchange, generating compound **2a**. In addition to unique intrinsic properties, such as increased capacity for halogen bonding, $ArCF_2X$ compounds are common intermediates for redox and cross-coupling reactions that generate a range of high value difluoro derivatives ($ArCF_2R$, Figure 2).[12] [13]

Optimizing a single halex on a trifluoromethyl center is a challenge, as the C–F bond strength decreases with each fluorine removal.[14] Encouragingly, lowering of the reaction temperature increased conversion to $ArCF_2Br$ (**2a**) relative to the $ArCBr_3$ (**4a**) (entry 19). This observation indicated that, despite the unfavorable

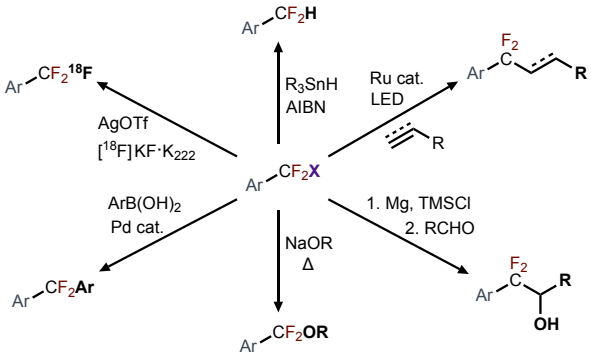

Figure 2. Transformations of $ArCF_2X$ (X = Br, Cl) reported in the literature.[12]

thermodynamic profile for selective mono halogen exchange, appropriate reaction tuning could provide synthetically viable amounts of the $ArCF_2Br$ product.

This complexity led us to use the statistical method Design of Experiments (DOE) for refined optimization. DOE uses regression analysis to generate a mathematical model of a selected reaction outcome as a function of defined reaction parameters (variables).[15] The relative importance of each parameter, as well as interaction effects between parameters is determined by analysis of variance (ANOVA).

We first performed a 5-variable fractional factorial DOE to evaluate the main linear effects of the following variables/parameters on conversion to $ArCF_2Br$: temperature, time, solvent molarity, FeF_3 loading, and BBr_3 equivalents (see SI for details). This model indicated the FeF_3 loading parameter was not significant (likely due to its solubility limit in dichloromethane).

Therefore, FeF_3 loading was fixed at 10% in the subsequent DOE, which utilized a response surface design, a more predicative model that accounts for non-linear effects. Evaluation of data normalcy, R^2 fit, a test for over-fitting ($R^2_{adjusted}$), a test for predictive

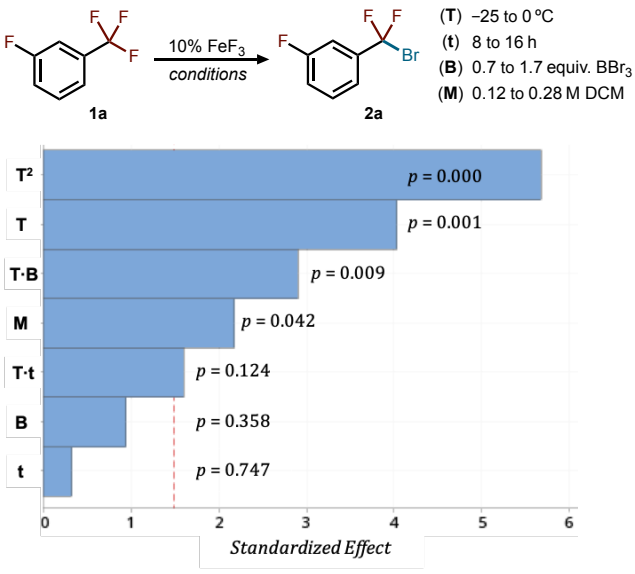

Figure 3. Pareto chart with added *p*-values for a response surface model of **2a** formation. The red dotted line is a reference corresponding to the standardized effect *t*-value determined by significance level α = 0.15, where α is the probability of obtaining a false positive on a statistical test.

power ($R^2_{predicted}$), and analysis of error versus reaction order (test for systematic experimental error), indicated that we had a well-fitted model for $ArCF_2Br$ conversion. We also performed test reactions to confirm that experimental conversion values were comparable to those predicted by the model (See SI).

The significance of each variable in the DOE model is shown the Pareto chart depicted in Figure 3. Such information can reflect mechanistic nuance. Temperature was found to be strongly correlated with $ArCF_2Br$ conversion and has a significant interaction effect with BBr_3.

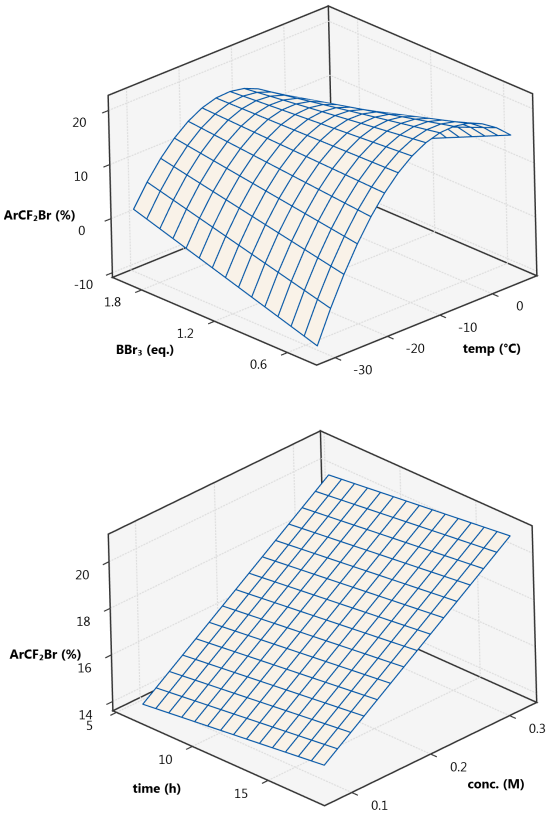

Figure 4. Surface plots from the DOE model. [Above] $ArCF_2Br$ conversion as a function of BBr_3 equivalents and temperature (constants: time = 12 h, concentration = 0.2 M). [Below] $ArCF_2Br$ conversion as a function of time and concentration (constants: BBr_3 = 1.2 equivalents, temperature = –12.5 °C).

Figure 4 shows the parabolic shape of the temperature effect, with a maximum at –3 °C, and the benefit of low BBr_3 equivalents (maximium at 0.45 equiv.). On the other hand, time has a relatively small effect, as shown by the very shallow slope in Figure 3 (see SI for other surface plots). These results suggest that optimal conversion is more complex than identifying a time point where a statistical mixture of products favors $ArCF_2Br$. In such a scenario, time would be highly significant to the model. The DOE model identified optimal conditions corresponding to a maximum $ArCF_2X$ conversion of 25%. Evaluation of these conditions experimentally, resulted in 28% conversion to $ArCF_2X$ **2a**, slightly outperforming the model (Scheme 1).

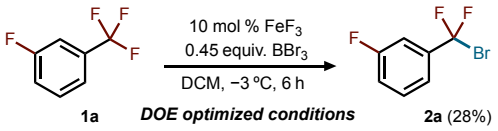

Scheme 1. DOE optimized conditions for the synthesis of $ArCF_2Br$

Given optimized reaction parameters for meta-fluoro substrate **1a**, we sought to apply conditions favoring $ArCF_2X$ formation to a selection of substrates (Scheme 2). The reaction was observed to progress more rapidly with electron rich aromatic complexes, which was easily compensated for with shorter reaction times. Gratifyingly, similar conversions to the desired $ArCF_2Br$ could be obtained for most substrates examined. For compounds with coordinating Lewis basic functionalities, additional equivalents of BBr_3 were necessary to account for competing coordination preferences (**2i**, **2j**, **2k**). Substitution at ortho, meta, and para positions, including halides, alkyl, and hydroxy groups were all well tolerated. Isolation of $ArCF_2X$ was achieved using reverse-phase HPLC, whereas small molecule substrates are reported as conversions, due to volatility affecting isolated yields. No evidence was observed of styrene derivatives or Friedel-Crafts alkylation arising from iron(III) activation of the alkyl bromide side chain with substrate **1h**. Chlorination was also achieved using similar conditions (compound **2c**).

To our delight, phosphine **1i** was converted to desymmetrized mono-brominated compound **2i** in 17% isolated yield, despite 9 different fluorines which can participate in the halex reaction. Further, commercial insecticide flufenoxuron (**1k**), was converted to mono-brominated derivative **2k** in 21% conversion and 13% isolated yield (Scheme 3).

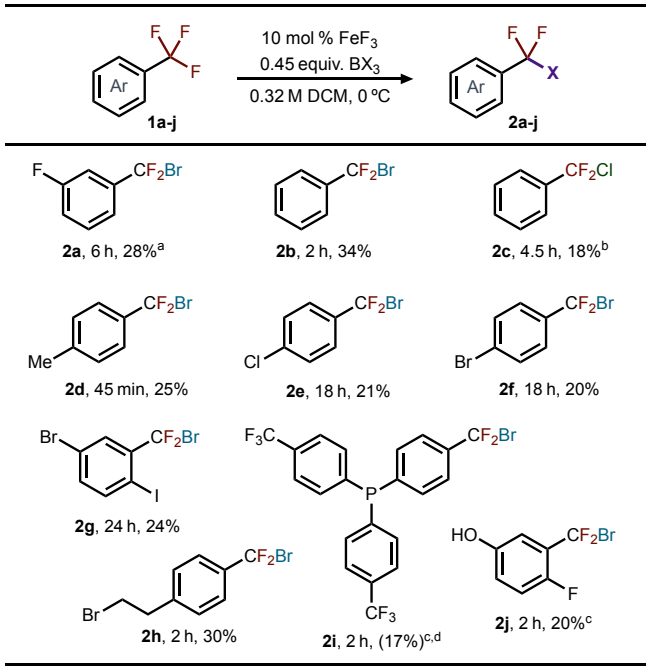

Scheme 2. Scope investigations for the mono-halex of trifluoromethyl arenes (0.40 mmol scale). Conversions determined by ^{19}F NMR (relative to 4-fluorotoluene internal standard), isolated yields in parentheses. [a] Performed at -3 °C. [b] 0.2 M NO_2Me/DCM (2:1), 0.45 equiv. $FeCl_3$, 1.2 equiv. BCl_3, 10 °C. [c] $Fe(OTf)_3$ in place of FeF_3. [d] 1.45 equivalents BBr_3 used.

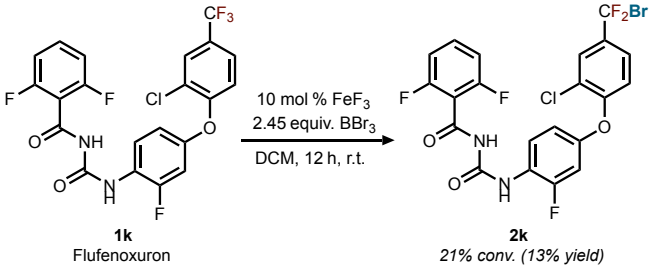

Scheme 3. Halogen exchange with a commercial insecticide flufenoxuron.

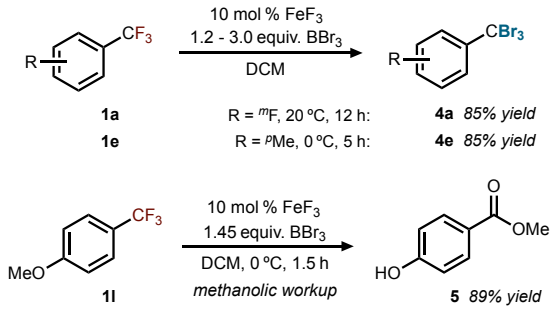

Scheme 4. Yields of tribromomethyl arenes produced using triple-halex.

Further, substrates **1a**, **1e** and **1l** were converted to tribromomethylarenes **4a**, **4e**, and compound **5** with excellent isolated yields (85-89%). Compound **5** was generated from an methanolic workup, resulting from rapid hydrolysis/methanolysis of the tribromomethyl group. These substrates demonstrate that electron deficient and electron rich arenes are competent in triple halogen exchange of benzylic trifluoromethyl groups.

Theoretical calculations were used to investigate the mechanistic role of the iron catalyst. Using unrestricted Kohn-Sham density functional theory B3LYP/6-31G**,[16] coordination energies between $PhCF_3$ **1b**, BCl_3, and $FeCl_3$ were determined in dimeric and trimeric orientations (see SI for a complete library of calculated complexes). Since the halex exchange works similarly well with BCl_3 as BBr_3, a BCl_3 reaction to introduce chloride was chosen. The background halex reaction with BCl_3 (without iron) is slow enough to be non-competitive.

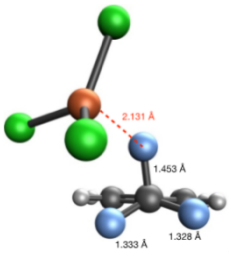

Figure 5. Computed geometries & bond lengths for $FeCl_3$ coordination to $PhCF_3$

The lowest dimeric coordination energy observed was between $PhCF_3$ and $FeCl_3$ at –14.65 kcal/mol (Figure 5). This interaction is predicted to stretch the coordinated C–F bond by approximately 0.1 Å. In contrast, the binding energy of $PhCF_3$ and BCl_3 is much less significant at –1.34 kcal/mol. ^{19}F NMR experiments support these calculations. The fluorine signal in $PhCF_3$ is shifted downfield by 2.5 ppm in the presence of $FeCl_3$, whereas BCl_3 only elicits a downfield shift of 0.2 ppm.

The lowest energy trimers ($PhCF_3$, BCl_3, $FeCl_3$) have interactions dominated by $PhCF_3$ and $FeCl_3$ binding; the lowest energy trimer is calculated to be at –15.35 kcal/mol relative to the monomers (See SI for details). Therefore, while iron activation of the boron trichloride remains a valid mechanistic possibility, calculations and NMR shift experiments suggest direct interaction with the $PhCF_3$ substrate is energetically favorable and weakens the C–F bond.

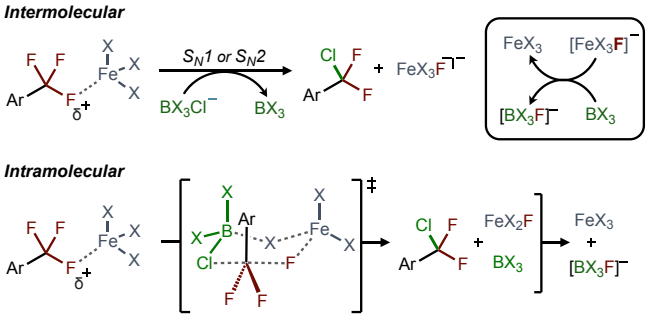

Figure 6. Plausible mechanisms for the halex reaction.

Figure 6 shows plausible mechanisms based on these data, where iron initiates activation of the C–F bond, facilitating nucleophilic substitution, and ultimately abstracting the fluoride. The nucleophilic chloride is likely delivered from a boron halide complex, as the identity of the boron halide reagent determines the major halogen exchange product. Subsequent transfer of the fluoride to the boron center is required for the process to be exergonic overall (for the first Cl exchange: –5.17 kcal/mol B3LYP/6-31G**, –7.56 kcal/mol CCSD(T)/CBS),[17] and this is corroborated by experimental observations of gas evolution (BF_3) and the loss of the ^{11}B NMR signal in the reaction mixture.

In conclusion, we have demonstrated that ferric halides catalyze halogen-exchange between trifluoromethyl arenes and boron halides. While early conditions favor full exchange of benzylic fluorides, providing $ArCX_3$ products, DOE analyses provided conditions that maximize mono-exchange to generate $ArCF_2X$ products in synthetically viable yields. The tunable halex reaction was also shown to produce the analogous chlorodifluoromethyl and iododifluoromethyl groups. Scope investigations demonstrated successful application to electron-deficient and electron-rich arenes, with good functional group tolerance. The reaction is also eminently practical, using inexpensive, readily available reagents and run at easily maintained temperatures.

Significantly, mechanistic insight from computational analyses suggest that ferric halides are likely direct activators of the C–F bond, which has important implications for future C–F activation methodology development. Further investigations into the mechanistic role of the iron catalyst in halex reactions are ongoing.

Acknowledgements

The authors thank Dr. Pamela Tadross, of Merck Industries, for her feedback and advice regarding Design of Experiments.

This work was primarily supported by NSERC RGPIN-2016-04843, the ACS Petroleum Research Fund PRF 59191-ND1, and the Canadian Foundation for Innovation IOF-34997 (FW and AD: experimental work and DOE). Additional support (AD) is acknowledged from Dr. Ralf Schirrmacher, through NSERC RGPIN-2019-04481. Electronic structure calculations (JS, EL, and HRP) were supported by the University of Iowa.

References

[1] D. O'Hagan, *Chem. Soc. Rev.* **2008**, *37*, 308-319.

[2] a.) E. P. Gillis, K. J. Eastman, M. D. Hill, D. J. Donnelly, N. A. Meanwell, *J. Med. Chem.* **2015**, *58*, 8315-8359; b.) R. Berger, G. Resnati, P. Metrangolo, E. Weber, J. Hulliger, *Chem. Soc. Rev.* **2011**, *40*, 3496-3508.

[3] a.) M. Inoue, Y. Sumii, N. Shibata, *ACS Omega* **2020**, *5*, 10633-10640; b.) C. Alonso, E. Martinez de Marigorta, G. Rubiales, F. Palacios, *Chem. Rev.* **2015**, *115*, 1847-1935.

[4] a.) T. Fujita, K. Fuchibe, J. Ichikawa, *Angew. Chem. Int. Ed.* **2019**, *58*, 390-402; b.) F. Jaroschik, *Chem. Euro. J.* **2018**, *24*, 14572-14582; c.) J. D. Hamel, J. F. Paquin, *Chem. Commun.* **2018**, *54*, 10224-10239; d.) T. Ahrens, J. Kohlmann, M. Ahrens, T. Braun, *Chem. Rev.* **2015**, *115*, 931-972; e.) H. Amii, K. Uneyama, *Chem. Rev.* **2009**, *109*, 2119-2183.

[5] a.) K. K. K. Goh, A. Sinha, C. Fraser, R. D. Young, *RSC Adv.* **2016**, *6*, 42708-42712; b.) M. Janjetovic, A. Ekebergh, A. M. Traff, G. Hilmersson, *Org. Lett.* **2016**, *18*, 2804-2807; c.) A. M. Traff, M. Janjetovic, L. Ta, G. Hilmersson, *Angew. Chem. Int. Ed.* **2013**, *52*, 12073-12076; d.) Y. Mizukami, Z. Song, T. Takahashi, *Org. Lett.* **2015**, *17*, 5942-5945; e.) K. Matsubara, T. Ishibashi, Y. Koga, *Org. Lett.* **2009**, *11*, 1765-1768; f.) J. Terao, S. A. Begum, Y. Shinohara, M. Tomita, Y. Naitoh, N. Kambe, *Chem. Commun.* **2007**, 855-857; g.) M. Namavari, N. Satyamurthy, J. R. Barrio, *J. F. Chem.* **1995**, *72*, 89-93; h.) G. A. Olah, S. C. Narang, L. D. Field, *J. Org. Chem.* **1981**, *46*, 3727-3728; i.) J. San Filippo Jr., A. F. Sowinski, L. J. Romano, *J. Org. Chem.* **1975**, *40*, 3295-3296.

[6] a.) D. Mandal, R. Gupta, A. K. Jaiswal, R. D. Young, *J. Am. Chem. Soc.* **2020**, *142*, 2572-2578; b.) G. K. S. Prakash, J. Hu, J. Simon, D. R. Bellew, G. A. Olah, *J. F. Chem.* **2004**, *125*, 595-601; c.) F. Dankert, H. L. Deubner, M. Müller, M. R. Buchner, F. Kraus, C. von Hänisch, *Z. Anorg. Allg. Chem.* **2020**, *646*, 1501-1507; d.) A. L. Henne, M. S. Newman, *J. Am. Chem. Soc.* **1938**; e.) J. Riera, J. Castaiier, J. Carilla, A. Robert, *Tet. Lett.* **1989**, *30*; f.) R. K. Ramchandani, R. D. Wakharkar, A. Sudalai, *Tet. Lett.* **1996**, *37*, 4063-4064; g.) M. Ikeda, T. Matsuzawa, T. Morita, T. Hosoya, S. Yoshida, *Chem. Eur. J.* **2020**, *26*, 12333-12337.

[7] T. Stahl, H. F. T. Klare, M. Oestreich, *ACS Catal.* **2013**, *3*, 1578-1587.

[8] a.) D. J. Grant, D. A. Dixon, *J. Phys. Chem. A* **2009**, *113*, 777-787; b.) R. Walsh, *J. Chem. Soc., Faraday Trans. 1* **1983**, *79*, 2233-2248.

[9] a.) Y. Wang, A. Liu, *Chem. Soc. Rev.* **2020**, *49*, 4906-4925; b.) G. M. Amaya, R. Durandis, D. S. Bourgeois, J. A. Perkins, A. A. Abouda, K. J. Wines, M. Mohamud, S. A. Starks, R. N. Daniels, K. D. Jackson, *Chem. Res. Toxicol.* **2018**, *31*, 570-584.

[10] A. I. Shipilov, L. A. Kolpashchikova, S. M. Igumnov, *Russ. J. Org. Chem.* **2003**, *39*, 975-978.

[11] a.) Q. Sun, X. Yu, M. Bao, M. Liu, J. Pan, Z. Zha, L. Cai, H. Ma, C. Yuan, X. Qiu, W. Xu, *Angew. Chem. Int. Ed.* **2018**, *57*, 4035-4038; b.) H. Liu, S.-i. Kondo, N. Takeda, M. Unno, *Eur. J. Inorg. Chem.* **2009**, 1317-1319.

[12] a.) M. Yoshida, M. Morinaga, M. Iyoda, *J. F. Chem.* **1994**; b.) S. Sumino, M. Uno, T. Fukuyama, I. Ryu, M. Matsuura, A. Yamamoto, Y. Kishikawa, *J. Org. Chem.* **2017**, *82*, 5469-5474; c.) J. Guidotti, C. Wakselman, F. Metz, M. Tordeux, *Synlett* **2004**, 1759-1762; d.) J. Guidotti, V. Schanen, M. Tordeux, C. Wakselman, *J. F. Chem.* **2005**, *126*, 443-447; e.) J.-W. Gu, W.-H. Guo, X. Zhang, *Org. Chem. Front.* **2015**, *2*, 38-41; f.) S. Verhoog, L. Pfeifer, T. Khotavivattana, S. Calderwood, T. Collier, K. Wheelhouse, M. Tredwell, V. Gouverneur, *Synlett* **2015**, *27*, 25-28.

[13] a.) X. J. Tang, Z. Zhang, W. R. Dolbier, Jr., *Chem. Eur. J.* **2015**, *21*, 18961-18965; b.) Z. Zhang, X. Tang, W. R. Dolbier, Jr., *Org. Lett.* **2015**, *17*, 4401-4403; c.) H. Jiang, W. Lu, K. Yang, G. Ma, M. Xu, J. Li, J. Yao, W. Wan, H. Deng, S. Wu, S. Zhu, J. Hao, *Chem. Eur. J.* **2014**, *20*, 10084-10092.

[14] G. Glockler, *J. Phys. Chem.* **1959**, *63*, 828-832.

[15] S. A. Weissman, N. G. Anderson, *Org. Process Res. Dev.* **2015**, *19*, 1605-1633.

[16] a.) A. D. Becke, *J. Chem. Phys.* **1993**, *98*, 1372-1377; b.) V. A. Rassolov, M. A. Ratner, J. A. Pople, P. C. Redfern, L. A. Curtiss, *J. Comput. Chem.* **2001**, *22*, 976-984.

[17] R. J. Bartlett, M. Musiał, *Rev. Mod. Phys.* **2007**, *79*, 291-352.

Supporting Information

Iron-Catalyzed Halogen Exchange of Trifluoromethyl Arenes

Andreas Dorian,[a] Emily J. Landgreen,[b] Hayley R. Petras,[b] James J. Shepherd,[b] Florence J. Williams[b]*

[a] University of Alberta, Edmonton, Alberta, Canada
[b] University of Iowa, Iowa City, Iowa, United States
email: florence-williams@uiowa.edu

Table of Contents

General Information

Reactions were performed in glass test-tubes (16x100mm) that were fitted with a stir bar and rubber septum, and then flame-dried under high vacuum. Solid reagents were weighed directly into the test tube, via temporary removal of the septum. Reactions were kept under a static dry nitrogen atmosphere, and all liquid reagent additions were performed using standard Schlenk techniques. Dichloromethane (DCM) was obtained from a LC Technology Solutions SP-1 solvent purification system. Nitromethane was stored over CaH_2 and distilled under nitrogen prior to use. All other reagents were obtained commercially and used without additional purification. Temperature control was achieved using a Neslab CryoCool (CC-65) immersion cooler, or an ice bath for 0 °C.

GC-MS were obtained using a Bruker Scion TQ 456 System. HRMS were obtained from a Kratos Analytical MS50G EI-MS. FTIR were obtained using a Thermo Nicolet 8700 with an attached continuum microscope. HPLC purification was performed using an Agilent 1260 preparatory system, with a C8 Zorbax column (PrepHT, 21.2 x 150 mm, 7 µm). NMR spectra were obtained using one of the following Varian (Agilent) spectrometers: MR DD2 400 MHz, VNMRS 500 MHz, VNMRS 600 MHz, VNMRS 700 MHz.

NMR chemical shifts (δ) are reported in ppm, and are referenced to residual protonated solvent in ^{1}H NMR (7.26 ppm for $CHCl_3$), deuterated solvent in ^{13}C NMR (77.06 ppm for $CDCl_3$), or internal standard in ^{19}F NMR (*vide infra*). Coupling constants (*J*) are reported in Hertz (Hz). The following splitting pattern abbreviations are used: d = *doublet*, t = *triplet*, q = *quartet*, dt = *doublet of triplets*, td = *triplet of doublets*, m = *multiplet*, app. = *apparent*, br. = *broad*. Carbon multiplicities were determined using HSQC, with the following abbreviations used: C = *no attached hydrogens*, CH = *one attached hydrogen*, CH_2 = *two attached hydrogens*, CH_3 = *three attached hydrogens*.

Reaction conversions calculated from ^{19}F NMR spectra are reported to one decimal place. To validate this level of precision, a general baseline deviation error was calculated based on integration values of the baseline. Three spectral regions (3000 Hz): left of peaks, center of the spectra, and right of the peaks, were evaluated in four different representative ^{19}F NMR experiments (with *internal standard integral* = 100). The average baseline error was calculated to be $6.6 \pm 2.2 \times 10^{-4}$ integration per Hz, with no significant difference between the spectra examined (ANOVA, $p = 0.163$). When applied to the $ArCF_2Br$ peak, this translates to an error of $0.12 \pm 0.04\%$ for $ArCF_2Br$ conversion, including for low conversion experiments (e.g. 1.6% $ArCF_2Br$, error = 0.08%).

Using this higher level of precision for ^{19}F NMR derived conversions was deemed beneficial for use in DOE analysis, in particular, due to the presence of many low value numbers. We readily acknowledge that workup procedures (separate from NMR precision), likely produce an additional 1-2% error. Nevertheless, the combined effects of these errors were small enough (or systematic enough) to provide good fits for the DOE analysis.

DOE experiments were created and analyzed using Minitab 19 software. Model fitting utilized stepwise regression, in which terms were added to maintain a hierarchy at each step. In other words, if higher order terms (i.e. T^2) were included, then the respective lower order term (i.e. T) was also included. In the DOE experimental procedures below, the values shown in brackets correspond to the high and low values of the model.

Reaction Screening

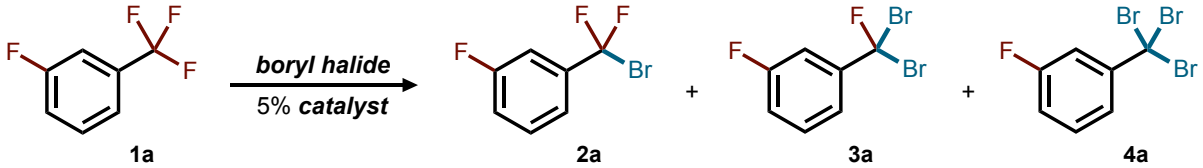

Reaction vessels were charged with the metal catalyst (0.05 mmol), followed by the reaction solvent (5 mL, 0.2M) and 3-fluoro(trifluoromethyl)benzene (126 µL, 1.00 mmol). The boryl halide reagent was slowly added, and the mixture stirred at the target temperature for the designated reaction time. The mixture was quenched by adding 2–3 mL DCM and a few drops of water (fuming frequently observed). The mixture was then transferred to a separatory funnel containing saturated aqueous $NaHCO_3$ (20 mL), brine (20 mL) and DCM (20 mL). The test tube was rinsed with 15 mL water and 15 mL DCM, both washes were added to the separatory funnel. The DCM layer was removed, and the aqueous layer washed with additional DCM (20 mL). The combined organic layers were then filtered through a bed of Na_2SO_4 into a beaker, followed by a DCM wash. The internal standard (100 µL of 4-fluorotoluene) was then added to the beaker, and the solution was stirred well, before an aliquot was taken and combined with equal parts $CDCl_3$ in an NMR tube. Analysis with ^{19}F NMR showed $ArCF_3$ **1a** (–63.2 ppm CF_3, –111.5 ppm ^{m}F), $ArCF_2Br$ **2a** (–44.5 ppm CF_2, –111.5 ppm ^{m}F), $ArCFBr_2$ **3a** (–54.4 ppm CF, –111.8 ppm ^{m}F) and $ArCBr_3$ **4a** (–112.5 ppm ^{m}F) which were quantified relative to the 4-fluorotoluene internal standard (–119.5 ppm). In entries 16 and 17, $ArCF_2Cl$ (–49.4 CF_2, –111.5 ppm ^{m}F), and $ArCF_2I$ (–38.4 ppm CF_2, –111.5 ppm ^{m}F) were observed respectively.

Table S1. Experimental details for screening reactions

entry	temp	time	solvent	metal catalyst		boryl halide			^{19}F NMR Conversion (%)				C-F_{total}
				reagent	*amount*	*reagent*	*mmol*	*amount*	1a	2a	3a	4a	
1	20 °C	5 h	DCM	-	-	BBr_3	1.00	96.5 µL	89.3	7.1	0.1	0.0	7
2	20 °C	5 h	DCM	AgBr	9.4 mg	BBr_3	1.00	96.5 µL	87.7	7.6	0.7	0.0	9
3	20 °C	5 h	DCM	CuI	9.5 mg	BBr_3	1.00	96.5 µL	88.2	7.3	0.5	0.0	8
4	20 °C	5 h	DCM	$Fe(CO)_5$	6.6 µL	BBr_3	1.00	96.5 µL	88.7	7.3	0.5	0.0	8
5	20 °C	5 h	DCM	$FeCl_2$	6.3 mg	BBr_3	1.00	96.5 µL	81.2	5.9	0.7	0.0	7
6	20 °C	5 h	DCM	$FeCl_3$	8.1 mg	BBr_3	1.00	96.5 µL	4.3	3.8	0.3	89.2	272
7	20 °C	5 h	DCM	$FeBr_3$	14.8 mg	BBr_3	1.00	96.5 µL	7.3	6.1	0.9	82.6	256
8	20 °C	5 h	DCM	FeF_3	5.6 mg	BBr_3	1.00	96.5 µL	5.5	4.7	0.5	83.1	255
9	20 °C	5 h	DCM	$Fe(OTf)_3$	25.2 mg	BBr_3	1.00	96.5 µL	0.8	0.5	0.5	90.6	273
10	20 °C	5 h	DCM	$Ga(OTf)_3$	25.8 mg	BBr_3	1.00	96.5 µL	1.5	0.3	0.0	82.9	249
11	20 °C	5 h	heptane	FeF_3	5.6 mg	BBr_3	1.00	96.5 µL	92.5	0.9	0.0	0.0	1
12	20 °C	5 h	PhCl	FeF_3	5.6 mg	BBr_3	1.00	96.5 µL	82.8	14.1	3.2	2.3	27
13	20 °C	5 h	$MeNO_2$	FeF_3	5.6 mg	BBr_3	1.00	96.5 µL	96.7	0.0	0.0	0.0	0
14	20 °C	5 h	DCM	FeF_3	5.6 mg	Me_2BBr	3.00	293 µL	42.5	20.8	1.0	35.2	128
15	20 °C	5 h	DCM	FeF_3	5.6 mg	(cat)BBr[a]	3.00	596 mg	92.8	0.7	0.0	0.0	1
16	20 °C	5 h	DCM	FeF_3	5.6 mg	BCl_3[b]	1.00	1.00 mL	83.8	6.0	0.0	0.0	6
17	20 °C	5 h	DCM	FeF_3	5.6 mg	BI_3	1.00	392 mg	87.5	5.1	0.0	0.0	5
18	20 °C	12 h	DCM	FeF_3	5.6 mg	BBr_3	3.00	289 µL	0.0	0.0	0.0	91.6	277
19	-10 °C	5 h	DCM	FeF_3	5.6 mg	BBr_3	1.00	96.5 µL	83.8	11.8	1.5	0.0	15

[a] B-bromocatechol borane. [b] 1M solution in DCM. [c] C-F_{total} = [$\mathbf{CF_2Br}$] + 2×[$\mathbf{CFBr_2}$] + 3×[$\mathbf{CBr_3}$]

Chloride Halex Investigation I

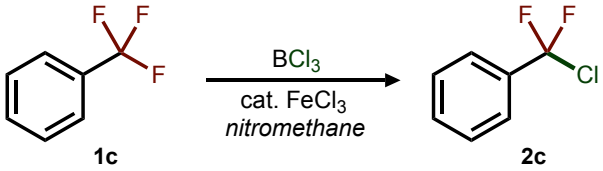

1c 2c

$FeCl_3$	10 mol %	50 mol %
temp.	-10 °C	30 °C
BCl_3	0.25 eq.	1.25 eq.
time	5 h	17 h
conc.	0.05 M	0.50 M

The chloride halex was initially investigated with this wide-ranging set of variables, allowing for the relative importance of each reaction parameter to be determined. Temperature and molarity were found to be the key parameters, without significant interaction effects with the other three variables. As such, temperature and molarity could be set at fixed values in the second set of experiments (investigation II).

A 5-factor *Fractional Factorial* DOE (2^{5-1}) was performed (with 4 center points), followed by augmentation with 10 axial points ($\alpha = 1.2$), forming a *Response Surface Design*. Reaction vessels were charged with ferric chloride (5 mg, 50 mg), nitromethane (1.25 mL, 12.3 mL), and α,α,α-trifluorotoluene (75.5 µL, 0.615 mmol). After adjusting the mixture to the target temperature, boron trichloride (1M in DCM) was added (155 µL, 770 µL). Additional DCM was added (615 µL) such that the total DCM volume was equal to 770 µL. After the target reaction time, C_6F_6 was added directly to the mixture (20 µL). An aliquot was taken and combined with equal parts $CDCl_3$ in an NMR tube. Immediate analysis with ^{19}F NMR showed $PhCF_3$ (–62.8 ppm), $PhCF_2Cl$ (–48.6 ppm) and $PhCFCl_2$ (–52.6 ppm), which were quantified relative to the C_6F_6 internal standard (–162 ppm). DOE regression analysis was performed using stepwise regression (α=0.05).

Table S2. Full data set for the chloride halex investigation I

$FeCl_3$ (mol %)	temp. (°C)	BCl_3 (eq.)	time (h)	conc. (M)	$PhCF_2Cl$ (conv %)
5.0	-10	0.25	5	0.50	**0.6**
50.0	-10	0.25	5	0.05	**0.0**
5.0	30	0.25	5	0.05	**0.0**
50.0	30	0.25	5	0.50	**1.2**
5.0	-10	1.25	5	0.05	**0.0**
50.0	-10	1.25	5	0.50	**7.0**
5.0	30	1.25	5	0.50	**0.0**
50.0	30	1.25	5	0.05	**7.9**
5.0	-10	0.25	17	0.05	**0.0**
50.0	-10	0.25	17	0.50	**5.6**
5.0	30	0.25	17	0.50	**1.5**
27.5	10	0.75	11	0.28	**15.1**
27.5	10	0.75	11	0.28	**14.4**
27.5	10	0.75	11	0.28	**14.0**
27.5	10	0.75	11	0.28	**13.6**

$FeCl_3$ (mol %)	temp. (°C)	BCl_3 (eq.)	time (h)	conc. (M)	$PhCF_2Cl$ (conv %)
50.0	30	0.25	17	0.05	**0.7**
5.0	-10	1.25	17	0.50	**8.3**
50.0	-10	1.25	17	0.05	**1.5**
5.0	30	1.25	17	0.05	**4.3**
50.0	30	1.25	17	0.50	**0.0**
0.5	10	0.75	11	0.28	**8.6**
54.5	10	0.75	11	0.28	**11.3**
27.5	-14	0.75	11	0.28	**0.6**
27.5	34	0.75	11	0.28	**0.4**
27.5	10	0.15	11	0.28	**4.0**
27.5	10	1.35	11	0.28	**14.7**
27.5	10	0.75	3.8	0.28	**8.2**
27.5	10	0.75	18.2	0.28	**13.5**
27.5	10	0.75	11	0.00	**0.4**
27.5	10	0.75	11	0.55	**3.1**

Figure S1: Statistical analysis for the chloride halex surface model I

Regression Parameters

S	R^2	R^2 (adj)	R^2 (pred)
1.73	94%	90%	85%

Coded Coefficients

Term	Coef	SE Coef	T-Value	P-Value	VIF
Constant	12.17	0.559	21.8	0.000	
$FeCl_3$ **(A)**	0.66	0.399	1.64	0.117	1.00
temp **(B)**	-0.41	0.399	-1.02	0.323	1.00
BCl_3 **(C)**	1.71	0.399	4.28	0.000	1.00
time **(D)**	0.60	0.399	1.51	0.147	1.00
conc **(E)**	0.70	0.399	1.75	0.096	1.00
temp*temp	-6.45	0.729	-8.84	0.000	1.46
conc*conc	-5.56	0.729	-7.63	0.000	1.46
$FeCl_3$*time	-1.36	0.433	-3.13	0.005	1.00
temp*conc	-1.89	0.433	-4.36	0.000	1.00

Regression Equation

$$PhCF_2Cl = -7.1 + 0.14\mathbf{A} + 0.42\mathbf{B} + 3.4\mathbf{C} + 0.38\mathbf{D} + 68\mathbf{E} - 0.016\mathbf{B}^2 - 110\mathbf{E}^2 - 0.010\mathbf{AD} - 0.42\mathbf{BE}$$

Analysis of Variance

Source	DF	Adj SS	Adj MS	F-Value	P-Value
Model	10	830.9	83.1	27.6	0.000
Blocks	1	94.3	94.3	31.4	0.000
Linear	5	82.4	16.5	5.5	0.003
$FeCl_3$	1	8.1	8.1	2.7	0.117
temp	1	3.1	3.1	1.0	0.323
BCl_3	1	55.0	55.0	18.3	0.000
time	1	6.9	6.9	2.3	0.147
conc	1	9.2	9.2	3.1	0.096
Square	2	642.5	321.2	106.9	0.000
temp*temp	1	235.0	235.0	78.2	0.000
conc*conc	1	175.0	175.0	58.2	0.000
2-Way	2	86.6	43.3	14.4	0.000
$FeCl_3$*time	1	29.5	29.5	9.8	0.005
temp*conc	1	57.1	57.1	19.0	0.000
Error	19	57.1	3.0		
Lack-of-Fit	16	55.8	3.5	8.1	0.055
Pure Error	3	1.3	0.4		
Total	29	888.1			

Figure S2. Pareto chart for the chloride halex surface model I

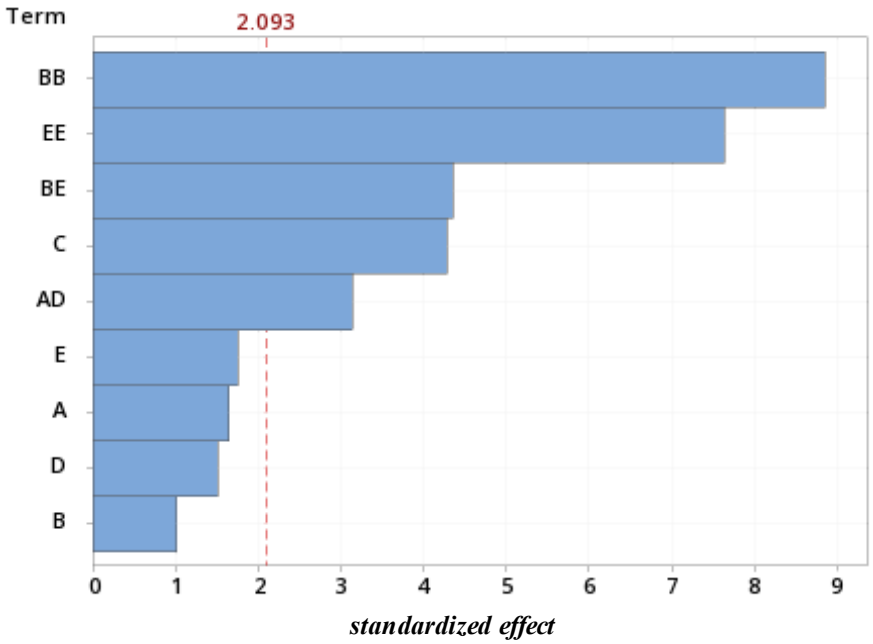

Figure S3. Residual plots for the chloride halex surface model I

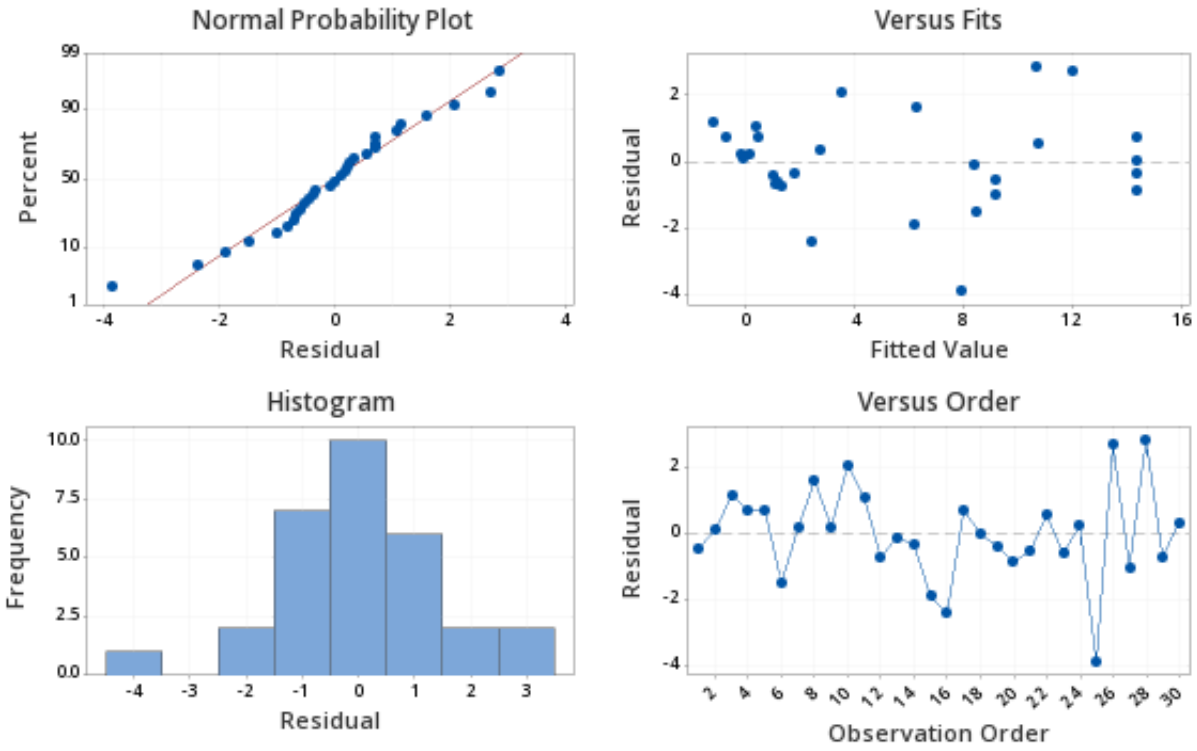

Chloride Halex Investigation II

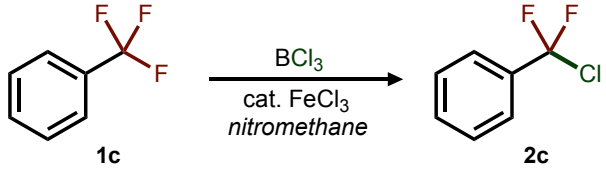

$FeCl_3$	35 mol %	55 mol %
temp.	9 °C	
BCl_3	0.80 eq.	1.50 eq.
time	5 h	17 h
conc.	0.29 M	

Based on the results from the previous model (investigation I), temperature and molarity were fixed for the following set of experiments. A full response surface design was used (as opposed to fractional), using a more narrow parameter range, in order to hone in on the maximum value for conversion to the monochloride ***2c****.*

A 3-factor *Response Surface* DOE was performed (4 center points, axial points at $\alpha = 1.63$). Vessels were charged with ferric chloride (44.0 mg, 69.0 mg), nitromethane (2.65 mL), and α,α,α-trifluorotoluene (95 µL, 0.77 mmol). After adjusting the mixture to the 9 °C, boron trichloride (1M in DCM) was added (620 µL, 1160 µL). Additional DCM was added (710 µL, 170 µL) such that the total DCM volume was equal to 1330 µL. After the desired time, the mixture was slowly quenched by adding a few drops of water. The mixture was transferred to a separatory funnel containing sat. $NaHCO_3$ solution (15 mL), brine (15 mL) and DCM (20 mL). The test tube was rinsed forward with 5 mL water and 10 mL DCM. The DCM layer was removed, and the aqueous layer washed with additional DCM (20 mL). The combined organic layers were then filtered through a bed of Na_2SO_4, into a beaker, followed by the addition of 100 µL of 4-fluorotoluene. After stirring well, an aliquot was taken and combined with equal parts $CDCl_3$ in an NMR tube. Analysis with ^{19}F NMR showed $PhCF_3$ (–62.8 ppm), $PhCF_2Cl$ (–48.6 ppm) and $PhCFCl_2$ (–52.6 ppm), quantified relative to the 4-fluorotoluene internal standard (–119.5 ppm). Regression analysis was performed using stepwise regression (α=0.05), in which terms were added to maintain a hierarchical model at each step.

Table S3. Full data set for the chloride halex optimization II

$FeCl_3$ (mol %)	temp. (°C)	BCl_3 (eq.)	time (h)	conc. (M)	$PhCF_2Cl$ (conv %)
35.0	9	0.8	7.0	0.29	**16.3**
55.0		0.8	7.0		**14.3**
35.0		1.5	7.0		**12.2**
55.0		1.5	7.0		**14.8**
35.0		0.8	15.0		**11.6**
55.0		0.8	15.0		**1.6**
35.0		1.5	15.0		**9.4**
55.0		1.5	15.0		**5.2**
45.0		1.2	11.0		**13.5**
45.0		1.2	11.0		**14.3**

$FeCl_3$ (mol %)	temp. (°C)	BCl_3 (eq.)	time (h)	conc. (M)	$PhCF_2Cl$ (conv %)
45.0	9	1.2	11.0	0.29	**13.8**
45.0		1.2	11.0		**13.0**
28.7		1.2	11.0		**15.7**
61.3		1.2	11.0		**8.3**
45.0		0.6	11.0		**15.2**
45.0		1.7	11.0		**13.7**
45.0		1.2	4.5		**17.8**
45.0		1.2	17.5		**1.2**
45.0		1.2	11.0		**11.8**
45.0		1.2	11.0		**15.5**

Figure S4. Statistical analysis for the chloride halex surface model II

Regression Parameters

S	R^2	R^2 (adj)	R^2 (pred)
1.34	95%	92%	81%

Coded Coefficients

Term	Coef	SE Coef	T-Value	P-Value	VIF
Constant	13.8	0.468	29.4	0.000	
$FeCl_3$ **(A)**	-1.93	0.368	-5.23	0.000	1.00
BCl_3 **(B)**	-0.35	0.368	-0.95	0.362	1.00
time **(C)**	-4.27	0.368	-11.6	0.000	1.00
$FeCl_3$*$FeCl_3$	-0.88	0.369	-2.37	0.035	1.00
time*time	-1.81	0.369	-4.92	0.000	1.00
$FeCl_3$*BCl_3	1.30	0.475	2.74	0.018	1.00
$FeCl_3$*time	-1.85	0.475	-3.89	0.002	1.00

Regression Equation

$$PhCF_2Cl = 0.20 + 0.68\mathbf{A} + 18\mathbf{B} + 3.5\mathbf{C} - 0.0088\mathbf{A}^2 - 0.11\mathbf{C}^2 + 0.37\mathbf{AB} - 0.046\mathbf{AC}$$

Analysis of Variance

Source	DF	Adj SS	Adj MS	F-Value	P-Value
Model	7	386.1	55.2	30.5	0.000
Linear	3	294.0	98.0	54.3	0.000
$FeCl_3$	1	49.5	49.5	27.4	0.000
BCl_3	1	1.6	1.6	0.9	0.362
time	1	242.9	242.9	134.5	0.000
Square	2	51.3	25.6	14.2	0.001
$FeCl_3$*$FeCl_3$	1	10.2	10.2	5.6	0.035
time*time	1	43.7	43.7	24.2	0.000
2-Way	2	40.9	20.5	11.3	0.002
$FeCl_3$*BCl_3	1	13.5	13.5	7.5	0.018
$FeCl_3$*time	1	27.4	27.4	15.2	0.002
Error	12	21.7	1.8		
Lack-of-Fit	8	13.9	1.7	0.9	0.585
Pure Error	4	7.7	1.9		
Total	19	407.8			

Figure S5. Pareto chart for the chloride halex surface model II

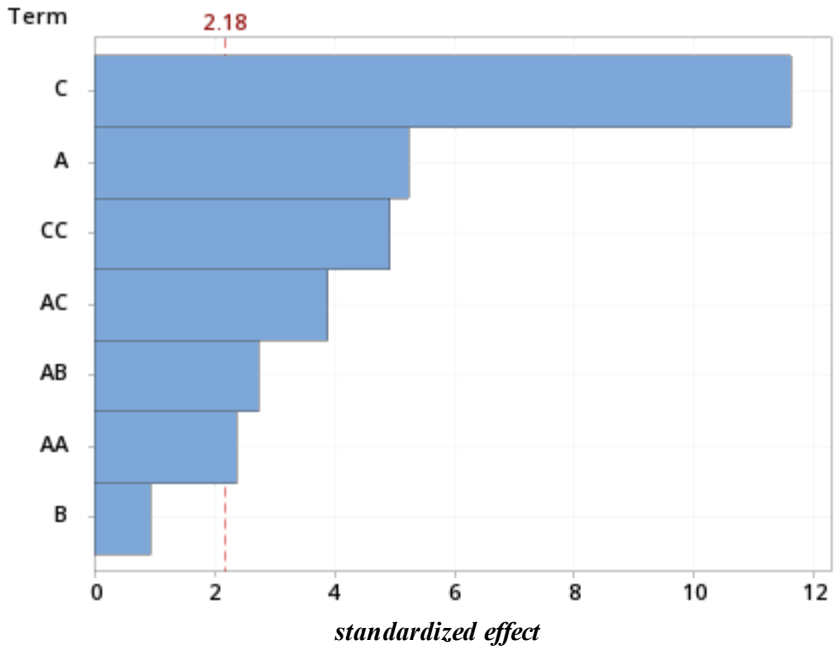

Figure S6. Residual plots for the chloride halex surface model II

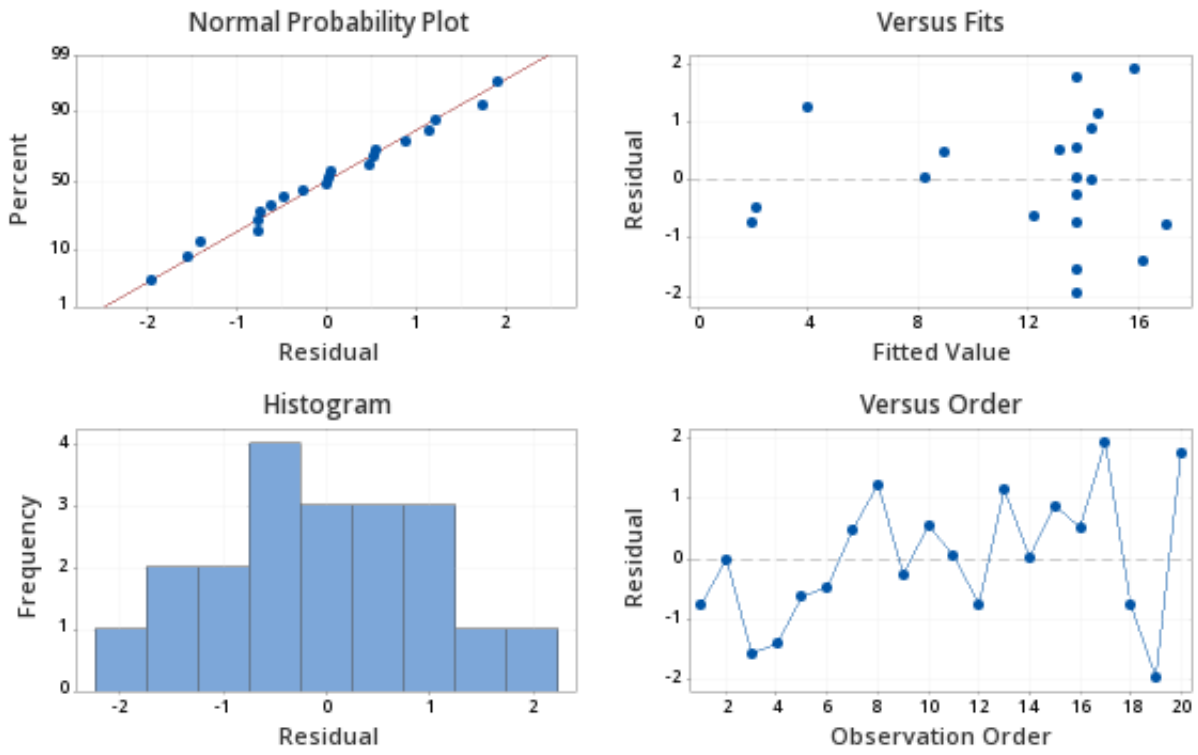

Bromide Halex Investigation I

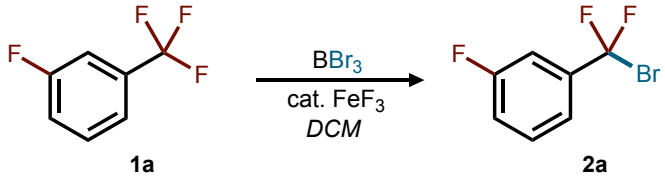

1a 2a

FeF_3	6 mol %	18 mol %
temp.	-50 °C	-10 °C
BBr_3	0.30 eq.	1.30 eq.
time	5 h	15 h
conc.	0.10 M	0.30 M

A new broad-ranging set of parameters were investigated for the bromide halex (due to the differences in behavior between BBr_3 and BCl_3), allowing for the relative importance of each parameter to be determined. Iron loading was found to have little effect on conversion, allowing for it to be fixed for the next set of experiments (investigation II).

A 5-factor *Fractional Factorial* DOE (2^{5-1}) was performed (3 center points). Reaction vessels were charged with ferric fluoride (4.3 mg, 12.9 mg), DCM (2.1 mL, 6.4 mL), and 3-fluoro(trifluoromethyl)benzene (80 µL, 0.63 mmol). The mixture was place in a –78 °C bath, before the addition of boron tribromide (18.5 µL, 79.5 µL). The mixture was transferred to a bath at the target reaction temperature. After the desired reaction time, the mixture was quenched by adding 2–3 mL DCM and a few drops of water (fuming is expected). The mixture was then slowly transferred to a separatory funnel containing saturated $NaHCO_3$ solution (15 mL), brine (15 mL) and DCM (20 mL). The test tube was rinsed forward with 5 mL water and 10 mL DCM. The DCM layer was removed, and the aqueous layer washed with additional DCM (20 mL). The combined organic layers were then filtered through a bed of $NaSO_4$, into a beaker, followed by the addition of 100 µL of 4-fluorotoluene. The solution was stirred well, before an aliquot was taken and combined with equal parts $CDCl_3$ in an NMR tube. Analysis with ^{19}F NMR showed $ArCF_3$ **1b** (–63.2 ppm CF_3, –111.5 ppm ^{m}F), $ArCF_2Br$ **2b** (–44.5 ppm CF_2, –111.5 ppm ^{m}F), $ArCFBr_2$ **3b** (-54.4 ppm CF, –111.8 ppm ^{m}F) and $ArCBr_3$ **4b** (–112.5 ppm ^{m}F) which were quantified relative to the 4-fluorotoluene internal standard (–119.5 ppm). DOE regression analysis was performed using stepwise regression (α=0.05), in which terms were added to maintain a hierarchical model at each step.

Table S4. Full data set for the bromide halex optimization I

FeF_3 (mol %)	temp. (°C)	BBr_3 (eq.)	time (h)	conc. (M)	$ArCF_2Br$ (conv %)
6	-50	0.3	5	0.30	**0.6**
18	-50	0.3	5	0.10	**0.9**
6	-10	0.3	5	0.10	**1.7**
18	-10	0.3	5	0.30	**8.4**
6	-50	1.3	5	0.10	**1.4**
18	-50	1.3	5	0.30	**2.1**
6	-10	1.3	5	0.30	**14.5**
18	-10	1.3	5	0.10	**12.4**
6	-50	0.3	15	0.10	**0.3**
18	-50	0.3	15	0.30	**1.5**

FeF_3 (mol %)	temp. (°C)	BBr_3 (eq.)	time (h)	conc. (M)	$ArCF_2Br$ (conv %)
6	-10	0.3	15.0	0.30	**22.3**
18	-10	0.3	15.0	0.10	**11.0**
6	-50	1.3	15.0	0.30	**5.2**
18	-50	1.3	15.0	0.10	**7.5**
6	-10	1.3	15.0	0.10	**24.2**
18	-10	1.3	15.0	0.30	**18.7**
12	-30	0.8	10.0	0.20	**3.7**
12	-30	0.8	10.0	0.20	**4.0**
12	-30	0.8	10.0	0.20	**4.7**

Figure S7. Statistical analysis for the bromide halex surface model I

Statistical Summary

S	R^2	R^2 (adj)	R^2 (pred)
3.31	87%	81%	68%

Coded Coefficients

Term	Coef	SE Coef	T-Value	P-Value	VIF
Constant	7.64	0.8	10.1	0.000	
FeF_3 **(A)**	-	-	-	-	-
temp **(B)**	5.86	0.8	7.1	0.000	1.000
BBr_3 **(C)**	2.46	0.8	3.0	0.012	1.000
time **(D)**	3.04	0.8	3.7	0.003	1.000
conc **(E)**	0.87	0.8	1.1	0.315	1.000
temp*time	1.86	0.8	2.2	0.045	1.000
BBr_3*conc	-1.49	0.8	-1.8	0.096	1.000

Regression Equation

$ArCF_2Br = -5.7 + 0.11B + 11C + 1.2D + 33E - 0.019BD - 30CE$

Analysis of Variance

Source	DF	Adj SS	Adj MS	F-Value	P-Value
Model	6	896.4	149.4	13.63	0.000
Linear	4	805.6	201.4	18.37	0.000
temp	1	548.7	548.7	50.06	0.000
BBr_3	1	96.5	96.5	8.81	0.012
time	1	148.2	148.2	13.52	0.003
conc.	1	12.1	12.1	1.10	0.315
2-Way	2	90.8	45.4	4.14	0.043
temp*time	1	55.1	55.1	5.03	0.045
BBr_3*conc.	1	35.7	35.7	3.26	0.096
Error	12	131.5	11.0		
Curvature	1	43.7	43.7	5.48	0.039
Lack-of-Fit	9	87.3	9.70	36.82	0.027
Pure Error	2	0.53	0.26		
Total	18	1028			

Figure S8. Pareto chart for the bromide halex surface model I

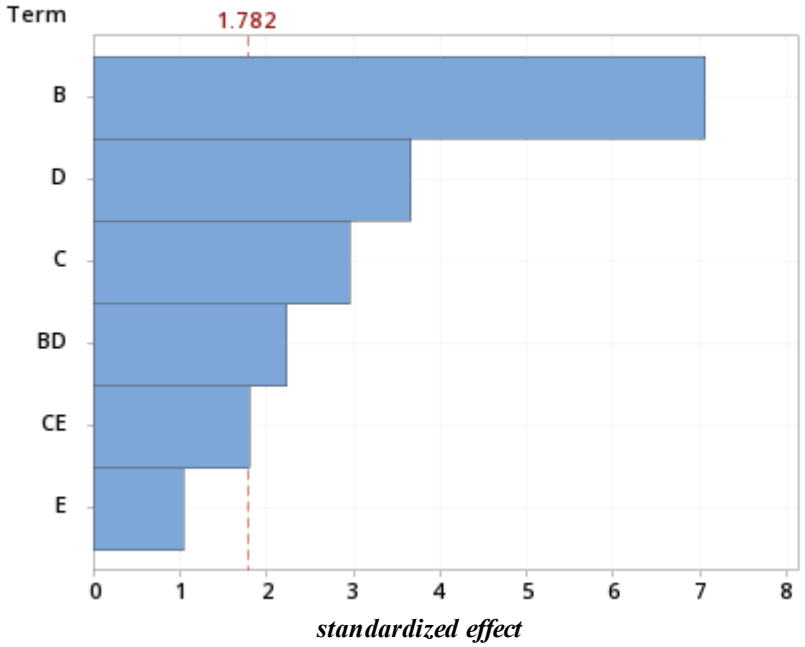

Figure S9. Residual plots for the bromide halex surface model I

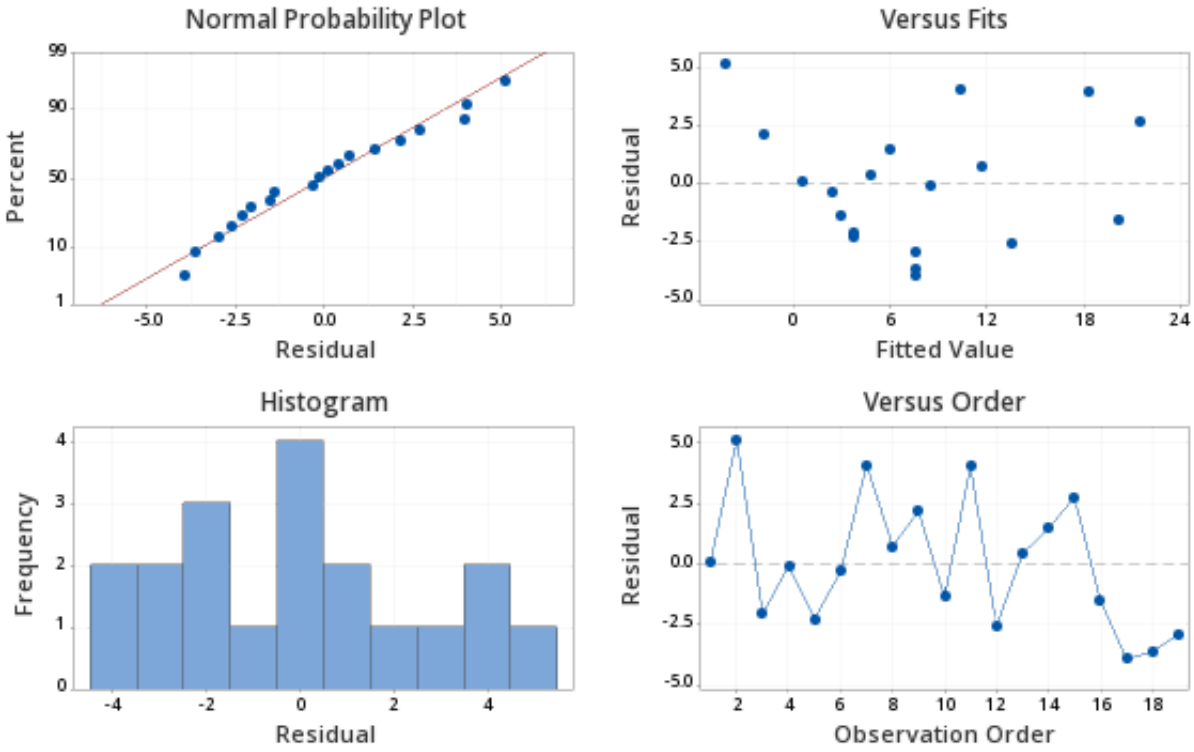

Bromide Halex Investigation II

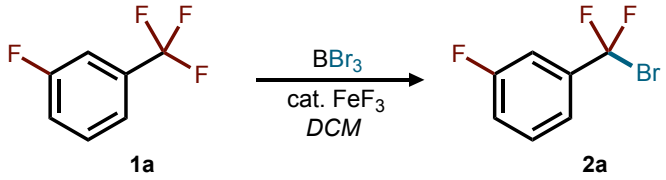

1a **2a**

FeF_3	10 mol %	
temp.	-25 °C	0 °C
BBr_3	0.7 eq.	1.7 eq.
time	8 h	16 h
conc.	0.12 M	0.28 M

*Based on the investigation I model, iron loading was fixed at 10 mol%. A full response surface design was used, using a more narrow parameter range, to hone in on the maximum conversion to the monobromide **2a**.*

A 4-factor *Response Surface* DOE was performed (4 center points, axial points at $\alpha = 1.5$). Reaction vessels were charged with ferric fluoride (7.2 mg), DCM (2.3 mL, 5.3 mL), and 3-fluoro(trifluoromethyl)benzene (80 µL, 0.63 mmol). The mixture was place in a -78 °C bath, before the addition of boron tribromide (43 µL, 104 µL). The mixture was transferred to a bath at the target reaction temperature. After the desired reaction time, the mixture was quenched by adding 2–3 mL DCM and a few drops of water (fuming is expected). The mixture was then slowly transferred to a separatory funnel containing saturated $NaHCO_3$ solution (15 mL), brine (15 mL) and DCM (20 mL). The test tube was rinsed forward with 5 mL water and 10 mL DCM. The DCM layer was removed, and the aqueous layer washed with additional DCM (20 mL). The combined organic layers were then filtered through a bed of $NaSO_4$, into a beaker, followed by the addition of 100 µL of 4-fluorotoluene. The solution was stirred well, before an aliquot was taken and combined with equal parts $CDCl_3$ in an NMR tube. Analysis with ^{19}F NMR showed $ArCF_3$ **1b** (–63.2 ppm CF_3, –111.5 ppm ^{m}F), $ArCF_2Br$ **2b** (–44.5 ppm CF_2, –111.5 ppm ^{m}F), $ArCFBr_2$ **3b** (-54.4 ppm CF, –111.8 ppm ^{m}F) and $ArCBr_3$ **4b** (–112.5 ppm ^{m}F) which were quantified relative to the 4-fluorotoluene internal standard (–119.5 ppm). DOE regression analysis was performed using stepwise regression (α=0.15).

Table S5. Full data set for the bromide halex optimization II

FeF_3 (mol %)	temp. (°C)	BBr_3 (eq.)	time (h)	conc. (M)	$ArCF_2Br$ (conv %)
10	-25	0.70	8	0.12	**1.9**
	0	0.70	8	0.12	**20.4**
	-25	1.70	8	0.12	**4.7**
	0	1.70	8	0.12	**13.1**
	-25	0.70	16	0.12	**1.6**
	0	0.70	16	0.12	**18.3**
	-25	1.70	16	0.12	**5.2**
	0	1.70	16	0.12	**0.1**
	-13	1.20	6	0.20	**9.7**
	-13	1.20	18	0.20	**22.4**
	-13	1.20	12	0.08	**13.8**
	-13	1.20	12	0.32	**20.6**
	-13	1.20	12	0.20	**18.8**
	-13	1.20	12	0.20	**20.7**

FeF_3 (mol %)	temp. (°C)	BBr_3 (eq.)	time (h)	conc. (M)	$ArCF_2Br$ (conv %)
10	-25	0.70	8	0.28	**5.3**
	0	0.70	8	0.28	**20.1**
	-25	1.70	8	0.28	**5.7**
	0	1.70	8	0.28	**15.6**
	-25	0.70	16	0.28	**5.5**
	0	0.70	16	0.28	**17.7**
	-25	1.70	16	0.28	**11.9**
	0	1.70	16	0.28	**13.5**
	-31	1.20	12	0.20	**4.1**
	6	1.20	12	0.20	**2.4**
	-13	0.45	12	0.20	**15.8**
	-13	1.95	12	0.20	**18.2**
	-13	1.20	12	0.20	**17.2**
	-13	1.20	12	0.20	**20.4**

Figure S10. Statistical analysis for the bromide halex surface model II

Regression Parameters

S	R^2	R^2 (adj)	R^2 (pred)
4.08	77%	68%	50%

Coded Coefficients

Term	Coef	SE Coef	T-Value	P-Value	VIF
Constant	17.4	1.18	14.7	0.000	
temp **(A)**	3.63	0.90	4.03	0.001	1.00
BBr_3 **(B)**	-0.85	0.90	-0.94	0.358	1.00
time **(C)**	0.30	0.90	0.33	0.747	1.00
conc **(D)**	1.96	0.90	2.17	0.042	1.00
temp*temp	-6.94	1.22	-5.67	0.000	1.00
temp*BBr_3	-2.96	1.02	-2.90	0.009	1.00
temp*time	-1.64	1.02	-1.60	0.124	1.00

Regression Equation

$$ArCF_2Br = 22 + 0.14A + 7.6B + 0.34C + 25D - 0.044A^2 - 0.47AB - 0.033AC$$

Analysis of Variance

Source	DF	Adj SS	Adj MS	F-Value	P-Value
Model	7	1084.5	154.9	9.29	0.000
Linear	4	365.8	91.4	5.49	0.004
temp	1	270.4	270.4	16.22	0.001
BBr_3	1	14.8	14.8	0.89	0.358
time	1	1.8	1.8	0.11	0.747
conc.	1	78.8	78.8	4.73	0.042
Square	1	535.4	535.4	32.12	0.000
temp*temp	1	535.4	535.4	32.12	0.000
2-Way	2	183.3	91.7	5.5	0.013
temp*BBr_3	1	140.4	140.4	8.42	0.009
temp*time	1	42.9	42.9	2.57	0.124
Error	20	333.4	16.7		
Lack-of-Fit	17	325.6	19.2	7.34	0.063
Pure Error	3	7.8	2.6		
Total	27	1417.9			

Figure S11. Pareto chart for the bromide halex surface model II

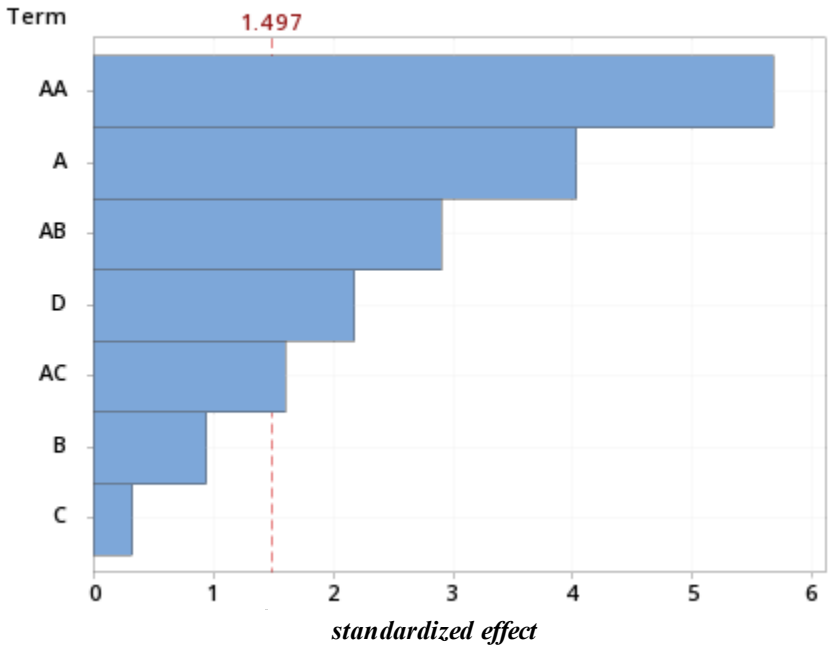

Table S6. Test points for the surface model

temp. (°C)	BBr_3 (eq.)	time (h)	conc. (M)	$ArCF_2Br$ (%) model	$ArCF_2Br$ (%) actual
-3	0.45	6	0.32	**25.2**	**28.1**
-9	1.70	13	0.32	**19.0**	**14.4**
-9	1.70	16	0.32	**19.0**	**15.4**
-13	1.95	15	0.32	**19.4**	**21.1**
-13	1.50	14	0.25	**18.2**	**22.9**

Figure S12. Residual plots for the bromide halex surface model II

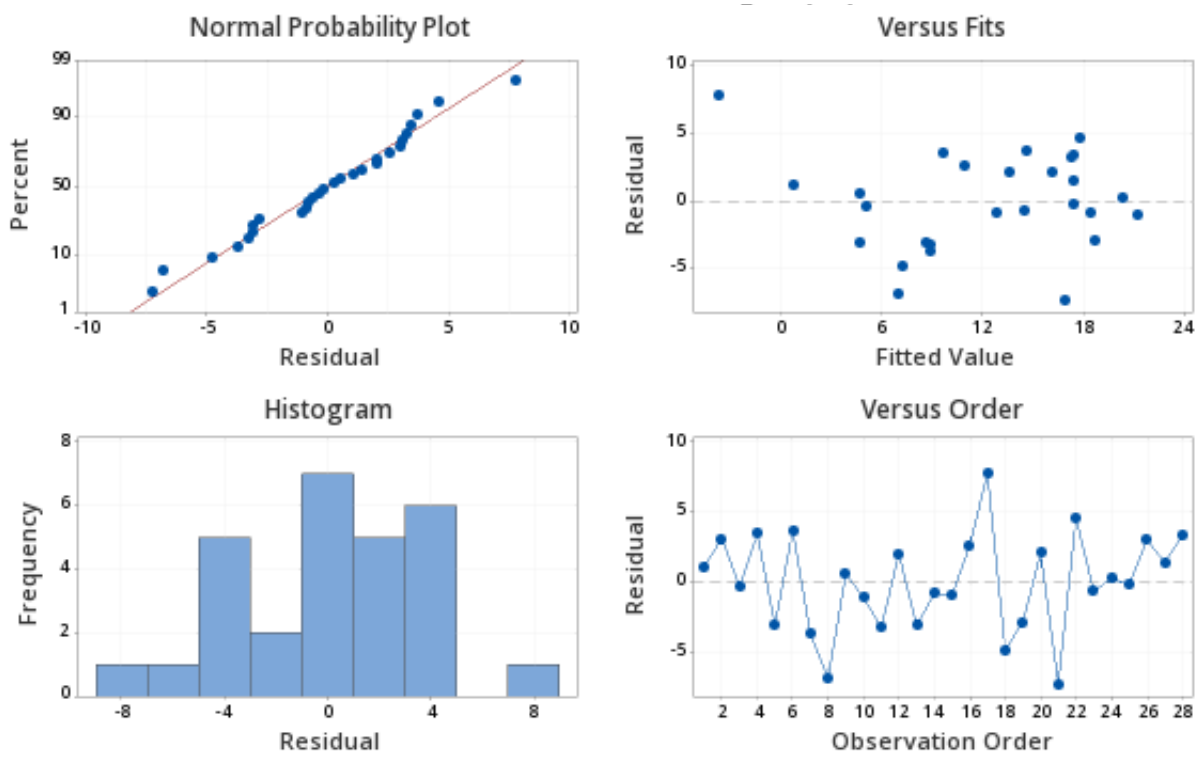

Figure S13. Complete set of surface plots for bromide halex response surface model II

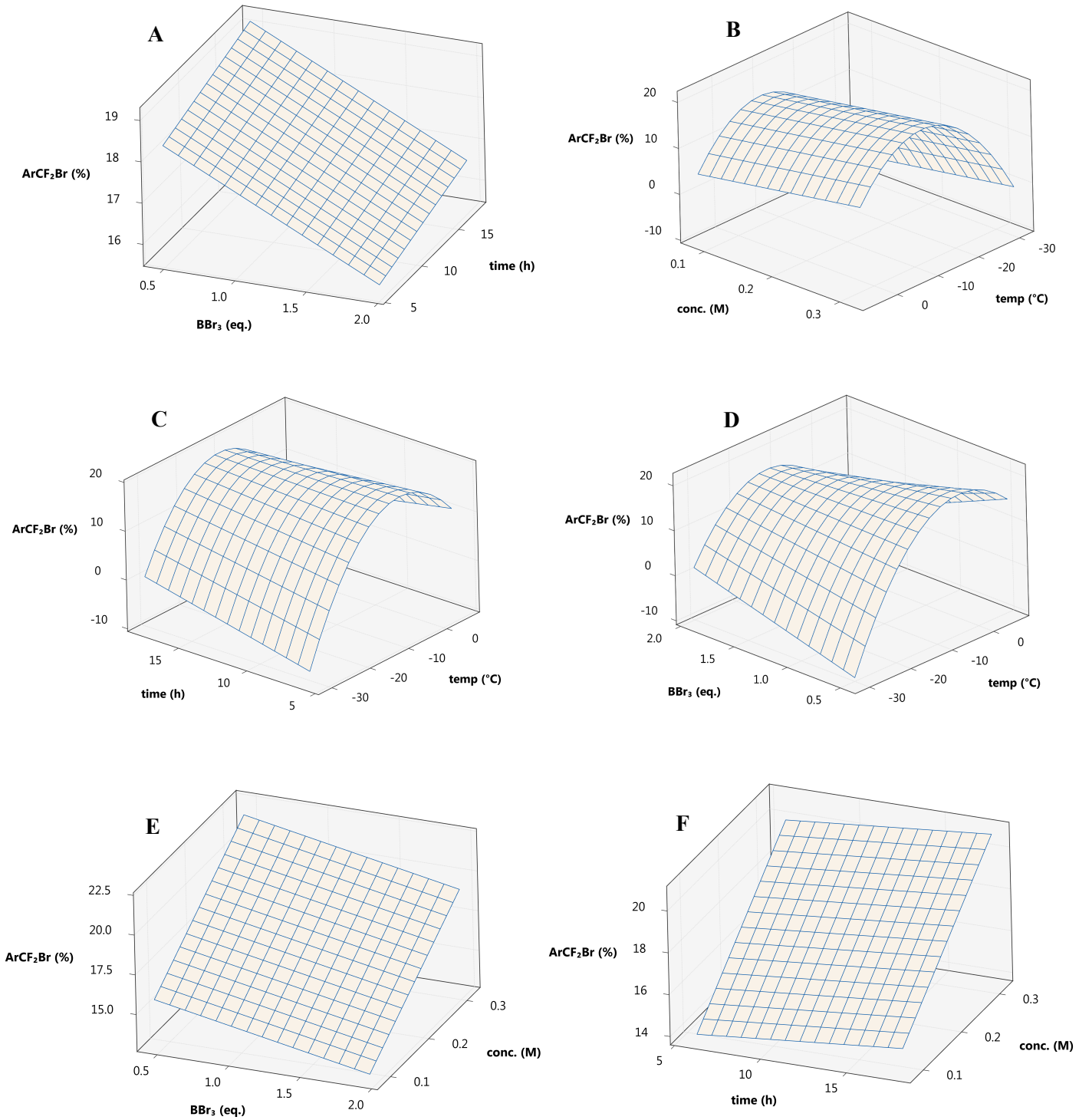

General Procedure: $ArCF_2X$ Scope

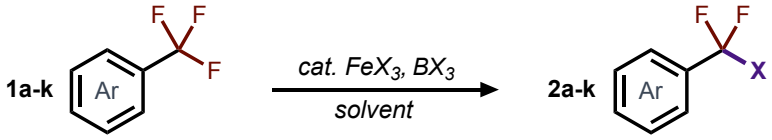

The reaction vessel was charged with ***FeX_3*** catalyst (0.040 mmol, 0.1 eq.), then dry ***solvent***. It was adjusted to target temperature ***T***, and the ***$ArCF_3$*** reagent was added (0.400 mmol, 1.0 eq.), followed by addition of ***BX_3***. After stirring for reaction time ***t***, the mixture was quenched with H_2O, added dropwise at 0 °C (fuming is expected). It was then transferred to a separatory funnel containing saturated aq. $NaHCO_3$ (15 mL), brine (15mL) and DCM (20 mL). The test tube was rinsed forward with 5 mL H_2O and 10 mL DCM. The DCM layer was removed, and the aqueous layer washed with additional DCM (20 mL). The combined organic layers were filtered through Na_2SO_4, into a beaker, followed by addition of 100 µL of 4-fluorotoluene. After stirring well, an aliquot was combined with equal parts $CDCl_3$ in an NMR tube. Conversion to $ArCF_2X$ (**2a-k**) was quantified by ^{19}F NMR, relative to 4-fluorotoluene (–119.5 ppm).[†]

Table S7. Experimental details for the synthesis of various $ArCF_2X$ substrates

product	*FeX_3*	*solvent*	*$ArCF_3$*	*BX_3*	*T*	*t*
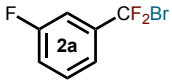	see *Bromide Halex II* (page 12) for **2a** conditions				–3 °C	6 h
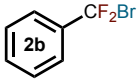	4.5 mg FeF_3	1.25 mL DCM	49.0 µL	0.45 eq. BBr_3 (17.5 µL)	0 °C	2 h
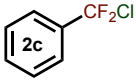	29.2 mg $FeCl_3$	1.4 mL NO_2Me 0.22 mL DCM	49.0 µL	1.2 eq. BCl_3 *1M in DCM* (480 µL)	10 °C	4.5 h
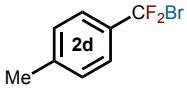	4.5 mg FeF_3	1.25 mL DCM	56.0 µL	0.45 eq. BBr_3 (17.5 µL)	0 °C	45 min
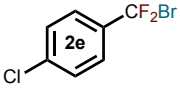	4.5 mg FeF_3	1.25 mL DCM	53.5 µL	0.45 eq. BBr_3 (17.5 µL)	0 °C	18 h
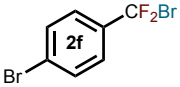	4.5 mg FeF_3	1.25 mL DCM	56.0 µL	0.45 eq. BBr_3 (17.5 µL)	0 °C	18 h
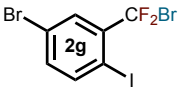	4.5 mg FeF_3	1.25 mL DCM	140.5 mg	0.45 eq. BBr_3 (17.5 µL)	0 °C	24 h
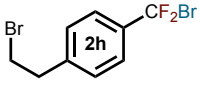	4.5 mg FeF_3	1.25 mL DCM	68.0 µL	0.45 eq. BBr_3 (17.5 µL)	0 °C	2 h
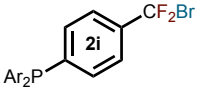	20.1 mg $Fe(OTf)_3$	1.25 mL DCM	186.5 mg	1.45 eq. BBr_3 (56 µL)	0 °C	2 h
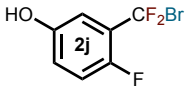	4.5 mg FeF_3	1.25 mL DCM	50.0 µL	1.45 eq. BBr_3 (56 µL)	0 °C	2 h
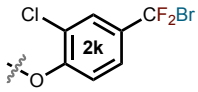	4.5 mg FeF_3	1.25 mL DCM	195.5 mg	2.45 eq. BBr_3 (94 µL)	20 °C	12 h

[†] *conversion not determined for **2i** due to overlap of multiple possible products in the ^{19}F NMR spectrum*

Identification of Compounds 2b, 2c, 2d, 2e, 2f

Known compounds **2b**,[1] **2c**[2], **2d**[3], **2e**[4], **2f**[5] all matched their respective reported ^{19}F NMR chemical shifts. GC-MS analysis was also performed to verify the identity of these products, using the following method.

column:	Zebron ZB-5MS (30m x 0.25cm), 0.25µm film	*injection:*	1 µL, (50:1 split)
gradient:	50°C to 300°C gradient (20 min). 300°C (8 min)	*mass range:*	35 – 500 amu

The synthesis of **2a** was scaled-up, allowing for isolation by distillation. The duplicate runs (*0.40 mmol*) for **2g**, **2h**, **2i**, **2j**, **2k** were combined (*0.80 mmol total*) before using prep-HPLC to isolate the target $ArCF_2Br$ product (*vide infra*).

Large Scale Synthesis of Compound 2a

A flame-dried 50 mL RBF was charged with ferric fluoride (113 mg, 1.0 mmol, 0.10 eq.), followed by dichloromethane (31 mL, 0.32M). The mixture was cooled to 0 °C, and 3-fluoro(trifluoromethyl)benzene was added (1.26 mL, 10.0 mmol), followed by the dropwise addition of boron tribromide (434 µL, 4.5 mmol, 0.45 eq.). After 4 hours, the mixture was diluted with ~10 mL DCM and quenched by adding water dropwise at 0 °C (significant fuming). The mixture was slowly transferred to a separatory funnel containing aq. saturated $NaHCO_3$ solution (30 mL), brine (30 mL) and DCM (50 mL). The RBF was rinsed forward with 10 mL water and 20 mL DCM. The DCM layer was removed, and the aqueous layer washed with additional DCM (40 mL). The combined organic layers were then dried over $NaSO_4$. Analysis with ^{19}F NMR revealed the following *relative* ratio of products:

50 % $ArCF_3$	**1a** (–63.2 ppm CF_3, –111.5 ppm ^{m}F)	*24 % $ArCF_2Br$*	**2b** (–44.5 ppm CF_2, –111.5 ppm ^{m}F)
5 % $ArCFBr_2$	**3b** (–54.4 ppm CF, –111.8 ppm ^{m}F)	*21 % $ArCBr_3$*	**4b** (–112.5 ppm ^{m}F)

The DCM was gently evaporated using a rotovap (not heating above 20 °C, and using mild vacuum). The resulting orange oil was purified using a Hickman still apparatus, with a combination of mild vacuum and heating, affording a high purity (>95%) fraction of $ArCF_2Br$.

3-(bromodifluoromethyl)-1-fluoro-benzene (**2a**). Colorless oil (127 mg, 6 %). **^{1}H NMR** ($CDCl_3$, 500MHz): δ 7.43 (m, 2H), 7.32 (dt, 1H, J = 9.0 Hz, 2.5 Hz), 7.19 (t, 1H, J = 8.3 Hz) ppm. **^{13}C NMR** ($CDCl_3$, 126MHz): δ 162.3 (C, d, J_{CF} = 248.7 Hz), 140.2 (C, td, J_{CF} = 24.5 Hz, 7.8 Hz), 130.6 (CH, d, J_{CF} = 8.0 Hz), 120.1 (CH, app. q, J_{CF} = 13.3 Hz), 118.4 (CH, d, J_{CF} = 20.9 Hz), 117.2 (C, td, J_{CF} = 303.9 Hz, 2.8 Hz), 112.0 (CH, dt, J_{CF} = 24.5 Hz, 5.3 Hz) ppm. **^{19}F NMR** ($CDCl_3$, 376MHz): δ –44.3 (s, 2F), –110.8 (m, 1F) ppm. **HRMS** (EI, $C_7H_4F_3Br$, M^+): calcd.: 223.9448, found: 223.9448. **FTIR** (cast film): 3074, 2925, 2853, 1589, 1483, 1434, 1242, 1135, 700 cm^{-1}.

Isolation of Compounds 2g, 2h, 2i, 2j, 2k

The DCM solution produced after workup was gently concentrated under vacuum. The resulting residue was taken up in 3-5 mL acetonitrile. The solution was divided into 3–6 portions for injection into a preparative-HPLC, allowing for separation of the $ArCF_2Br$ compound from the other byproducts and starting material.

method A: 40 min gradient 58% ACN (H_2O) to 66% ACN (H_2O), 30mL/min, C8 column. (**2g**)
method B: 30 min gradient 50% ACN (H_2O) to 85% ACN (H_2O), 30mL/min, C8 column. (**2h**)
method C: 35 min gradient 78% ACN (H_2O) to 85% ACN (H_2O), 30mL/min, C8 column. (**2i**)
method D: 35 min gradient 30% ACN (H_2O) to 50% ACN (H_2O), 30mL/min, C8 column. (**2j**)
method E: 40 min gradient 55% ACN (H_2O) to 75% ACN (H_2O), 30mL/min, C8 column. (**2k**)

After combining the desired fractions from each injection, the solution was partially concentrated under vacuum to reduce the amount of acetonitrile present. The solution was transferred to a separatory funnel along with DCM (150 mL) and solid NaCl (until saturated). The organic phase was separated, and the aqueous layer was washed with additional DCM (75 mL x 2). The organic layers were combined, dried over $NaSO_4$, and the solvent evaporated under vacuum to afford the pure $ArCF_2Br$ compound.

4-bromo-2-(bromodifluoromethyl)-1-iodobenzene (**2g**). Beige solid (47 mg, 24%). HPLC (*method A*) R.T. = 13.8 min. **^{1}H NMR** ($CDCl_3$, 700MHz): δ 7.88 (d, 1H, J = 8.4 Hz), 7.75 (d, 1H, J = 2.4 Hz), 7.26 (dd, 1H, J = 8.4, 2.4 Hz) ppm. **^{13}C NMR** ($CDCl_3$, 176MHz): δ 143.9 (CH), 141.1 (C, t, $^2J_{CF}$ = 23.1 Hz), 135.3 (CH), 128.9 (CH, t, $^3J_{CF}$ = 8.6 Hz), 122.5 (C), 115.9 (C, t, $^1J_{CF}$ = 305.5 Hz), 89.6 (C, t, $^3J_{CF}$ = 2.7 Hz) ppm. **^{19}F NMR** ($CDCl_3$, 376MHz): δ –46.4 (s, 2F) ppm. **HRMS** (EI, $C_7H_3Br_2F_2I$, M^+): calcd.: 409.7614, found: 409.7613. **FTIR** (cast film): 3090, 2924, 1571, 1551, 1456, 1377, 1275, 1232, 906, 870, 752 cm^{-1}.

1-(bromodifluoromethyl)-4-(2-bromoethyl)-benzene (**2h**). Yellow oil (27 mg, 11%). HPLC (*method B*) R.T. = 11.7 min. **^{1}H NMR** ($CDCl_3$, 700MHz): δ 7.57 (d, 2H, J = 8.4 Hz), 7.31 (d, 2H, J = 8.4 Hz), 3.58 (t, 2H, J = 7.4 Hz), 3.22 (t, 2H, J = 7.4 Hz) ppm. **^{13}C NMR** ($CDCl_3$, 176MHz): δ 142.4 (C), 136.9 (C, t, J_{CF} = 23.7 Hz), 129.0 (CH), 124.7 (CH, t, J_{CF} = 5.0 Hz), 118.4 (C, t, J_{CF} = 303.9 Hz), 38.9 (CH_2), 32.1 (CH_2) ppm. **^{19}F NMR** ($CDCl_3$, 376MHz): δ –43.2 (s, 2F) ppm. **HRMS** (EI, $C_9H_8F_2Br_2$, M^+): calcd.: 311.8961, found: 311.8954. **FTIR** (cast film): 3043, 3015, 2966, 2852, 1615, 1418, 1277, 1055, 884 cm^{-1}.

4-(bromodifluoromethyl)phenyl bis[4-(trifluoromethyl)phenyl]phosphine (**2i**). Yellow oil (71 mg, 17%). HPLC (*method C*) R.T. = 14.5 min. **^{1}H NMR** ($CDCl_3$, 700MHz): δ 7.64 (d, 4H, J = 8.0 Hz), 7.61 (d, 2H, J = 7.6 Hz), 7.42 (app. t, 4H, $^3J_{HH}$, $^3J_{PH}$ = 7.6 Hz), 7.38 (app. t, 2H, $^3J_{HH}$, $^3J_{PH}$ = 7.8 Hz) ppm. **^{13}C NMR** ($CDCl_3$, 176MHz): δ 140.3 (C, d, $^1J_{CP}$ = 14.3 Hz), 139.7 (C, d, $^1J_{CP}$ = 14.0 Hz), 139.1 (C, t, $^2J_{CF}$ = 24.0 Hz), 134.0 (CH, d, $^2J_{CP}$ = 19.9 Hz), 133.9 (CH, d, $^2J_{CP}$ = 19.9 Hz), 131.6 (C, q, $^2J_{CF}$ = 32.6 Hz), 125.7 (CH, dq, $^3J_{CP}$ = 7.3 Hz, $^3J_{CF}$ = 3.7 Hz), 124.8 (CH, dt, $^3J_{CP}$ = 7.0 Hz, $^3J_{CF}$ = 5.0 Hz), 123.9 (C, q, $^1J_{CF}$ = 272.5 Hz), 117.9 (C, t, $^1J_{CF}$ = 303.9 Hz) ppm. **^{19}F NMR** ($CDCl_3$, 376MHz): δ –44.3 (s, 2F), –62.9 (s, 6F) ppm. **^{31}P NMR** ($CDCl_3$, 162MHz): δ –6.0 (s) ppm. **HRMS** (EI, $C_{21}H_{12}BrF_8P$, M^+): calcd.: 525.9732, found: 525.9741. **FTIR** (cast film): 3043, 1607, 1398, 1169, 1132, 1061, 1017, 889, 701 cm^{-1}.

3-(bromodifluoromethyl)-4-fluoro-1-phenol (**2j**). Yellow oil (24 mg, 12%). HPLC (*method D*) R.T. = 17.8 min. **^{1}H NMR** ($CDCl_3$, 500MHz): δ 7.05 (t, 1H, J = 9.5 Hz), 6.99 (dd, 1H, J = 5.8 Hz, 3.1 Hz), 6.93 (dt, 1H, J =

8.9 Hz, 3.4 Hz), 4.28 (br. s, 1H). **^{13}C NMR** ($CDCl_3$, 126MHz): δ 152.9 (C, dt, J_{CF} = 249.0 Hz, 3.4 Hz), 151.2 (C, d, J_{CF} = 2.3 Hz), 126.2 (C, td, J_{CF} = 24.6 Hz, 12.4 Hz), 119.8 (CH, d, J_{CF} = 8.0 Hz), 118.2 (CH, d, J_{CF} = 23.0 Hz), 114.0 (C, td, J_{CF} = 303.9 Hz, 2.2 Hz), 111.9 (CH, t, J_{CF} = 6.4 Hz) ppm. **^{19}F NMR** ($CDCl_3$, 376MHz): δ –44.7 (d, 2F, J = 15.5 Hz) , –123.0 (m, 1F) ppm. **HRMS** (EI, $C_7H_4OF_3Br$, M^+): calcd.: 239.9398, found: 239.9395. **FTIR** (cast film): 3388, 3081, 2930, 2856, 1602, 1503, 1303, 1228, 1109, 952, 836, 774 cm^{-1}.

N-[[4-[2-chloro-4-(bromodifluoromethyl)phenoxy]-2-fluorophenyl]aminocarbonyl]-2,6-difluorobenzamide (**2k**). Off-white solid (57 mg, 13%). HPLC (*method E*) R.T. = 20.1 min. **^{1}H NMR** ($CDCl_3$, 700MHz): δ 10.68 (s, 1H), 9.56 (s, 1H), 8.00 (t, 1H, J = 8.9 Hz), 7.74 (d, 1H, J = 2.3 Hz), 7.51 (tt, 1H, J = 8.5 Hz, 6.3 Hz), 7.47 (dd, 1H, J = 8.6 Hz, 2.3 Hz), 7.03 (t, 2H, J = 8.2 Hz), 6.99 (d, 1H, J = 8.5 Hz), 6.85 (dd, 1H, J = 10.9 Hz, 2.7 Hz), 6.77 (ddd, 1H, J = 8.9 Hz, 2.6 Hz, 1.2 Hz) ppm. **^{13}C NMR** ($CDCl_3$, 176MHz): δ 162.1 (C), 160.1 (C, dd, $^{1,3}J_{CF}$ = 256.0, 6.0 Hz), 154.9 (C), 153.5 (C, d, $^{1}J_{CF}$ = 248.8 Hz), 152.2 (C, d, $^{1}J_{CF}$ = 9.8 Hz), 150.9 (C), 134.5 (C, t, $^{2}J_{CF}$ = 24.7 Hz), 133.7 (CH, t, $^{3}J_{CF}$ = 10.5 Hz), 127.4 (CH, t, $^{3}J_{CF}$ = 5.2 Hz), 125.4 (C), 124.4 (CH, t, $^{3}J_{CF}$ = 5.1 Hz), 123.1 (CH, d, $^{3}J_{CF}$ = 2.0 Hz), 122.2 (C, d, $^{2}J_{CF}$ = 10.7 Hz), 119.1 (CH), 116.9 (C, t, $^{1}J_{CF}$ = 303.8 Hz), 114.7 (CH, d, $^{4}J_{CF}$ = 3.4 Hz), 112.4 (CH, dd, $^{2,4}J_{CF}$ = 21.6, 3.7 Hz), 112.2 (C, t, $^{2}J_{CF}$ = 18.1 Hz), 106.9 (CH, d, $^{2}J_{CF}$ =22.4 Hz) ppm. **^{19}F NMR** ($CDCl_3$, 376MHz): δ –44.0 (s, 2F), –113.9 (s, 2F), –125.9 (s, 1F) ppm. **HRMS** (ESI, $C_{21}H_{11}BrClF_5N_2O_3$, $(M+Na)^+$): calcd.: 547.9562, found: 547.9565. **FTIR** (cast film): 3234, 3134, 2966, 1701, 1626, 1599, 1555, 1492, 1289, 1260, 1068, 918, 797 cm^{-1}.

General Procedure: $ArCX_3$ Scope

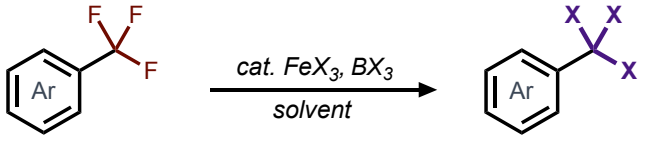

1a, **1e**, **1j** **4a**, **4e**, **5**

The flamed-dried reaction vessel was charged with ***FeX_3*** catalyst (0.040 mmol, 0.1 eq.), followed by dry ***solvent***. It was adjusted to target temperature ***T***, and the ***$ArCF_3$*** reagent was added (0.400 mmol, 1.0 eq.). The ***BX_3*** reagent was then added, and the mixture stirred for the specified reaction time ***t***.

Table S8. Experimental details for the synthesis of various $ArCX_3$ substrates

product	*FeX_3*	*solvent*	*$ArCF_3$*	*BX_3*	*T*	*t*
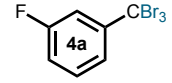	4.5 mg FeF_3	1.25 mL DCM	50.5 µL	3.00 eq. BBr_3 (116 µL)	20 °C	12 h
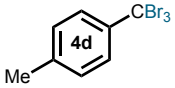	4.5 mg FeF_3	1.25 mL DCM	53.5 µL	1.20 eq. BBr_3 (46 µL)	0 °C	5 h
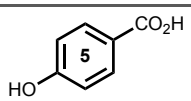	4.5 mg FeF_3	1.25 mL DCM	59.0 µL	1.45 eq. BBr_3 (56 µL)	0 °C	1.5 h

Isolation of Compound 4a, 4e

The mixture was quenched with H_2O, added dropwise at 0 °C (fuming is expected). It was then transferred to a separatory funnel containing saturated aq. $NaHCO_3$ (15 mL), brine (15mL) and DCM (20 mL). The test tube was rinsed forward with 5 mL H_2O and 10 mL DCM. The DCM layer was separated, and the aqueous layer washed with additional DCM (20 mL). The combined organic layers were dried over Na_2SO_4. The solution was concentrated with a rotovap, followed by drying under high vacuum for 2 hours, affording **4a**/**4e**. No further purification was required.

3-fluoro-1-(tribromomethyl)benzene (**4a**). Characterization is consistent with the literature.[6] Clear orange oil (186 mg, 85%). **^{1}H NMR** ($CDCl_3$, 700 MHz) δ 7.80 (ddd, 1H, J = 8.1, 2.2, 0.8 Hz), 7.73 (dt, 1H, J = 10.3, 2.3 Hz), 7.37 (td, 1H, J = 8.3, 5.9 Hz), 7.06 (tdd, 1H, J = 8.1, 2.5, 0.8 Hz) ppm. **^{13}C NMR** ($CDCl_3$, 176 MHz) δ 161.6 (C, d, $^1J_{CF}$ = 247.9 Hz), 149.0 (C, d, $^3J_{CF}$ = 7.6 Hz), 129.6 (CH, d, $^3J_{CF}$ = 7.9 Hz), 122.4 (CH, d, $^4J_{CF}$ = 2.5 Hz), 117.1 (CH, d, $^2J_{CF}$ = 21.0 Hz), 114.3 (CH, d, $^2J_{CF}$ = 25.5 Hz), 33.9 (C, s) ppm. **^{19}F NMR** ($CDCl_3$, 376MHz): δ –111.5 (s, 1F) ppm.

4-methyl-1-(tribromomethyl)benzene (**4e**). Characterization is consistent with the literature.[7] Beige solid (233 mg, 85%). **^{1}H NMR** ($CDCl_3$, 700 MHz) δ 7.90 (d, 2H, J = 8.6 Hz), 7.20 (d, 2H, J = 8.3 Hz), 2.41 (s, 3H) ppm. **^{13}C NMR** ($CDCl_3$, 176 MHz) δ 144.5 (C), 140.5 (C), 128.6 (CH), 126.4 (CH), 36.2 (C), 21.1 (CH_3) ppm.

Isolation of Compound 5

The mixture was quenching by slowly adding 5mL of methanol, followed by potassium hydroxide (500 mg). The mixture was removed from the cool bath and stirred at 20 °C for 1 hour, before being concentrated to dryness under vacuum. The resulting residue was taken up in DCM (30mL) and brine (30mL), and transferred to a separatory funnel. The mixture was adjusted to ~ pH 4, using 2M HCl. The DCM layer was removed, and the aqueous layer washed with additional DCM (20 mL). The combined organic layers were dried over Na_2SO_4. Removal of the solvent under vacuum afforded compound **5** as a white powder. No further purification was required.

Methyl 4-hydroxybenzoate (**5**). Characterization is consistent with the literature.[8] White solid (54 mg, 89%). **^{1}H NMR** ($CDCl_3$, 600 MHz) δ 7.94 (d, J = 8.4 Hz, 2H), 6.89 (d, J = 8.4 Hz, 2 H), 3.99 (s, 3 H). **^{13}C NMR** ($CDCl_3$, 151 MHz) δ 167.5, 160.3, 132.0, 122.3, 115.3, 52.1.

Computational Methods

Gas phase density functional theory (DFT) calculations are commonplace in electronic structure studies of organic mechanisms.[9] We provide calculations on the reaction mixture containing $FeCl_3$, BCl_3 and $PhCF_3$, to provide theoretical evidence for how $FeCl_3$ catalyzes the single halogen-exchange between BCl_3 and $PhCF_3$.

Density functional theory details

The QChem 5.1 package[10] was used to perform unrestricted Kohn-Sham density functional theory calculations, using the B3LYP[11–13] functional and the 6-31G** basis set. All geometry optimization calculations were performed in the gas phase. The IQMol program was used to build structures and view optimized geometries. Here, we have chosen to investigate the reactants and a large variety of possible products in the form of monomers, dimers and trimers. A common heuristic for DFT errors associated with these calculations is 2.3 – 6.9 kcal/mol.[14] The likely error in our calculations is closer to the lower end of this range. Solvent calculations were performed with a polarizable continuum model (for dichloromethane and nitromethane) which yielded energies that closely agreed with the energies presented here. More details on sensitivity tests can be found below.

Selection of monomers

For investigation of all possible structures, a set of six monomers were considered: $FeCl_3$, BCl_3, $PhCF_3$, $FeCl_2F$, BCl_2F, $PhCClF_2$, where combinations (including dimers and trimers) of these could represent species in the reaction mixture.

Protocol for building dimers and trimers

First, three different pots were chosen, which could be arranged in various ways for the reactants and products. The 1st pot contained each of the reaction reactants: BCl_3, $FeCl_3$, and $PhCF_3$. The 2nd pot was one pathway that would allow for possible halogen exchange to occur for the reaction; $FeCl_3$, BCl_2F and $PhCClF_2$. The last pot was the other possible pathway this reaction could take for halex with BCl_3, $FeCl_2F$, and $PhCClF_2$. There were six monomers built and optimized based off possible products and reactants from the three pots. From these optimized geometries, three dimers were made up that would allow for all combinations to be investigated within each pot. The dimers were made from two monomers which were placed in orientations which would allow for possible interaction between a metal and a halogen after optimization. These were then optimized and analyzed to ensure that a reasonable geometry was achieved that highlights the metal/halogen interaction. For further investigation, trimers were made up and optimized as a type of sensitivity test. To make the trimers, for each dimer that was in a pot a monomer was added to it to allow for the full reactants or products to be present. Monomers were placed where possible metal/halogen interaction could take place. This was done for all three pots containing three dimers, resulting in nine trimers. To ensure all possibilities were covered for the trimer calculations, for all trimers made with one dimer, a different dimer was chosen from the three molecules, and the necessary monomer chosen to make it the complete reactants or products. For example, one of the trimers first modeled was with the optimized dimer structure of BCl_3 and $FeCl_3$ with $PhCF_3$ as the monomer added. The alternative trimer investigated was when $FeCl_3$ and $PhCF_3$ were a dimer and BCl_3 was the monomer added. Some of these trimer structures are conformational isomers and were included for completeness as we sought local minima.

Reaction energy calculations

To predict the most likely products given different combinations of reactants, reaction energies (ΔE_r) were calculated from products and reactants energies at their optimal geometries. Specifically, energies of reaction and dimerization were calculated as $\Delta E_r = \sum E(\text{products}) - \sum E(\text{reactants})$, with a negative signed ΔE_r indicating a favorable reaction. We investigated various reactions between monomers, dimers & trimers using optimized structures. The lowest energy dimer or trimer was chosen to calculate the reaction energy if there were conformational isomers to choose between. Note that, in the monomer reactions, only those species that participated directly in the reaction were included.

Dimer and trimer coordination energies

When investigating the reactant dimers, $PhCF_3$ and $FeCl_3$ dimerize where the C-F bond in $PhCF_3$ is stretched by 0.1 Å. This does not occur when $PhCF_3$ dimerizes with BCl_3. This bond elongation indicates a weakening of the bond, which may allow for a more facile reaction with BCl_3. This elongation of the C-F bond is also observed for the trimer reactants. Dimer coordination energies are shown in ***Table S9***.

Table S9. Dimer coordination energies of optimized reactant dimers

Dimer	Dimer coordination energies (kcal/mol)
$PhCF_3 \cdots FeCl_3$	-14.65
$PhCF_3 \cdots BCl_3$	-1.34
$BCl_3 \cdots FeCl_3$	-5.11

** dimers are represented as a (···) joining the two species.*

The reactant trimers were optimized with different arrangements of dimers and monomers. Activation of the C-F bond is shown in ***Figure S14***, with the iron species coordinated to a fluorine, stretching the C-F bond. This was the most favorable trimer out of six that were calculated, with a coordination energy of -15.35 kcal/mol. Other trimers were identified at similar energies with different placements of BCl_3.

Figure S14. Example trimer geometry involving all reactants

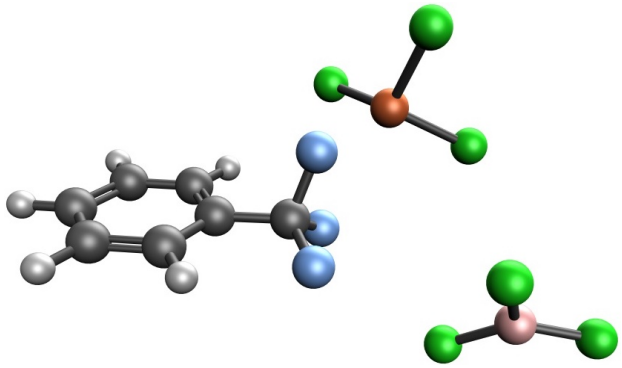

Iron cluster calculations

Calculations were performed to investigate what would occur if an $FeCl_3$ cluster were present. This cluster would involve two or more $FeCl_3$ structures which are coordinated to other $FeCl_3$ structures. In these calculations a cluster of only two $FeCl_3$ molecules were used. Two different monomers, $PhCF_3$ and BCl_3, were modeled with these Fe clusters to determine if they would have stronger interactions with the $FeCl_3$ cluster than with the monomer. The $FeCl_3$ clusters were modeled with odd multiplicities of 1 to 11, and the lowest energy structure was found to be the multiplicity of 11. The multiplicity is given as 2S+1, where S is the sum of the spins of the unpaired electrons. $PhCF_3$ and BCl_3 monomers were then added separately to the lowest energy $FeCl_3$ cluster, and had their geometries reoptimized. Coordination energies of $PhCF_3$ and BCl_3 to the $FeCl_3$ cluster were then calculated and compared to dimerization energies. Coordinating $PhCF_3$ or BCl_3 to $FeCl_3$ is more favorable when $FeCl_3$ is alone rather than in a $FeCl_3$ cluster. Additionally, $PhCF_3$ coordination to the $FeCl_3$ cluster shows no significant C-F bond elongation. Due to weaker interactions of $PhCF_3$ or BCl_3 with the $FeCl_3$ dimeric cluster than to monomeric $FeCl_3$, larger clusters of $FeCl_3$ were presumed to behave similarly and were not investigated computationally.

Table S10. Coordination energies of optimized $FeCl_3$ clusters with $PhCF_3$ or BCl_3

Trimer	Coordination energies (kcal/mol)
$PhCF_3 \cdots FeCl_3 \cdots FeCl_3$	-3.6
$BCl_3 \cdots FeCl_3 \cdots FeCl_3$	-0.07

Reaction Energies

Density functional theory calculations of isolated species

We find that the reaction of BCl_3 and $PhCF_3$ to form BCl_2F and $PhCClF_2$ is thermodynamically favorable when reactant/reactant and product/product dimeric interactions are neglected. For the reaction of $FeCl_3$ and $PhCF_3$ to form $FeCl_2F$ and $PhCClF_2$, we find that the reaction is thermodynamically unfavorable as seen in ***Table S11*** for the B3LYP/6-31G** functional and basis set.

Coupled cluster calculations

Calculations using coupled cluster singles and doubles with perturbative triples (CCSD(T)) were performed on all monomers investigated.[15] Calculations were performed with Dunning correlation consistent basis sets, cc-pVDZ and cc-pVTZ.[16] The reaction energies were then calculated from the monomer energies and compared to the reaction energies given in the main text, as shown in ***Table S11***. Extrapolations were performed on the monomer energies by calculating a straight-line fit with respect to the energies as a function of $1/X^3$, where X is the cardinal number associated with the basis set. [17]

Table S11. Comparison of reaction energies from DFT, CCSD(T) and extrapolated monomers energies

Reaction	B3LYP/ 6-31G** (kcal/mol)	CCSD(T)/ cc-pVDZ (kcal/mol)	CCSD(T)/ cc-pVTZ (kcal/mol)	CCSD(T) – extrapolation (kcal/mol)
$PhCF_3 + BCl_3 \rightarrow PhCClF_2 + BCl_2F$	-5.17	-2.62	-6.09	-7.56
$PhCF_3 + FeCl_3 \rightarrow PhCClF_2 + FeCl_2F$	14.10	18.66	19.60	20.00
$FeCl_2F + BCl_3 \rightarrow FeCl_3 + BCl_2F$	-19.28	-21.27	-25.70	-27.56

Sensitivity Tests

Functionals and basis sets

All monomers were run with two different functionals and basis sets to perform sensitivity tests. Dispersion calculations were also run to account for any van der Waals interactions that may not be accounted for in the DFT calculations. All calculations were run with the geometry inputs from the original B3LYP/6-31G** calculations before they were optimized. These combinations of functional and basis set were used: B3LYP/6-31G*[18], B3LYP/6-31G(d)+, PBE[19]/6-31G**, PBE/6-31G*, PBE0[20]/6-31G**, B3LYP – D3[21]/6-31G**. No significant changes were observed after the optimizations of the structures with these functionals and basis sets.

PCM results

Polarizable continuum models (PCM) were used as a solvation model for the studied molecules. These models allow for the calculations to account for the electrostatic interactions that may occur between the molecules and the solvent they are in. For these calculations, dichloromethane was used as the solvent which coincides with the solvents used in experiment, with a dielectric constant of 8.93. Another parameter needed to be added for molecules with Fe (the van der Waals radius was set to 1.94 Å).[22] After optimization of the structures using PCM no significant changes were observed relative to without PCM.

Optimized Coordinates

PhCClF$_2$

C	1.1854593948	0.2532849381	-0.2852599788
C	-0.3026645046	0.1016503357	-0.1425088098
C	-0.9126425639	-1.1119355247	-0.4726868368
H	-0.3115636053	-1.9345021981	-0.8441026335
C	-2.2913282283	-1.2532550860	-0.3256320127
H	-2.7659870431	-2.1945808244	-0.5846860536
C	-3.0587441025	-0.1880171479	0.1491026872
H	-4.1326709242	-0.3010102825	0.2628803589
C	-2.4457967338	1.0230219243	0.4760786477
H	-3.0407416135	1.8542974508	0.8414678860
C	-1.0676546625	1.1713524841	0.3315105345
H	-0.5860361555	2.1104118451	0.5807490623
F	1.6721267788	-0.5238551319	-1.2770254338
F	1.5312240790	1.5300567511	-0.5592618149
Cl	2.0702370152	-0.2189003096	1.2403554842

PhCF$_3$

C	1.4512727691	0.0075720241	0.0000000847
C	-0.0531330401	0.0227665345	0.0000020969
C	-0.7363212766	-1.1981670578	0.0000008881
H	-0.1781376969	-2.1290159831	0.0000019618
C	-2.1286390140	-1.2113957907	-0.0000005209
H	-2.6593397265	-2.1584698550	-0.0000011745
C	-2.8397742866	-0.0084313879	-0.0000008221
H	-3.9256047304	-0.0205007904	-0.0000016565
C	-2.1557391817	1.2070282754	0.0000003274
H	-2.7062207120	2.1427524450	0.0000003715
C	-0.7602063473	1.2257037204	0.0000016700
H	-0.2212086743	2.1660138275	0.0000027735
F	1.9414231317	-0.6382008022	-1.0844281792
F	1.9797486391	1.2499689793	0.0000301926
F	1.9414251547	-0.6382549385	1.0843950315

BCl_3

B	-0.0000339123	-0.0000588542	0.0000000000
Cl	-1.2241627931	-1.2545868701	0.0000000000
Cl	-0.4744446947	1.6875028266	0.0000000000
Cl	1.6986414001	-0.4328571023	0.0000000000

BCl_2F

B	-0.0000339123	-0.0000588542	0.0000000000
Cl	-1.2241627931	-1.2545868701	0.0000000000
Cl	-0.4744446947	1.6875028266	0.0000000000
Cl	1.6986414001	-0.4328571023	0.0000000000

$FeCl_3$

Fe	0.0000572409	-0.0000044377	0.0000000000
Cl	2.0661657680	0.5556640747	0.0000000000
Cl	-0.5518440359	-2.0671255165	0.0000000000
Cl	-1.5143852667	1.5114486937	0.0000000000

$FeCl_2F$

Fe	-0.0000063399	-0.2884902710	0.0000000000
Cl	-1.8637645300	0.7718012238	0.0000000000
Cl	1.8637772213	0.7717552573	0.0000000000
F	-0.0000242491	-2.0216626907	0.0000000000

$BCl_3 \cdots FeCl_3$

Fe	1.4865535755	-0.1187975874	0.4504033619
Cl	1.9621140694	1.5731765719	-0.7976652755
Cl	0.8378681782	0.2760947618	2.4678060322
Cl	2.5911483085	-1.9386939549	0.1110374066
B	-2.1537550701	0.0842187236	-0.7329489394
Cl	-3.6165353986	-0.4794495796	-1.4788269856
Cl	-0.7658171284	-1.0554539507	-0.6959202241
Cl	-1.9957596817	1.6644758277	-0.0443087006

$BCl_3 \cdots PhCF_3 \cdots FeCl_3$

C	1.2486868640	-0.9065521898	0.0023935403
C	2.6938992408	-1.2590805095	0.0026455664
C	3.1808812058	-2.1877723007	-0.9229729366
H	2.5026493997	-2.6699144430	-1.6180023675
C	4.5406062396	-2.4905633707	-0.9344404569
H	4.9248957151	-3.2135237207	-1.6464803938
C	5.4034085767	-1.8665050857	-0.0313736704
H	6.4625121124	-2.1047139598	-0.0437176075
C	4.9109029973	-0.9378413324	0.8886692769
H	5.5830997409	-0.4542306923	1.5897263549
C	3.5533155633	-0.6290554520	0.9110569306
H	3.1638020826	0.0918131228	1.6218759575
F	1.0525475723	0.3177038683	-0.7679075859
F	0.7506689799	-0.6108501364	1.2017794003
F	0.4601141875	-1.7861527647	-0.6008092894
Fe	0.2199792103	2.1934151839	-0.2238014909
Cl	0.4658561369	3.2295272977	-2.1011455663
Cl	-1.8179509280	1.7356767188	0.3400787332
Cl	1.5424615181	2.8154766822	1.3797463979
B	-3.4399853481	-1.7825969030	0.1762591532
Cl	-2.3630858859	-2.3197681377	1.4536685039
Cl	-2.9361523398	-1.9131906625	-1.4995879553
Cl	-5.0218802146	-1.1490009069	0.5710006962

$PhCF_3\cdots BCl_3$

C	-0.7818289706	-1.3165290834	-0.6511040525
C	-1.9925454529	-0.4783578882	-0.3487197700
C	-2.6393762532	-0.6158002053	0.8825730344
H	-2.2943933822	-1.3594749201	1.5926961815
C	-3.7297812680	0.1981819128	1.1842677303
H	-4.2352053980	0.0900795672	2.1388887973
C	-4.1724282971	1.1462207272	0.2597426162
H	-5.0229723534	1.7784862642	0.4962177159
C	-3.5249119844	1.2797821728	-0.9696951245
H	-3.8707554444	2.0133201198	-1.6913341307
C	-2.4334887550	0.4686145006	-1.2767137270
H	-1.9292289268	0.5618819794	-2.2322444044
F	0.3591749944	-0.7255441040	-0.1997447336
F	-0.6147820300	-1.5124848010	-1.9757953999
F	-0.8430645030	-2.5293537457	-0.0619381057
B	2.8571894714	0.6324931045	0.7123185171
Cl	1.8940071300	1.8308203479	1.5561709029
Cl	3.3762783344	-0.8191507921	1.5461102271
Cl	3.3410969440	0.9099268519	-0.9495601293

$PhCF_3\cdots FeCl_3$

C	-1.1341703741	-0.5659178341	0.9389614236
C	-2.4666482391	-0.2522272695	0.3554593781
C	-2.7709350479	1.0728085939	0.0204728774
H	-2.0515206425	1.8626563120	0.2089717694
C	-4.0048327783	1.3622124211	-0.5561007448
H	-4.2485014746	2.3866370046	-0.8176209967
C	-4.9242438475	0.3378188220	-0.7948169246
H	-5.8855164578	0.5688109994	-1.2433740599
C	-4.6136367114	-0.9812463153	-0.4588898083
H	-5.3300994410	-1.7750491960	-0.6431281026
C	-3.3810011334	-1.2829278268	0.1161676692
H	-3.1318063463	-2.3038576471	0.3828444249
F	-0.1535099181	-0.6613338052	-0.1288456791
F	-1.0548884323	-1.7417555677	1.5502183700
F	-0.6462822724	0.3826068895	1.7389234760
Fe	1.7304577439	0.3142244103	-0.3326285828
Cl	1.1254397405	2.3931145964	-0.4813428207
Cl	2.8161518408	-0.2639140182	1.4436005963
Cl	2.3796409992	-0.6028707472	-2.1778781884

$(FeCl_3)_2$

Fe	-1.6628800349	0.3623390994	-0.0338254380
Cl	-0.0776788978	-0.5077561555	-1.5709102830
Cl	-2.3629799235	2.2954880763	-0.6172236899
Cl	-3.1327158020	-1.0937799261	0.5014777963
Cl	0.0752875266	0.4991000712	1.5762963801
Fe	1.6620918640	-0.3613695542	0.0359706405
Cl	3.1259899301	1.0974736977	-0.5080224438
Cl	2.3728801703	-2.2914969236	0.6162404548

$(FeCl_3)_2\cdots BCl_3$

Fe	1.6245452423	-0.1970870158	-2.0637211665
Cl	0.0447529928	1.0434235947	-0.8013977640
Cl	2.7849574926	-1.5134313089	-0.8441369272
Cl	2.6822986476	1.0441788794	-3.4456209980
Cl	-0.1915609705	-1.3238180002	-3.0970792279
Fe	-1.7717533857	-0.0688183197	-1.8470349359
Cl	-2.8688219151	-1.2975368556	-0.4855395760
Cl	-2.8974471659	1.2573848915	-3.0893938489
B	0.1754143757	0.2767574622	4.3556743711
Cl	-1.2726614224	-0.3432517029	3.5865635481
Cl	0.0610882753	1.1331408407	5.8800568720
Cl	1.7384960449	0.0390042107	3.5983866892

$(FeCl_3)_2\cdots PhCF_3$

Fe	-2.2746885408	1.2525699921	1.2413054397
Cl	-2.4174489610	-1.0726779540	1.7042774864
Cl	-4.1572707802	2.2091087046	1.5928457142
Cl	-0.5933353760	2.1800580198	2.1812617612
Cl	-2.0649816797	0.7126021000	-1.0564543338
Fe	-2.4721449659	-1.5825404837	-0.6133023798
Cl	-4.4574089755	-2.0951502409	-1.2320010174
Cl	-0.9434727299	-2.9514919588	-1.2058985124
C	1.7096532769	0.2286384518	-0.6433178934
C	3.1761914461	0.1032001713	-0.3428766047
C	4.0856454905	-0.1439152459	-1.3735106695
H	3.7270139842	-0.2867083404	-2.3865945597
C	5.4487935498	-0.2141950027	-1.0873189990
H	6.1570674014	-0.4101349551	-1.8862542814
C	5.8991403919	-0.0361735831	0.2213802825
H	6.9605059215	-0.0942675892	0.4430869399
C	4.9861226129	0.2124186366	1.2488300182
H	5.3355723548	0.3485735060	2.2675091952
C	3.6231510251	0.2833313119	0.9699648100
H	2.9080046471	0.4707023622	1.7639343158
F	1.3692520814	-0.3465342308	-1.8158904353
F	0.9492309806	-0.3553236901	0.3241209617

References

1. G.K.S. Prakash, J. Hu, J. Simon, D. R. Bellew, G.A. Olah, *J. F. Chem.* **2004**, *125*, 595.
2. R.C. McAtee, J.W. Beatty, C.C. McAtee, C.R. Stephenson, *Org. Lett.* **2018**, *20*, 3491.
3. D. Mandal, R. Gupta, A. K. Jaiswal, R. D. Young, *J. Am. Chem. Soc.* **2020**, *142*, 2572.
4. J.-W. Gu, W.-H. Guo, X. Zhang, *Org. Chem. Front.* **2015**, *2*, 38.
5. A.B. Gome, M.A.C. Gonzalez, M. Lubcke, M.J. Johansson, M. Schou, K.J. Szabo, *J. F. Chem.* **2017**, *194*, 51.
6. W.A. Sheppard, *Tetrahedron*, **1971**, *27*, 945.
7. T. Chatterjee, D.I. Kim, E.J. Cho, *J. Org. Chem.*, **2018**, *83*, 7423.
8. H-M. Yang, M-L. Liu, J-W. Tu, E. Miura-Stempel, M.G. Campbell, G.J. Chuang, *J. Org. Chem.*, **2020**, *85*, 2040.
9. R.S. Payal, R. Bharath, G. Periyasamy, S. Balasubramanian, *J. Phys. Chem. B*, **2012**, *116*, 833.
10. Y. Shao et al., *Mol. Phys.*, **2015**, *113*, 184.
11. A.D. Becke, *J. Chem. Phys.*, **1993**, *98*, 1372.
12. C. Lee, W. Yang, R.G. Parr, *Phys. Rev. B*, **1988**, *37*, 785.
13. P.J. Stephens, F.J. Devlin, C.F. Chabalowski, M.J. Frisch, *J. Phys. Chem*., **1994**, *98*, 11623.
14. F.D. Sala, S. D'Agostino, *Handbook of Molecular Plasmonics*, CRC Press, **2013**.
15. R.J. Bartlett and M. Musiał, *Rev. Mod. Phys*., **2007**, *79*, 291.
16. T.H. Dunning, *J. Chem. Phys.,* **1989**, *90*, 1007.
17. A. Halkier, T. Helgaker, P. Jørgensen, W. Klopper, H. Koch, J. Olsen, A. Wilson, *Chem. Phys. Let.*, **1998**, *286*, 243.
18. V.A. Rassolov, M.A. Ratner, J.A. Pople, P.C. Redfern, L.A. Curtiss, *J. Comput. Chem.*, **2001**, *22*, 976.
19. M. Ernzerhof, G.E. Scuseria, *J. Chem. Phys.*, **1999**, *110*, 5029.
20. C. Adamo, V. Barone, *J. Chem. Phys.*, **1999**, *110*, 6158.
21. S. Grimme, J. Antony, S. Ehrlich, K. Helge, *J. Chem. Phys.*, **2010**, *132*, 154104.
22. Periodic Table of Elements: Los Alamos National Laboratory. *https://periodic.lanl.gov/26.shtml.*

Figure S15: GCMS chromatogram of compound **2a** reaction

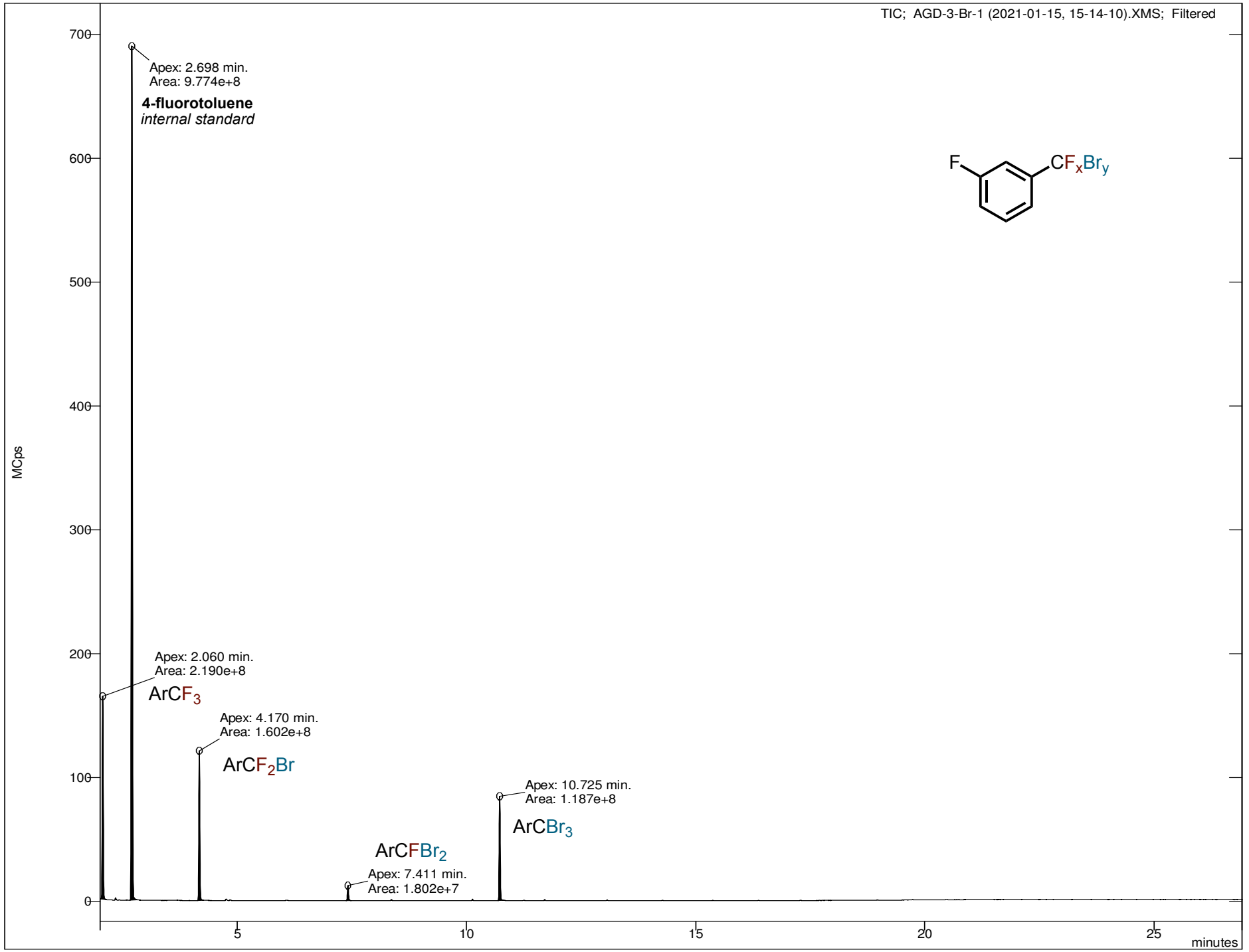

Figure S16: Mass spectrum for peak at 2.1 minutes (compound **2a** reaction)

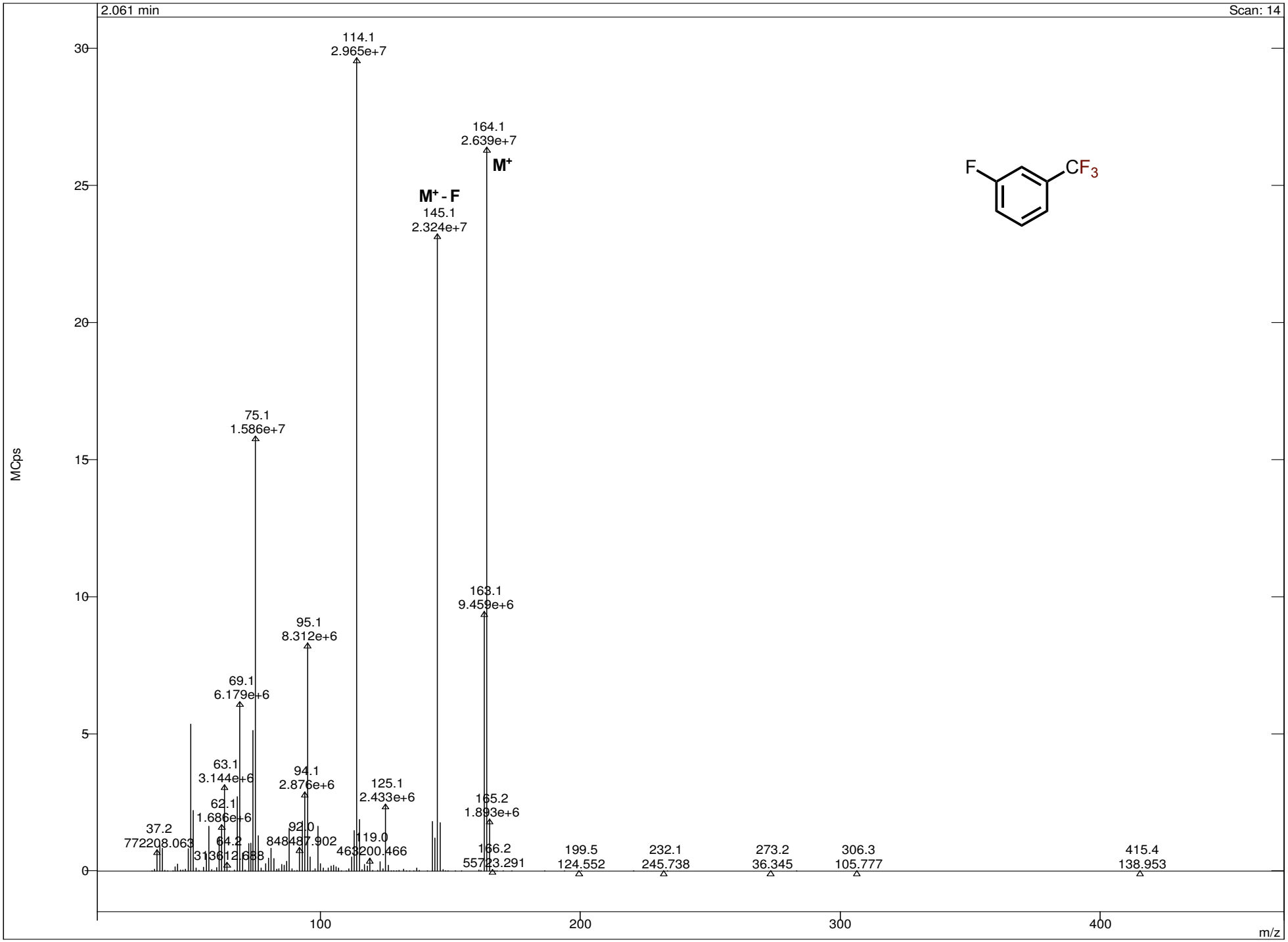

Figure S17: Mass spectrum for peak at 4.2 minutes (compound **2a** reaction)

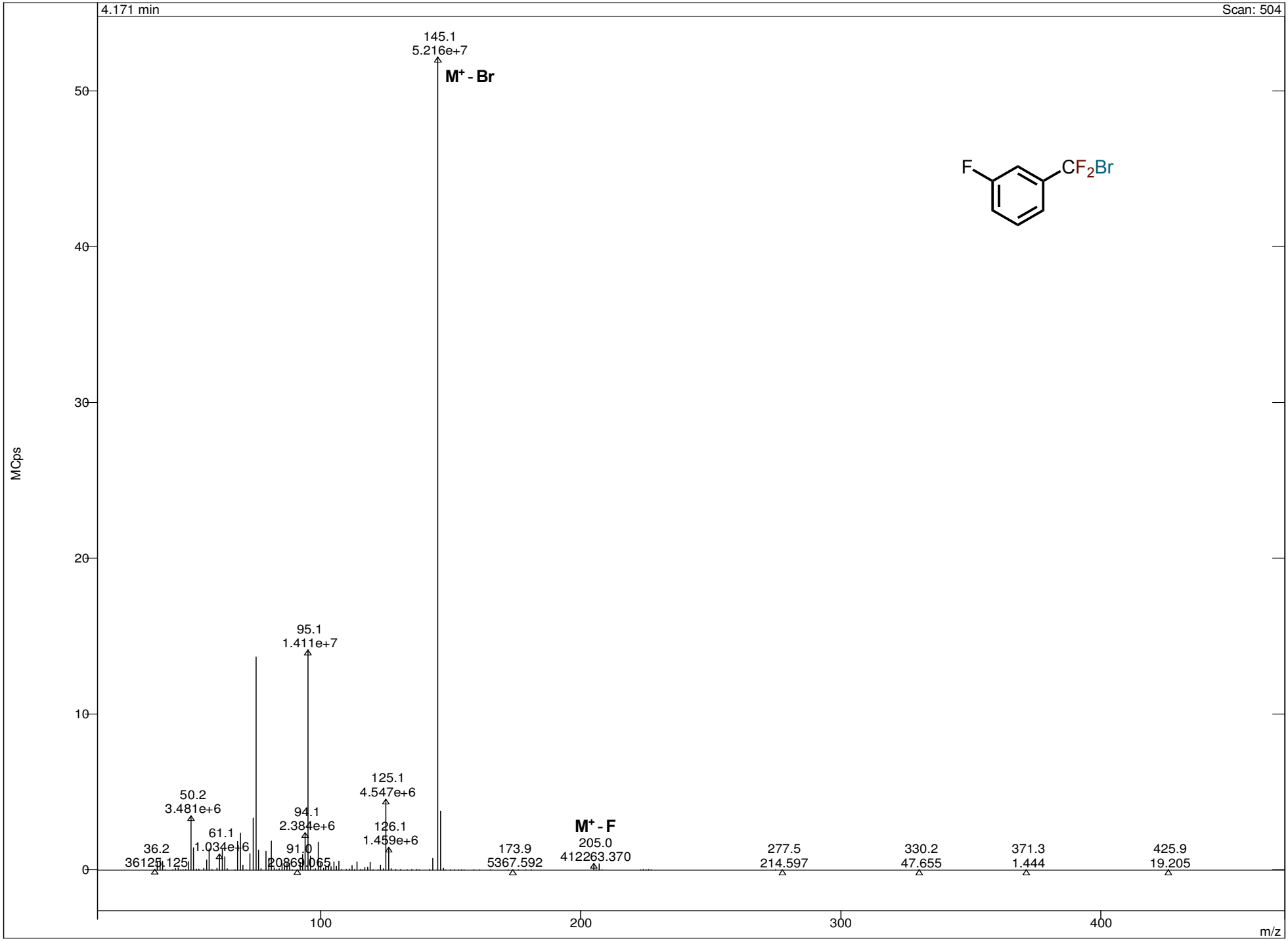

Figure S18: Mass spectrum for peak at 7.4 minutes (compound **2a** reaction)

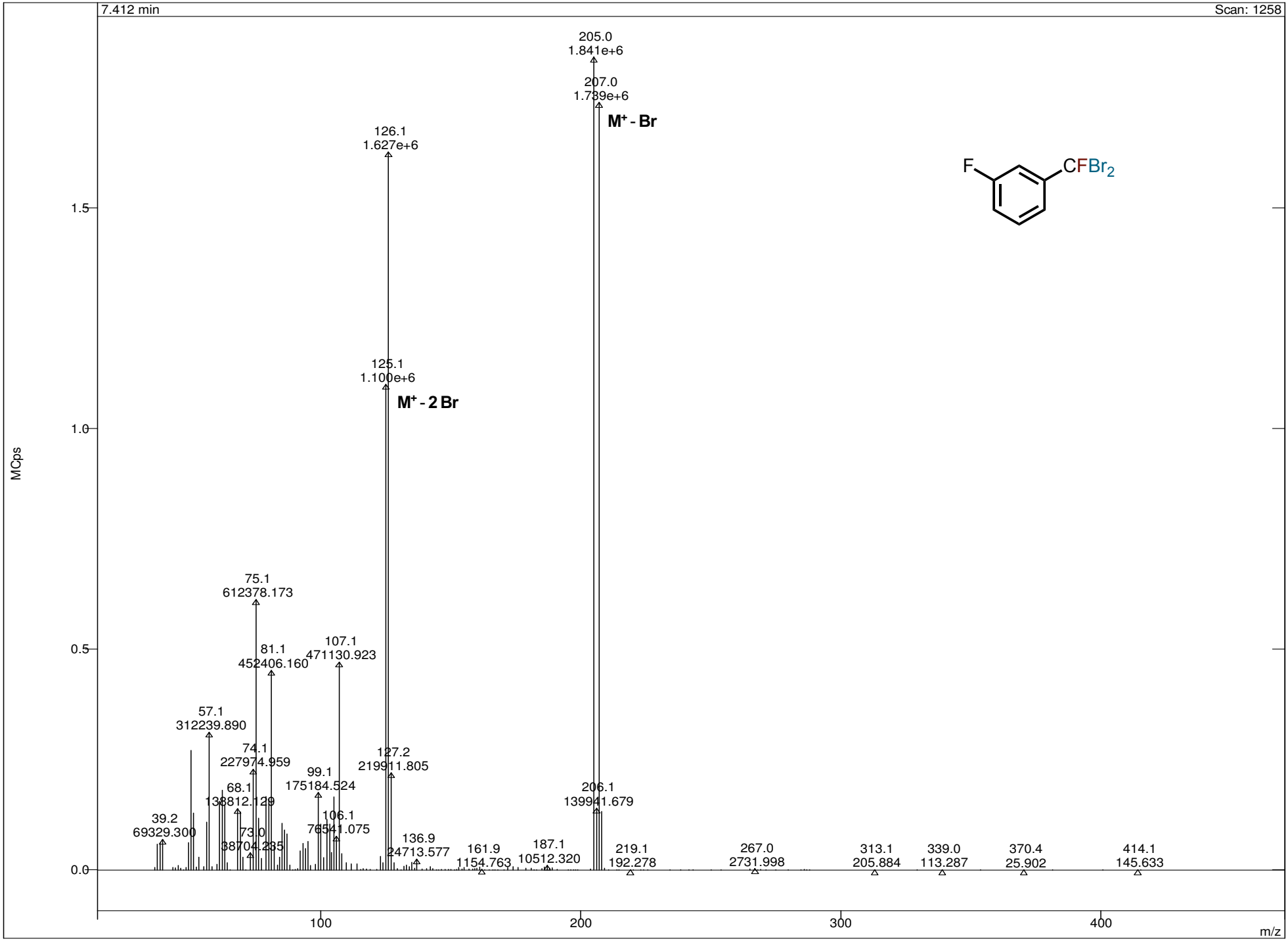

Figure S19: Mass spectrum for peak at 10.7 minutes (compound **2a** reaction)

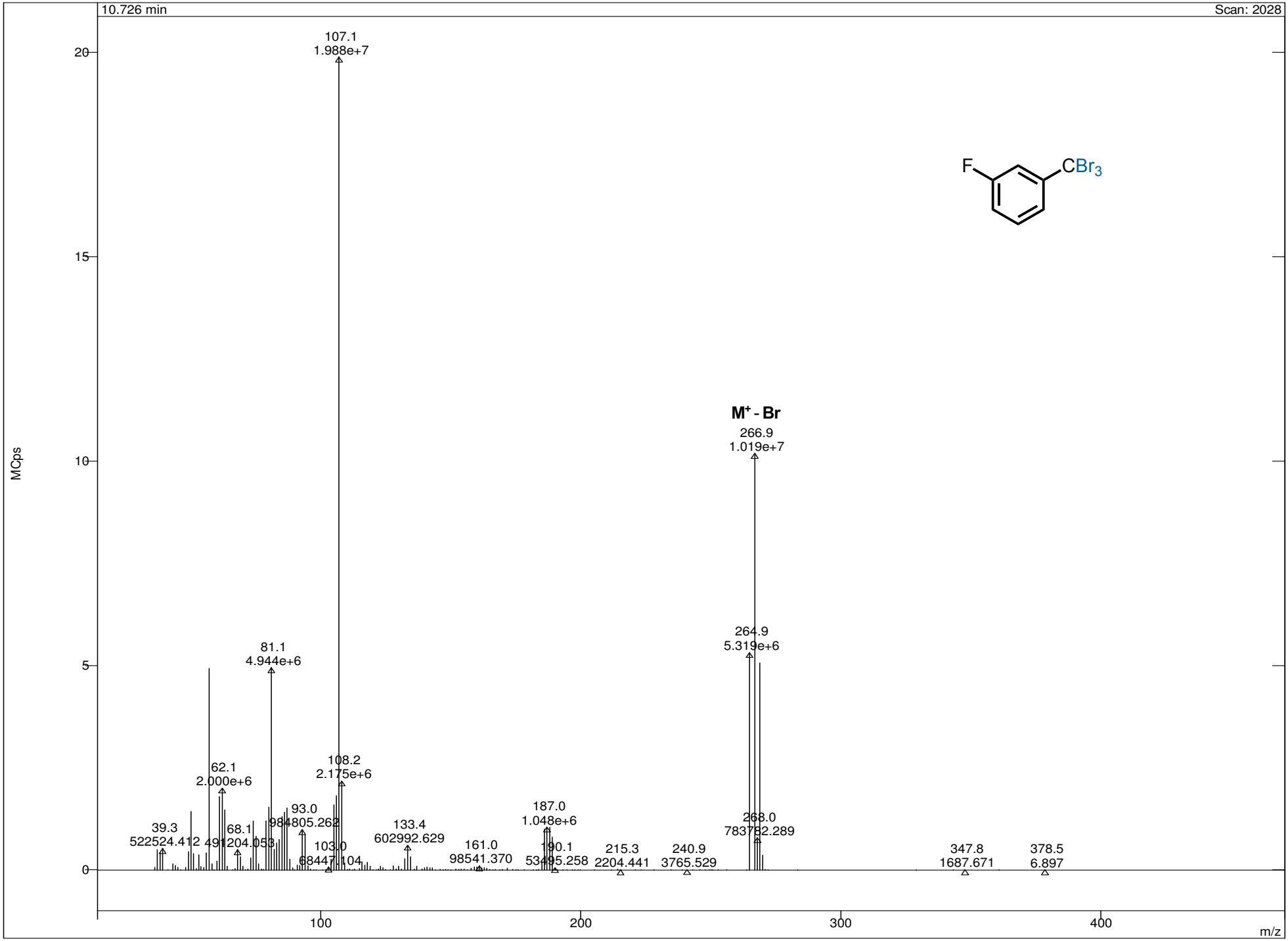

Figure S20: GCMS chromatogram of compound **2b** reaction

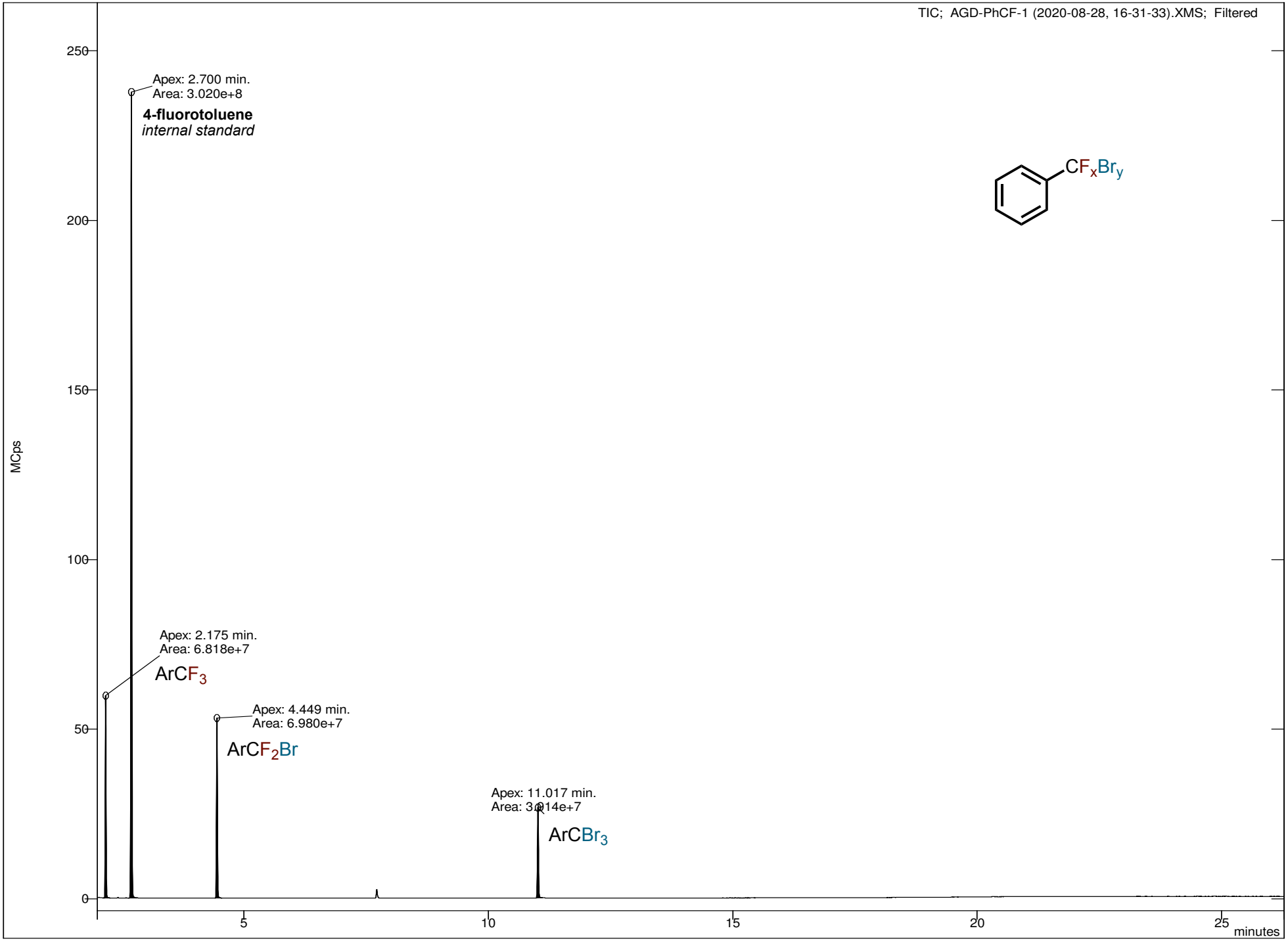

Figure S21: Mass spectrum for peak at 2.2 minutes (compound **2b** reaction)

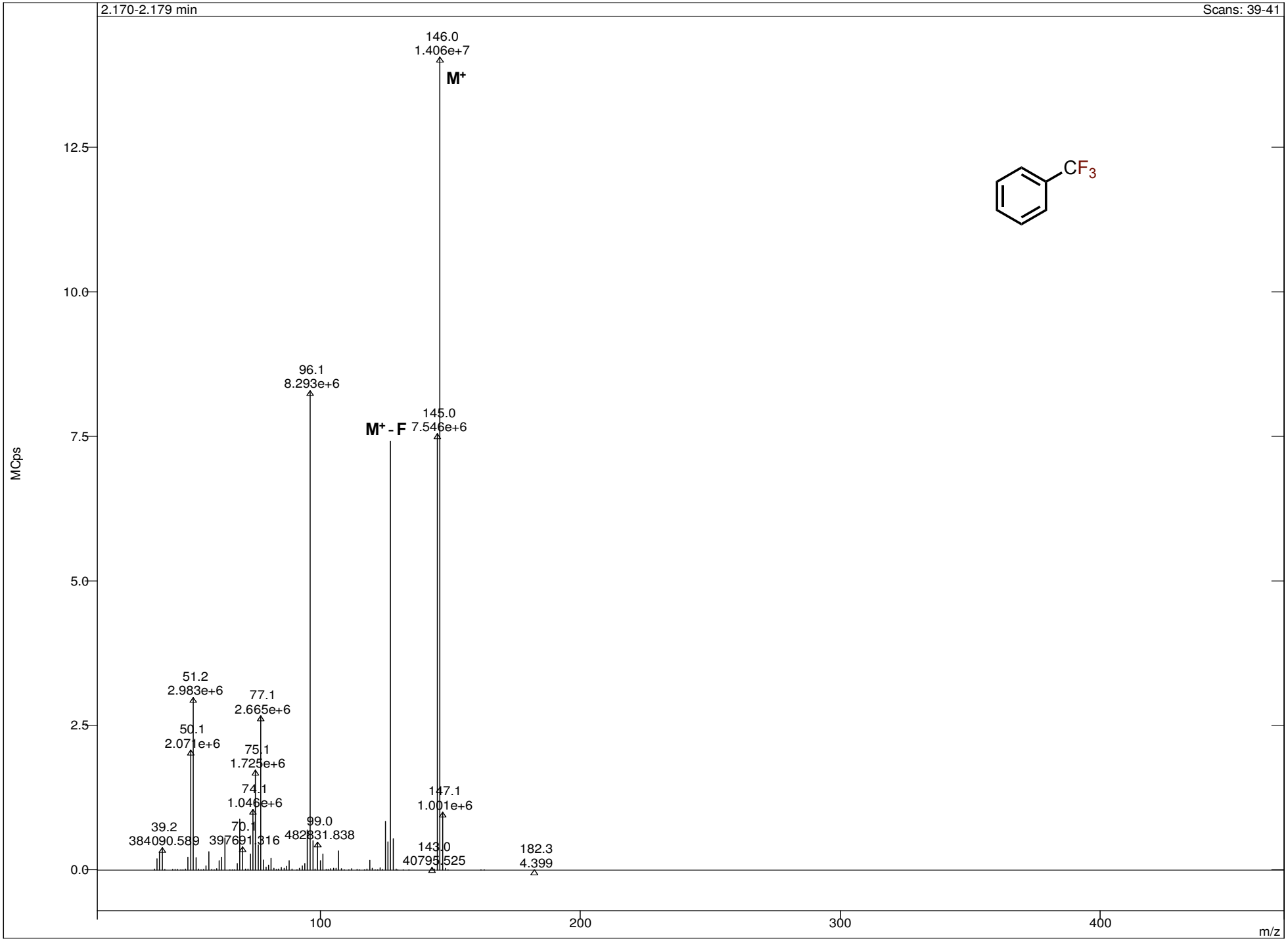

Figure S22: Mass spectrum for peak at 4.5 minutes (compound **2b** reaction)

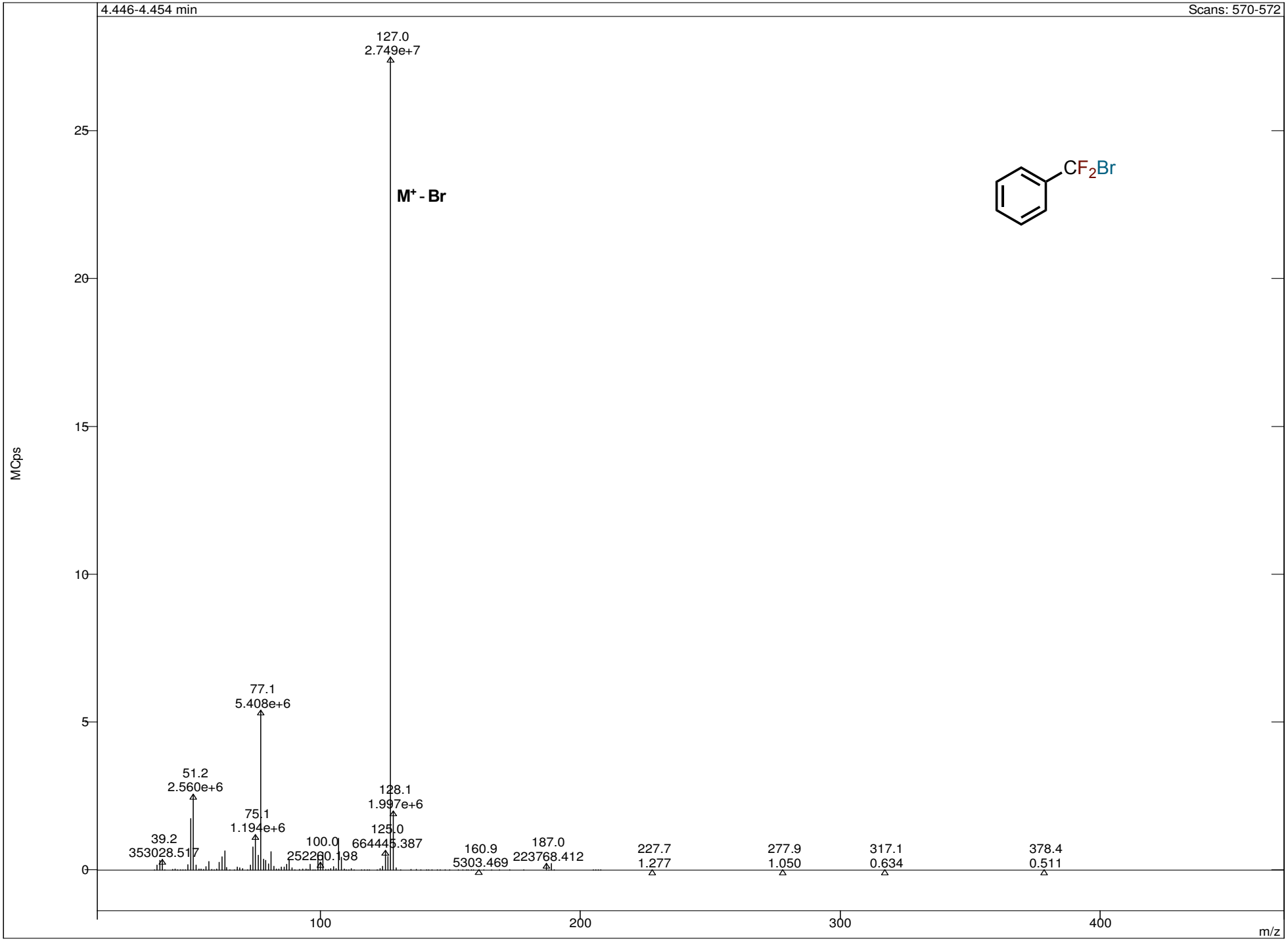

Figure S23: Mass spectrum for peak at 11.0 minutes (compound **2b** reaction)

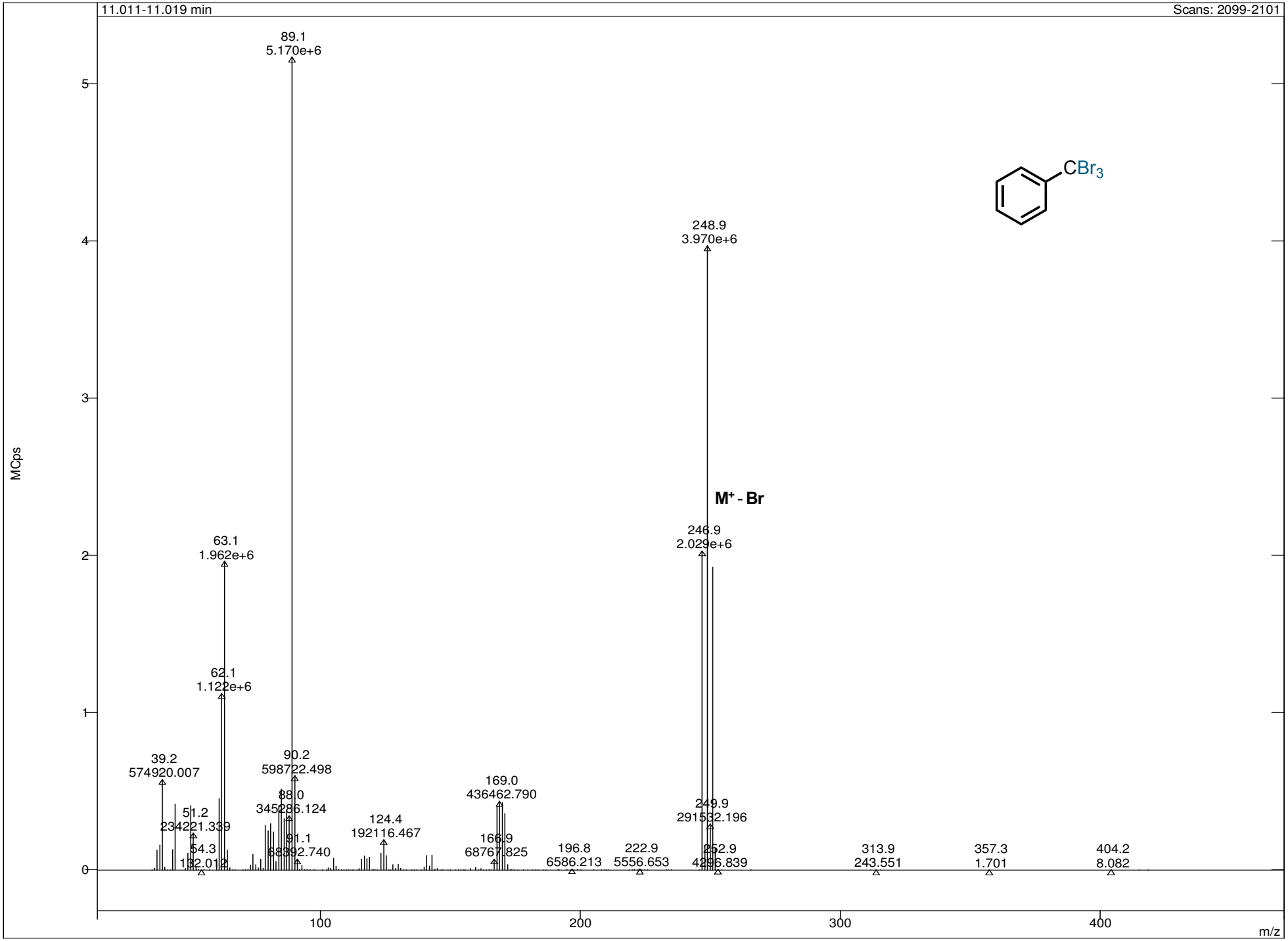

Figure S24: GCMS chromatogram of compound **2c** reaction

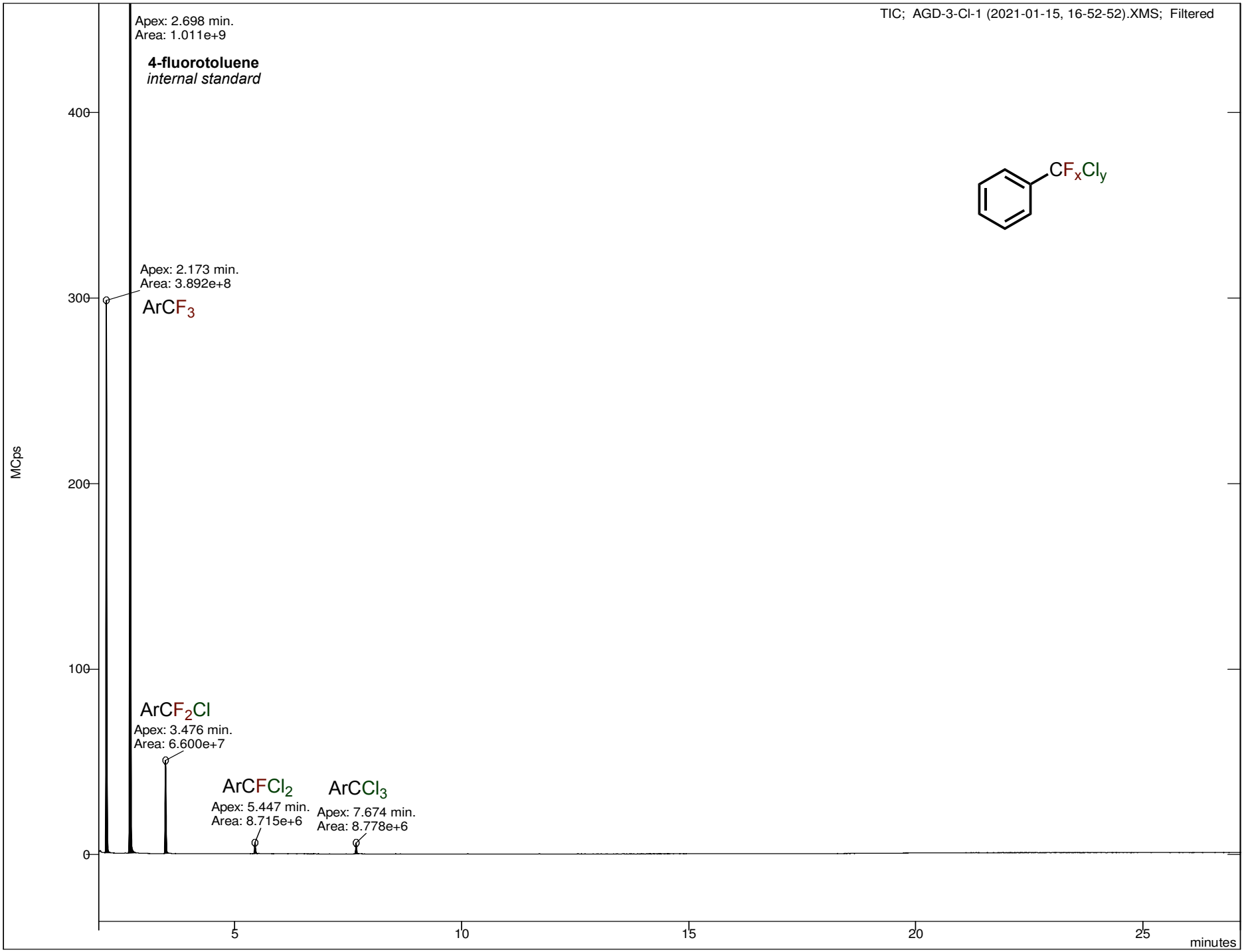

Figure S25: Mass spectrum for peak at 2.2 minutes (compound **2c** reaction)

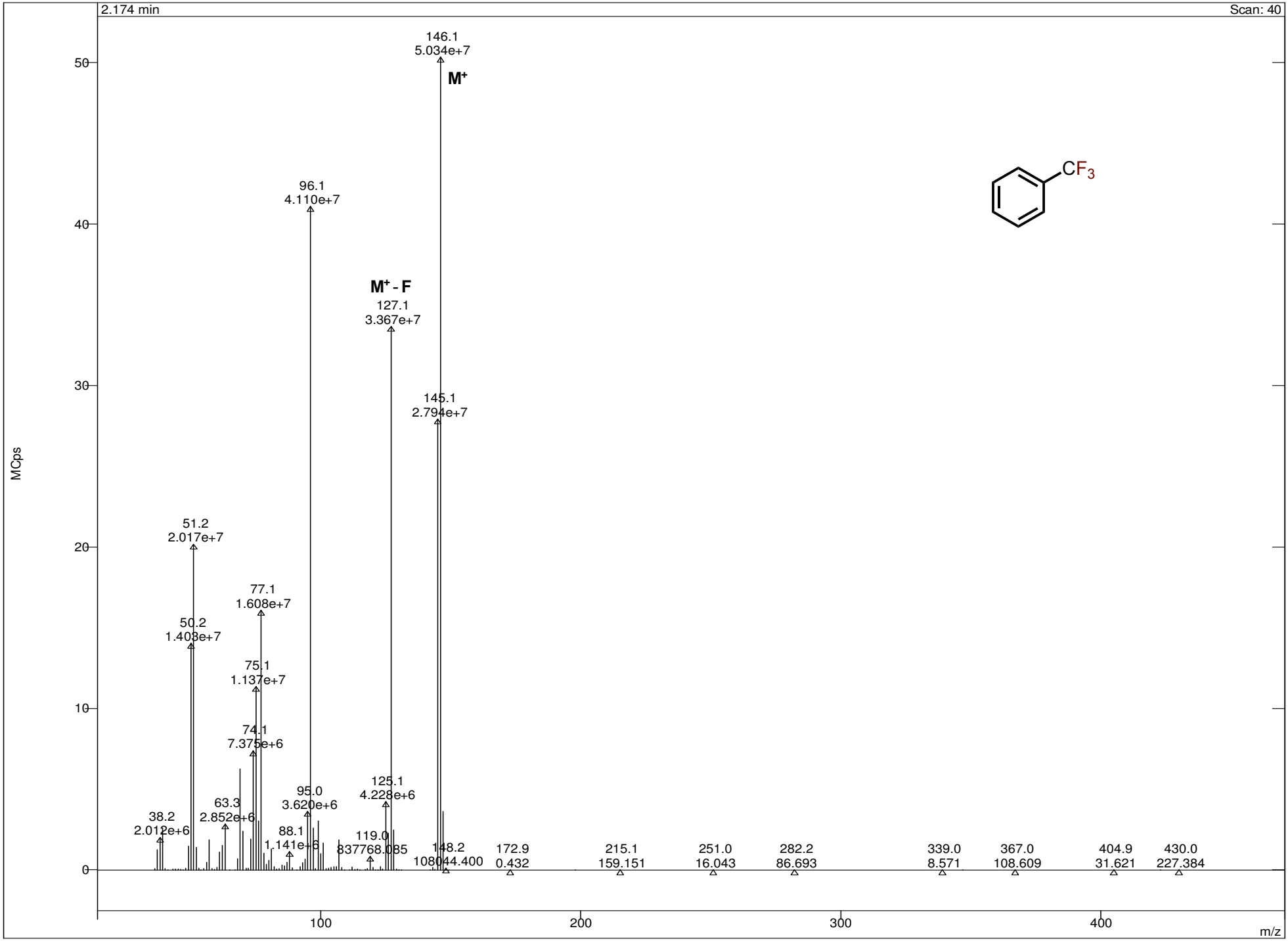

Figure S26: Mass spectrum for peak at 3.5 minutes (compound **2c** reaction)

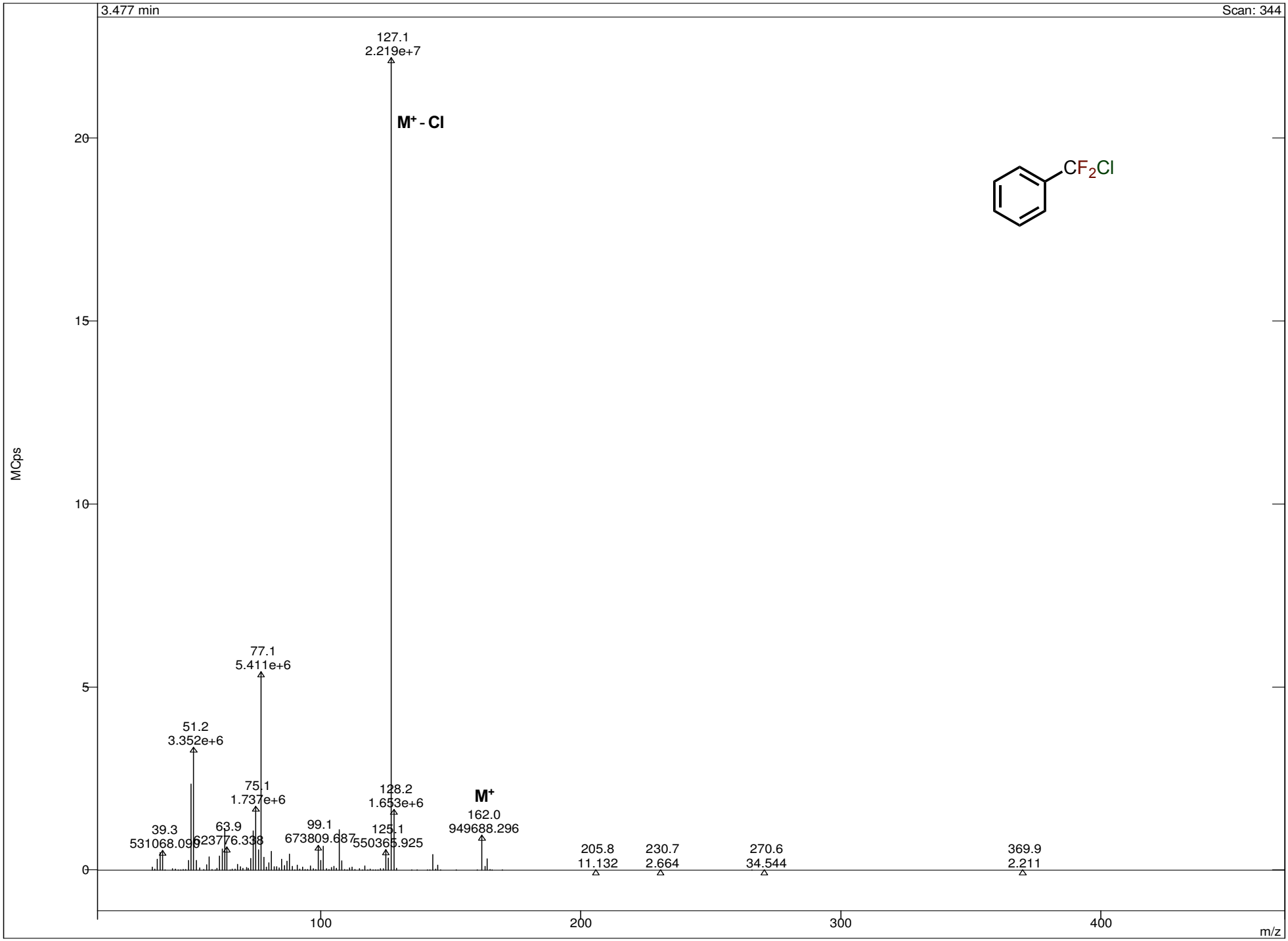

Figure S27: Mass spectrum for peak at 5.5 minutes (compound **2c** reaction)

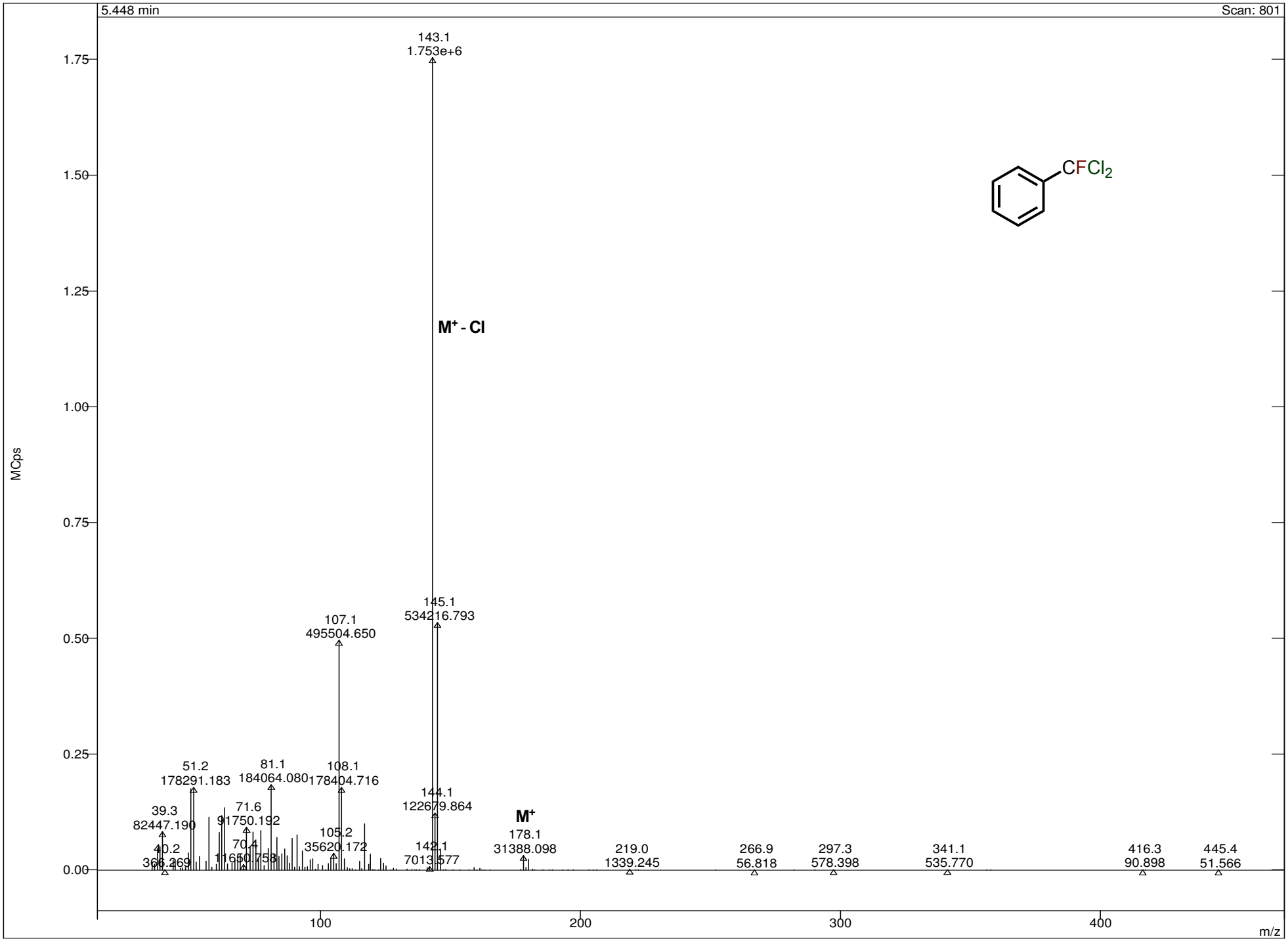

Figure S28: Mass spectrum for peak at 7.7 minutes (compound **2c** reaction)

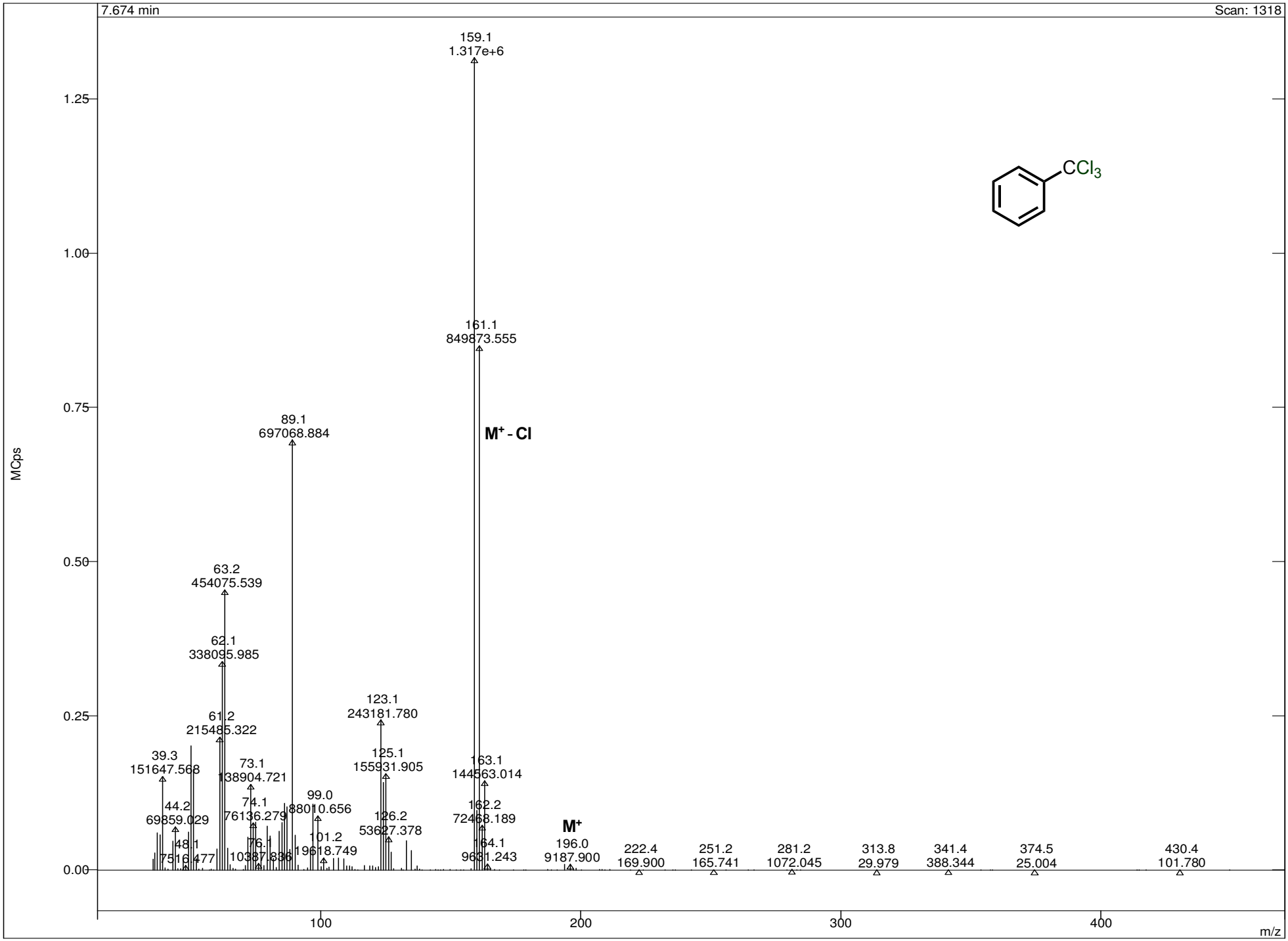

Figure S29: GCMS chromatogram of compound **2d** reaction

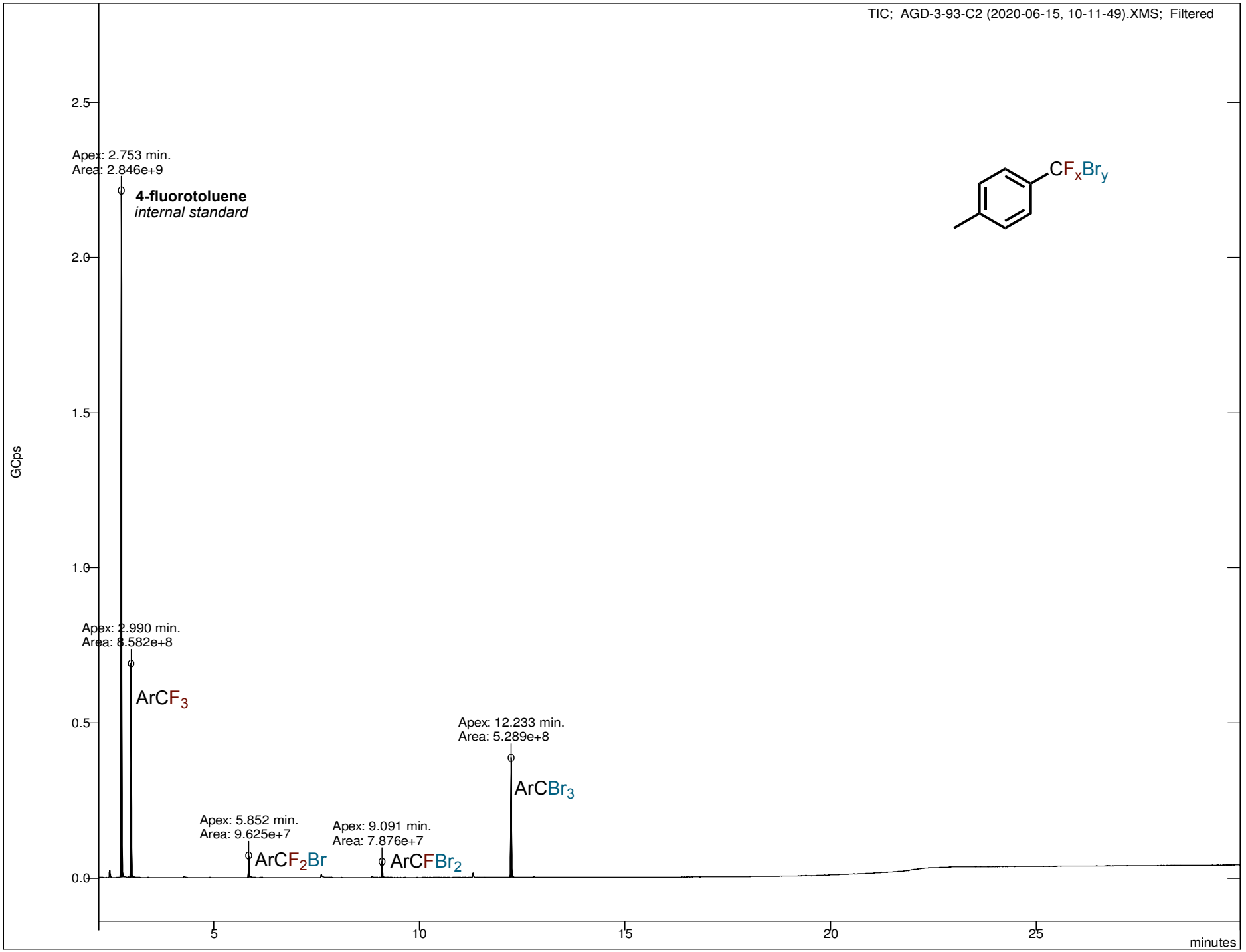

Figure S30: Mass spectrum for peak at 3.0 minutes (compound **2d** reaction)

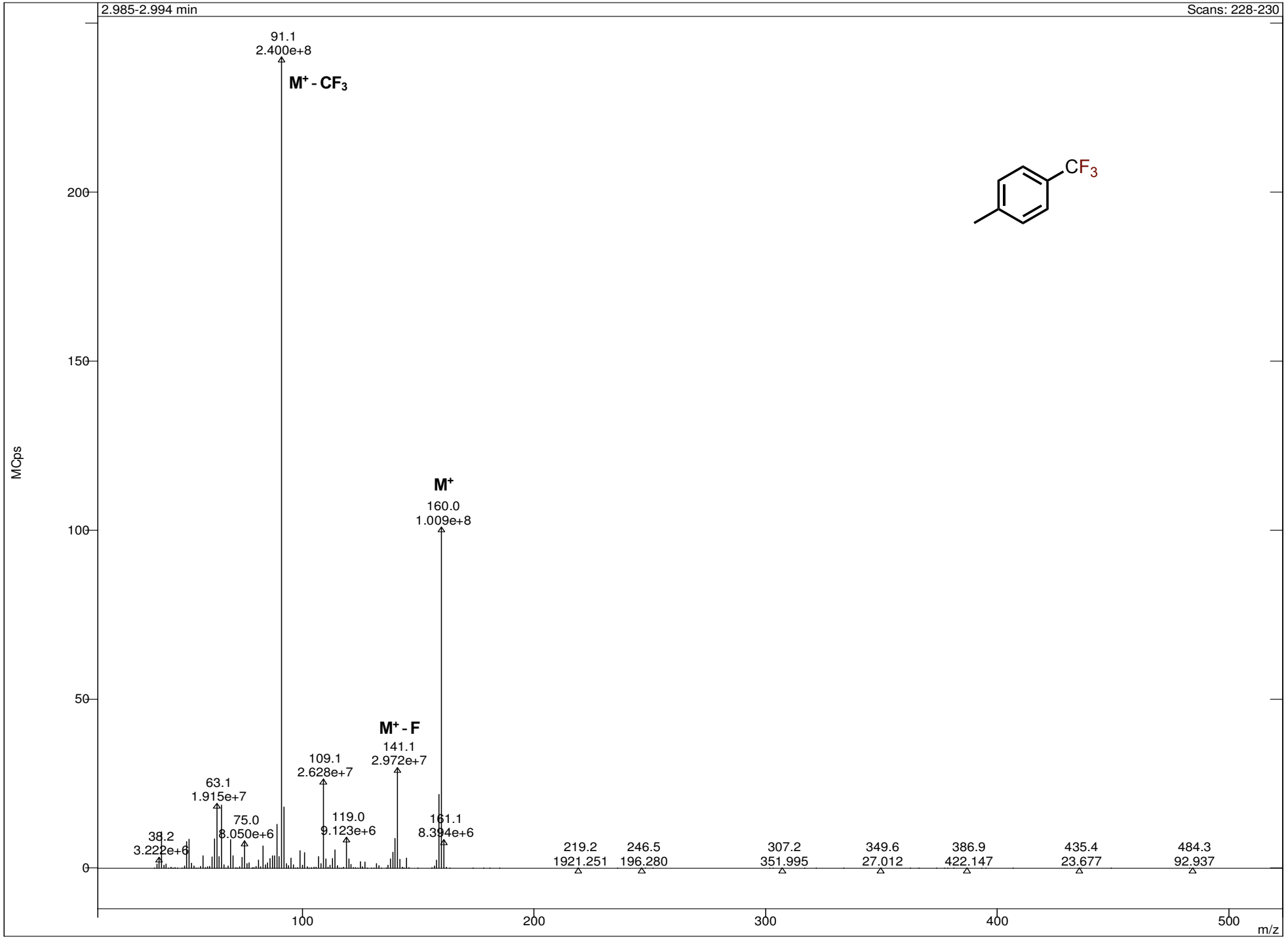

Figure S31: Mass spectrum for peak at 5.9 minutes (compound **2d** reaction)

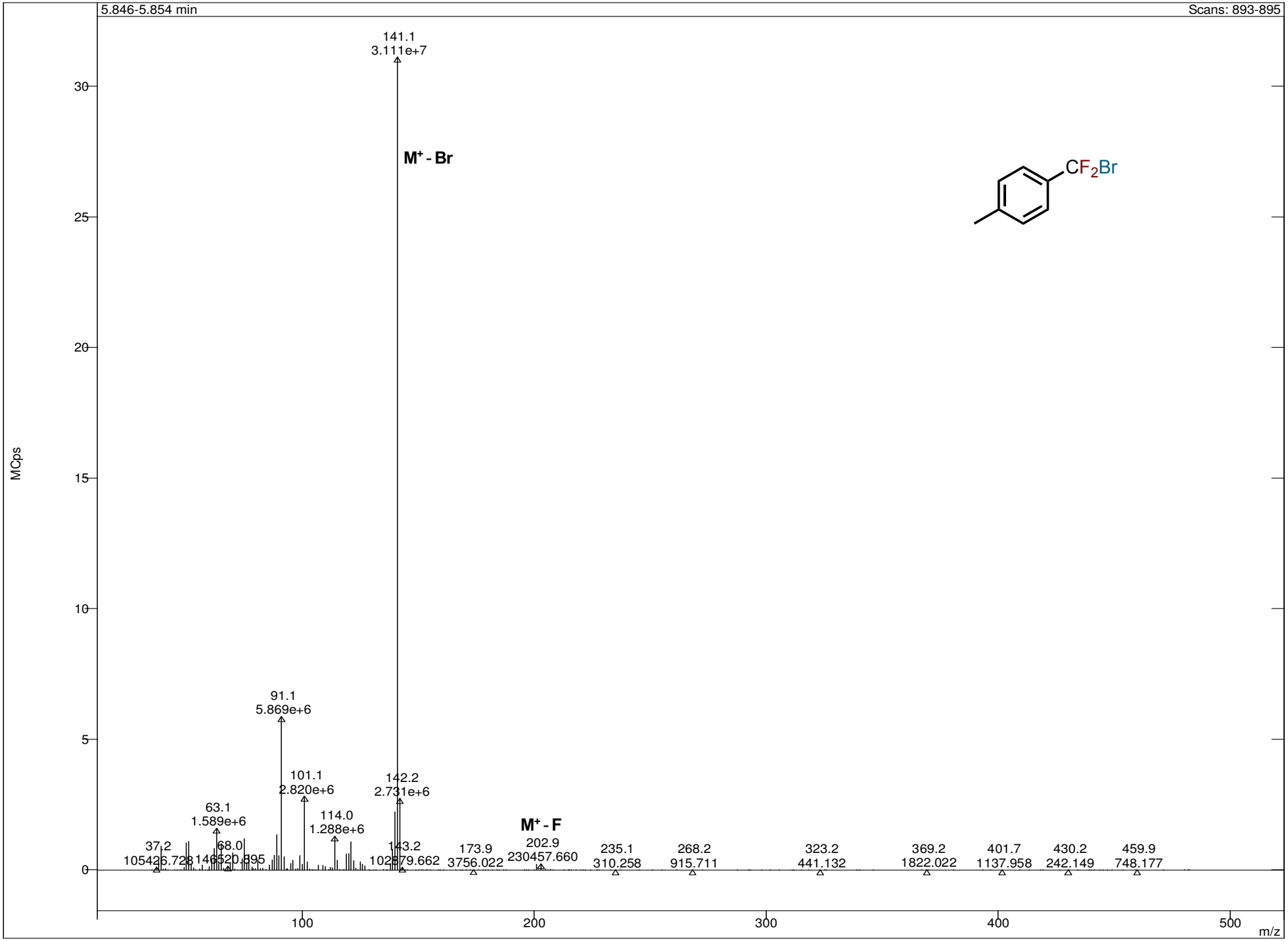

Figure S32: Mass spectrum for peak at 9.1 minutes (compound **2d** reaction)

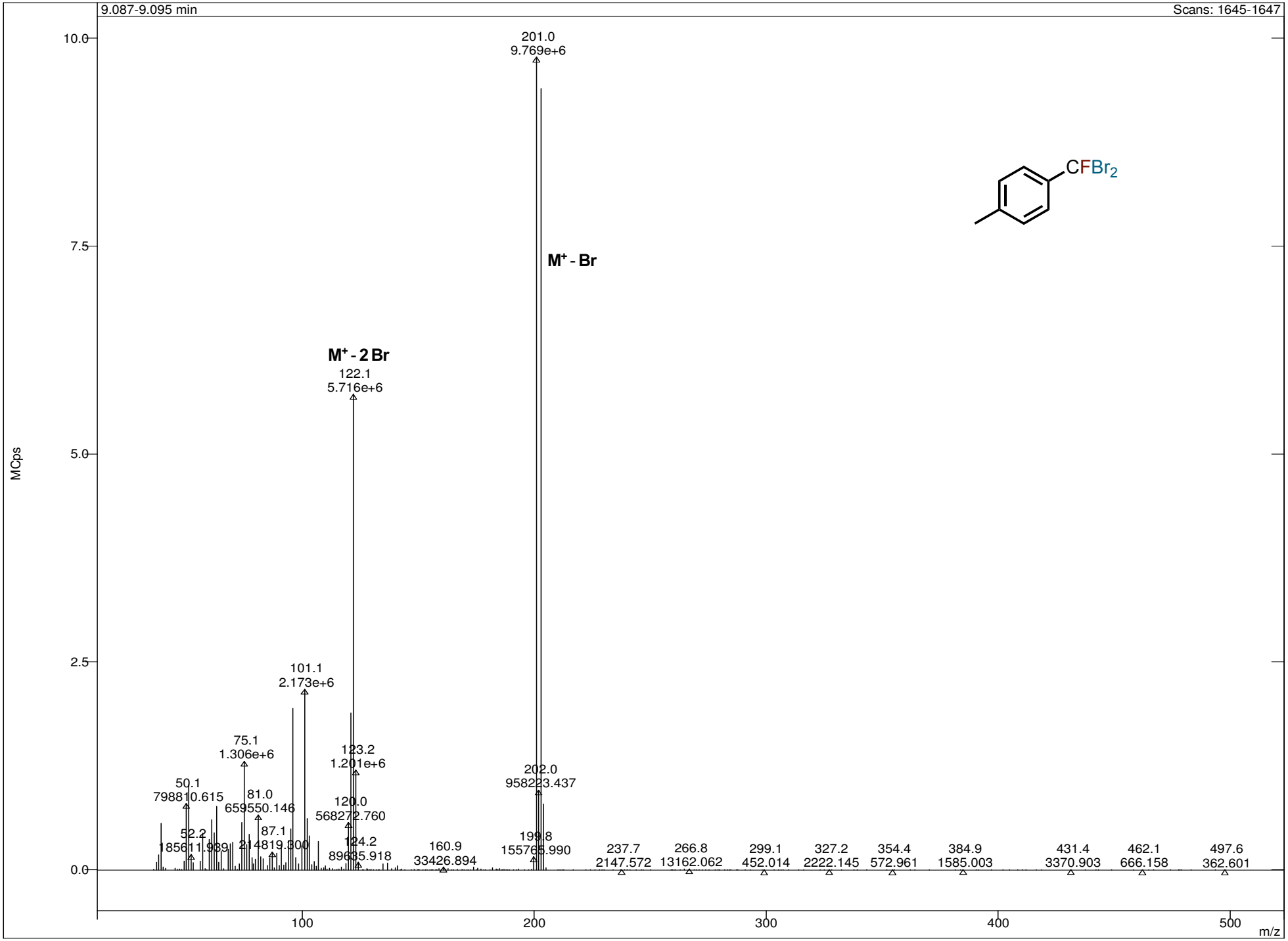

Figure S33: Mass spectrum for peak at 12.2 minutes (compound **2d** reaction)

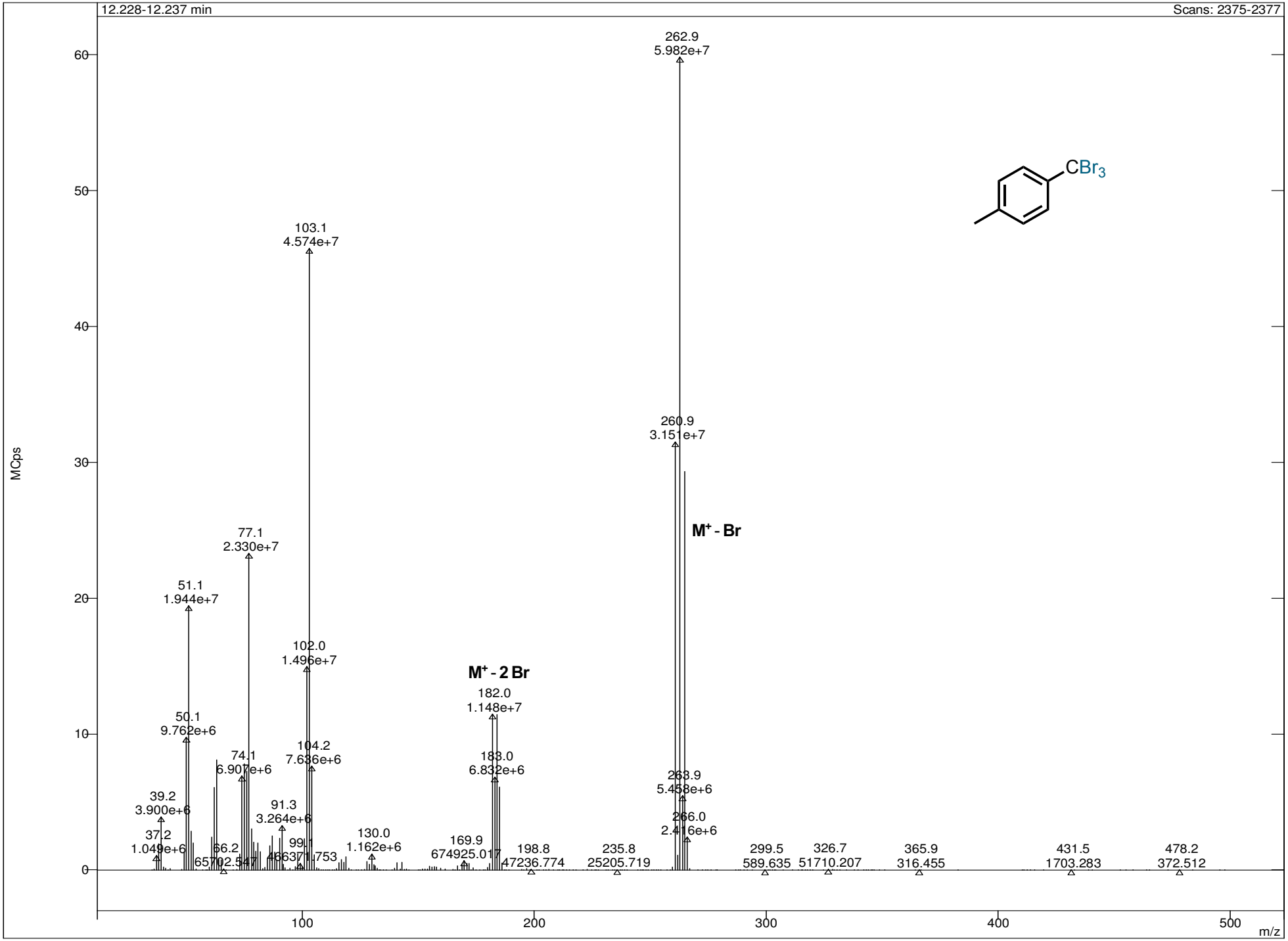

Figure S34: GCMS chromatogram of compound **2e** reaction

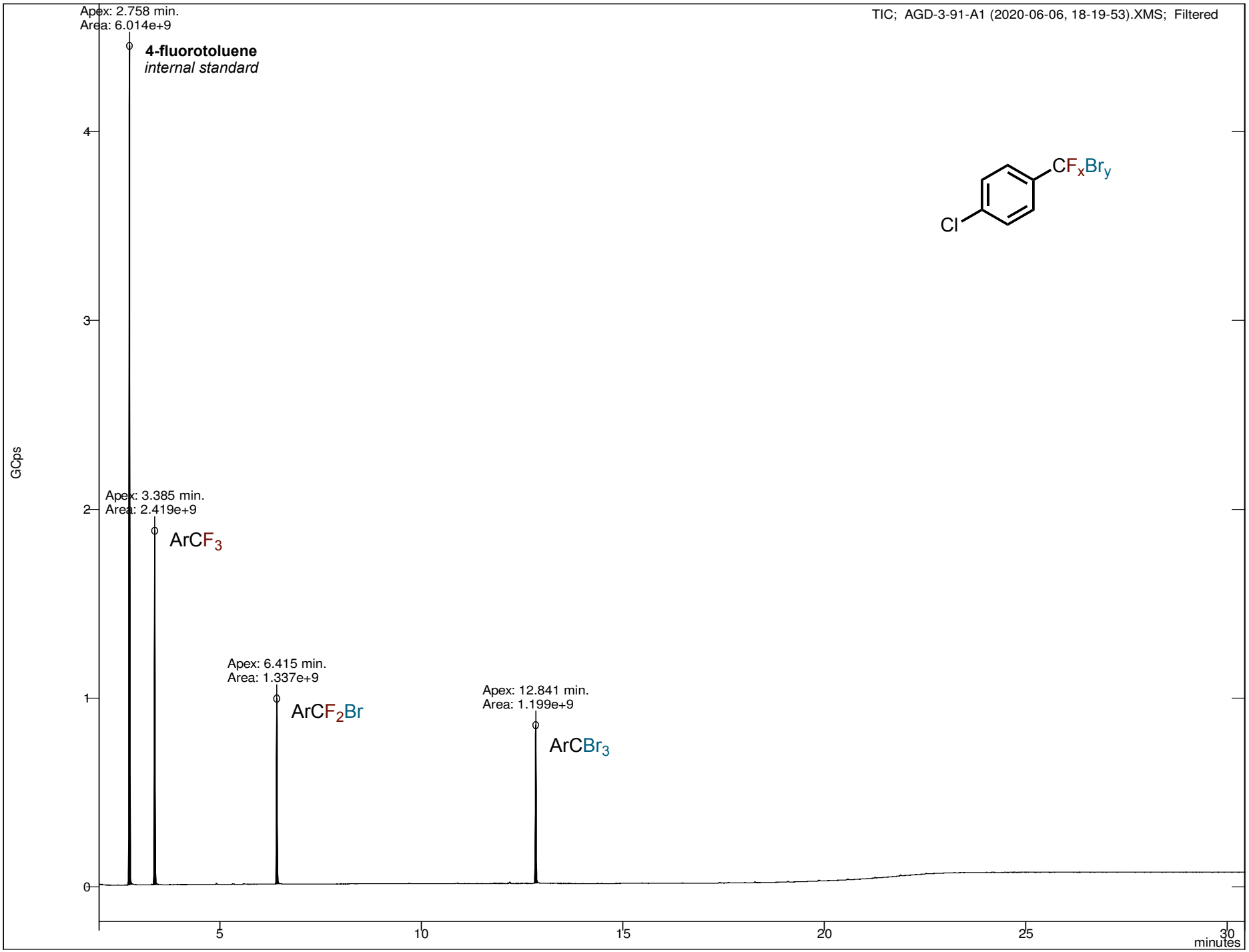

Figure S35: Mass spectrum for peak at 3.4 minutes (compound **2e** reaction)

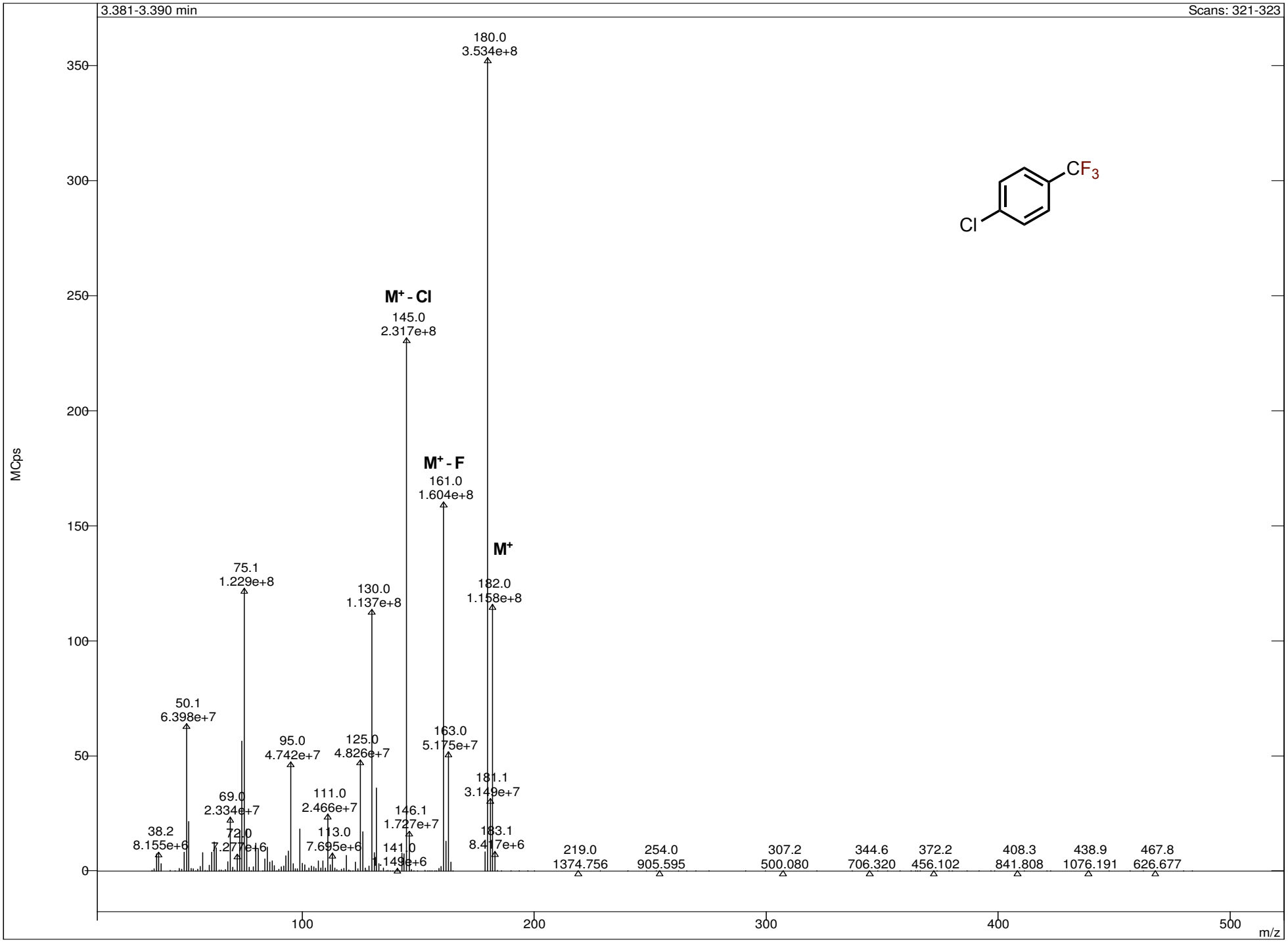

Figure S36: Mass spectrum for peak at 6.4 minutes (compound **2e** reaction)

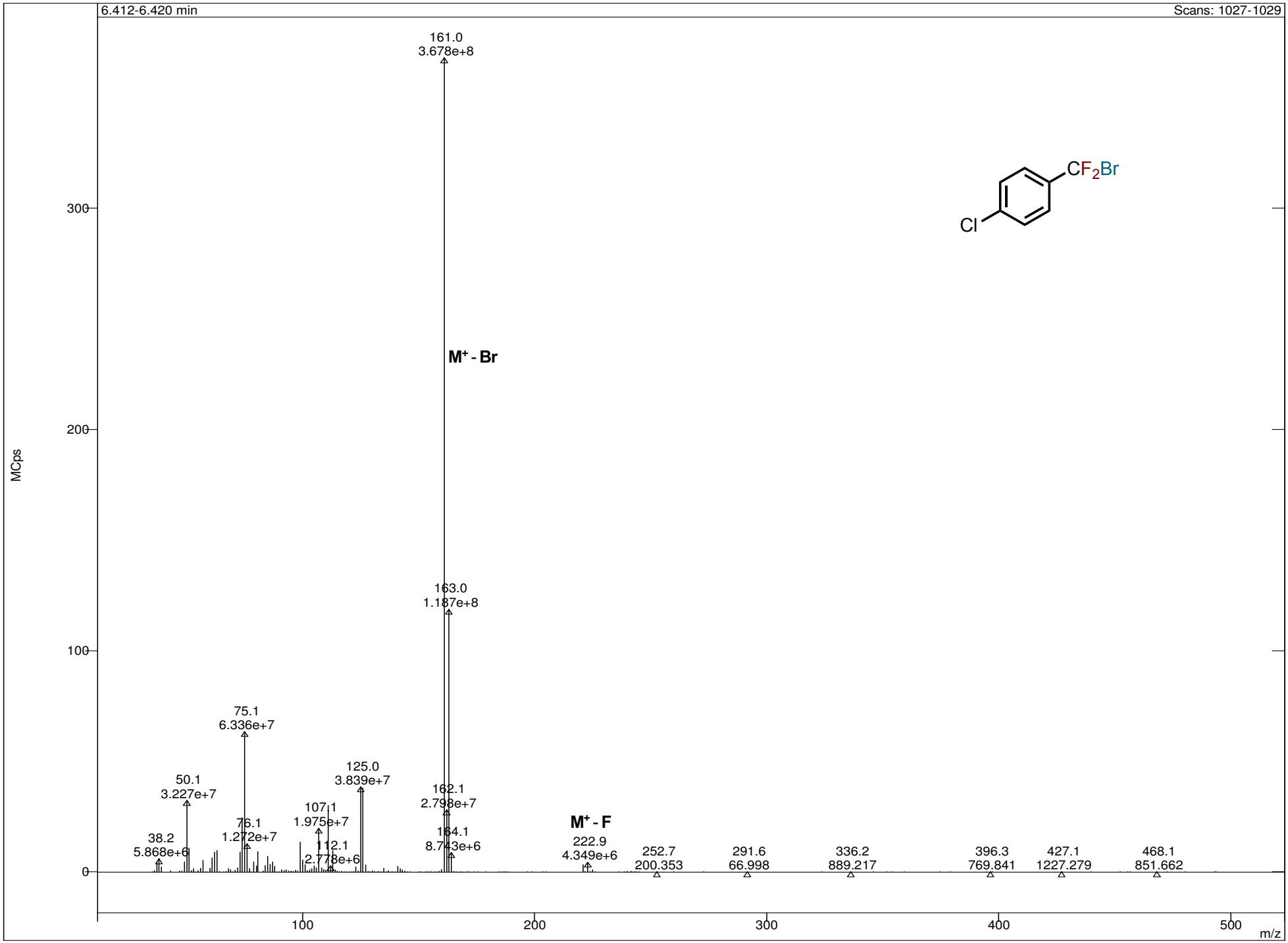

Figure S37: Mass spectrum for peak at 12.8 minutes (compound **2e** reaction)

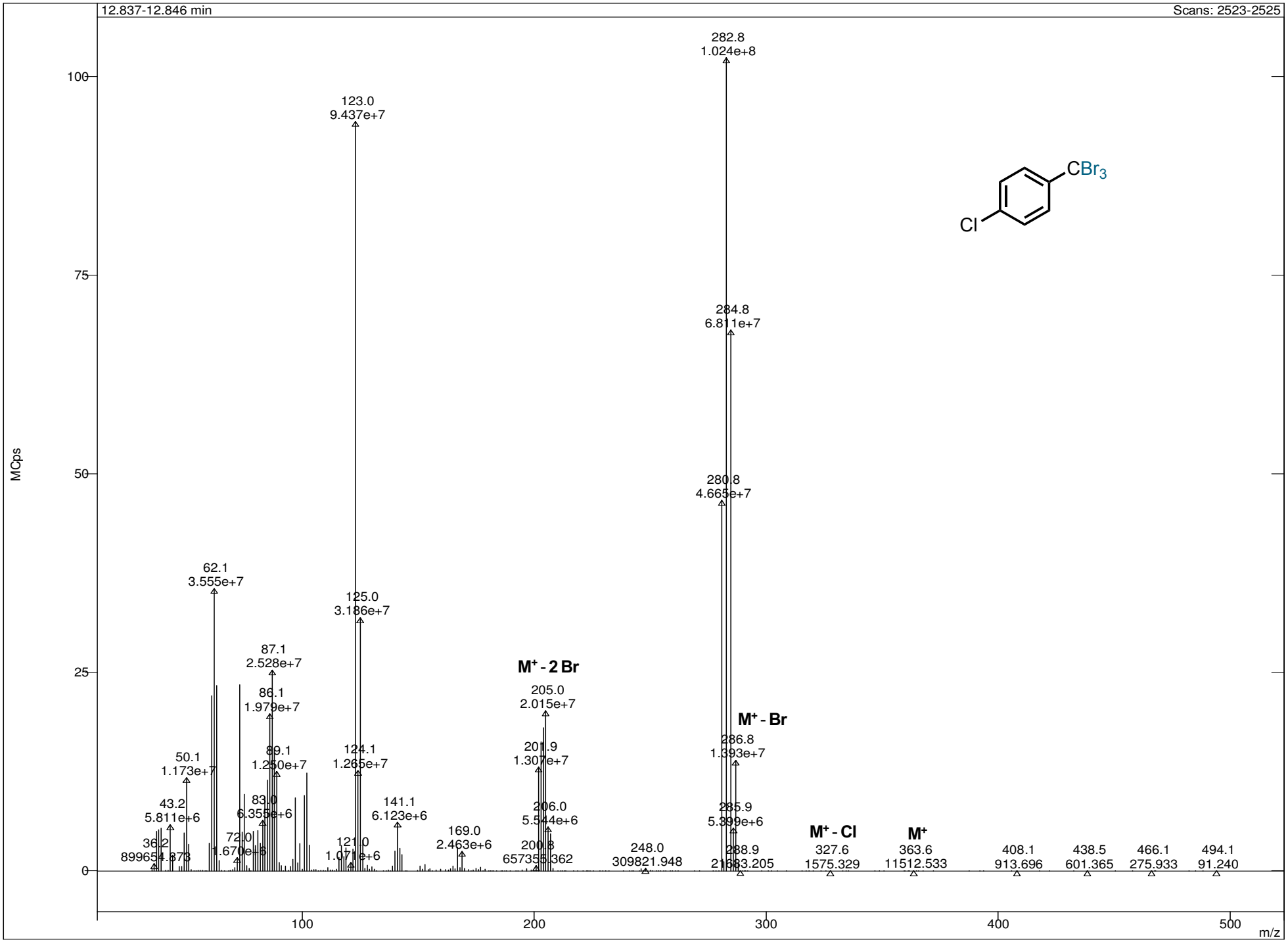

Figure S38: GCMS chromatogram of compound **2f** reaction

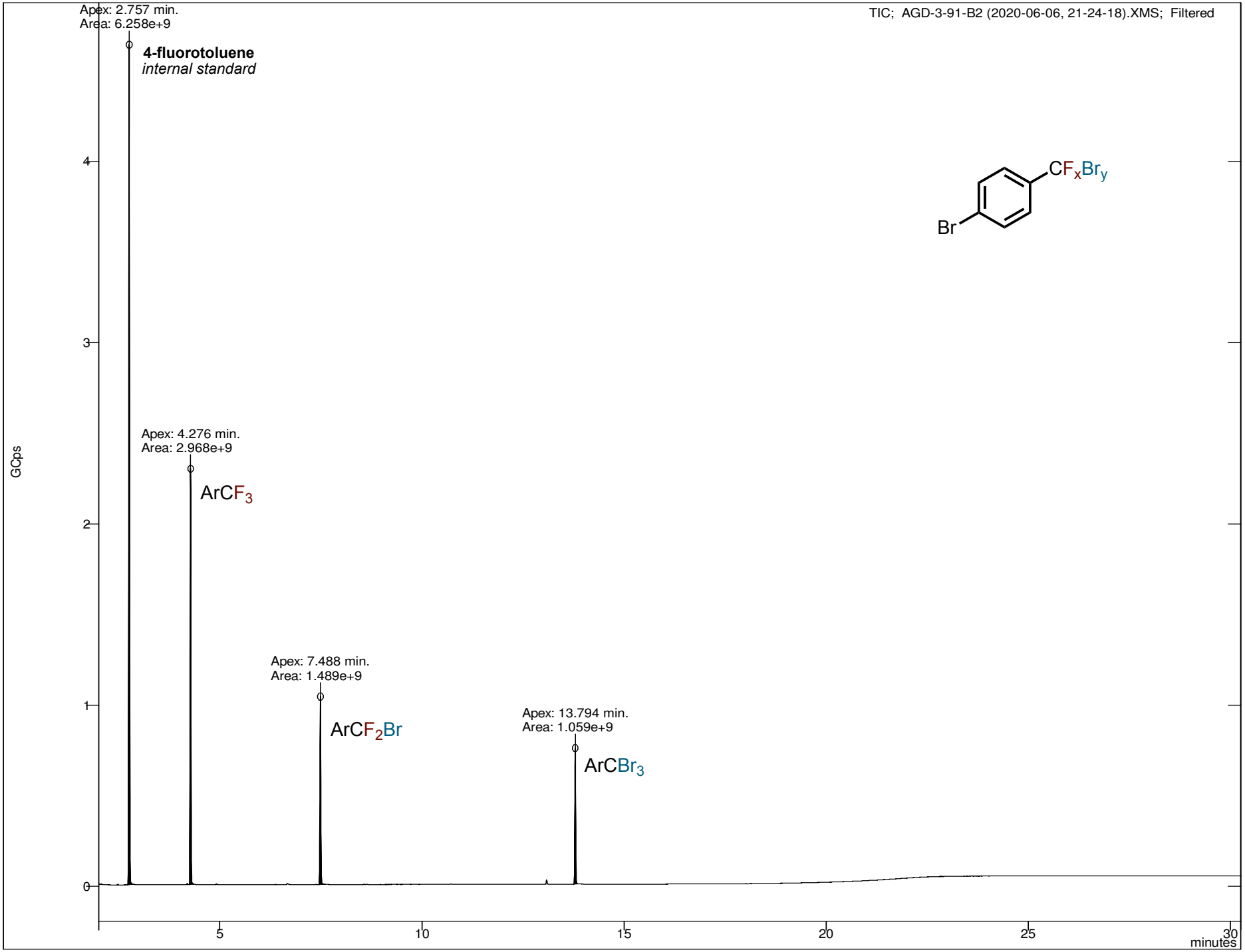

Figure S39: Mass spectrum for peak at 4.3 minutes (compound **2f** reaction)

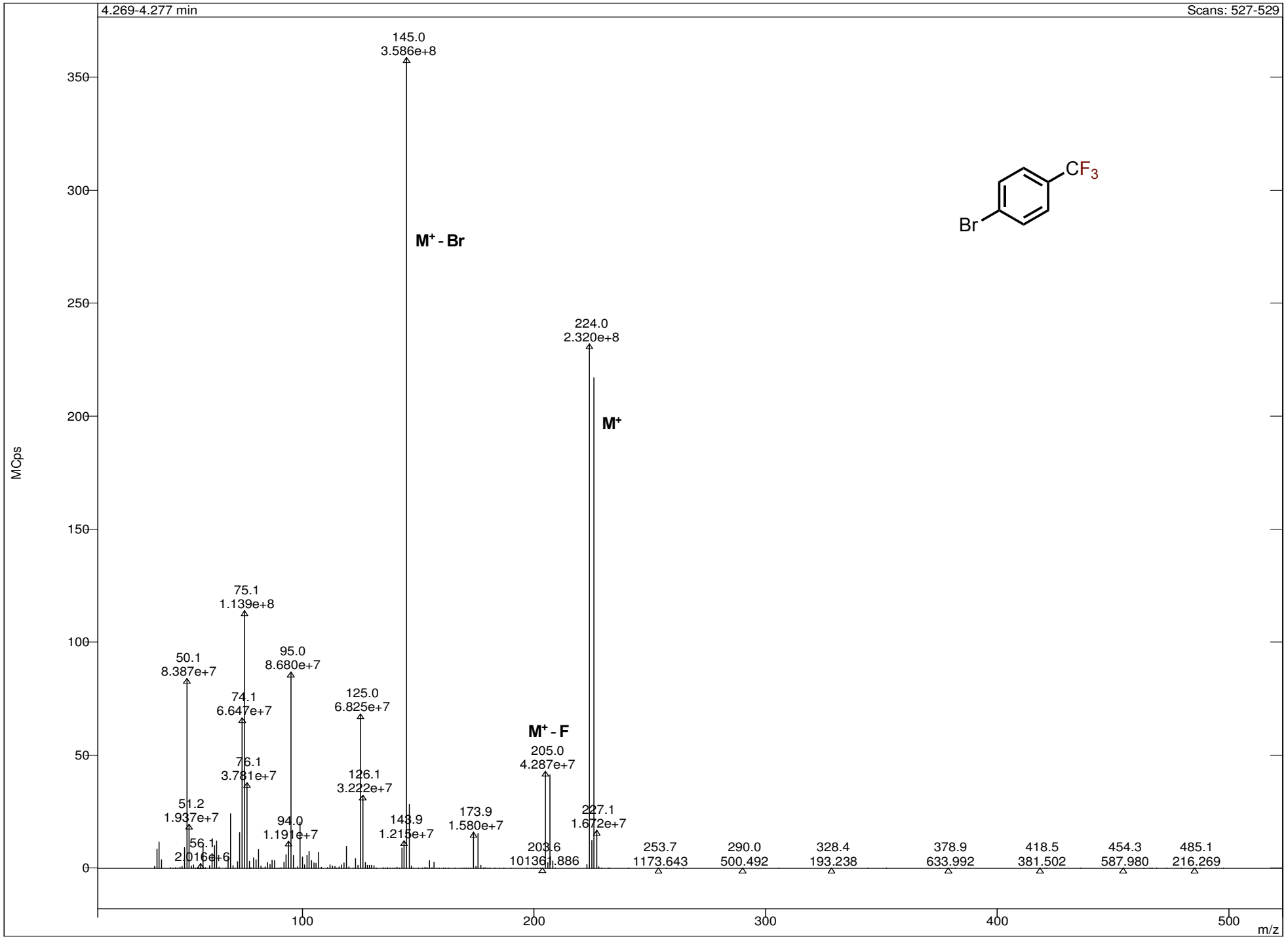

Figure S40: Mass spectrum for peak at 7.5 minutes (compound **2f** reaction)

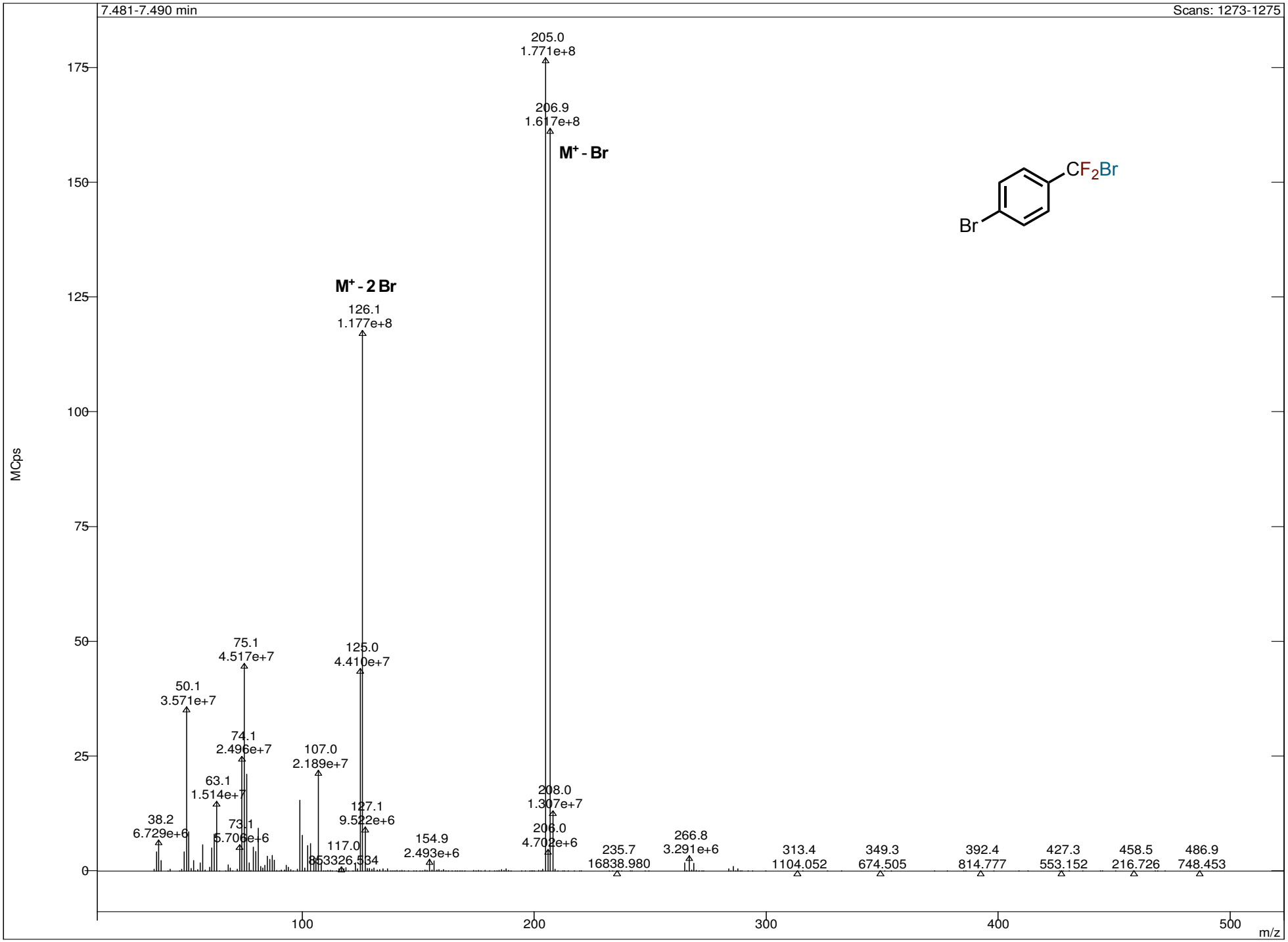

Figure S41: Mass spectrum for peak at 13.8 minutes (compound **2f** reaction)

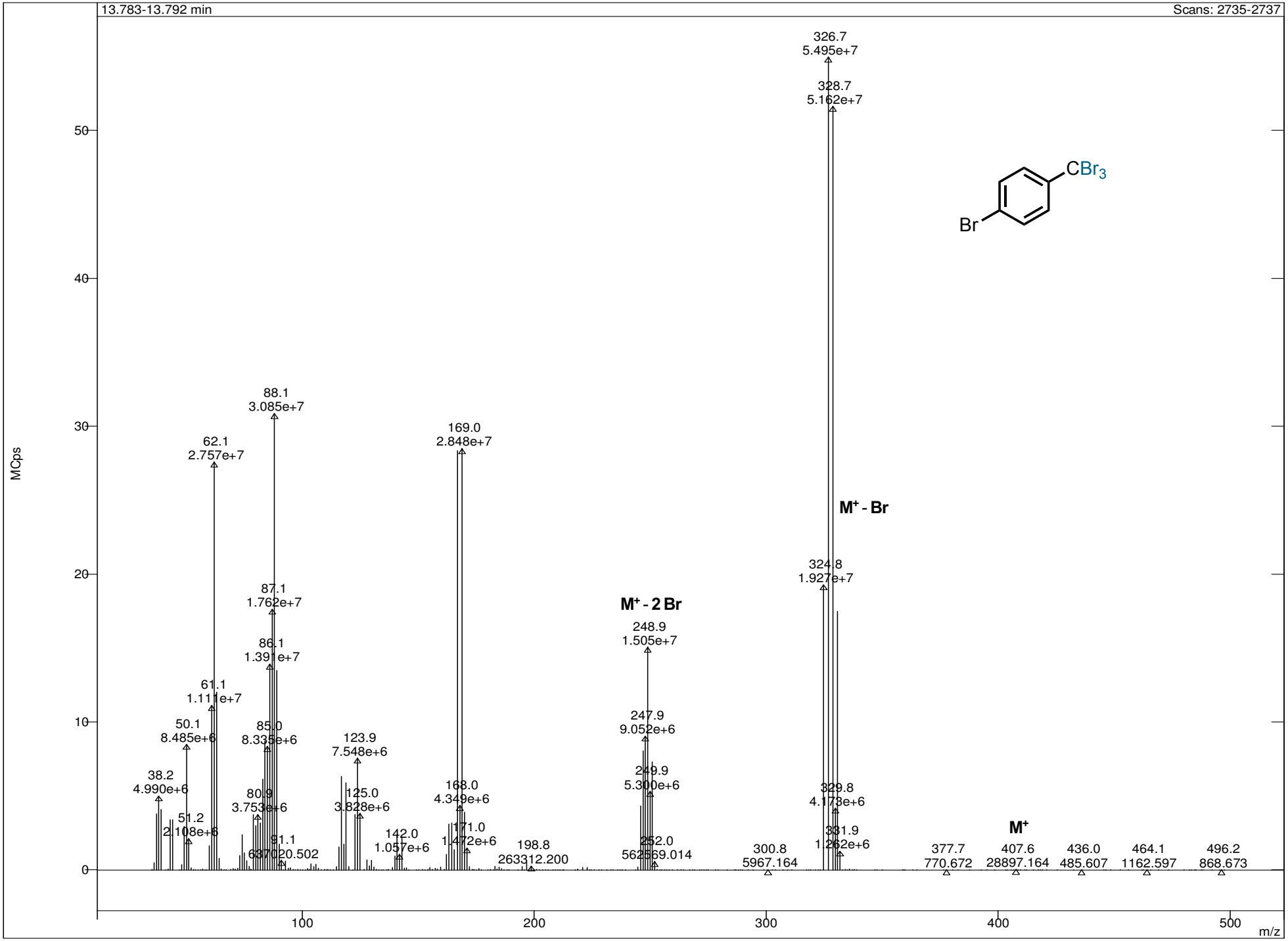

Figure S42: GCMS chromatogram of compound **2h** reaction

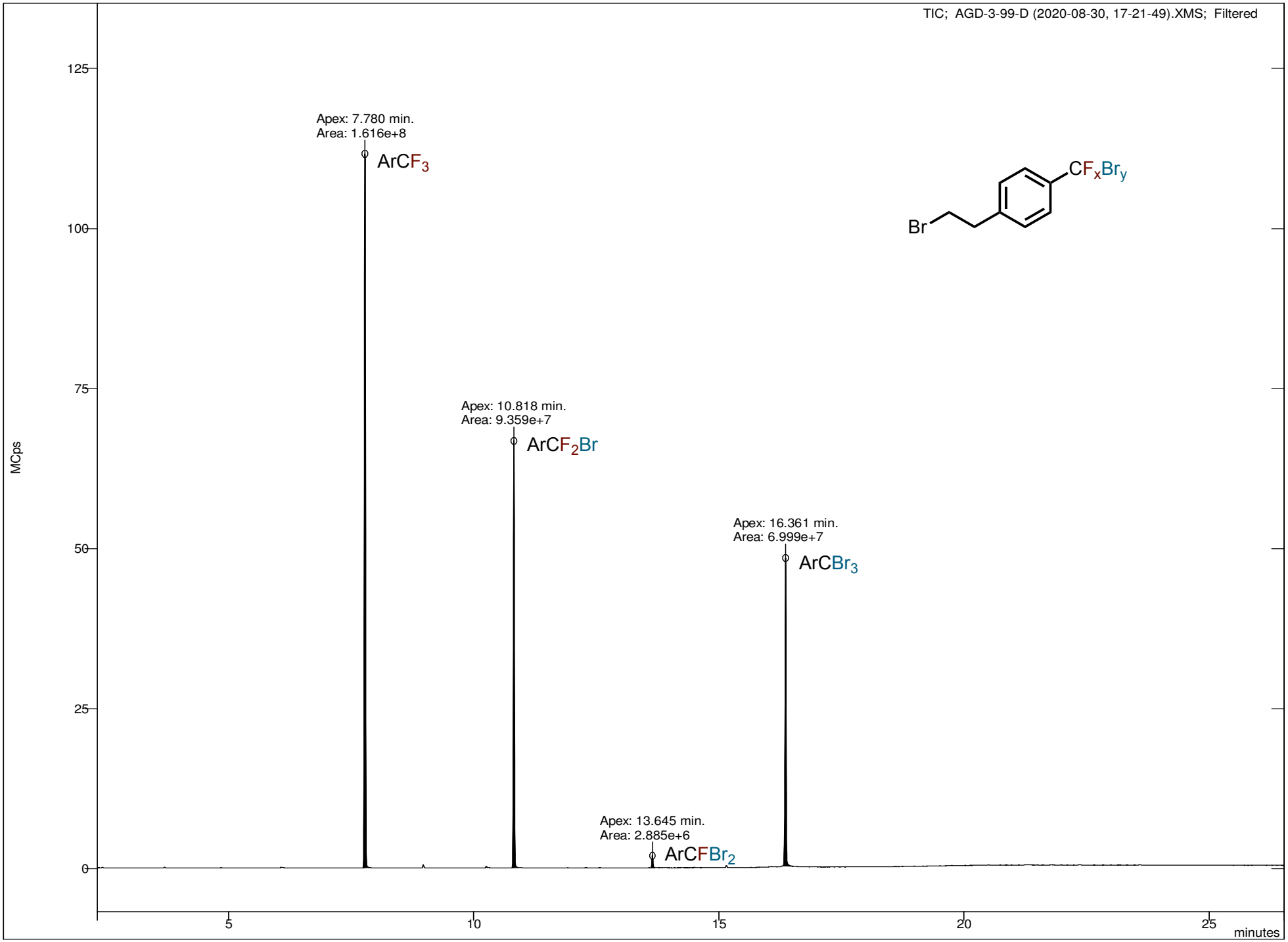

Figure S43: ^{19}F NMR spectrum of compound **2a** reaction ($CDCl_3$, 376.3 MHz)

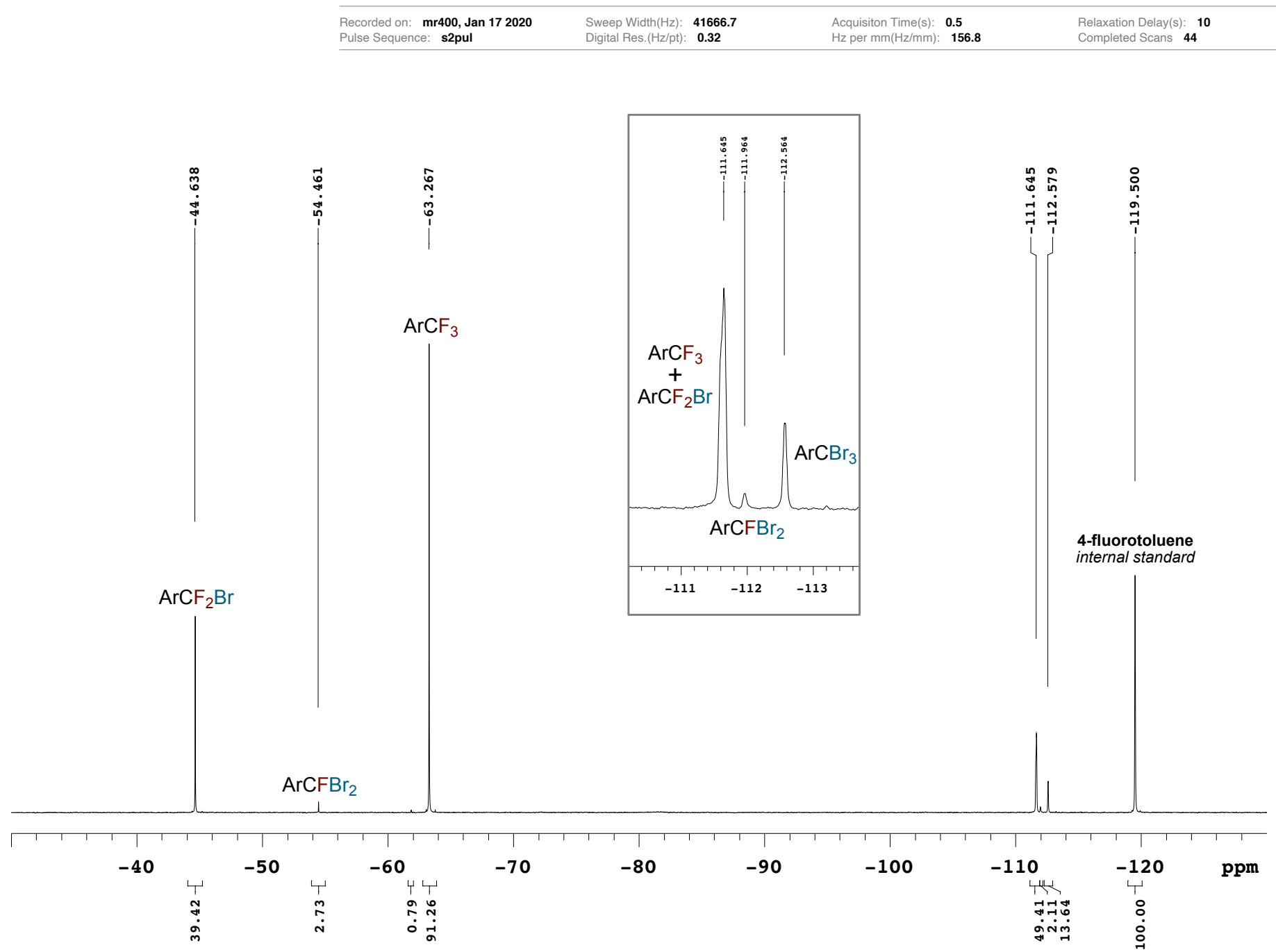

Figure S44: ^{19}F NMR spectrum of compound **2b** reaction I ($CDCl_3$, 376.3 MHz)

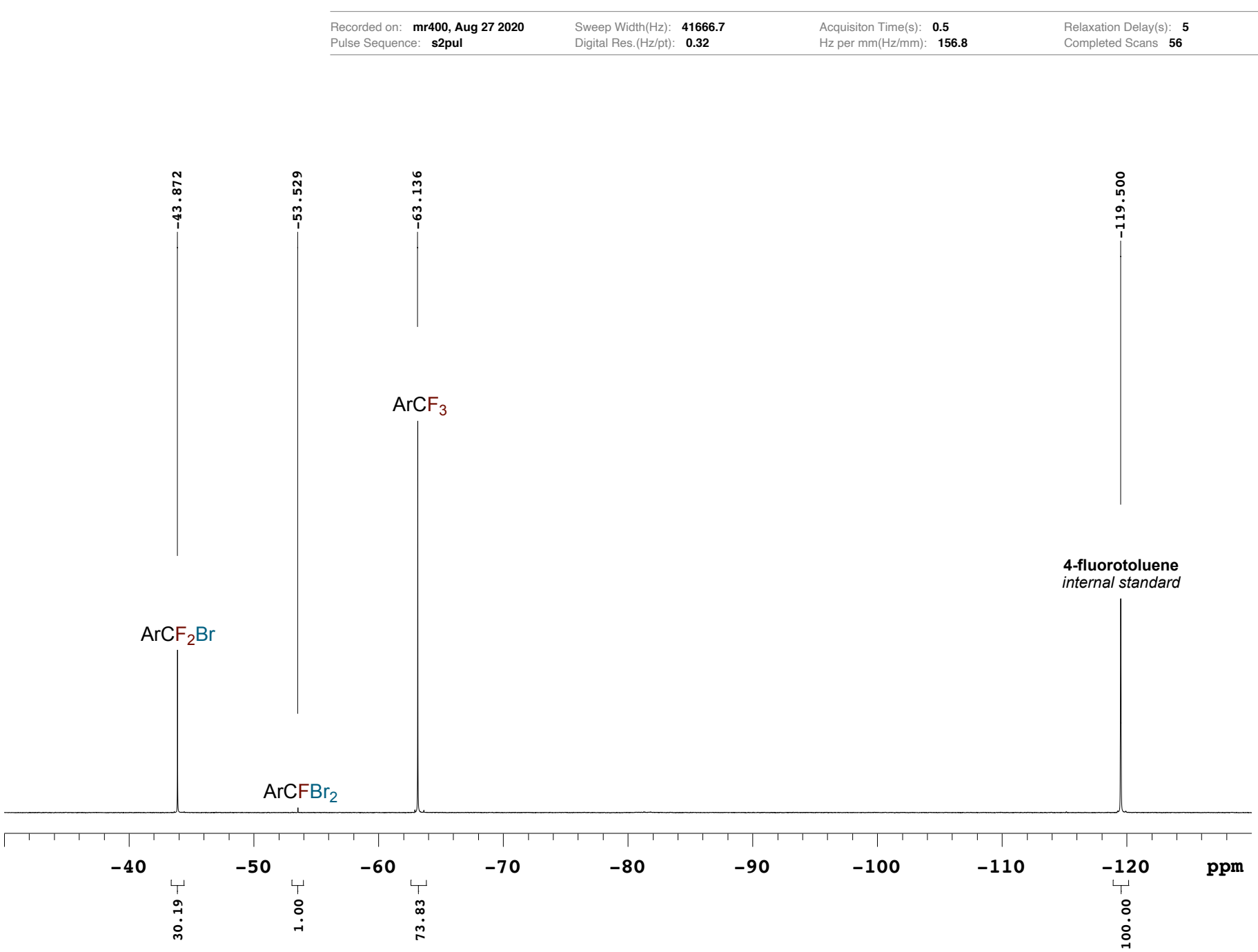

Figure S45: ^{19}F NMR spectrum of compound **2b** reaction II ($CDCl_3$, 376.3 MHz)

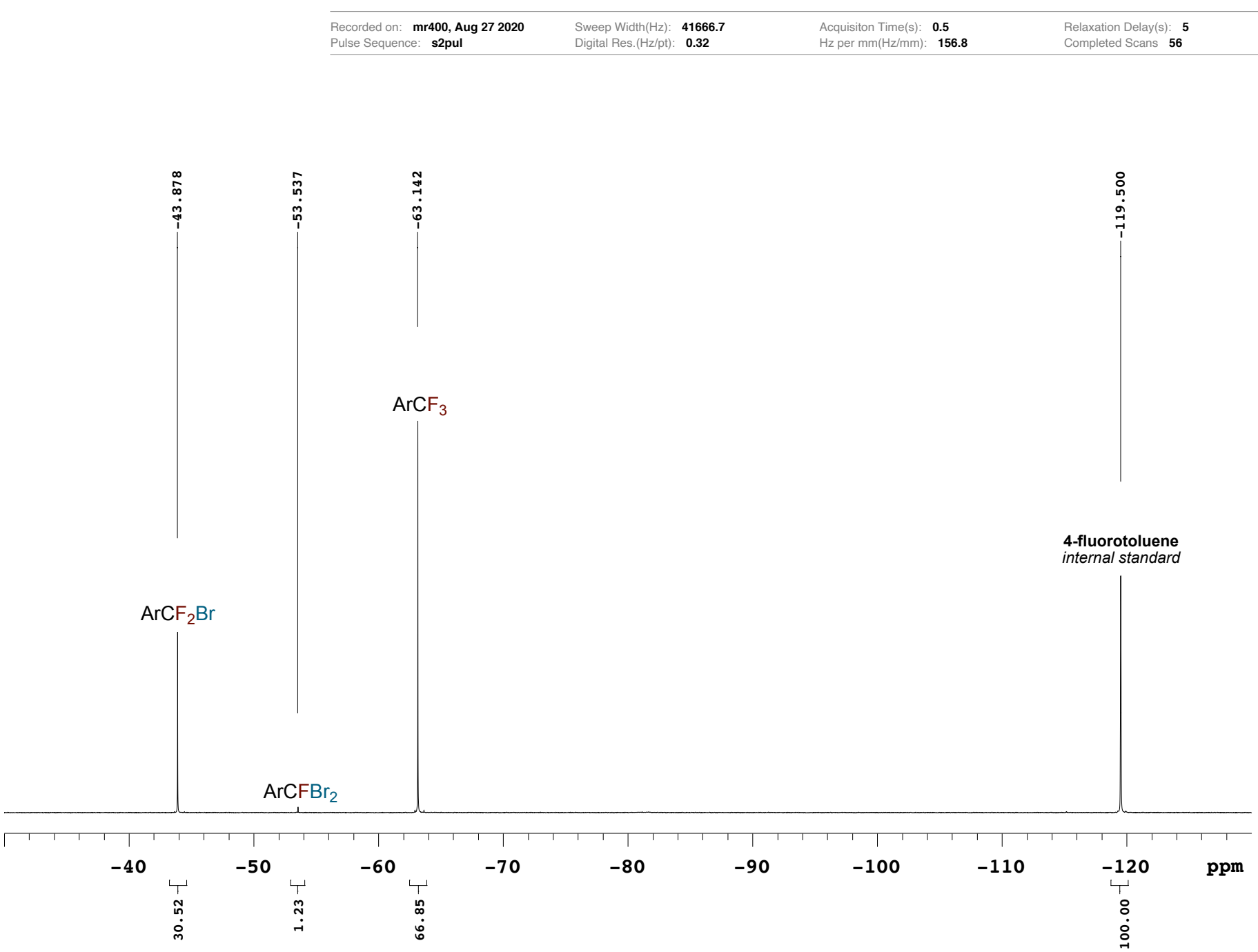

Figure S46: ^{19}F NMR spectrum of compound **2c** reaction ($CDCl_3$, 376.3 MHz)

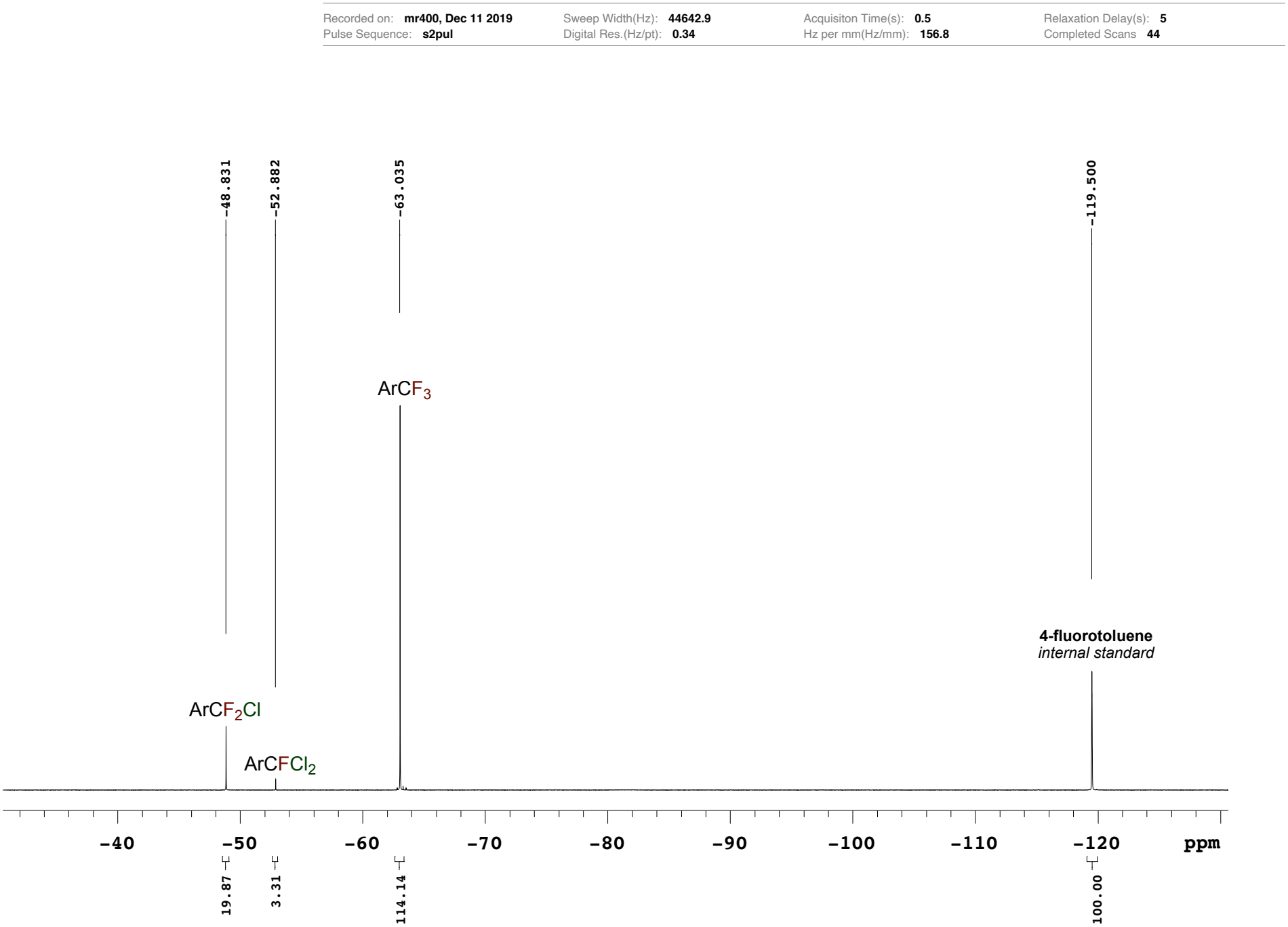

Figure S47: ^{19}F NMR spectrum of compound **2d** reaction I ($CDCl_3$, 376.3 MHz)

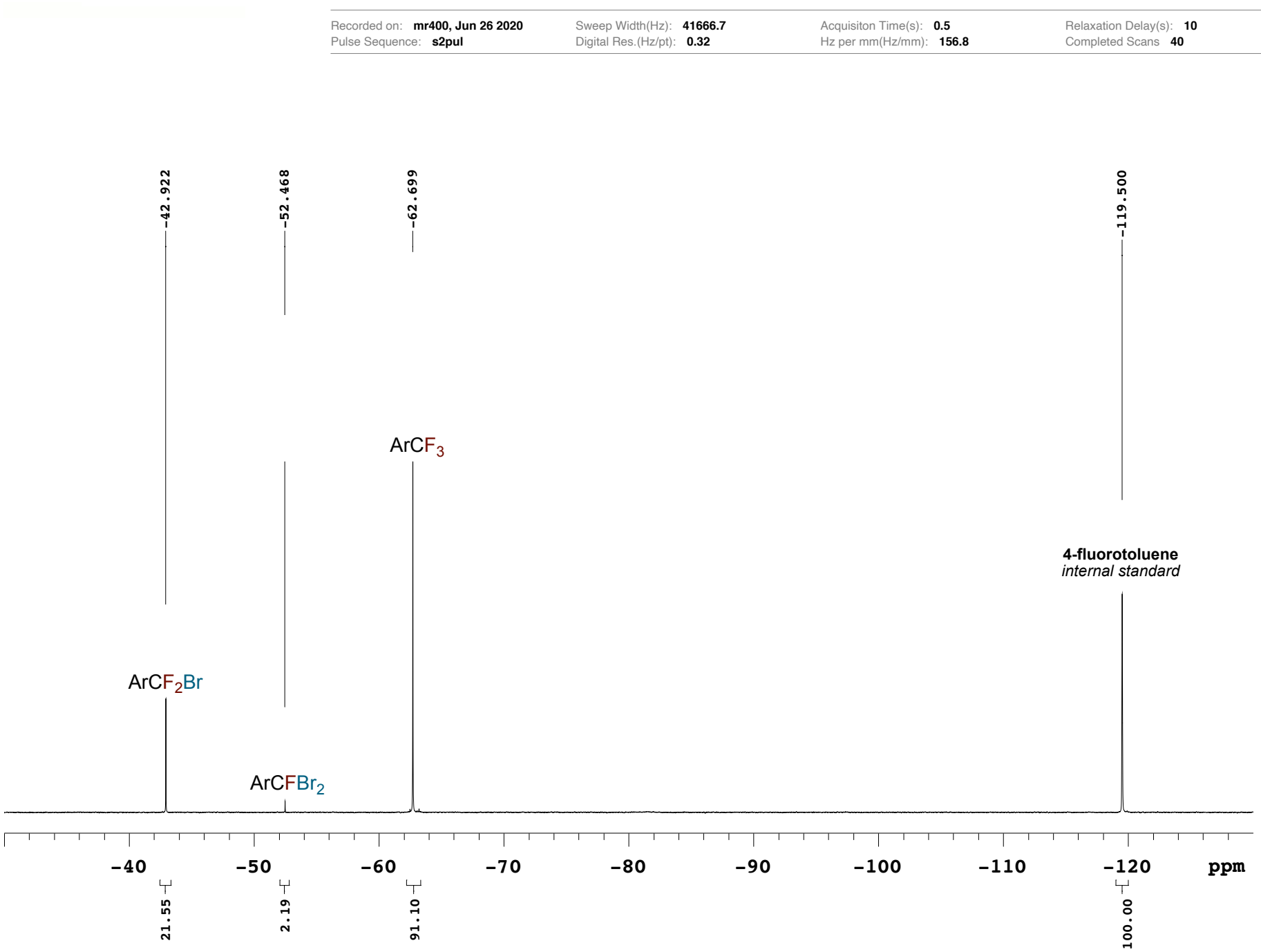

Figure S48: ^{19}F NMR spectrum of compound **2d** reaction II ($CDCl_3$, 376.3 MHz)

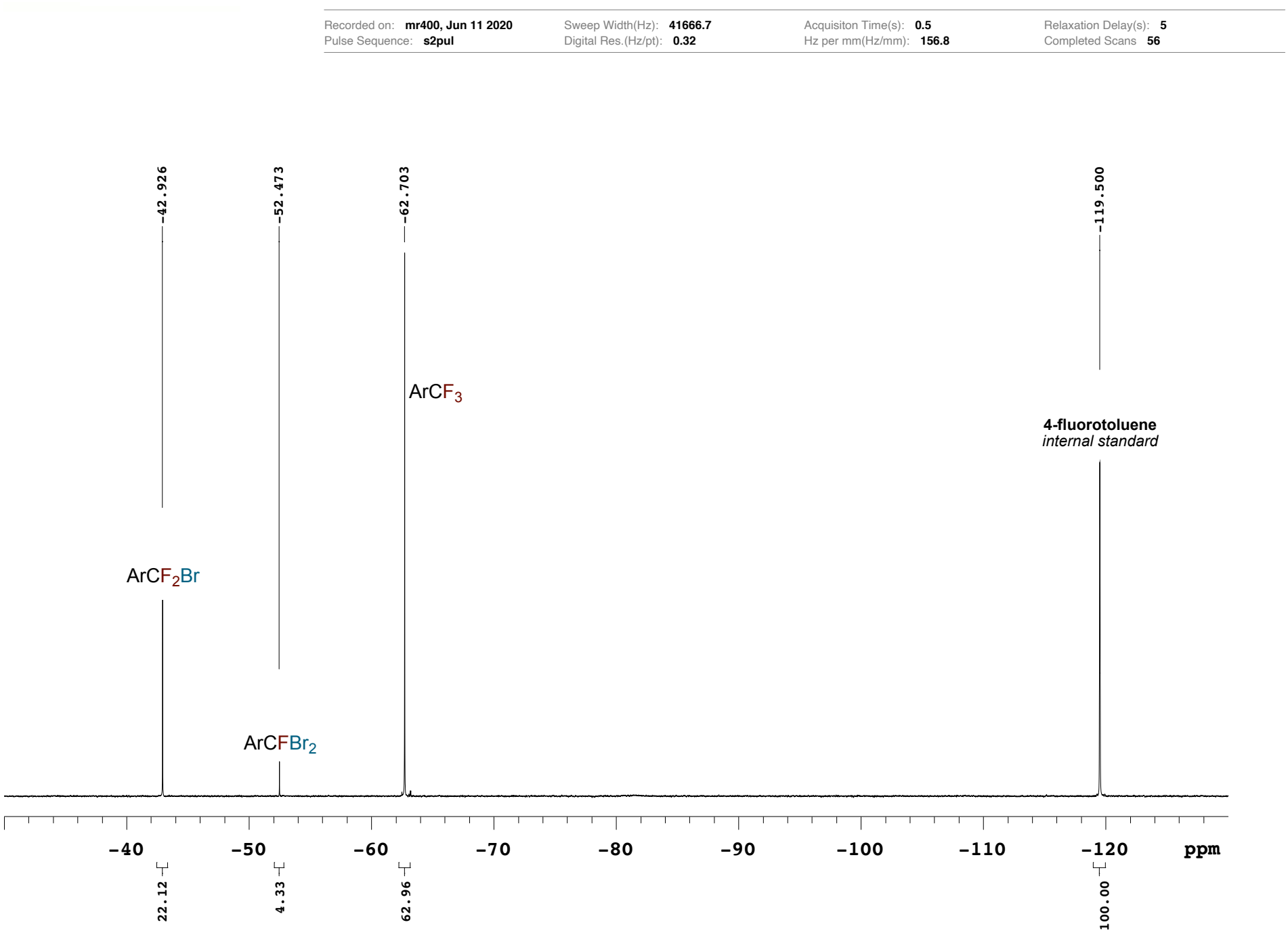

Figure S49: ^{19}F NMR spectrum of compound **2e** reaction I ($CDCl_3$, 376.3 MHz)

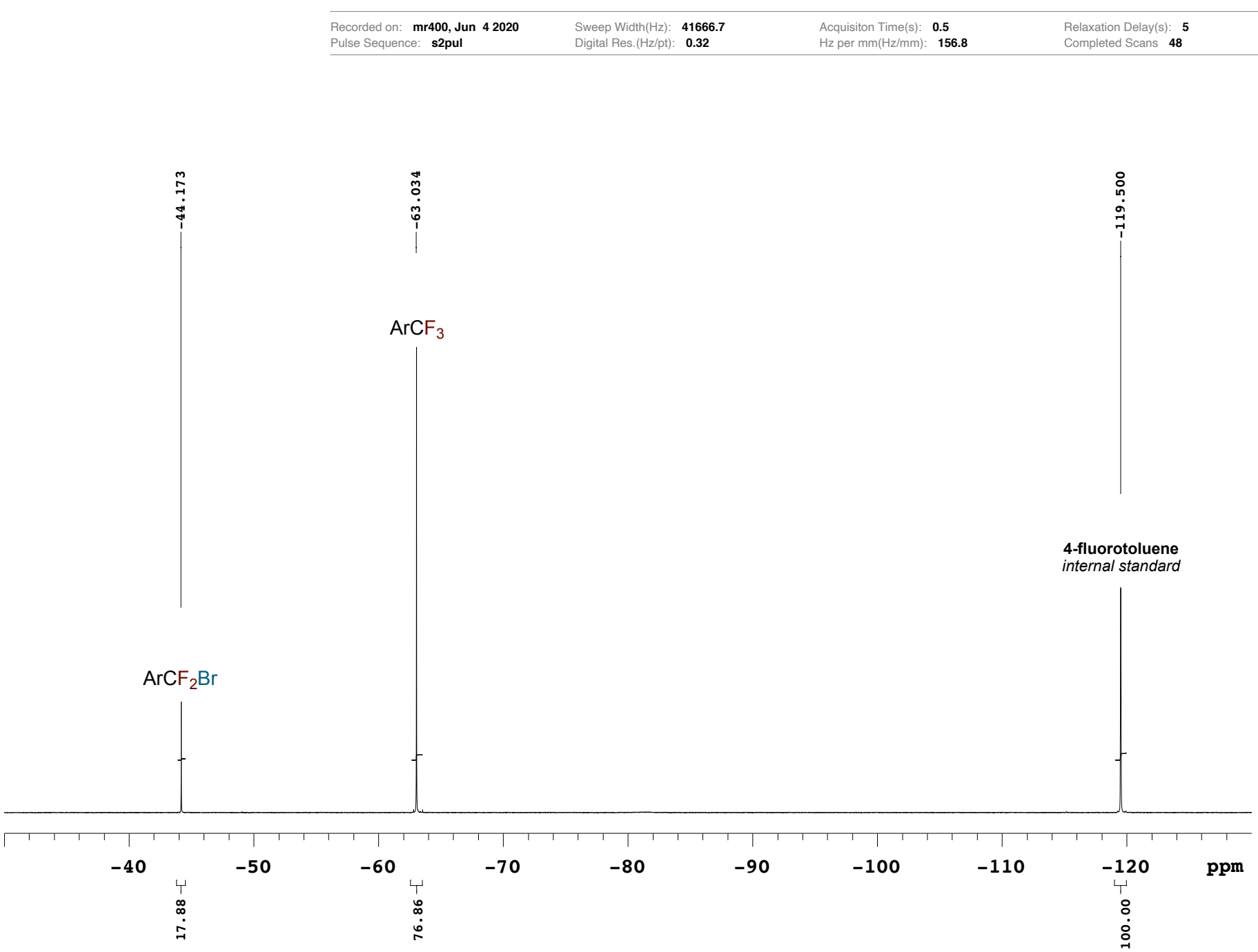

Figure S50: ^{19}F NMR spectrum of compound **2e** reaction II ($CDCl_3$, 376.3 MHz)

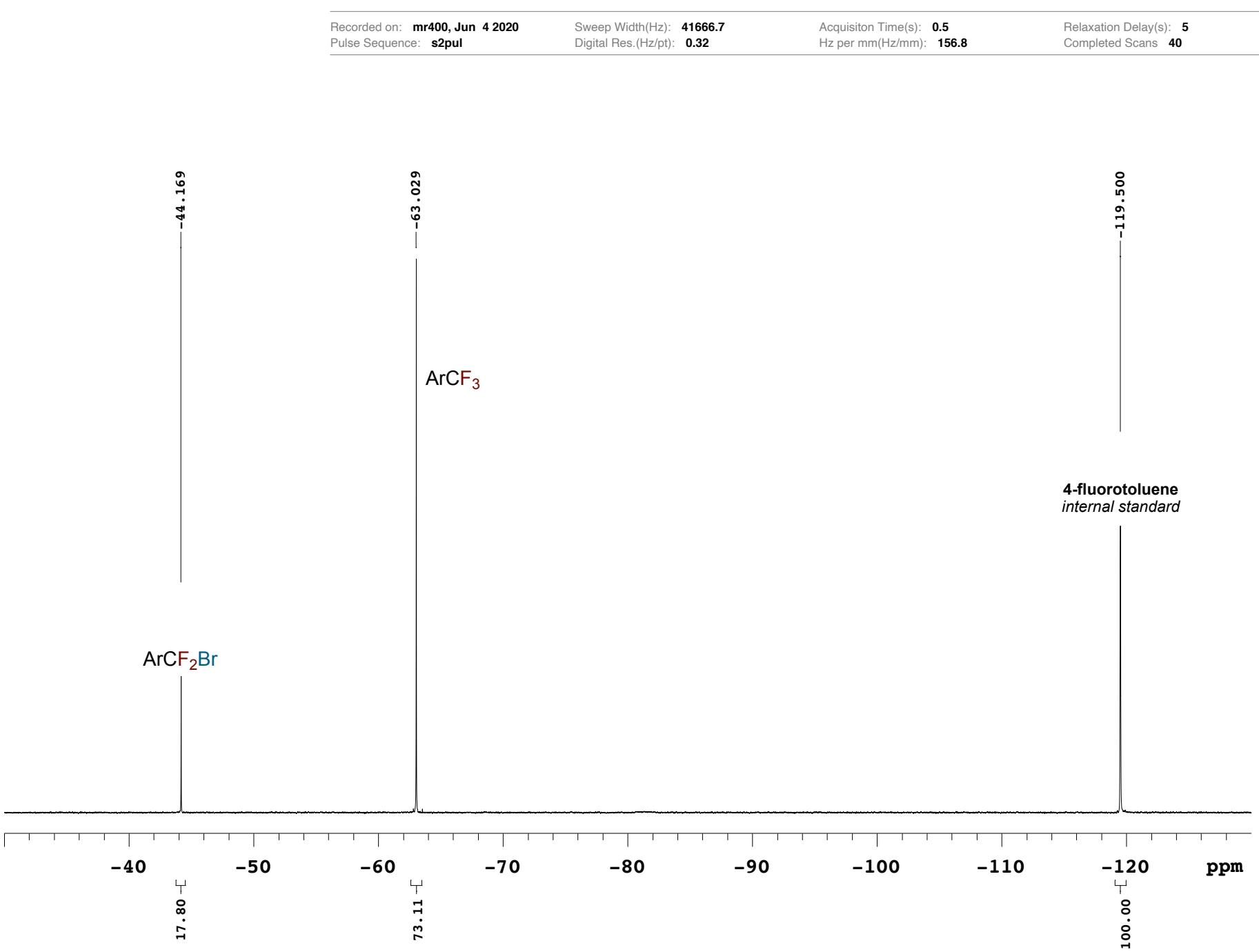

Figure S51: ^{19}F NMR spectrum of compound **2f** reaction I ($CDCl_3$, 376.3 MHz)

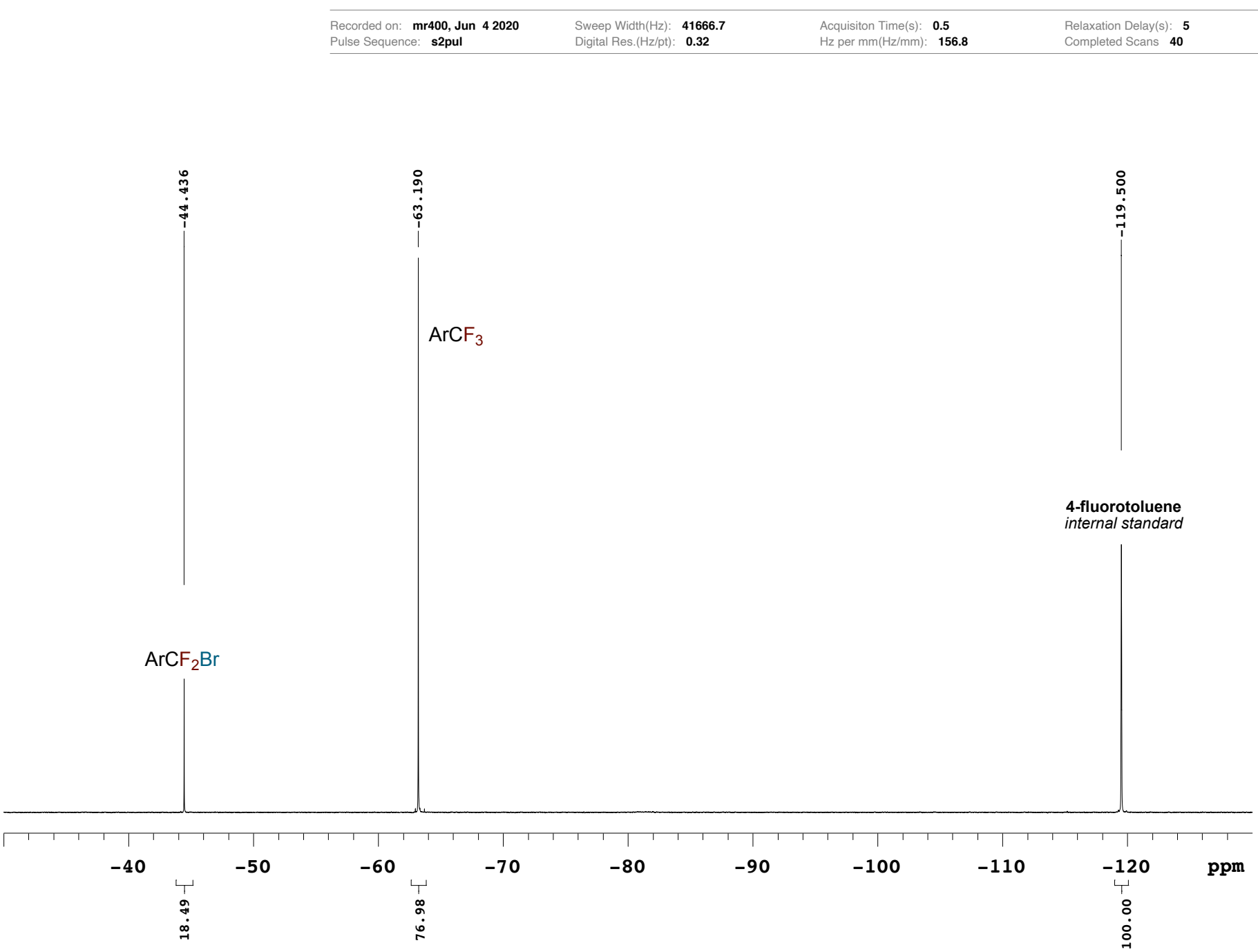

Figure S52: ^{19}F NMR spectrum of compound **2f** reaction II ($CDCl_3$, 376.3 MHz)

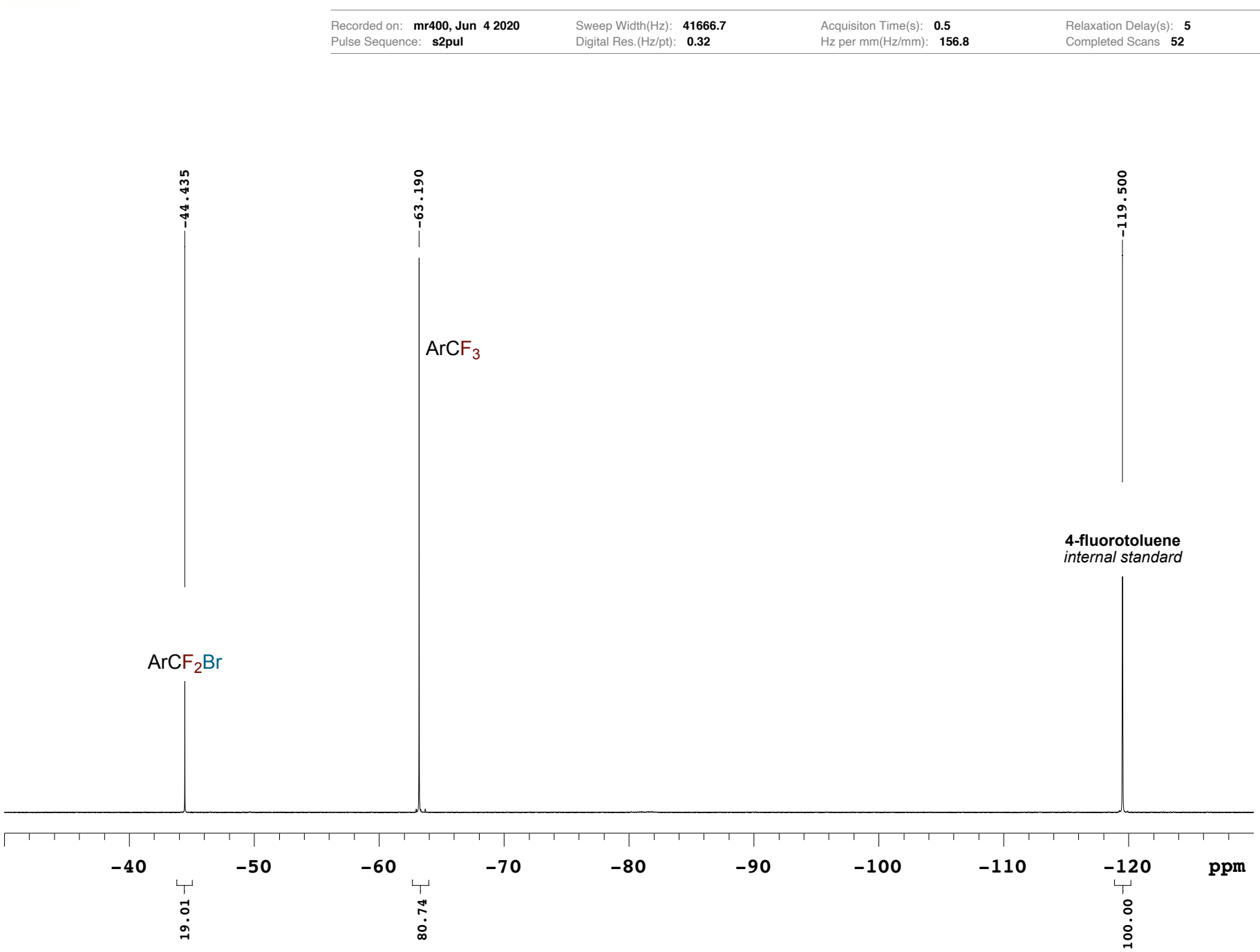

Figure S53: ^{19}F NMR spectrum of compound **2g** reaction I ($CDCl_3$, 376.3 MHz)

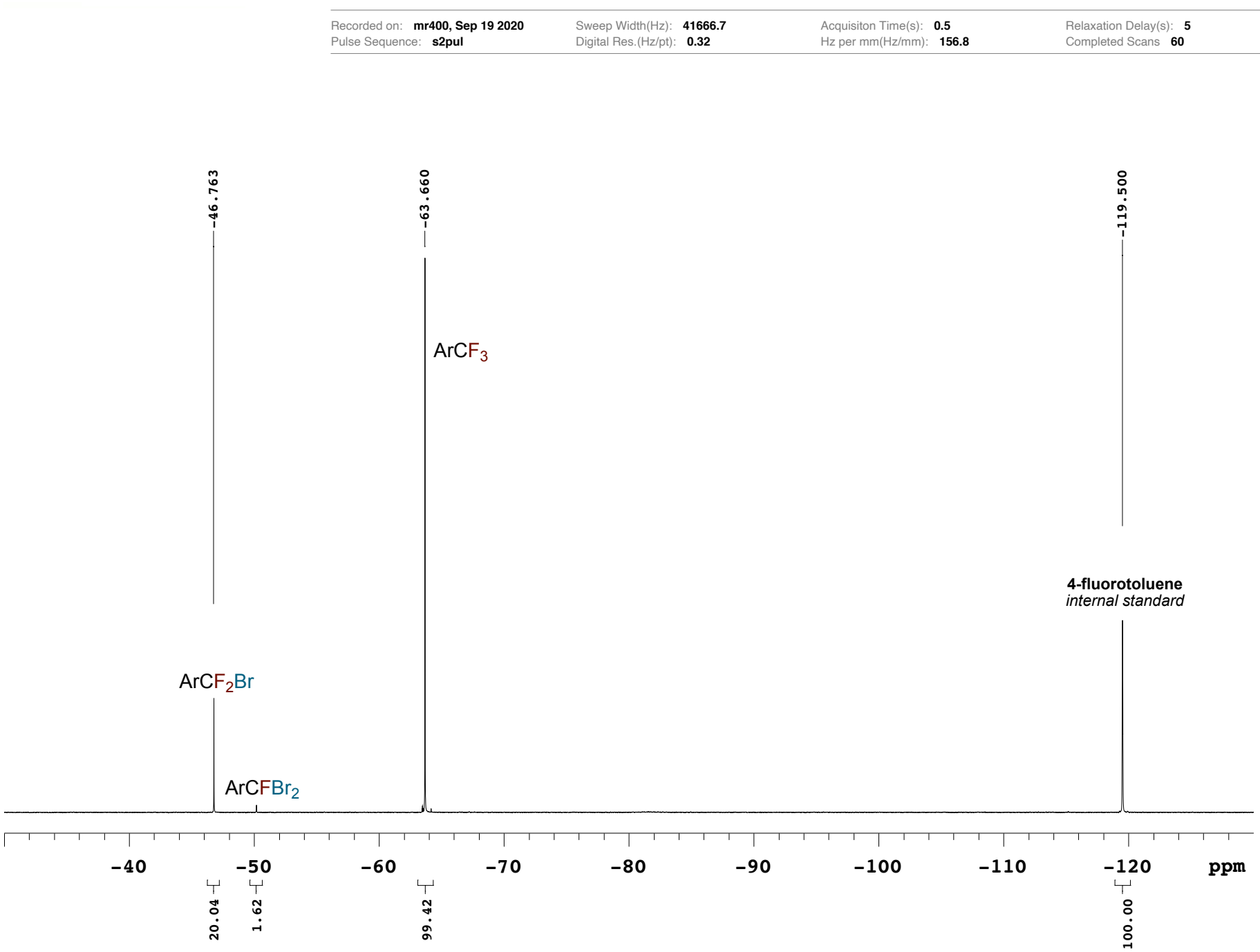

Figure S54: ^{19}F NMR spectrum of compound **2g** reaction II ($CDCl_3$, 376.3 MHz)

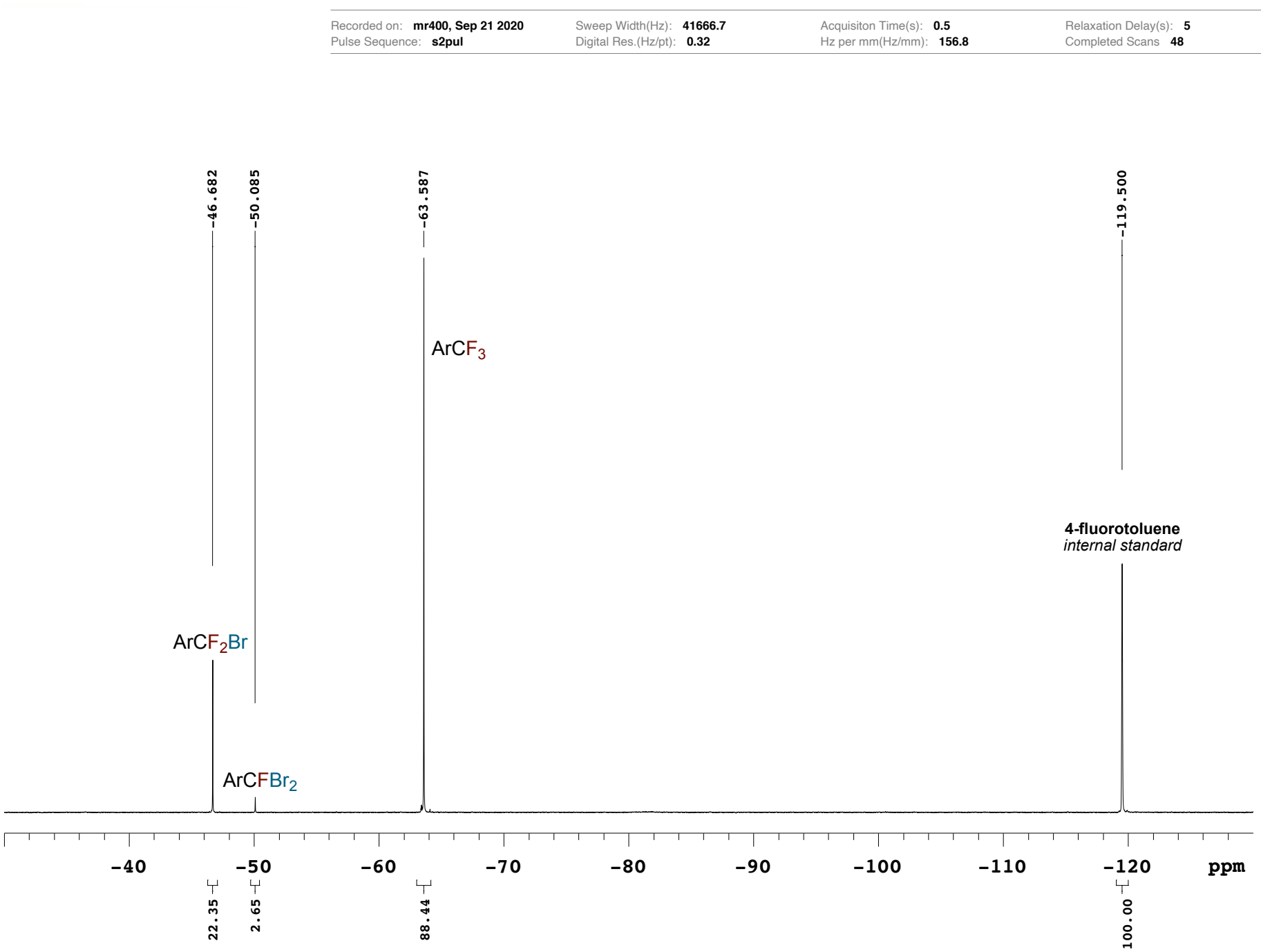

Figure S55: ^{19}F NMR spectrum of compound **2h** reaction I ($CDCl_3$, 376.3 MHz)

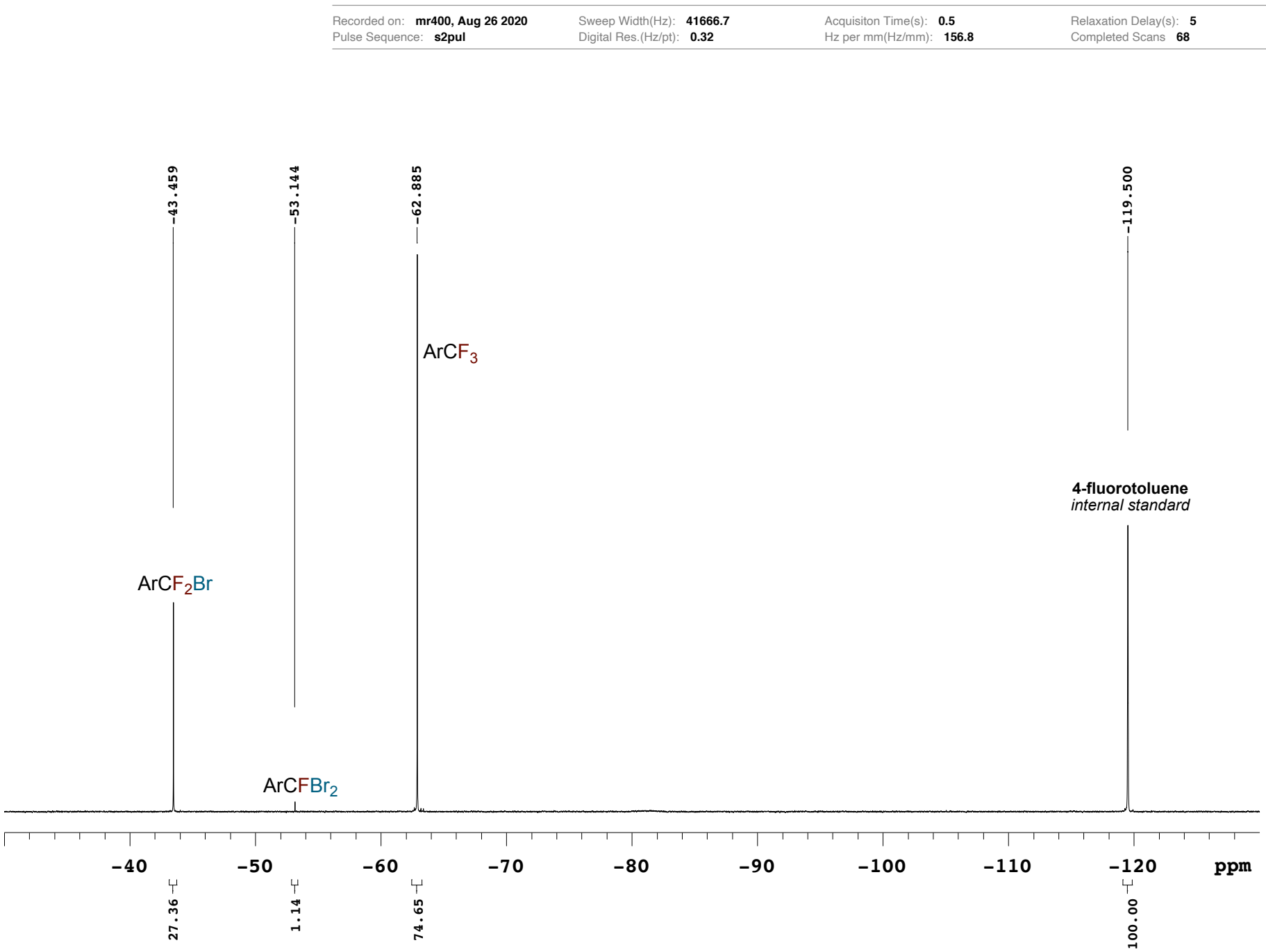

Figure S56: ^{19}F NMR spectrum of compound **2h** reaction II ($CDCl_3$, 376.3 MHz)

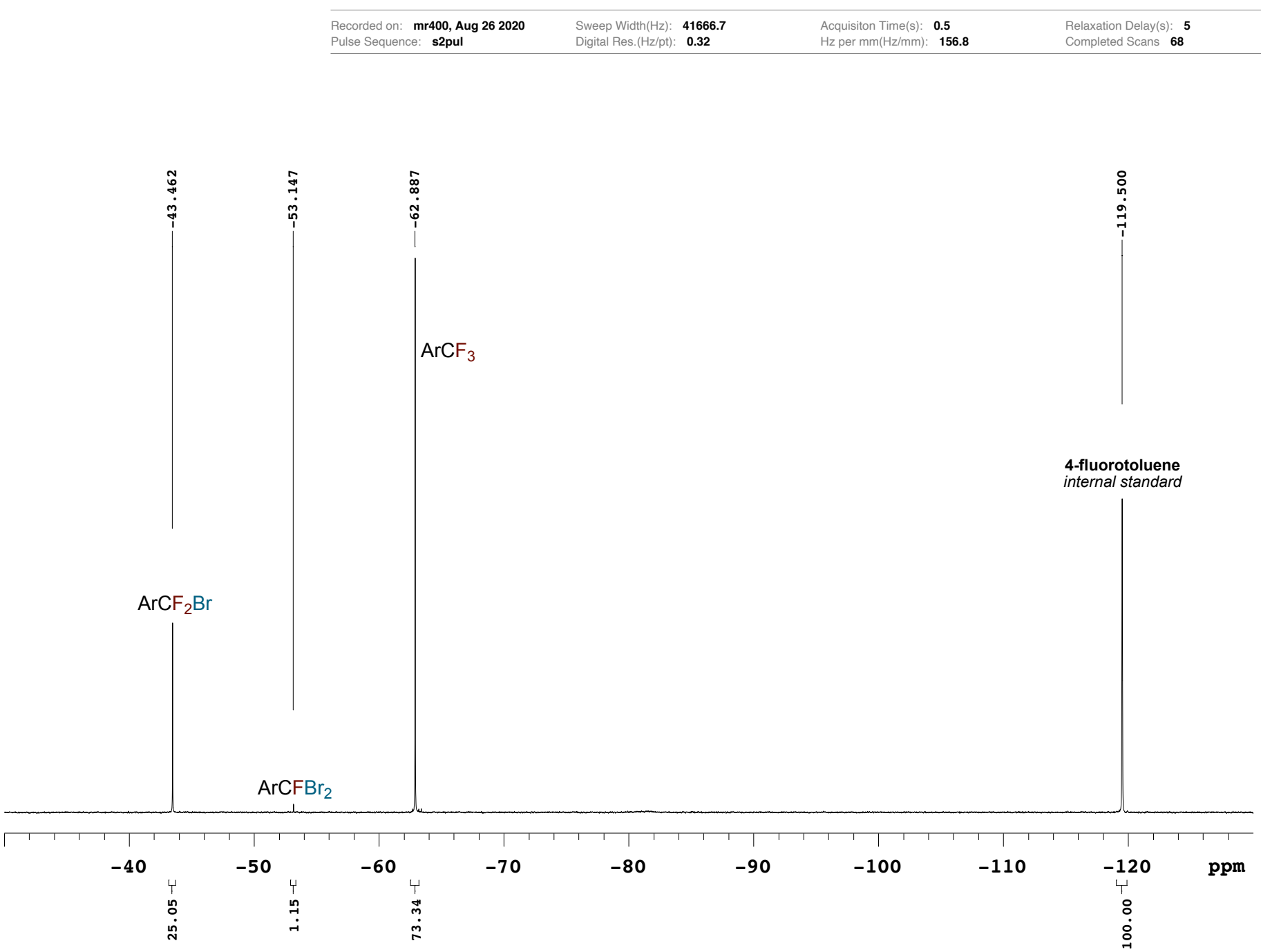

Figure S57: ^{19}F NMR spectrum of compound **2i** reaction I ($CDCl_3$, 376.3 MHz)

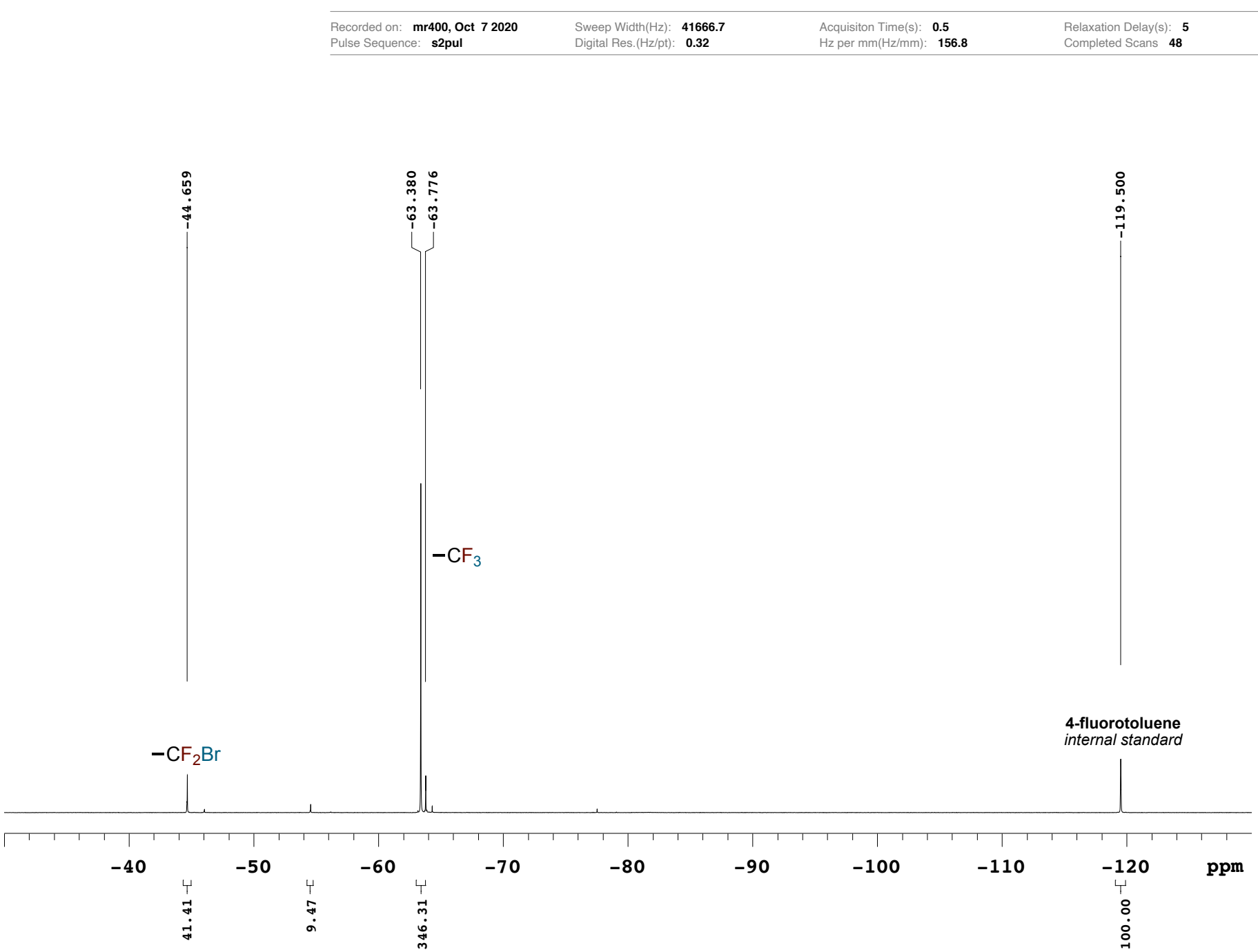

Figure S58: ^{19}F NMR spectrum of compound **2i** reaction II ($CDCl_3$, 376.3 MHz)

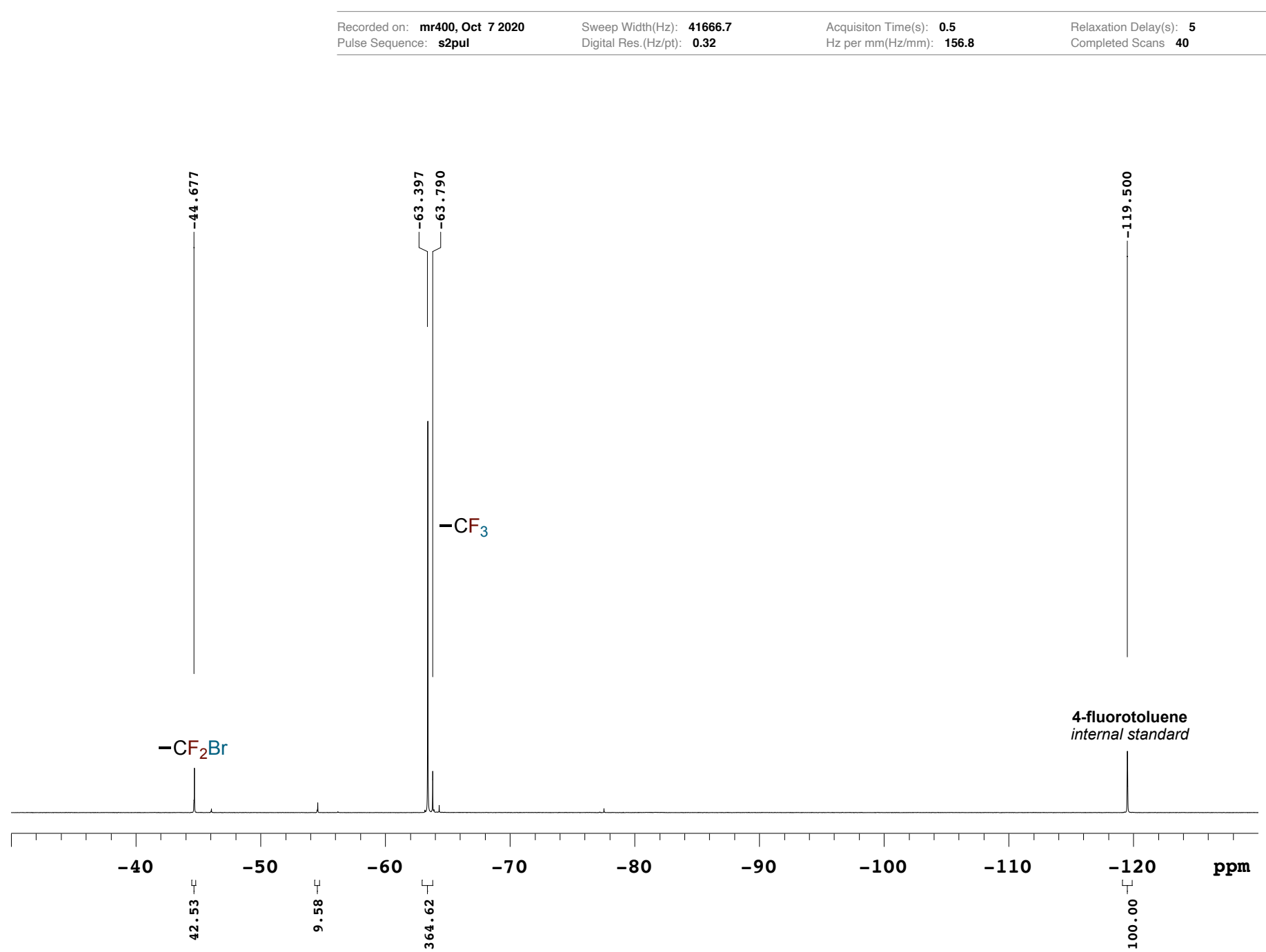

Figure S59: ^{19}F NMR spectrum of compound **2j** reaction I ($CDCl_3$, 376.3 MHz)

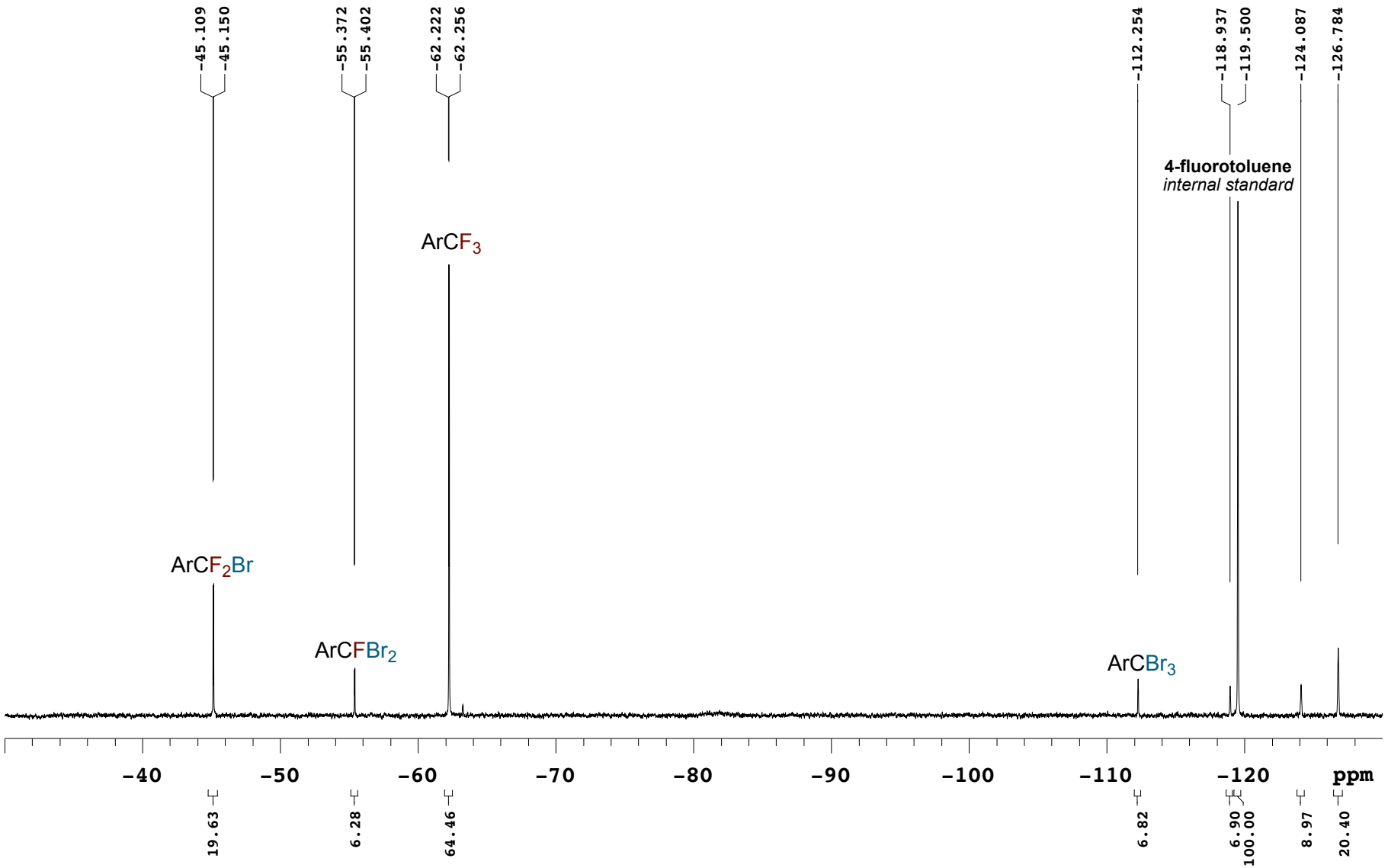

Figure S60: ^{19}F NMR spectrum of compound **2j** reaction II ($CDCl_3$, 376.3 MHz)

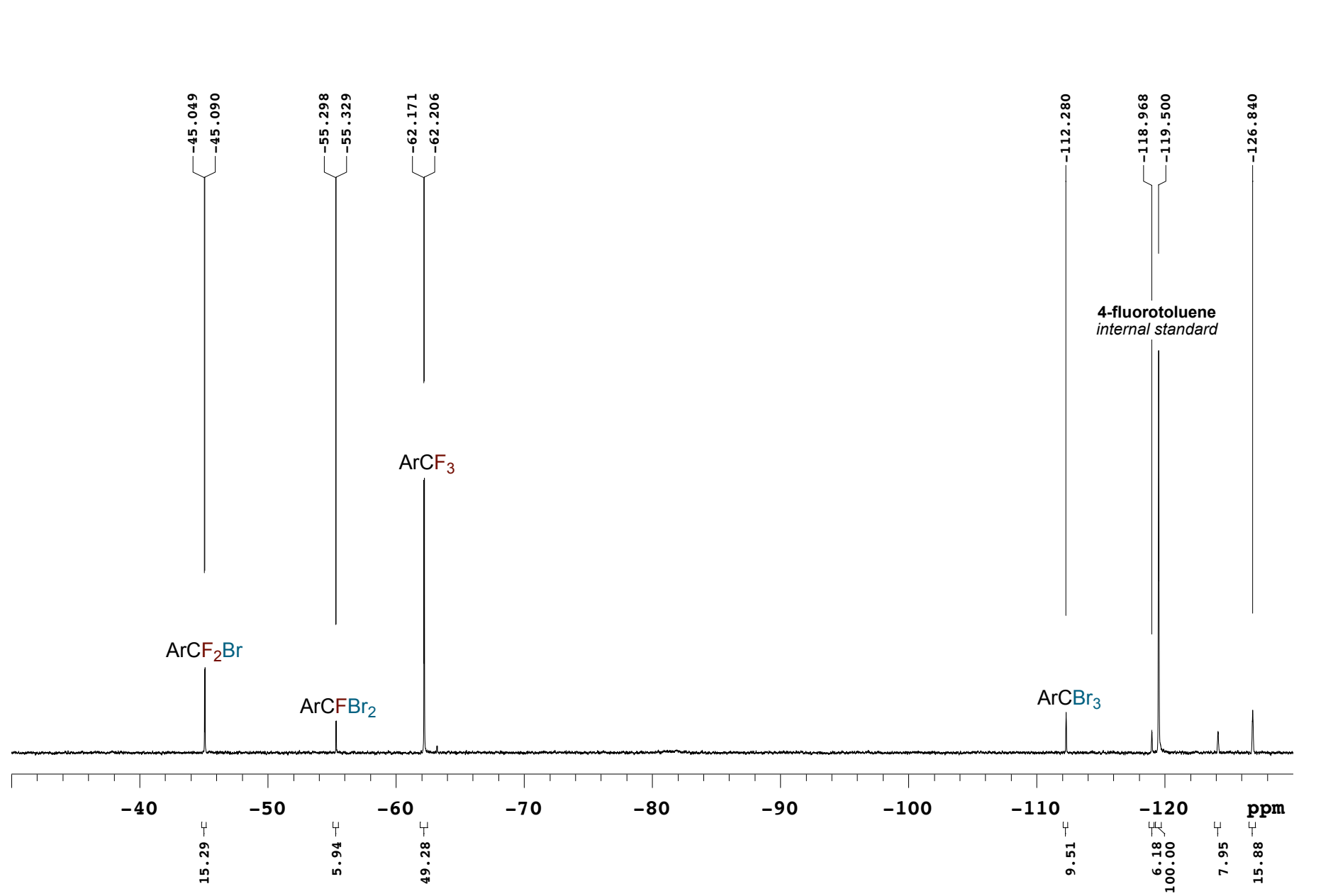

Figure S61: ^{19}F NMR spectrum of compound **2k** reaction I ($CDCl_3$, 376.3 MHz)

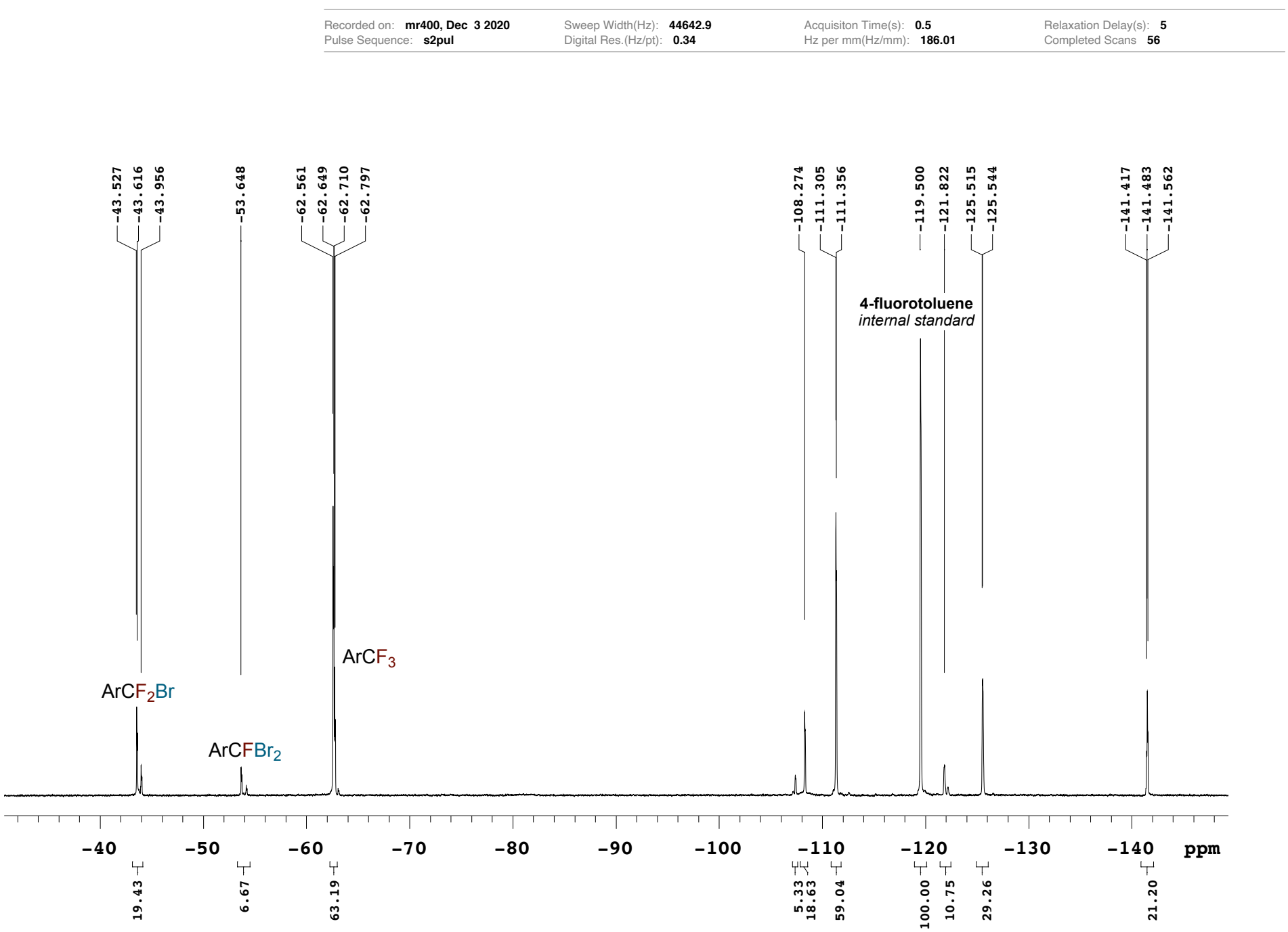

Figure S62: ^{19}F NMR spectrum of compound **2k** reaction II ($CDCl_3$, 376.3 MHz)

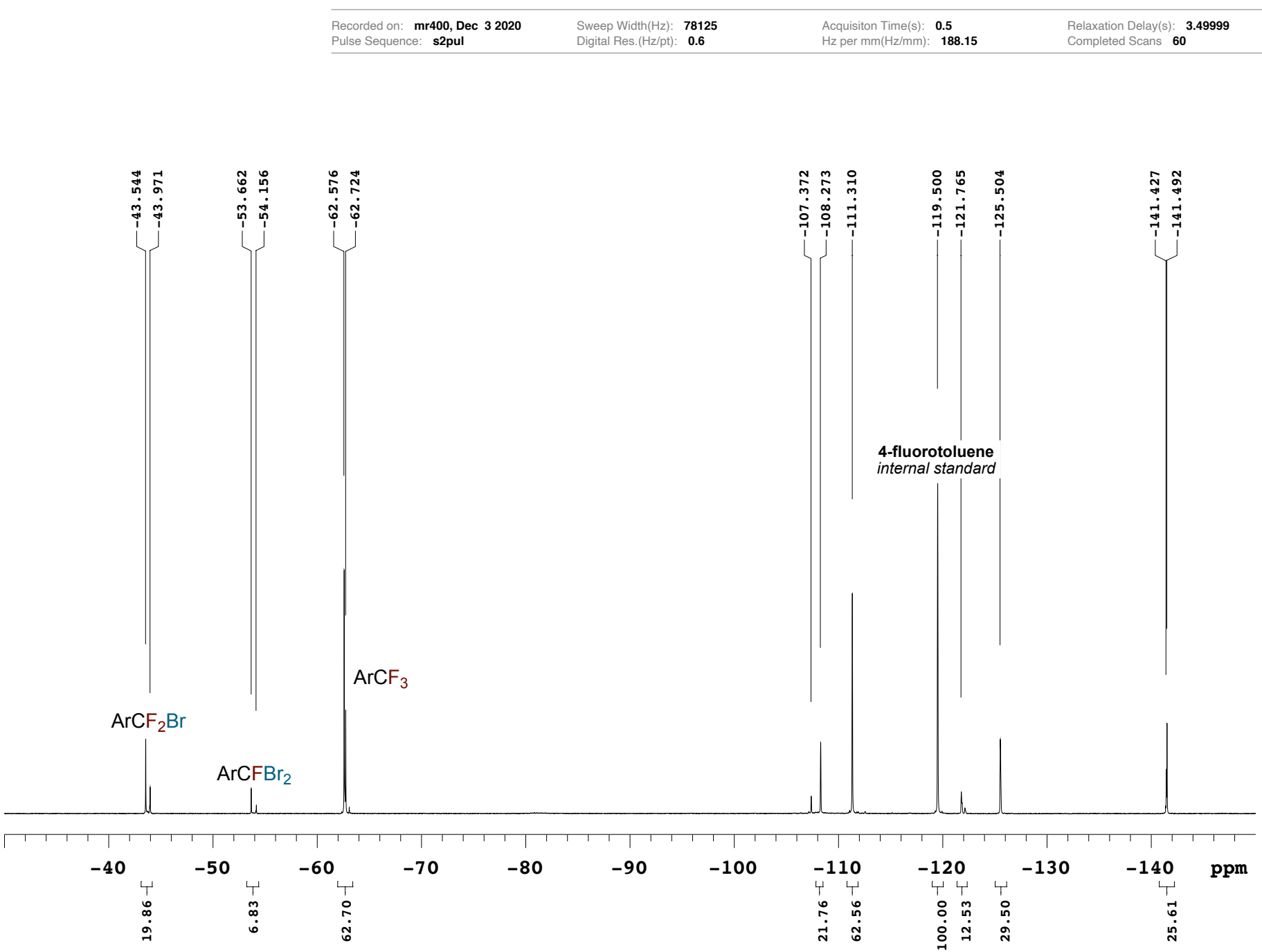

Figure S63: ^{1}H NMR spectrum of compound **2a** ($CDCl_3$, 499.8 MHz)

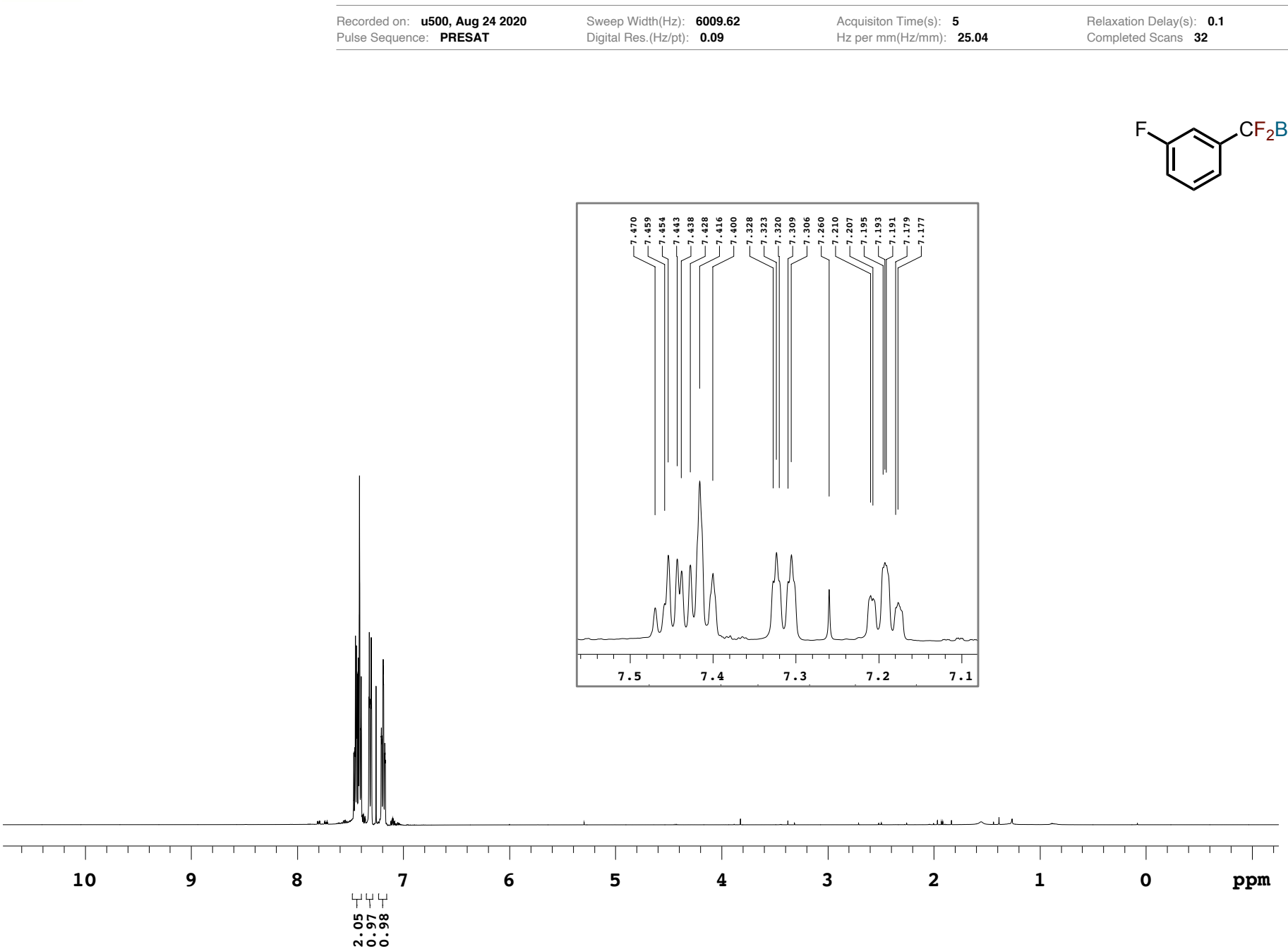

Figure S64: $^{13}C\{^{1}H\}$ NMR spectrum of compound **2a** ($CDCl_3$, 125.7 MHz)

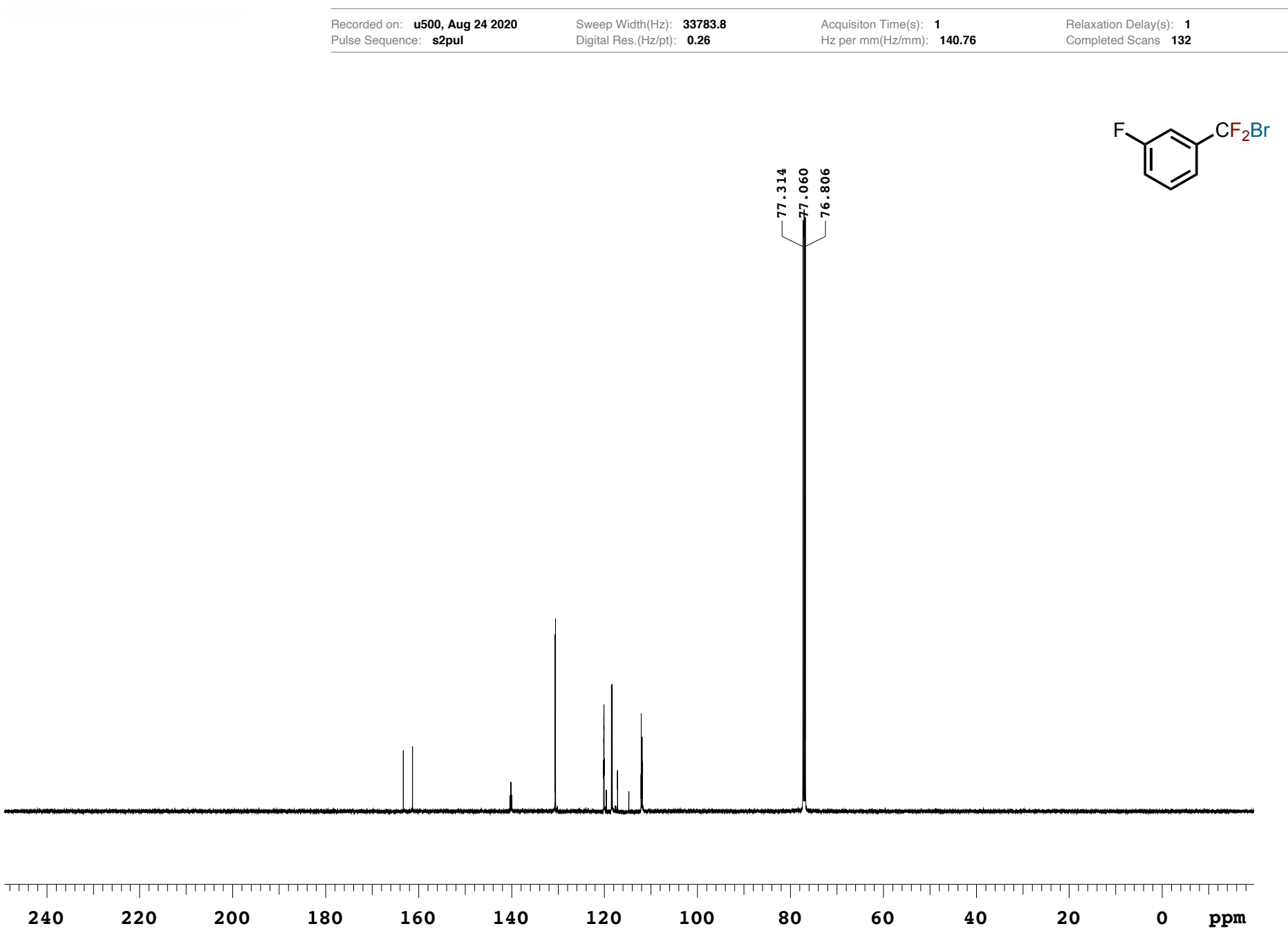

Figure S65: $^{13}C\{^{1}H\}$ NMR magnified spectrum of compound **2a** ($CDCl_3$, 125.7 MHz)

Recorded on: **u500, Aug 24 2020**	Sweep Width(Hz): **33783.8**	Acquisiton Time(s): **1**	Relaxation Delay(s): **1**
Pulse Sequence: **s2pul**	Digital Res.(Hz/pt): **0.26**	Hz per mm(Hz/mm): **140.76**	Completed Scans **132**

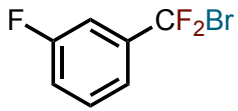

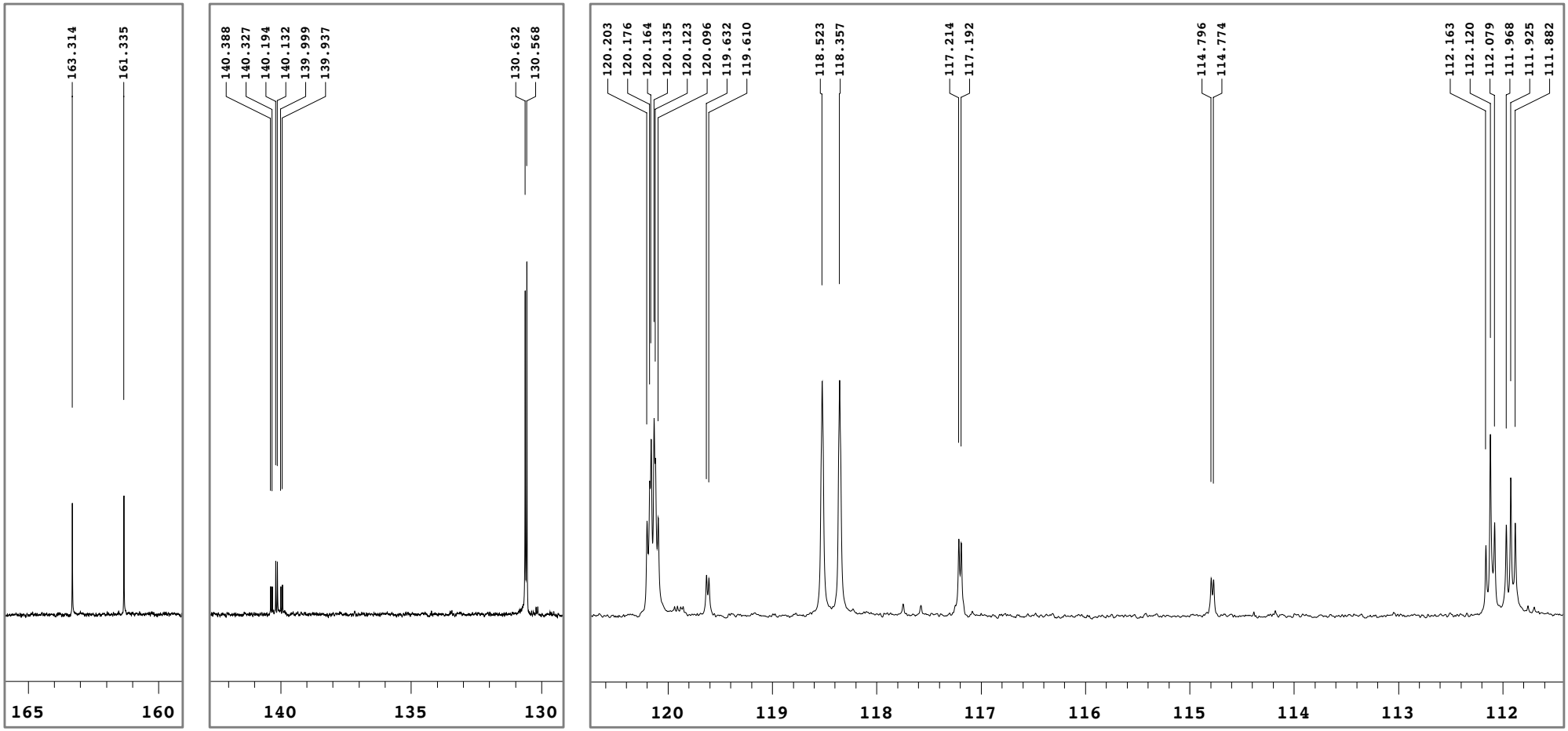

Figure S66: ^{19}F NMR spectrum of compound **2a** ($CDCl_3$, 367.3 MHz)

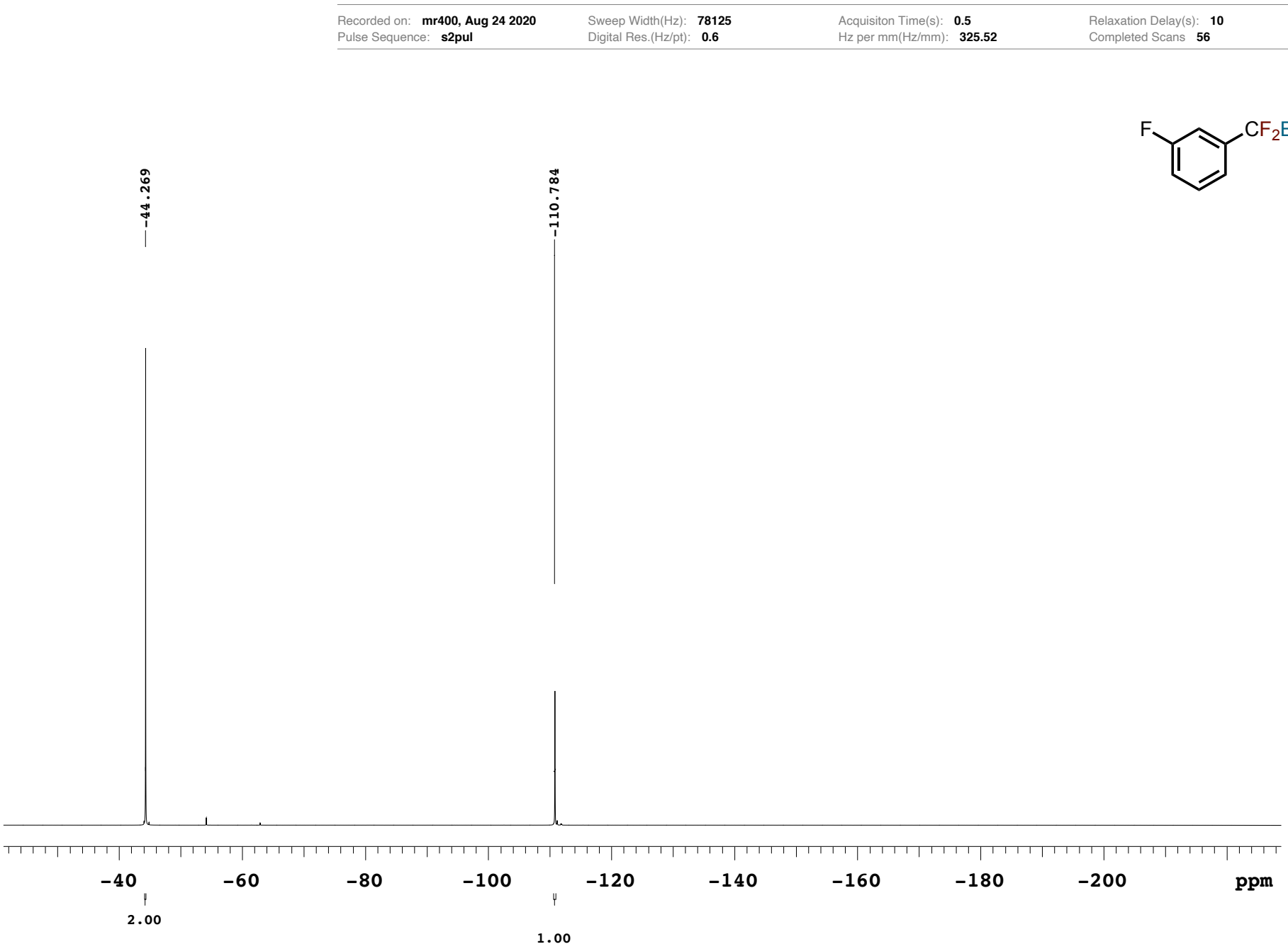

Figure S67: ^{1}H NMR spectrum of compound **2g** ($CDCl_3$, 699.8 MHz)

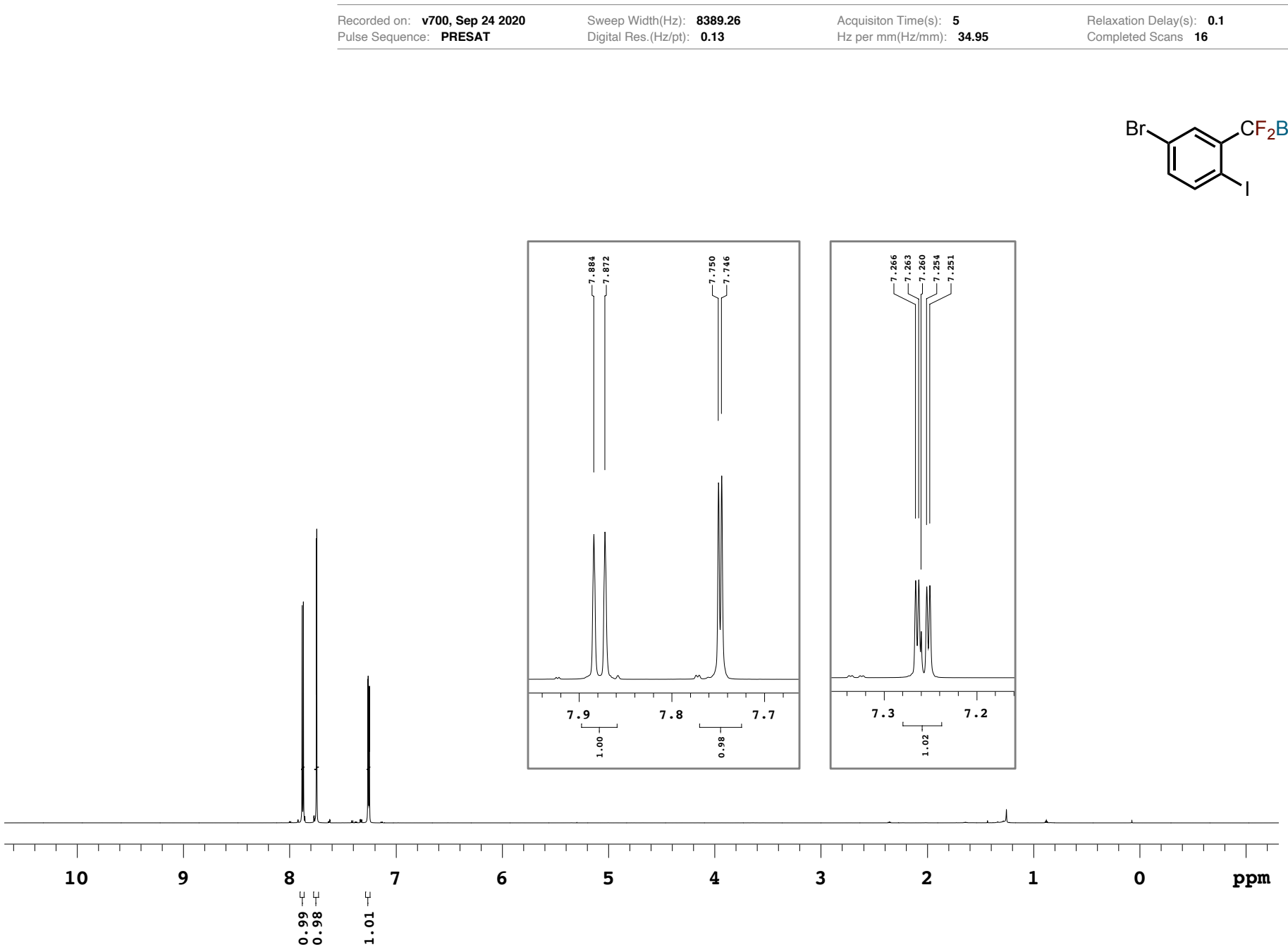

Figure S68: $^{13}C\{^{1}H\}$ NMR spectrum of compound **2g** ($CDCl_3$, 176.0 MHz)

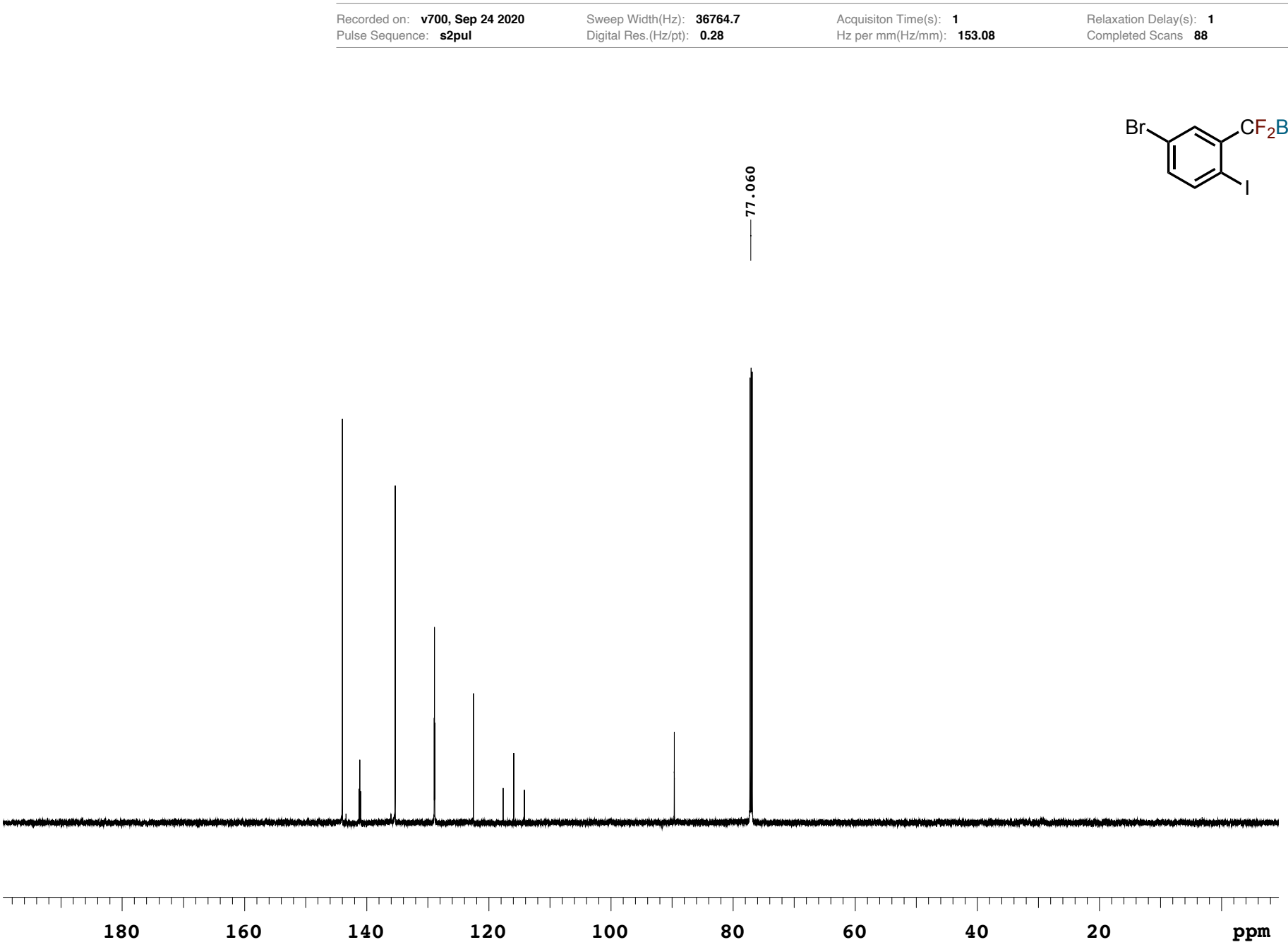

Figure S69: $^{13}C\{^{1}H\}$ NMR magnified spectrum of compound **2g** ($CDCl_3$, 176.0 MHz)

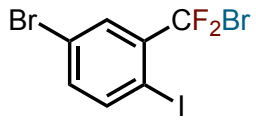

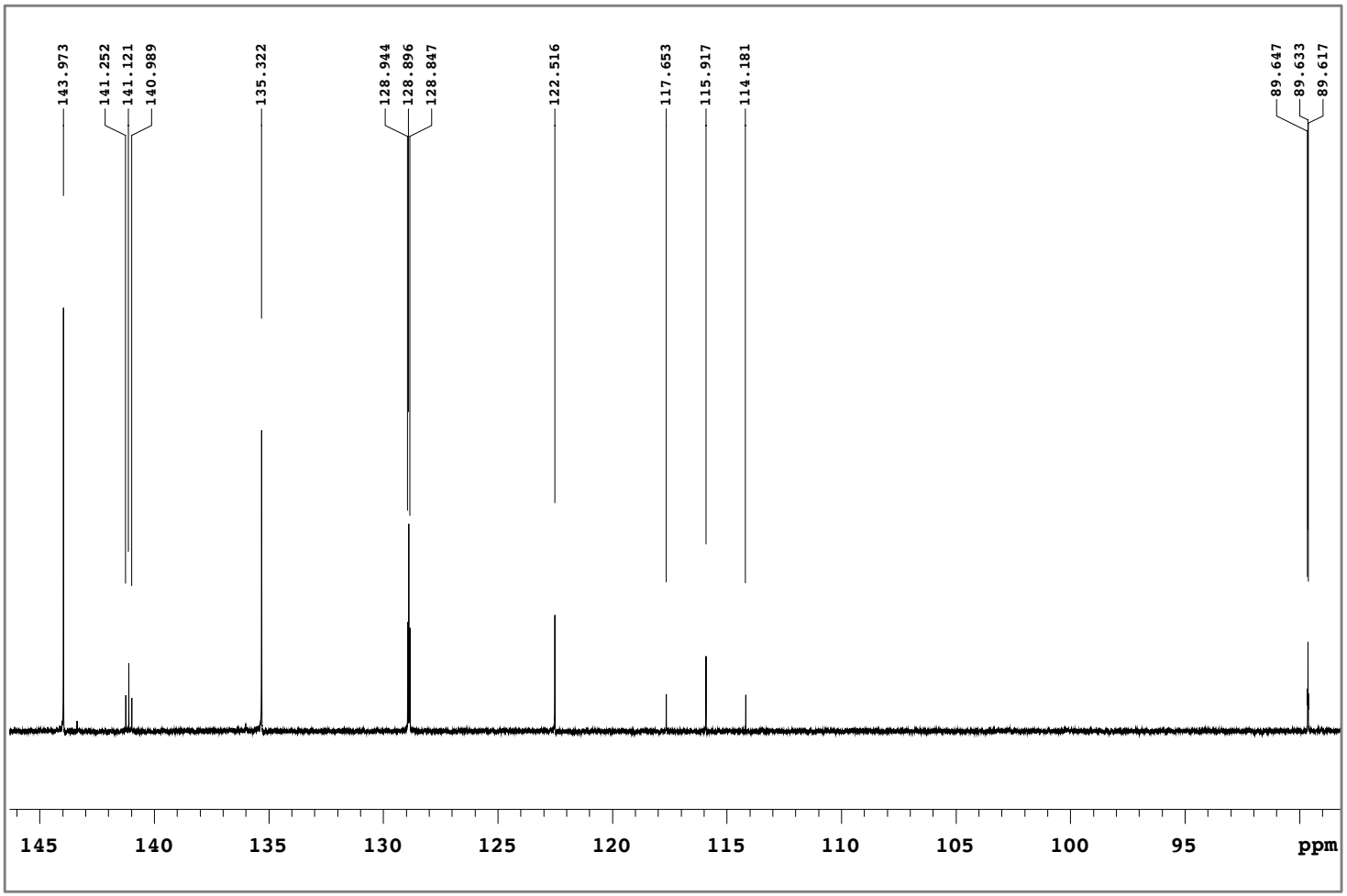

Figure S70: ^{19}F NMR spectrum of compound **2g** ($CDCl_3$, 367.3 MHz)

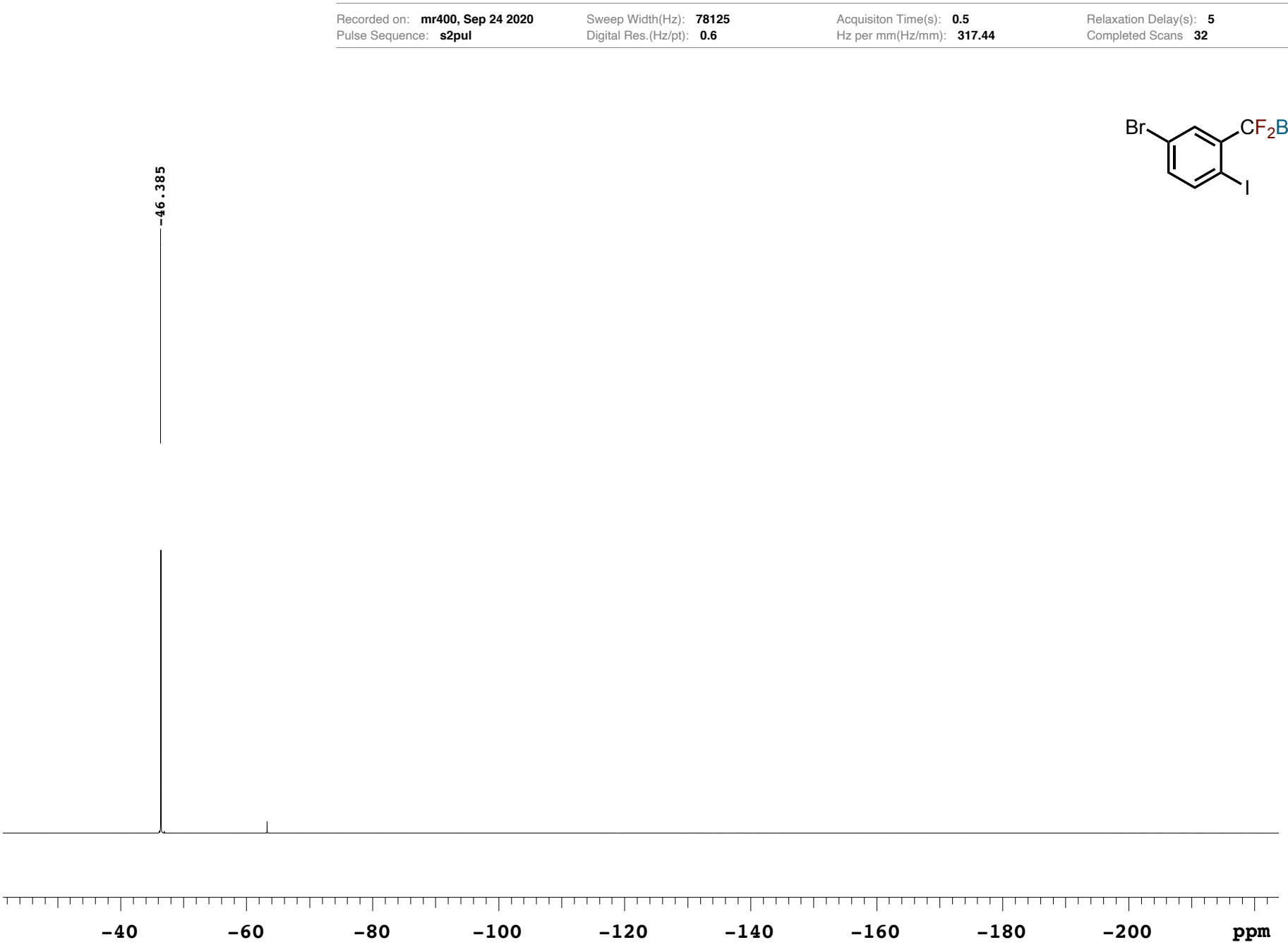

Figure S71: ^{1}H NMR spectrum of compound **2h** ($CDCl_3$, 699.8 MHz)

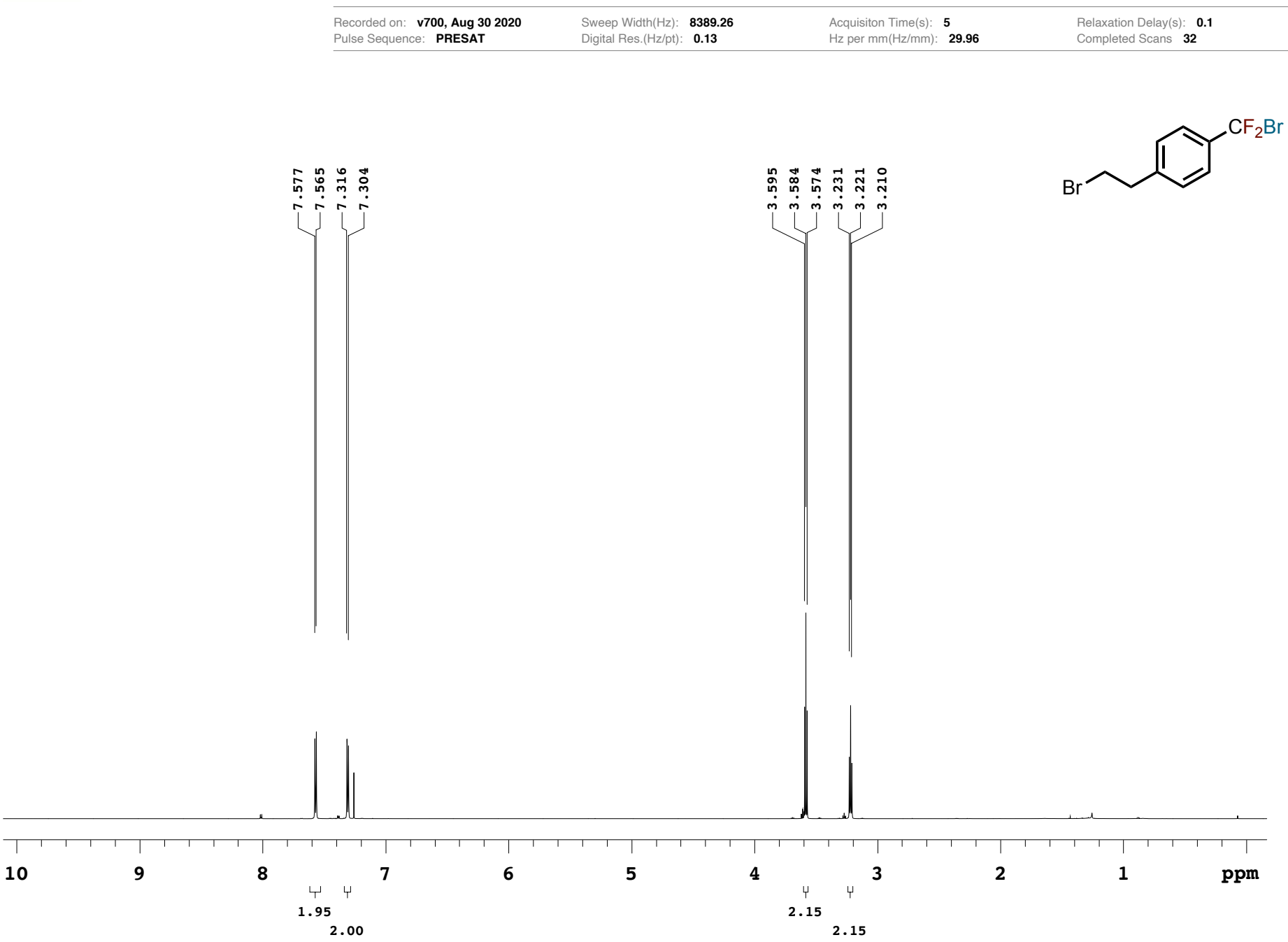

Figure S72: $^{13}C\{^{1}H\}$ NMR spectrum of compound **2h** ($CDCl_3$, 176.0 MHz)

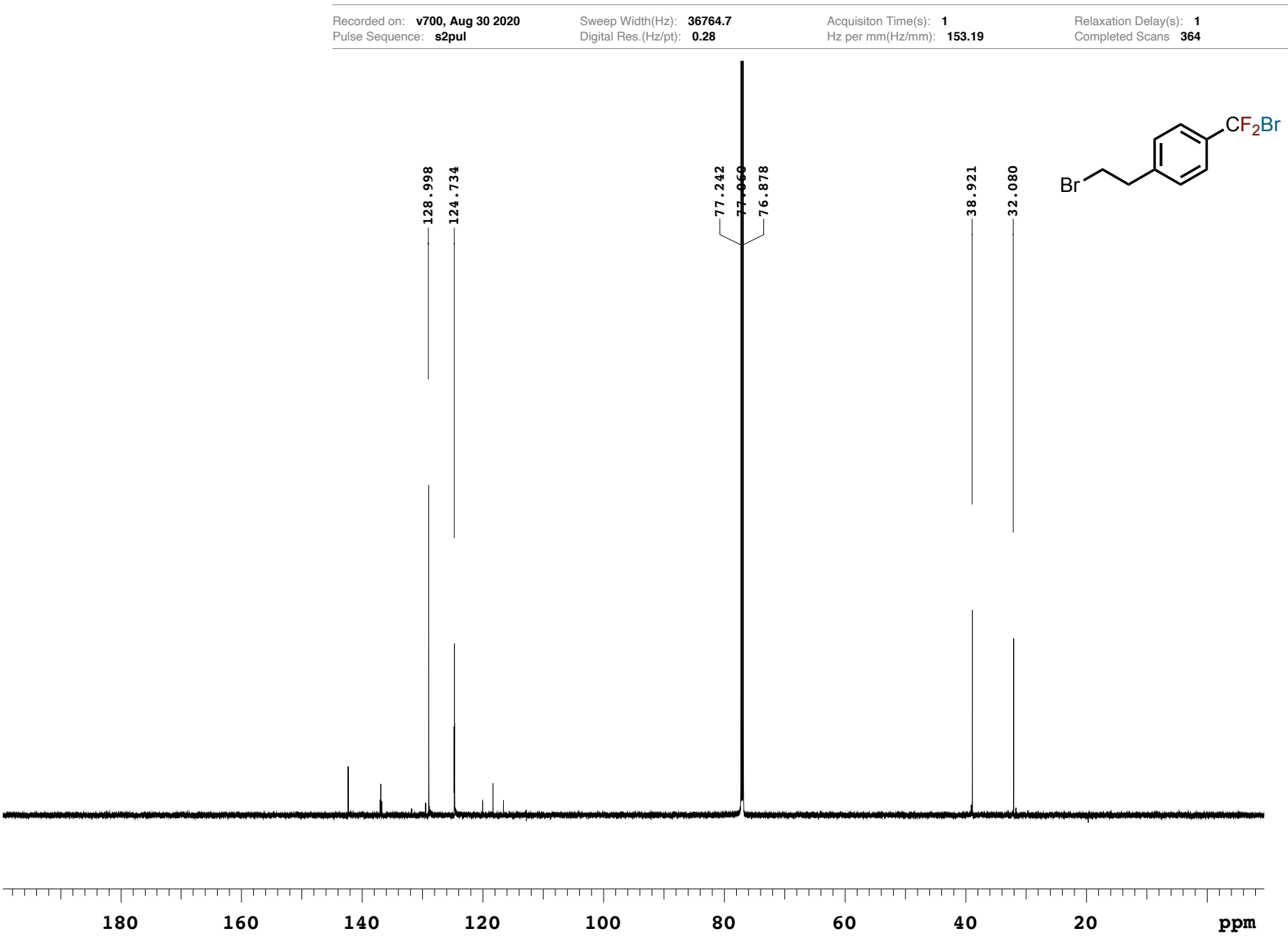

Figure S73: $^{13}C\{^{1}H\}$ NMR magnified spectrum of compound **2h** ($CDCl_3$, 176.0 MHz)

Recorded on: **v700, Aug 30 2020**	Sweep Width(Hz): **36764.7**	Acquisiton Time(s): **1**	Relaxation Delay(s): **1**
Pulse Sequence: **s2pul**	Digital Res.(Hz/pt): **0.28**	Hz per mm(Hz/mm): **153.19**	Completed Scans **364**

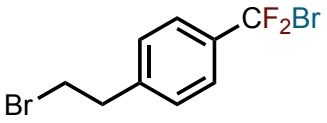

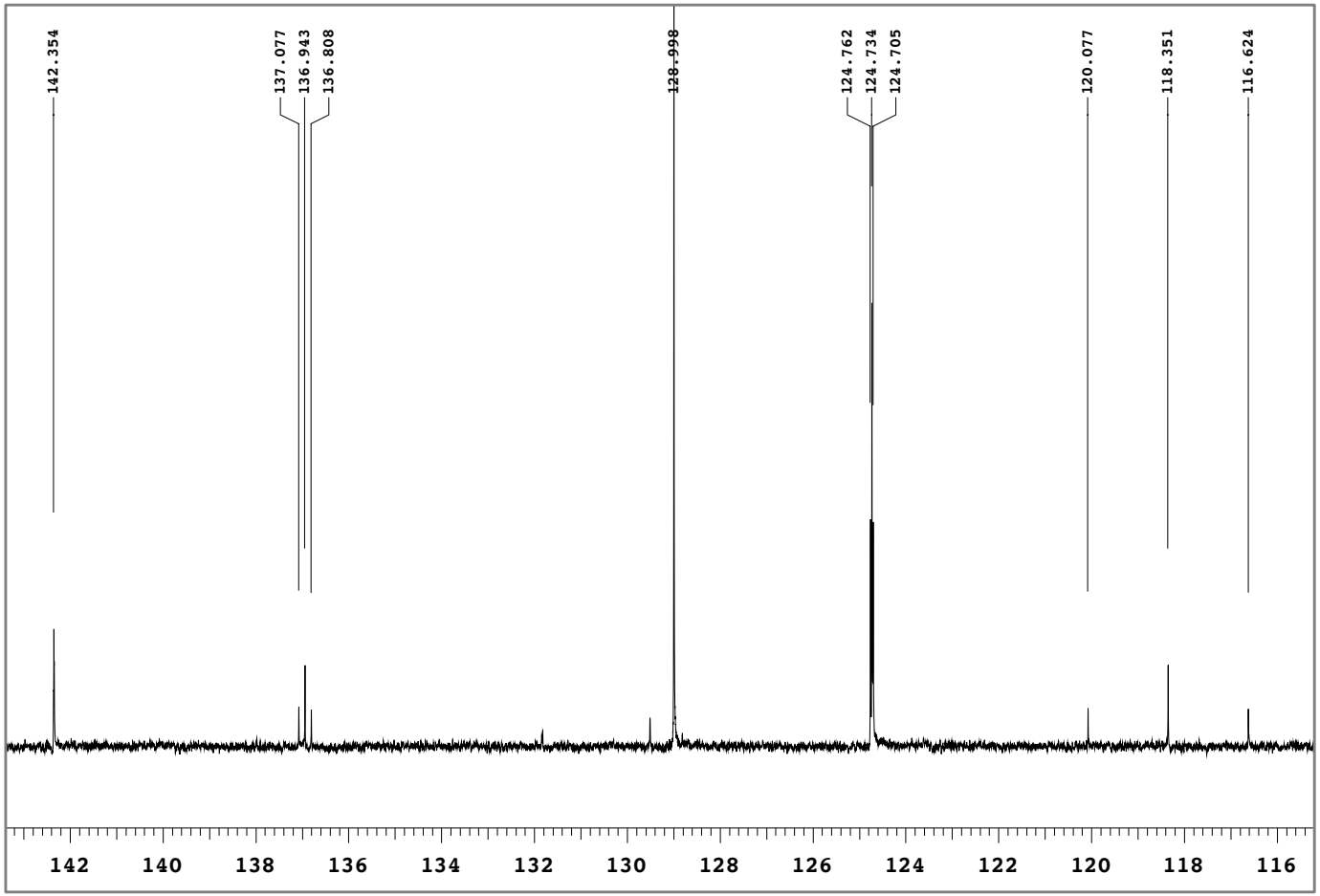

Figure S74: ^{19}F NMR spectrum of compound **2h** ($CDCl_3$, 367.3 MHz)

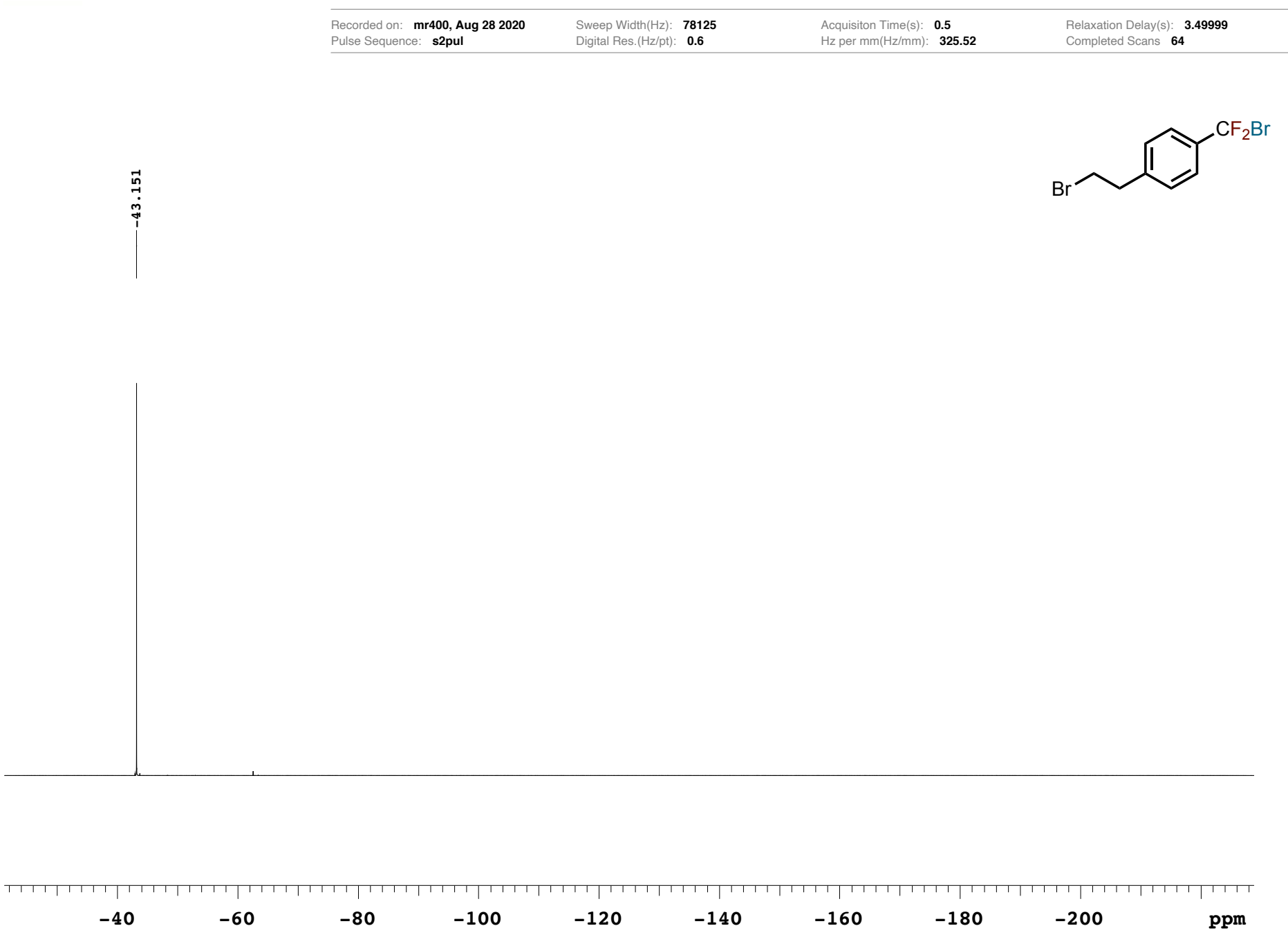

Figure S75: ^{1}H NMR spectrum of compound **2i** ($CDCl_3$, 699.8 MHz)

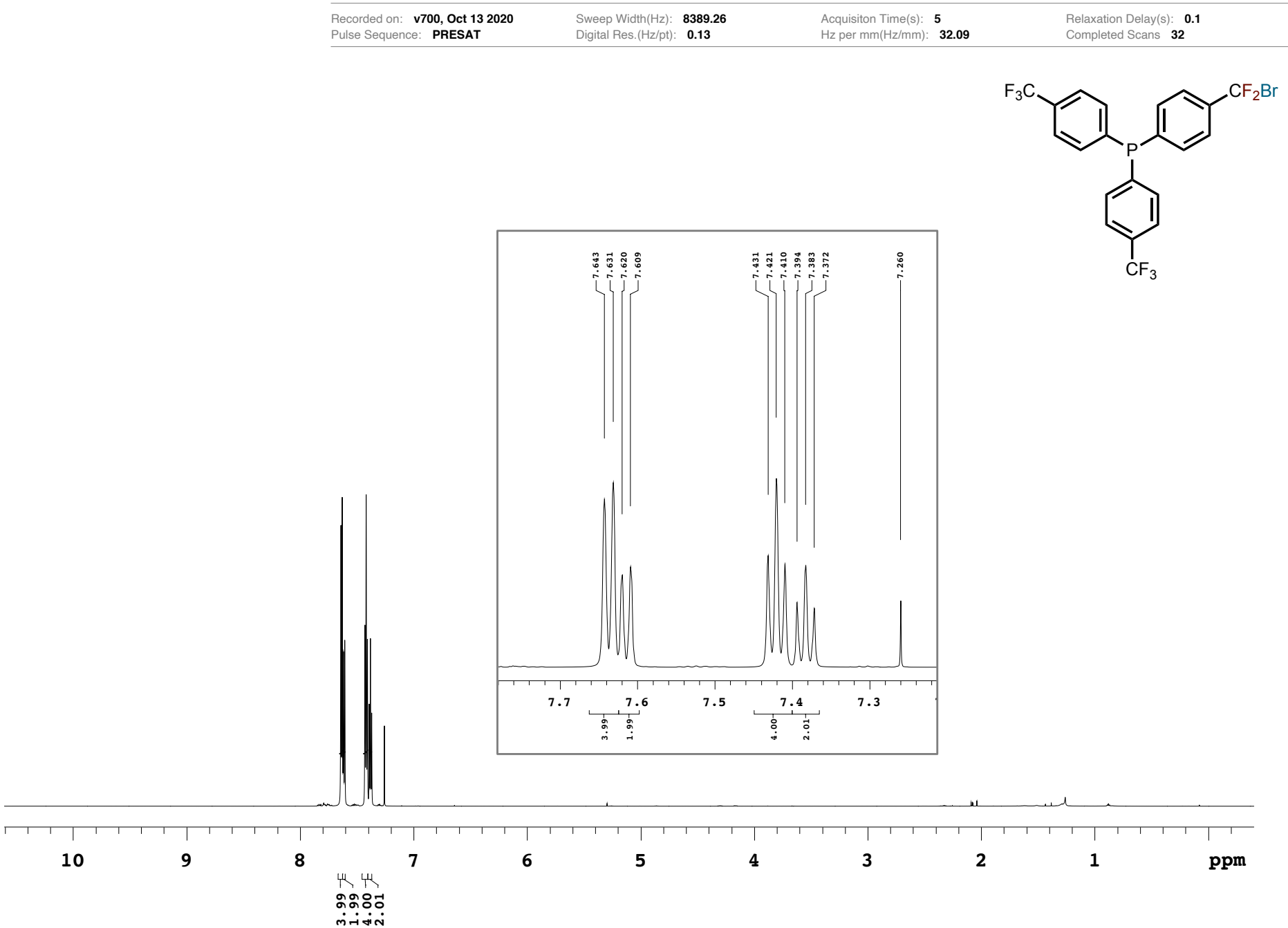

Figure S76: $^{13}C\{^{1}H\}$ NMR spectrum of compound **2i** ($CDCl_3$, 176.0 MHz)

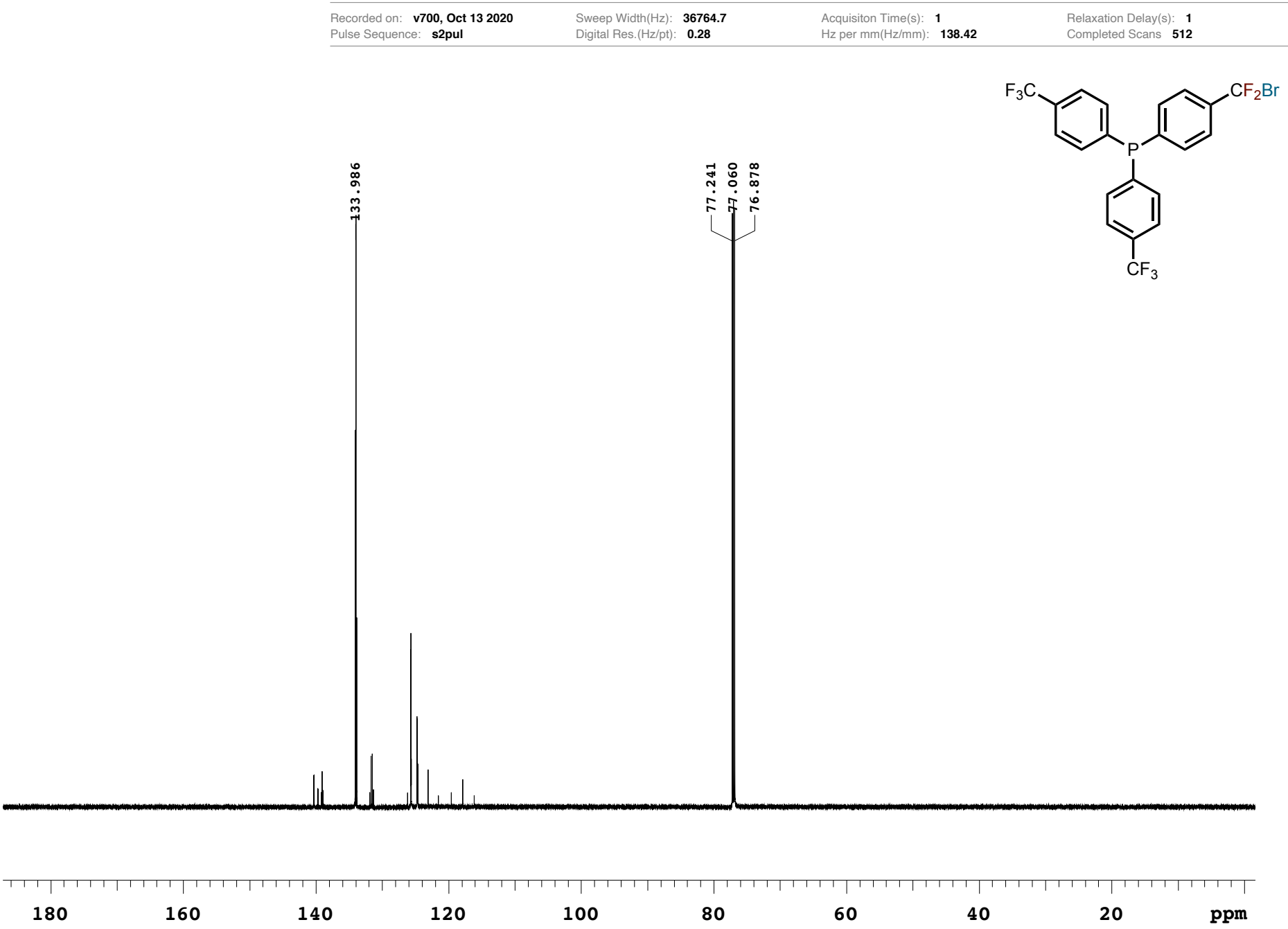

Figure S77: $^{13}C\{^{1}H\}$ NMR magnified spectrum of compound **2i** ($CDCl_3$, 176.0 MHz)

Recorded on: **v700, Oct 13 2020**	Sweep Width(Hz): **36764.7**	Acquisiton Time(s): **1**	Relaxation Delay(s): **1**
Pulse Sequence: **s2pul**	Digital Res.(Hz/pt): **0.28**	Hz per mm(Hz/mm): **138.42**	Completed Scans **512**

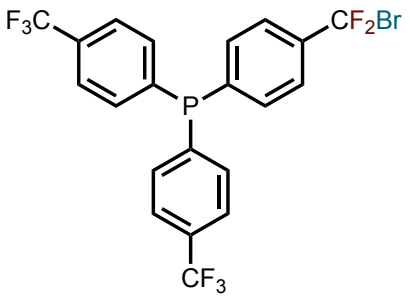

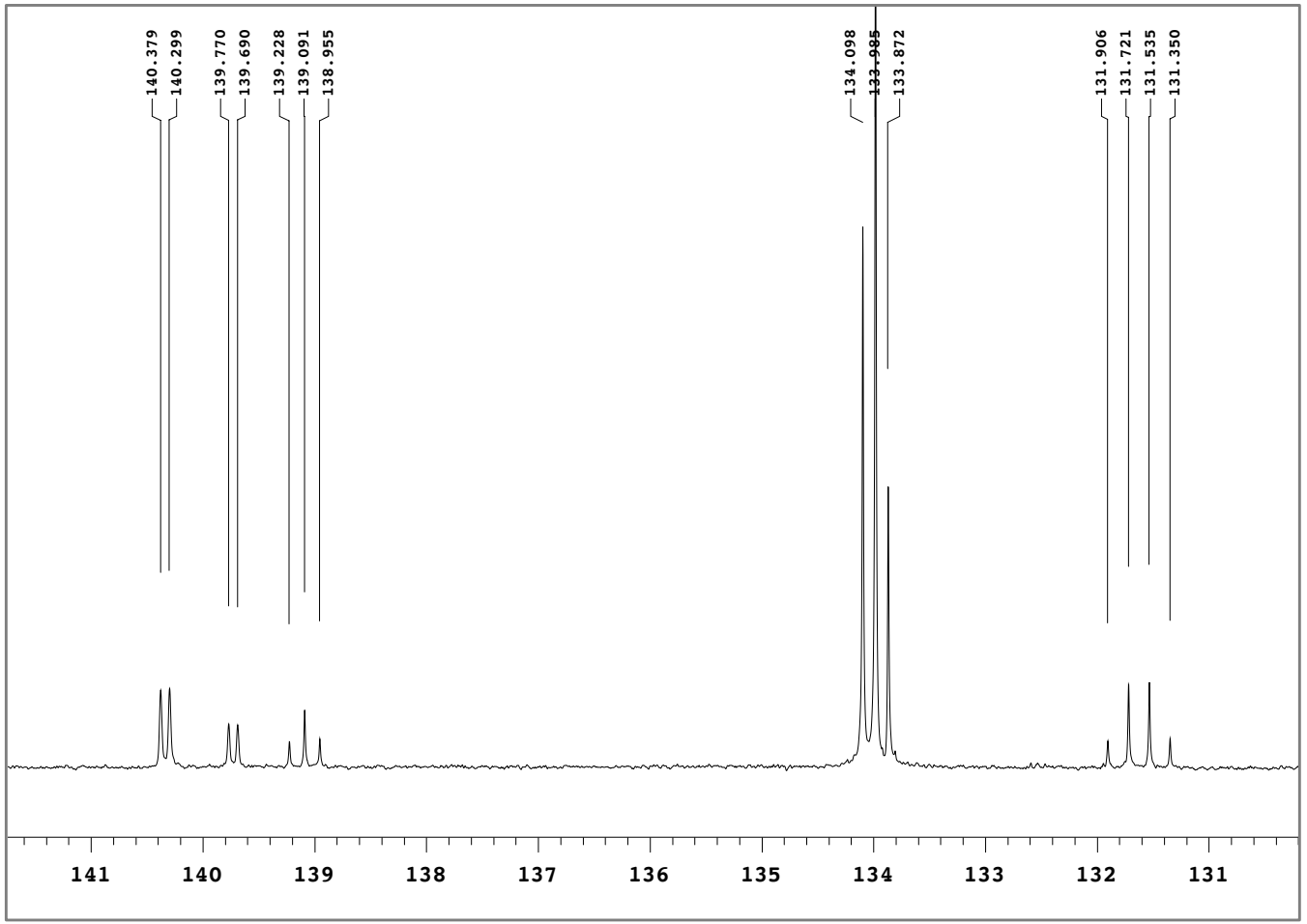

Figure S78: $^{13}C\{^{1}H\}$ NMR magnified spectrum of compound **2i** ($CDCl_3$, 176.0 MHz)

Recorded on: **v700, Oct 13 2020**	Sweep Width(Hz): **36764.7**	Acquisiton Time(s): **1**	Relaxation Delay(s): **1**
Pulse Sequence: **s2pul**	Digital Res.(Hz/pt): **0.28**	Hz per mm(Hz/mm): **138.42**	Completed Scans **512**

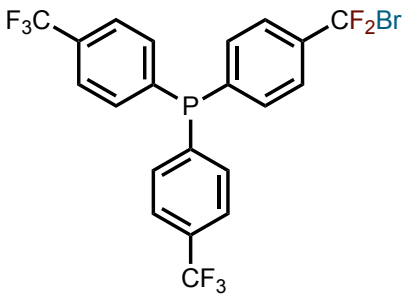

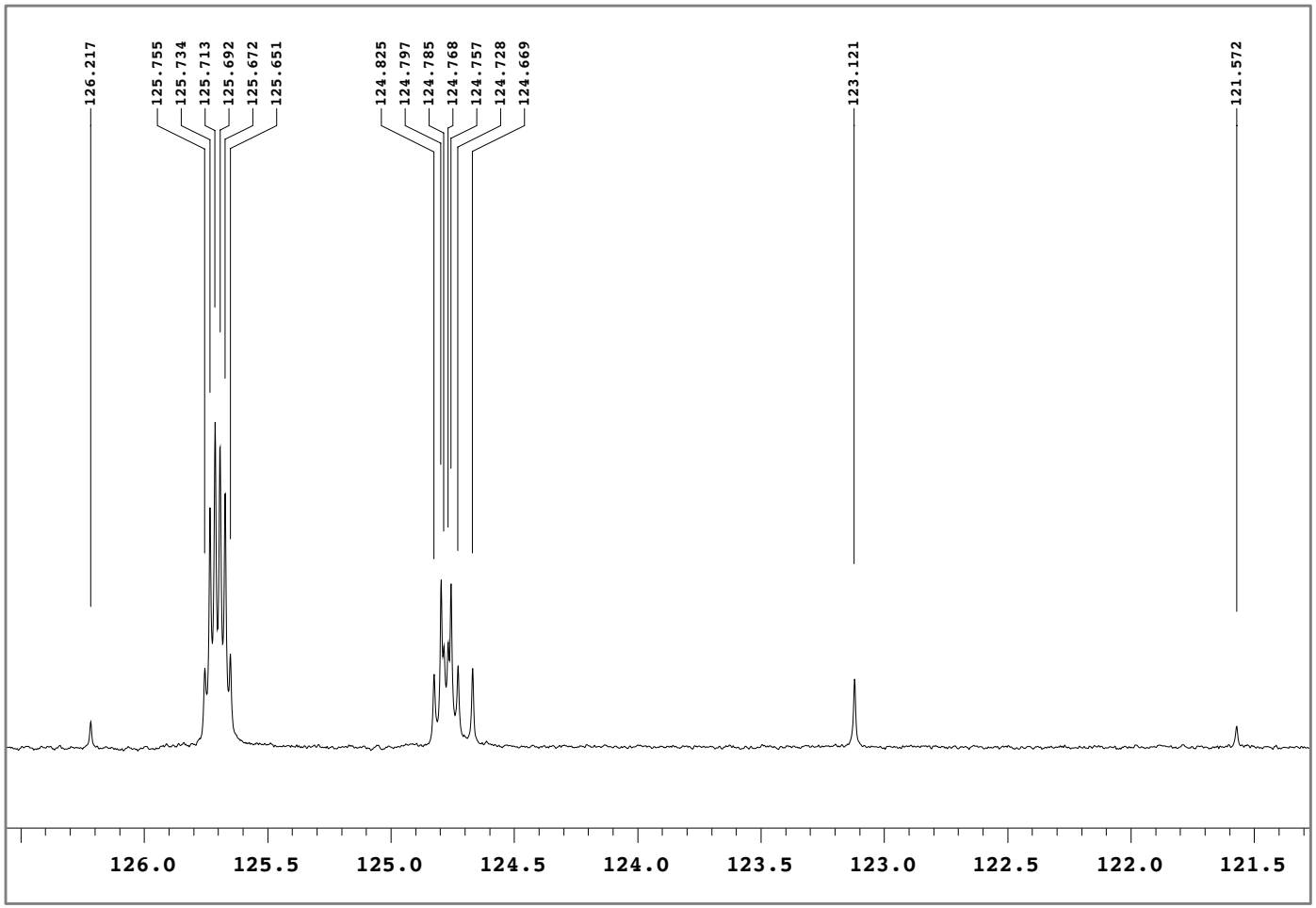

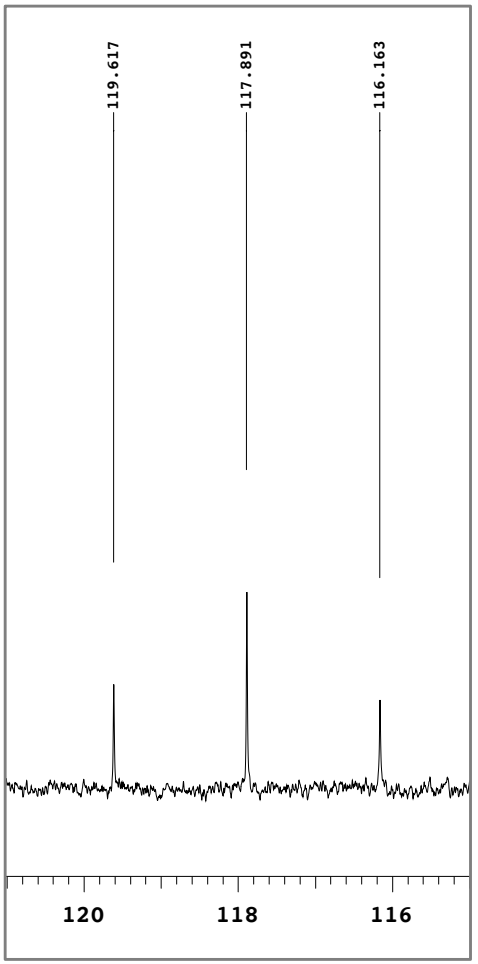

Figure S79: ^{19}F NMR spectrum of compound **2i** ($CDCl_3$, 376.3 MHz)

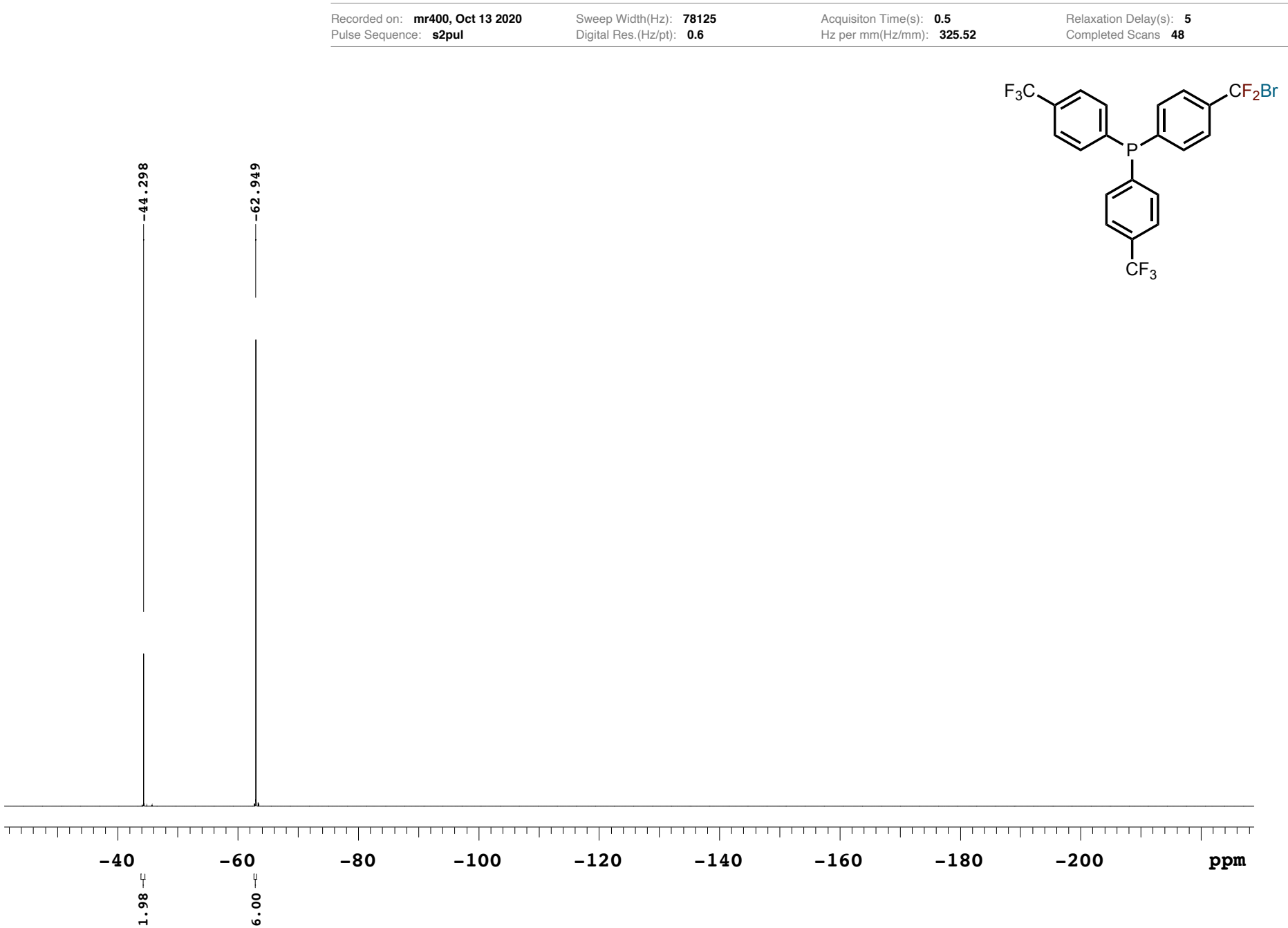

Figure S80: $^{31}P\{^{1}H\}$ NMR spectrum of compound **2i** ($CDCl_3$, 161.9 MHz)

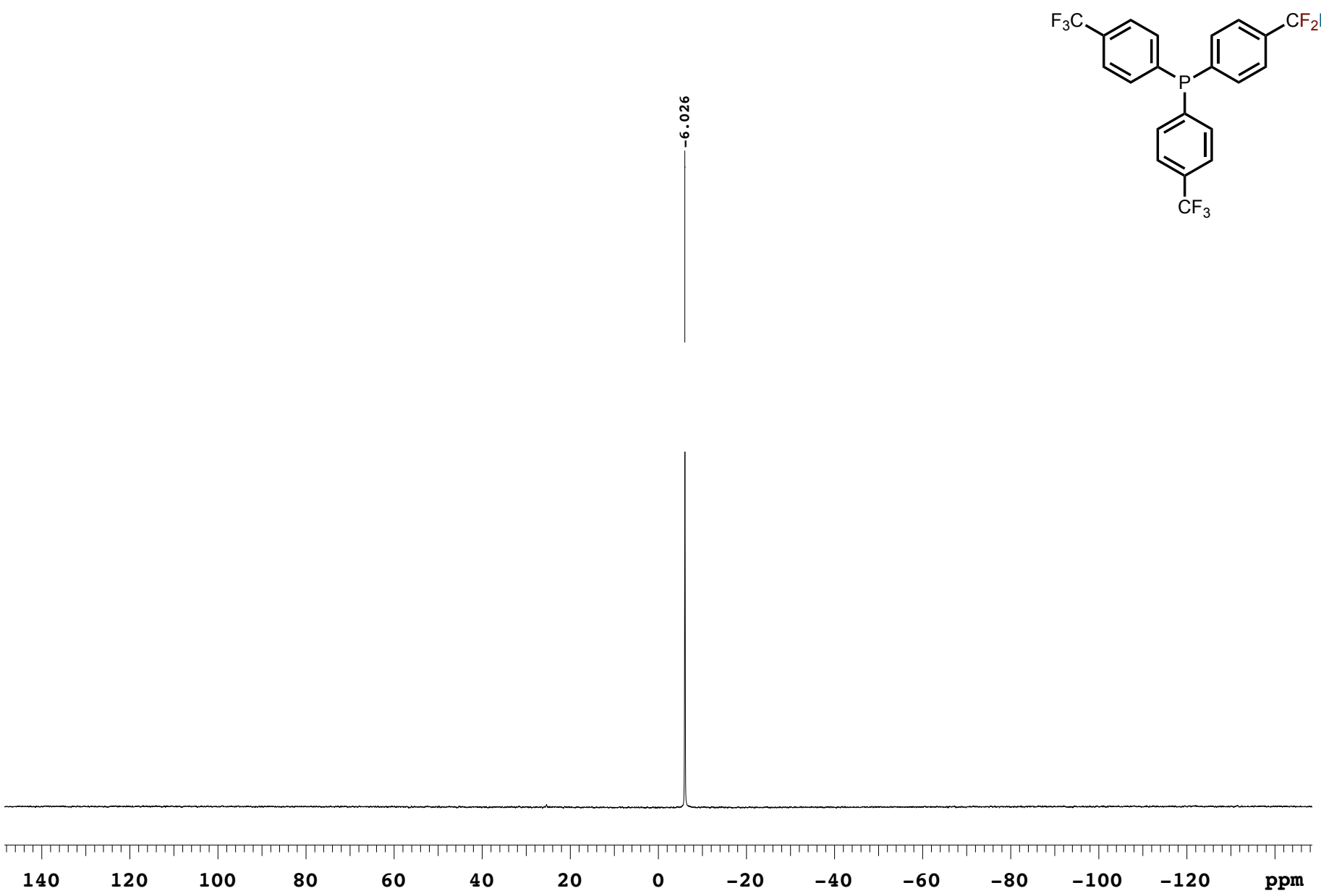

Figure S81: ^{1}H NMR spectrum of compound **2j** ($CDCl_3$, 499.8 MHz)

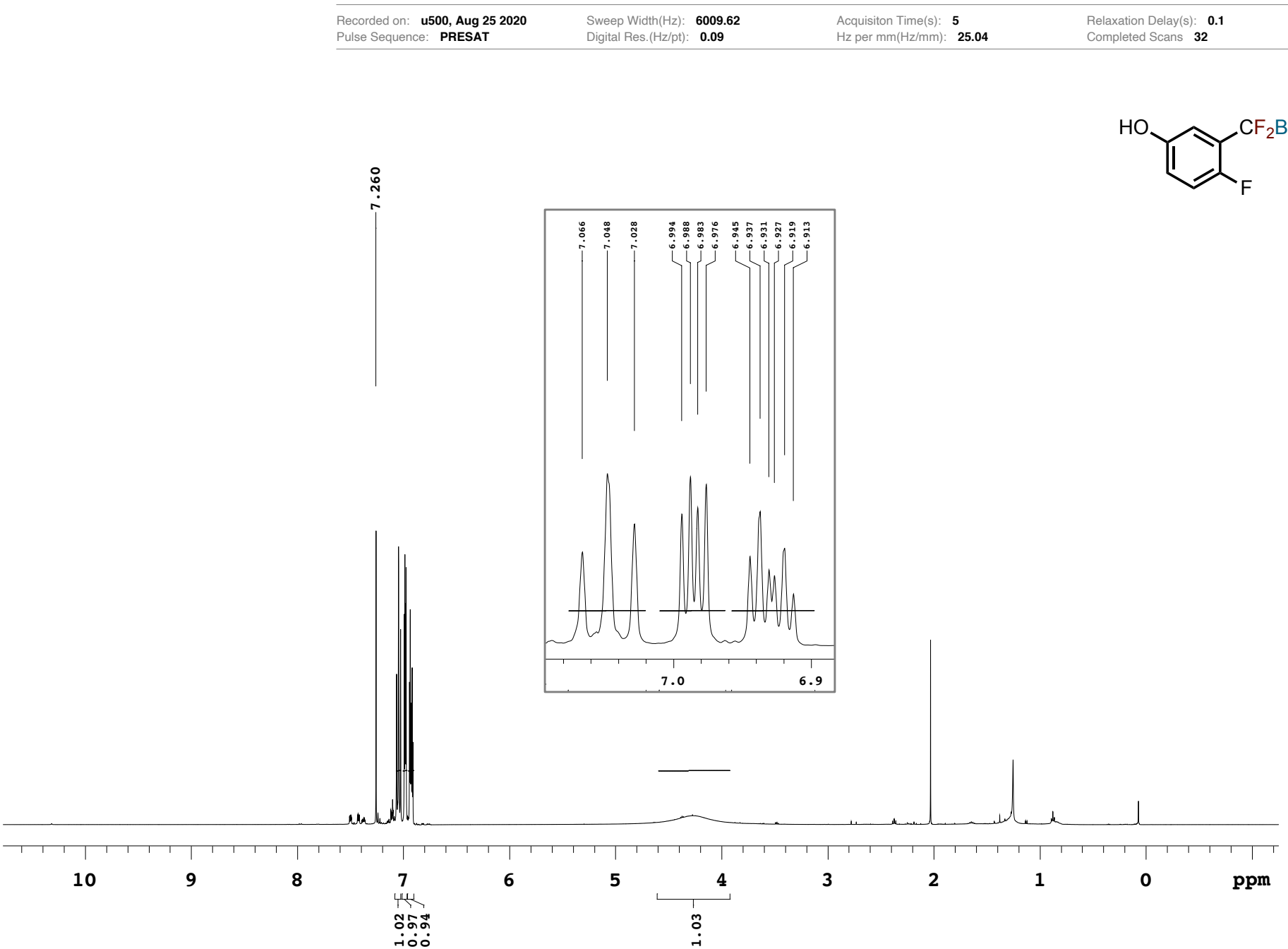

Figure S82: $^{13}C\{^{1}H\}$ NMR spectrum of compound **2j** ($CDCl_3$, 125.7 MHz)

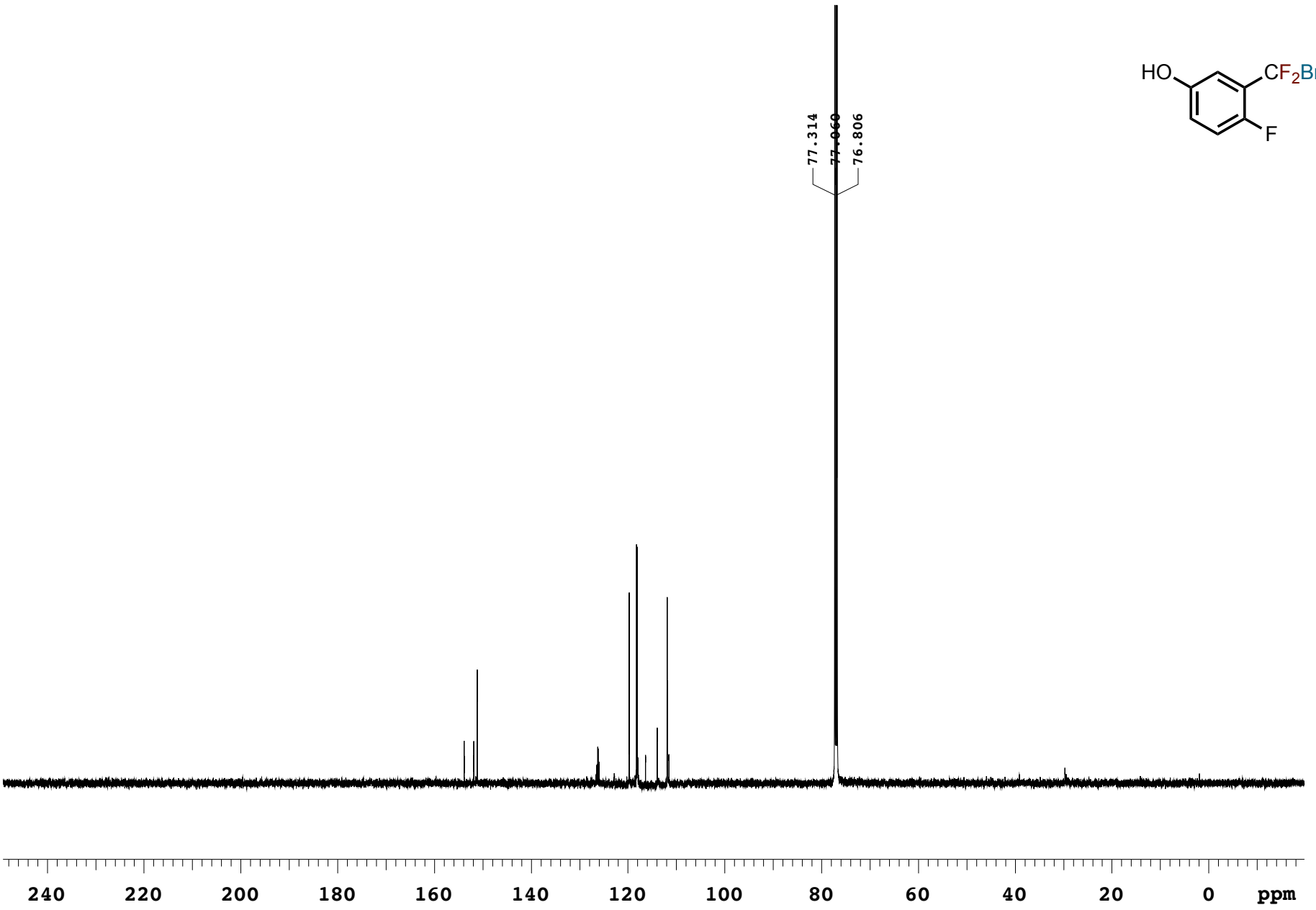

Figure S83: $^{13}C\{^{1}H\}$ NMR magnified spectrum of compound **2j** ($CDCl_3$, 125.7 MHz)

Recorded on: **u500, Aug 25 2020**	Sweep Width(Hz): **33783.8**	Acquisiton Time(s): **1**	Relaxation Delay(s): **1**
Pulse Sequence: **s2pul**	Digital Res.(Hz/pt): **0.26**	Hz per mm(Hz/mm): **140.76**	Completed Scans **256**

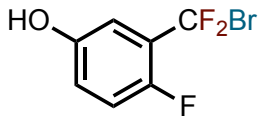

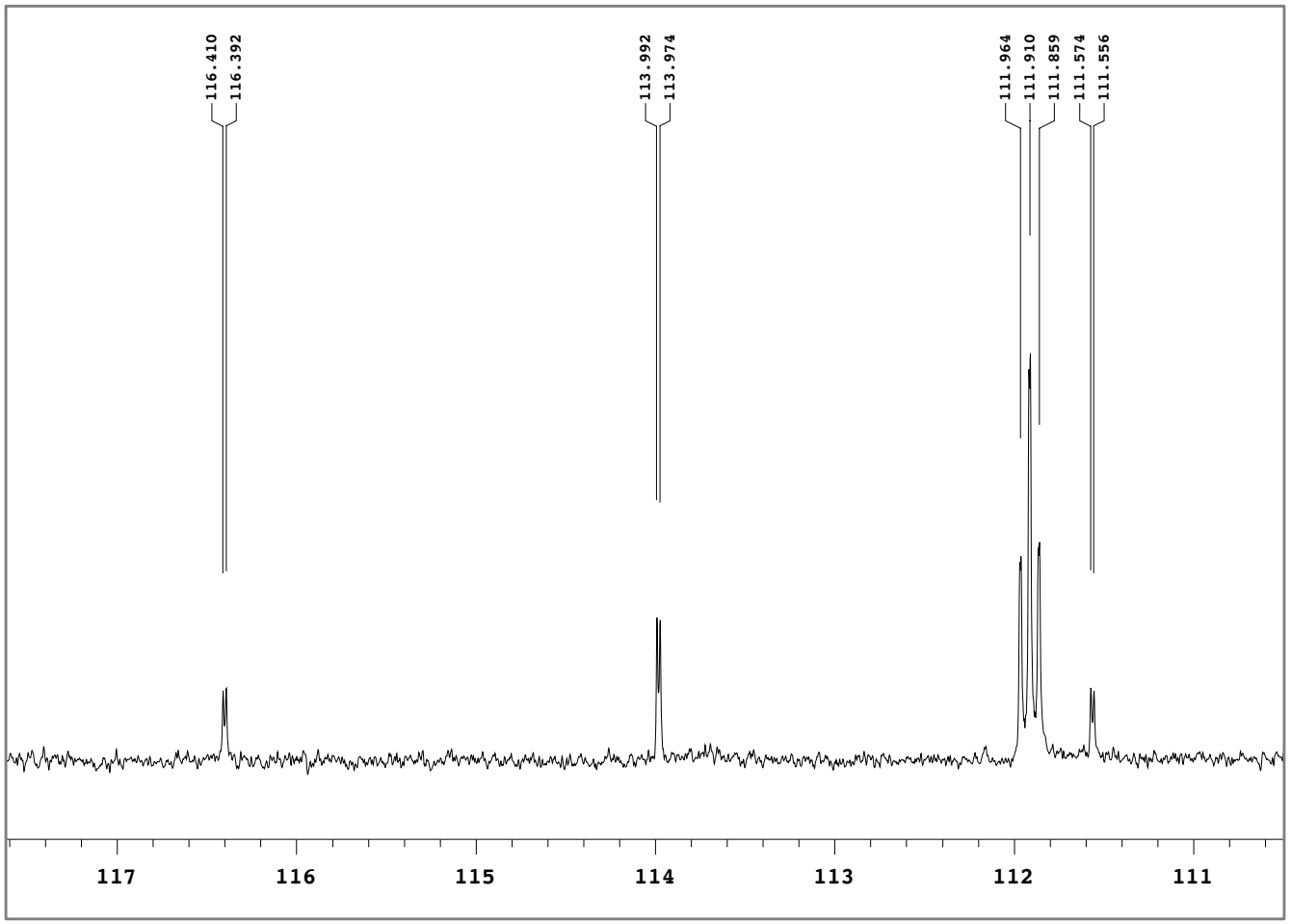

Figure S84: $^{13}C\{^{1}H\}$ NMR magnified spectrum of compound **2j** ($CDCl_3$, 125.7 MHz)

Recorded on: **u500, Aug 25 2020**	Sweep Width(Hz): **33783.8**	Acquisiton Time(s): **1**	Relaxation Delay(s): **1**
Pulse Sequence: **s2pul**	Digital Res.(Hz/pt): **0.26**	Hz per mm(Hz/mm): **140.76**	Completed Scans **256**

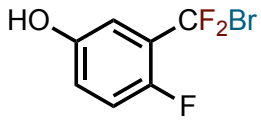

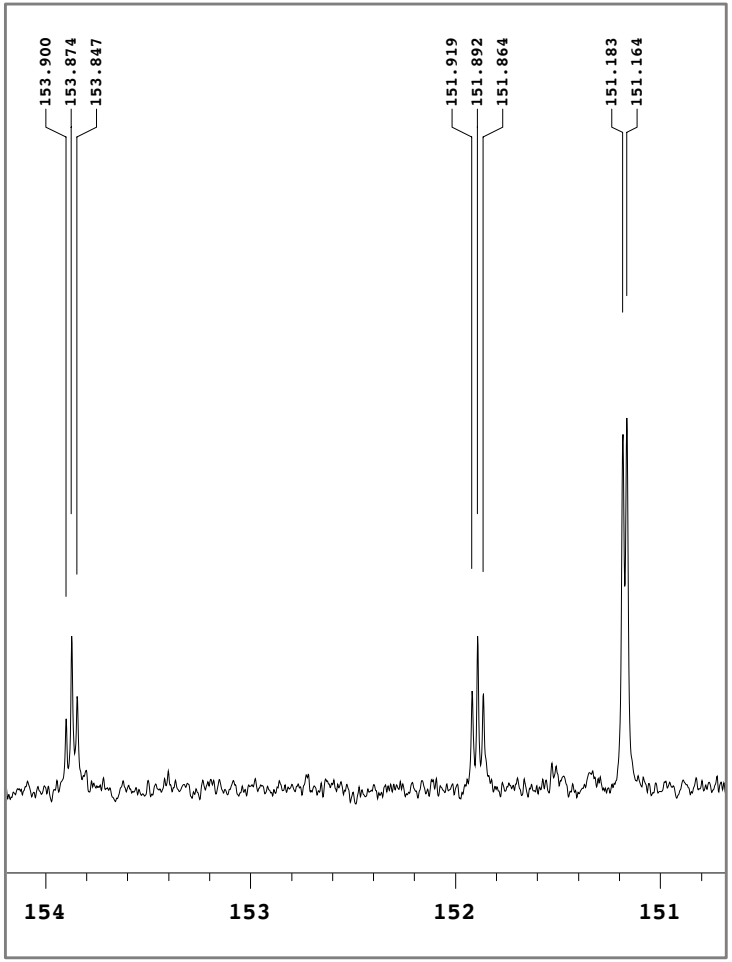

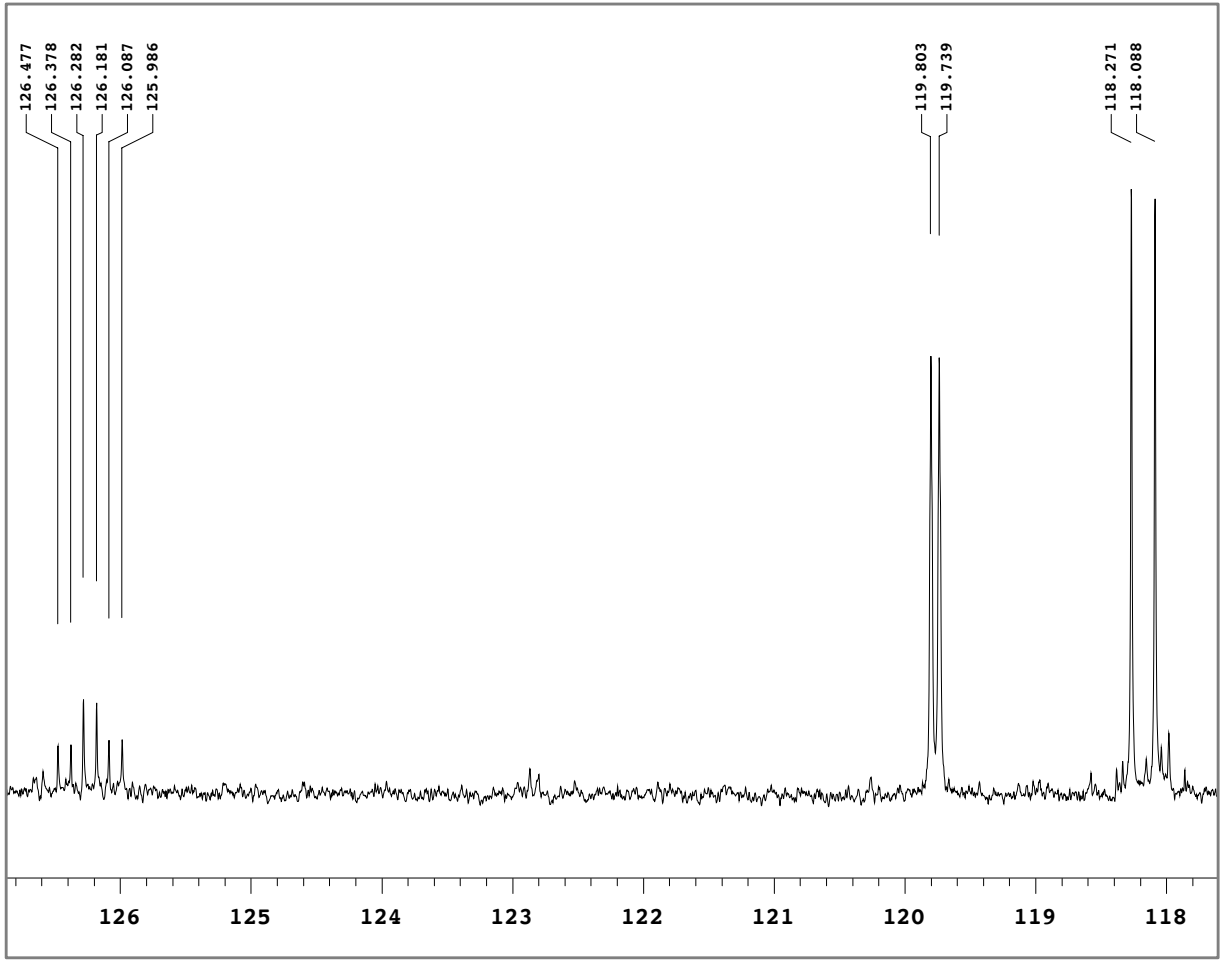

Figure S85: ^{19}F NMR spectrum of compound **2j** ($CDCl_3$, 367.3 MHz)

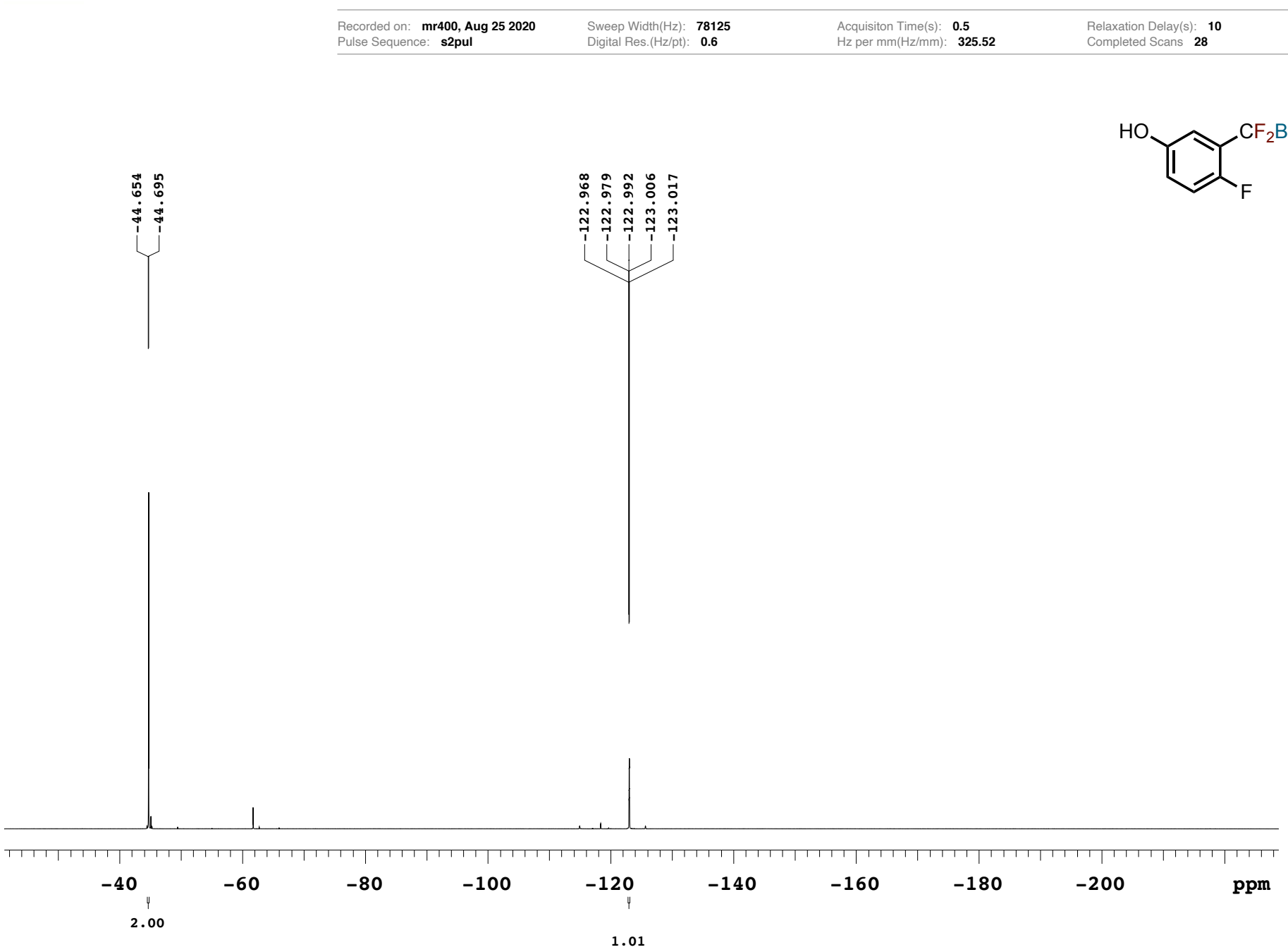

Figure S86: ^{1}H NMR spectrum of compound **2k** ($CDCl_3$, 699.8 MHz)

Recorded on: **v700, Dec 9 2020**	Sweep Width(Hz): **8741.26**	Acquisiton Time(s): **5**	Relaxation Delay(s): **0.1**
Pulse Sequence: **PRESAT**	Digital Res.(Hz/pt): **0.13**	Hz per mm(Hz/mm): **32.86**	Completed Scans **32**

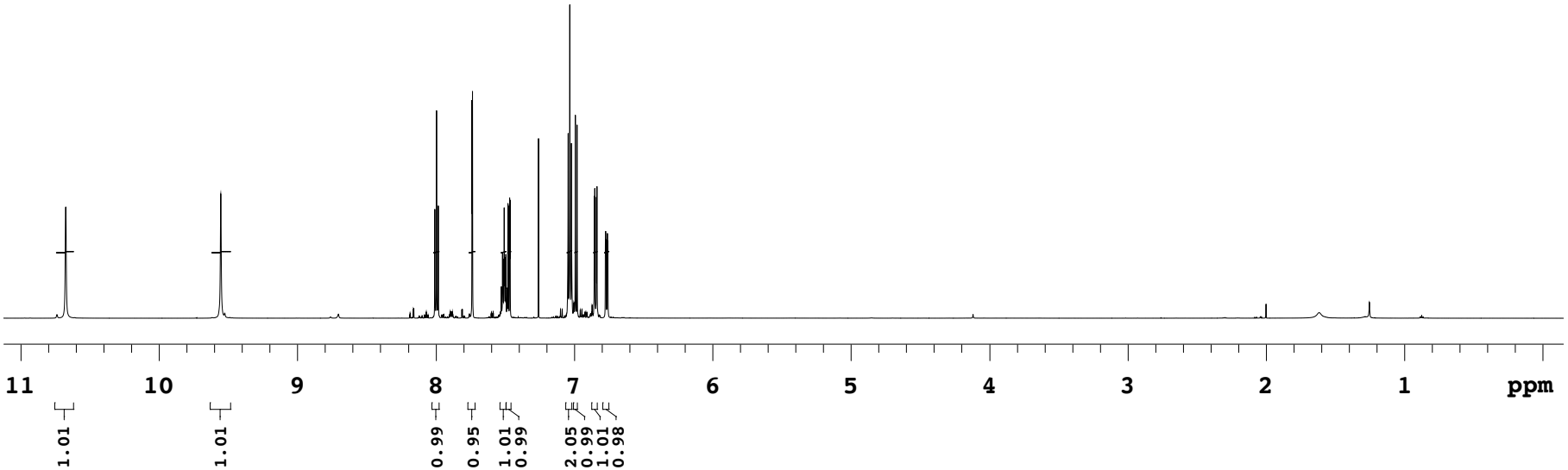

Figure S87: ^{1}H NMR magnified spectrum of compound **2k** ($CDCl_3$, 699.8 MHz)

Recorded on: **v700, Dec 9 2020**	Sweep Width(Hz): **8741.26**	Acquisiton Time(s): **5**	Relaxation Delay(s): **0.1**
Pulse Sequence: **PRESAT**	Digital Res.(Hz/pt): **0.13**	Hz per mm(Hz/mm): **32.86**	Completed Scans **32**

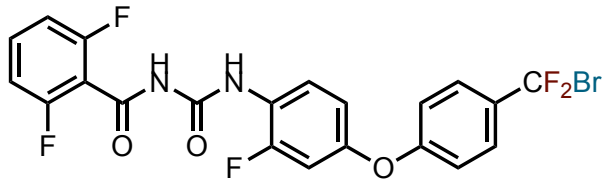

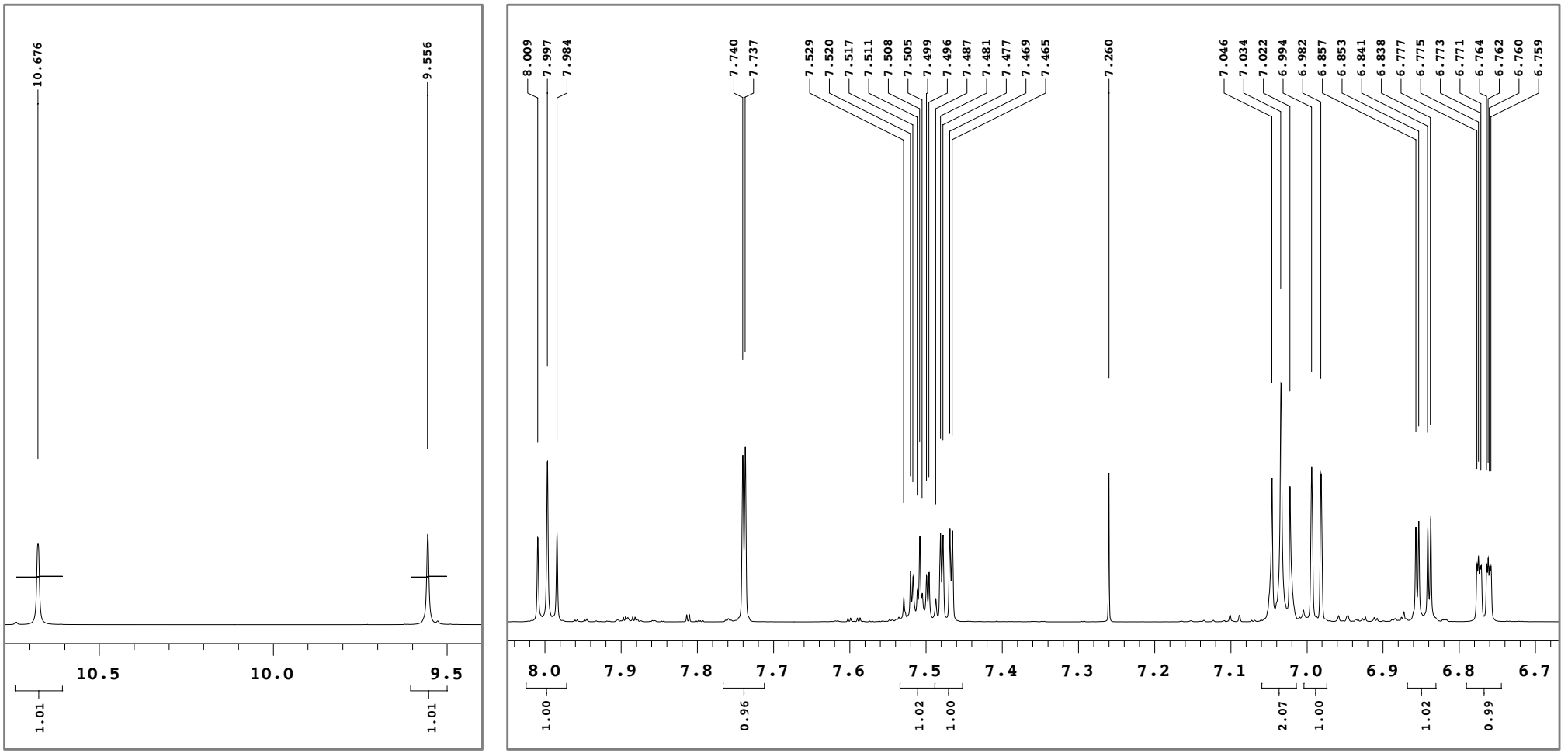

Figure S88: $^{13}C\{^{1}H\}$ NMR spectrum of compound **2k** ($CDCl_3$, 176.0 MHz)

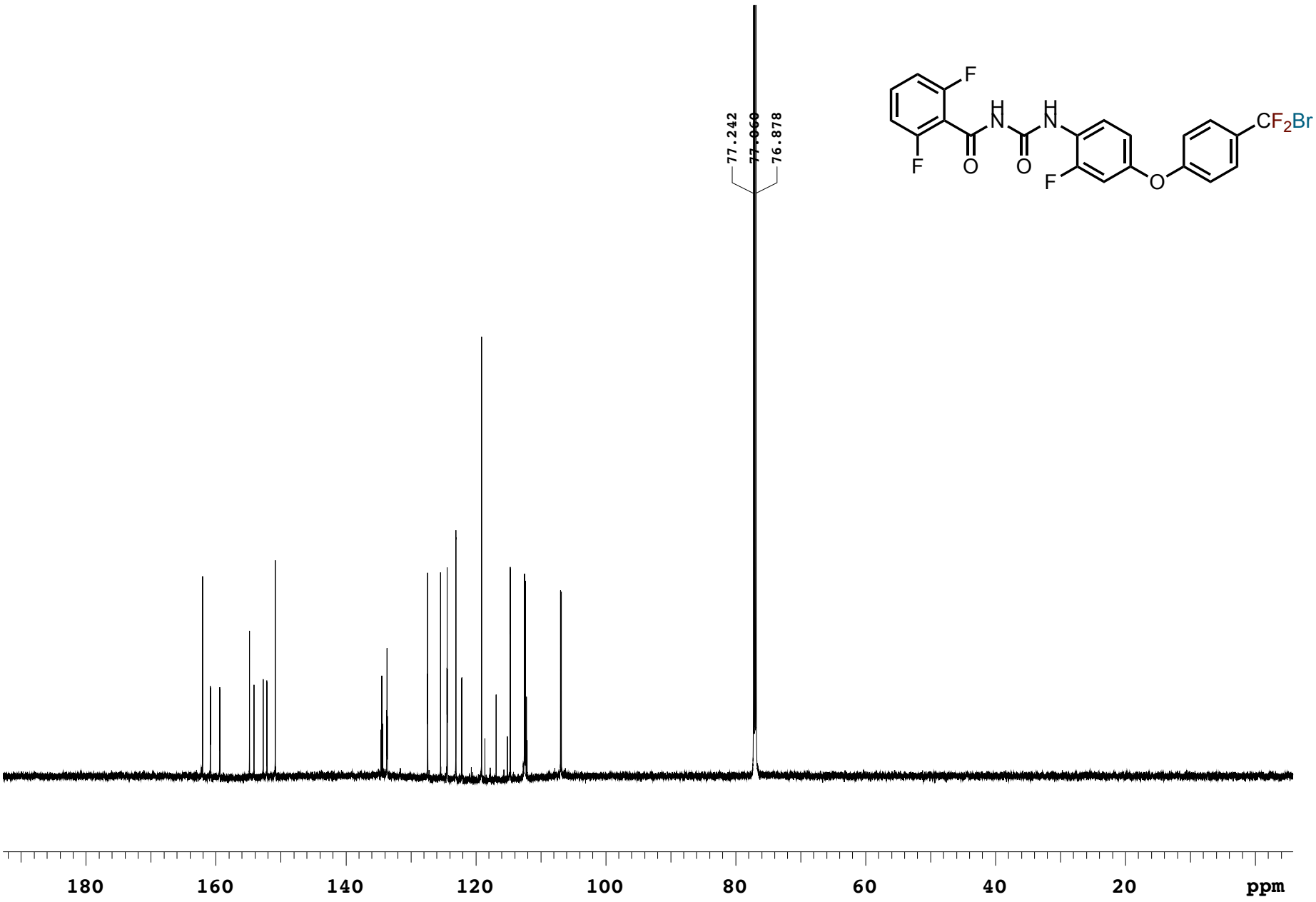

Figure S89: $^{13}C\{^{1}H\}$ NMR magnified spectrum of compound **2k** ($CDCl_3$, 176.0 MHz)

Recorded on: **v700, Dec 8 2020**	Sweep Width(Hz): **36764.7**	Acquisiton Time(s): **1**	Relaxation Delay(s): **1**
Pulse Sequence: **s2pul**	Digital Res.(Hz/pt): **0.28**	Hz per mm(Hz/mm): **145.56**	Completed Scans **512**

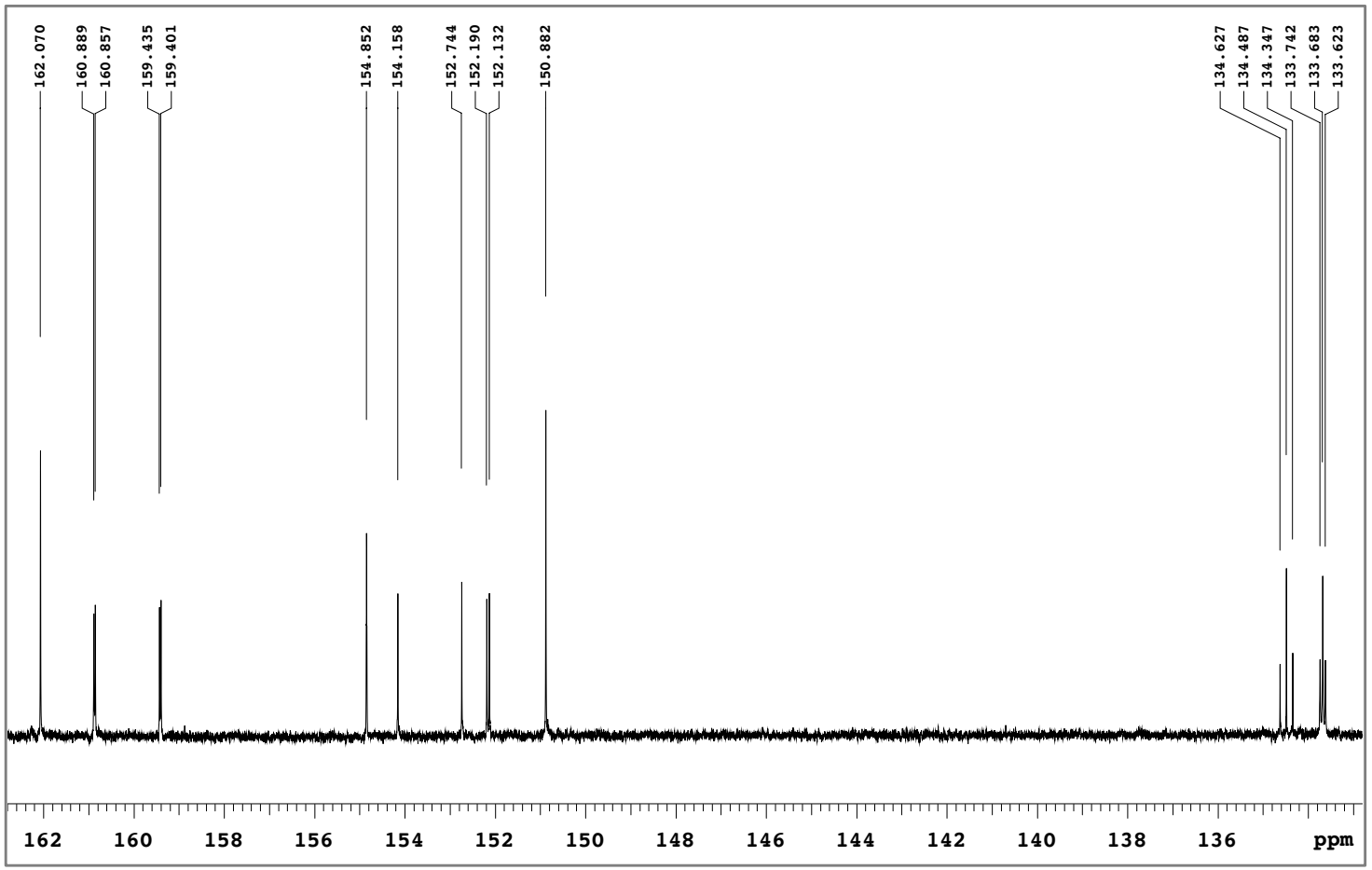

Figure S90: $^{13}C\{^{1}H\}$ NMR magnified spectrum of compound **2k** ($CDCl_3$, 176.0 MHz)

Recorded on: **v700, Dec 8 2020**	Sweep Width(Hz): **36764.7**	Acquisiton Time(s): **1**	Relaxation Delay(s): **1**
Pulse Sequence: **s2pul**	Digital Res.(Hz/pt): **0.28**	Hz per mm(Hz/mm): **145.56**	Completed Scans **512**

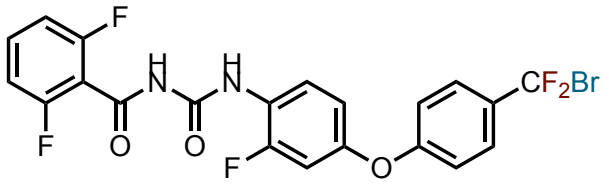

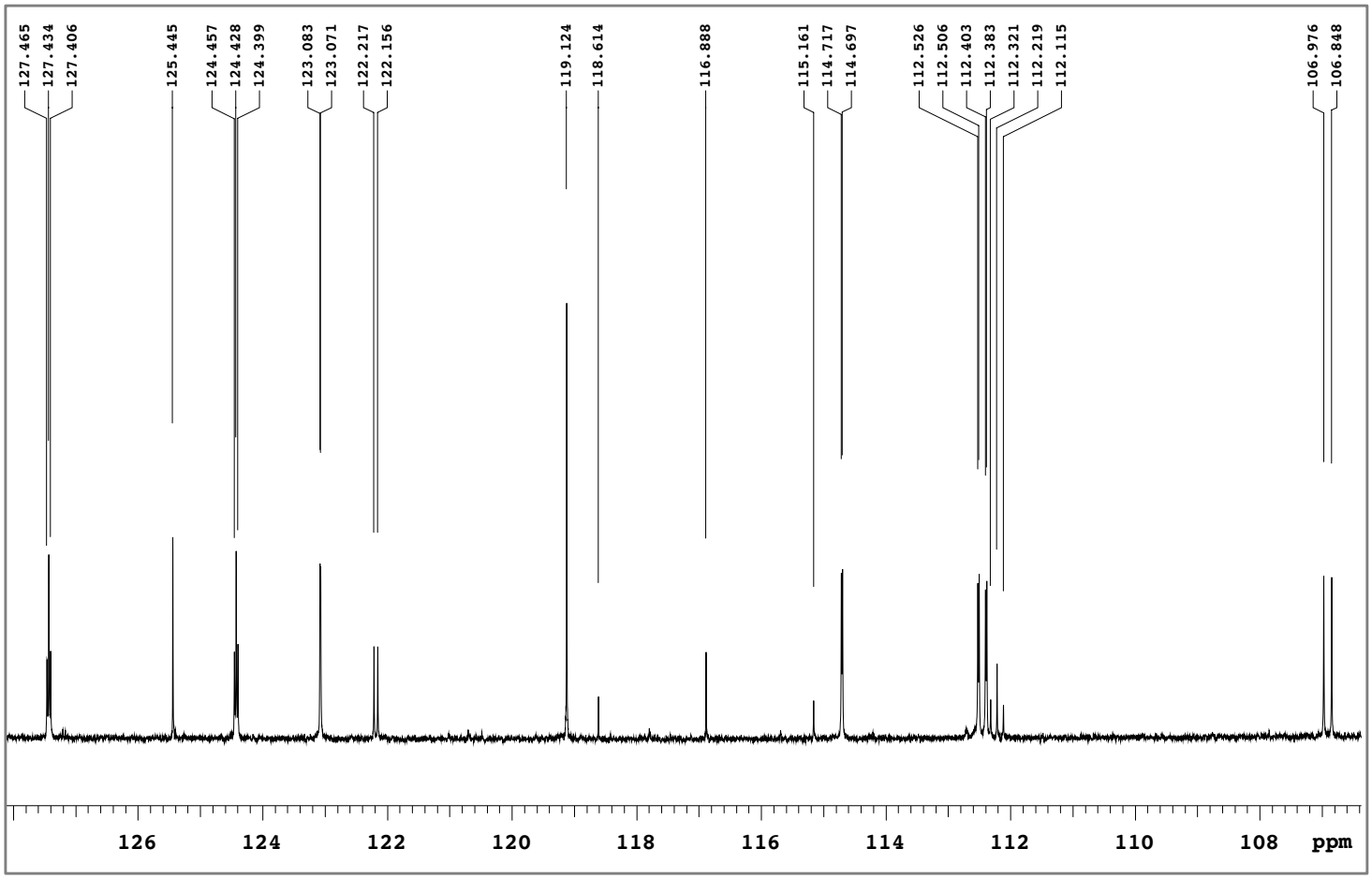

Figure S91: ^{19}F NMR spectrum of compound **2k** ($CDCl_3$, 376.3 MHz)

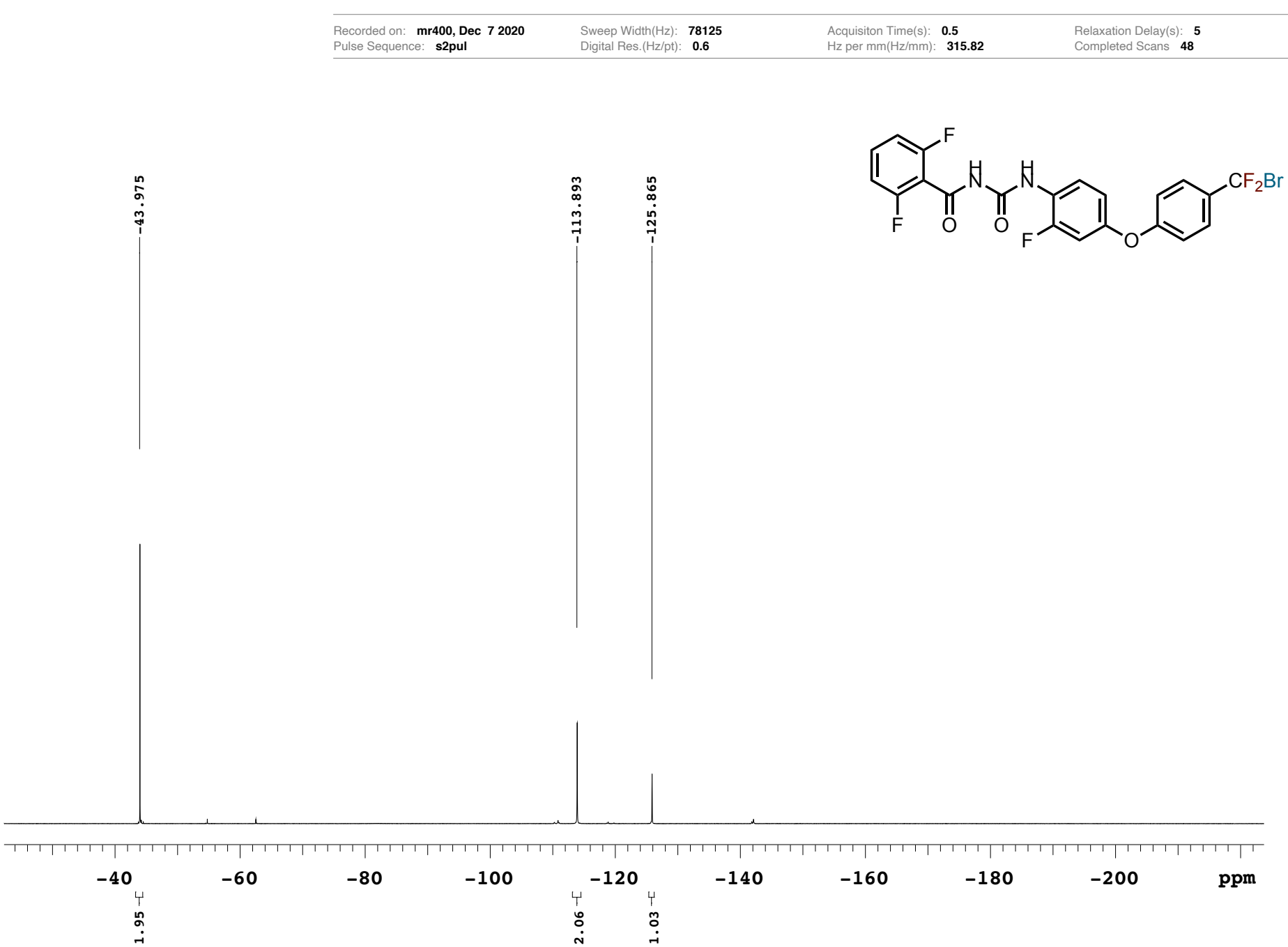

Figure S92: ^{1}H NMR spectrum of compound **4a** ($CDCl_3$, 699.8 MHz)

Recorded on: **v700, Dec 13 2020**	Sweep Width(Hz): **8389.26**	Acquisiton Time(s): **5**	Relaxation Delay(s): **0.1**
Pulse Sequence: **PRESAT**	Digital Res.(Hz/pt): **0.13**	Hz per mm(Hz/mm): **32.55**	Completed Scans **32**

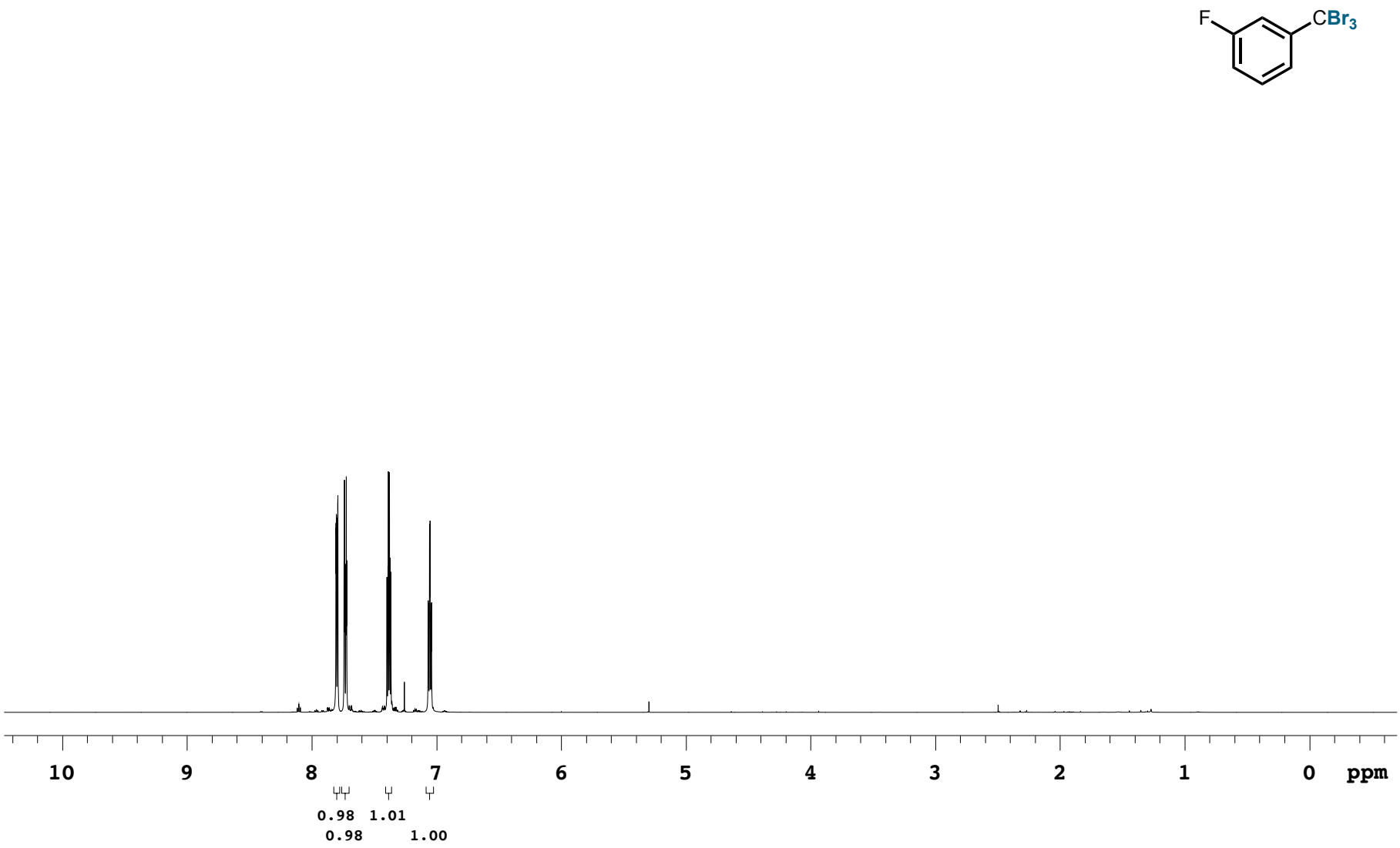

Figure S93: ^{1}H NMR magnified spectrum of compound **4a** ($CDCl_3$, 699.8 MHz)

Recorded on: **v700, Dec 13 2020**	Sweep Width(Hz): **8389.26**	Acquisiton Time(s): **5**	Relaxation Delay(s): **0.1**
Pulse Sequence: **PRESAT**	Digital Res.(Hz/pt): **0.13**	Hz per mm(Hz/mm): **32.55**	Completed Scans **32**

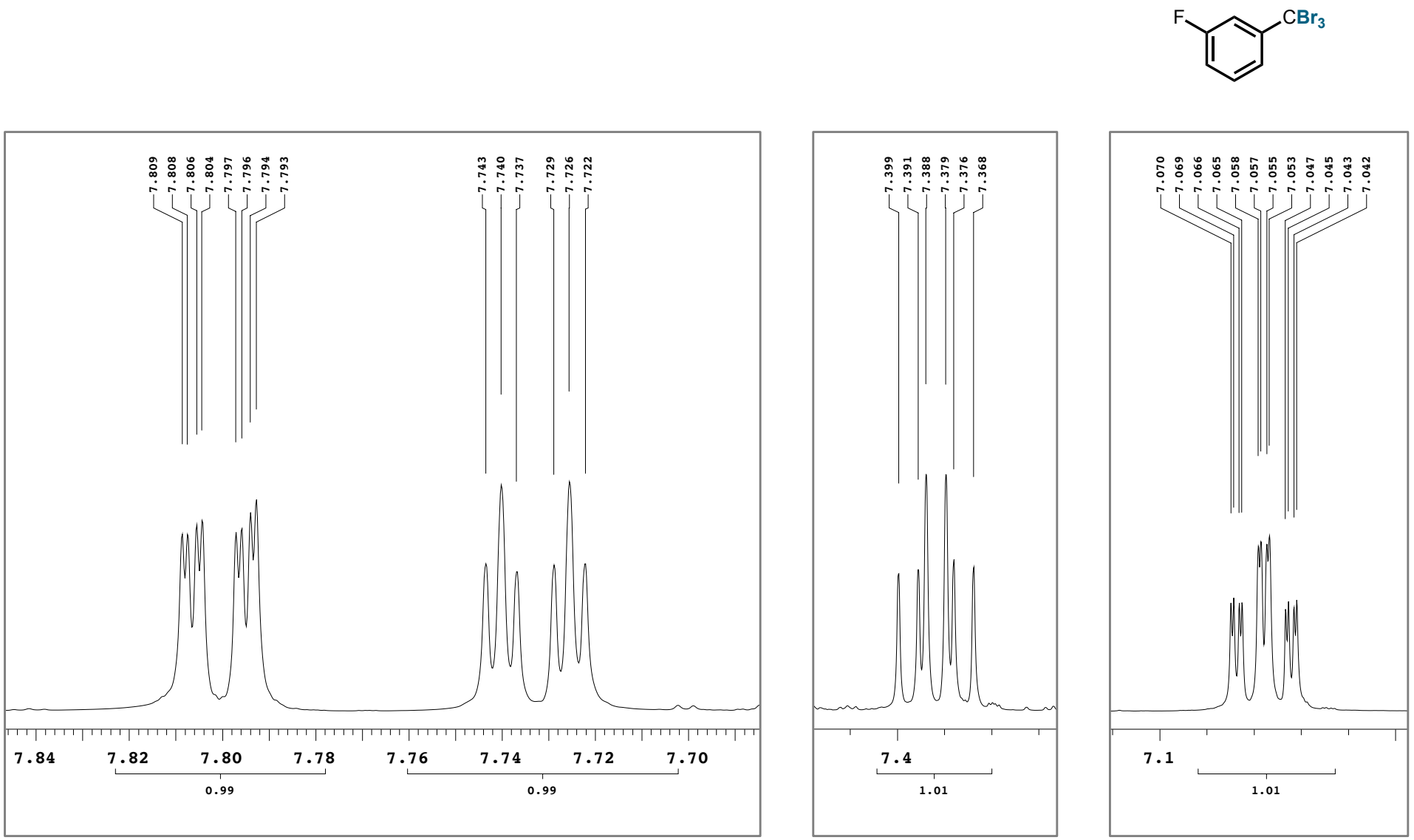

Figure S94: $^{13}C\{^{1}H\}$ NMR spectrum of compound **4a** ($CDCl_3$, 176.0 MHz)

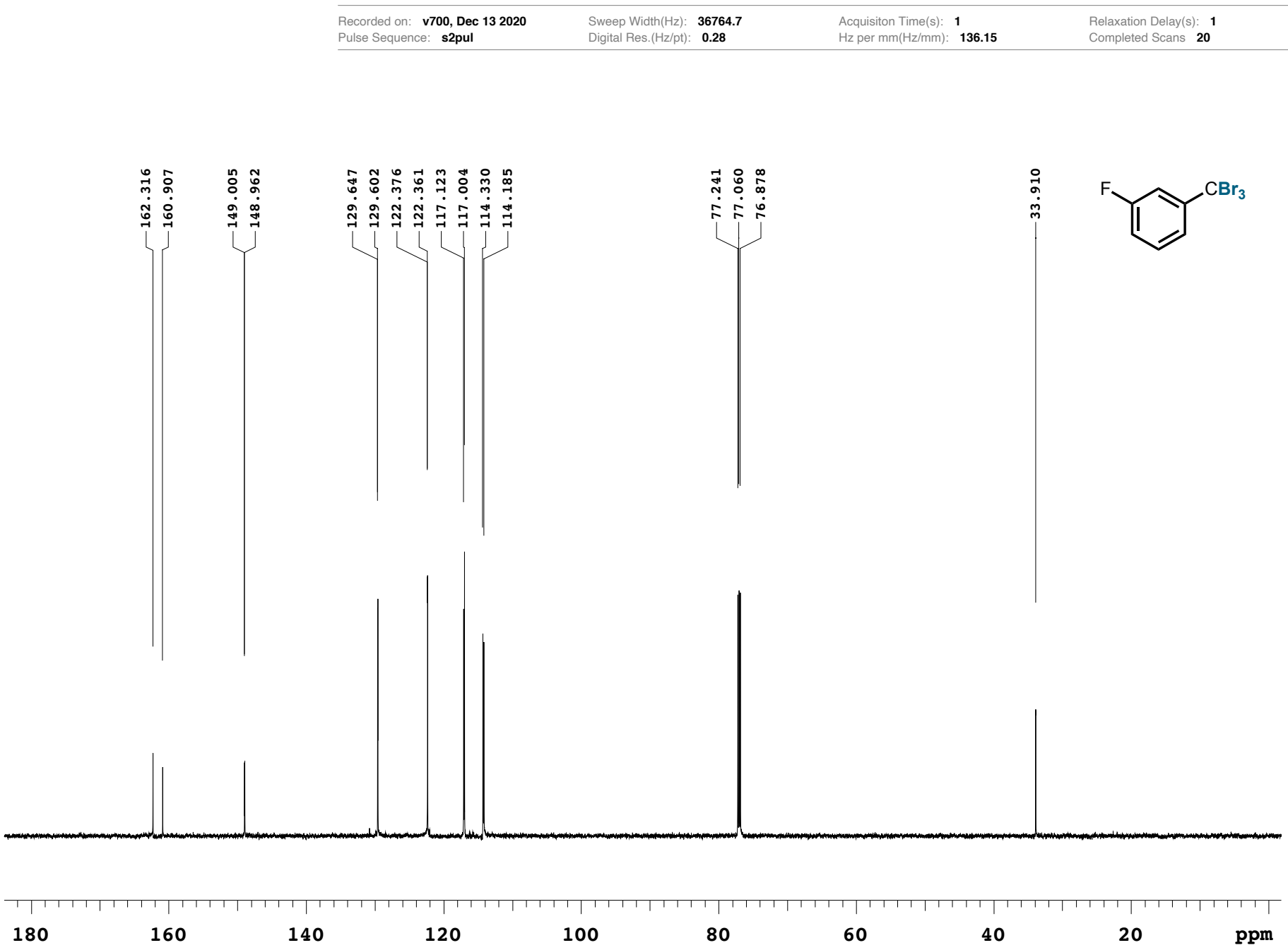

Figure S95: ^{19}F NMR spectrum of compound **4a** ($CDCl_3$, 376.3 MHz)

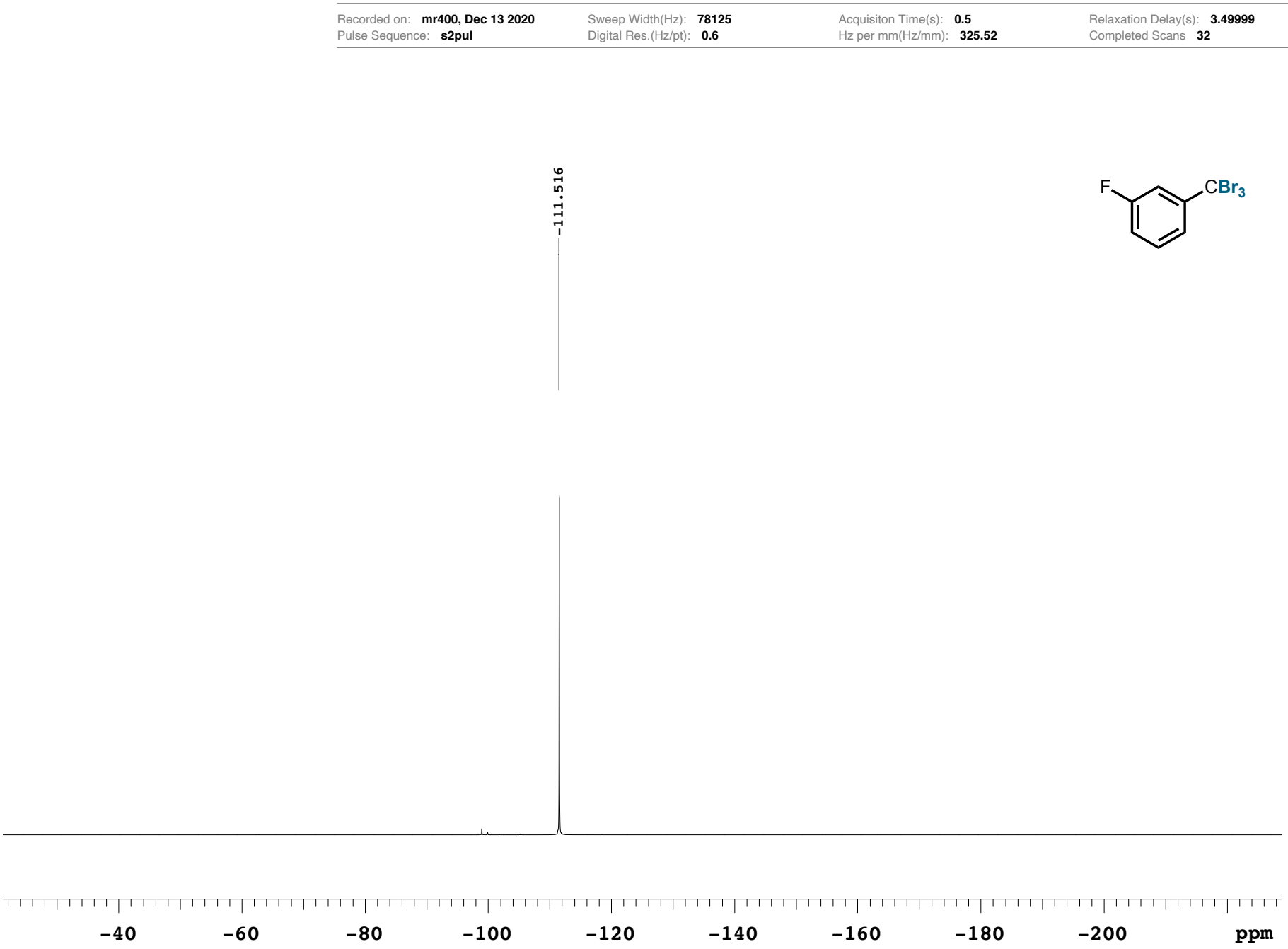

Figure S96: ^{1}H NMR spectrum of compound **4e** ($CDCl_3$, 699.8 MHz)

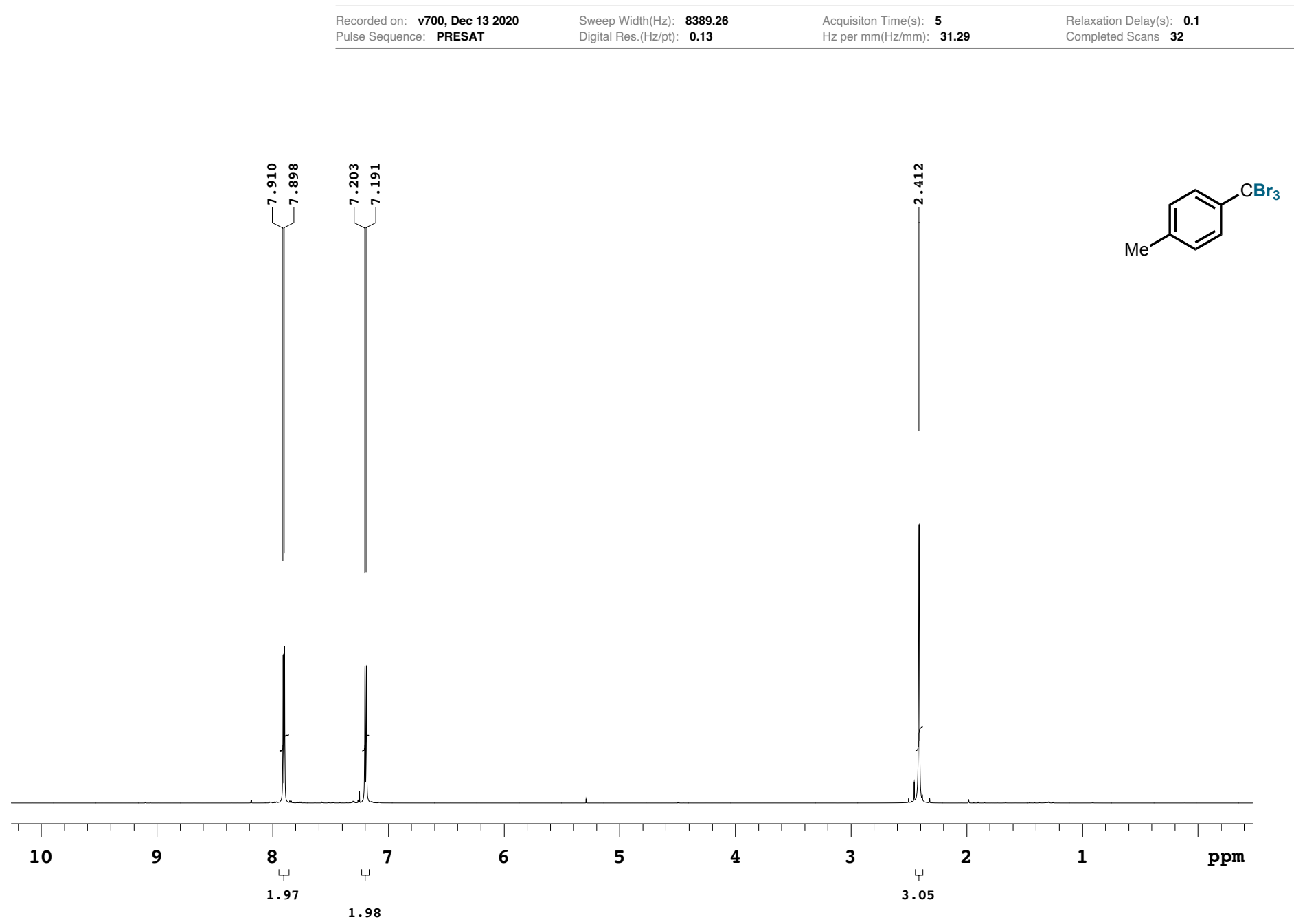

Figure S97: $^{13}C\{^{1}H\}$ NMR spectrum of compound **4e** ($CDCl_3$, 176.0 MHz)

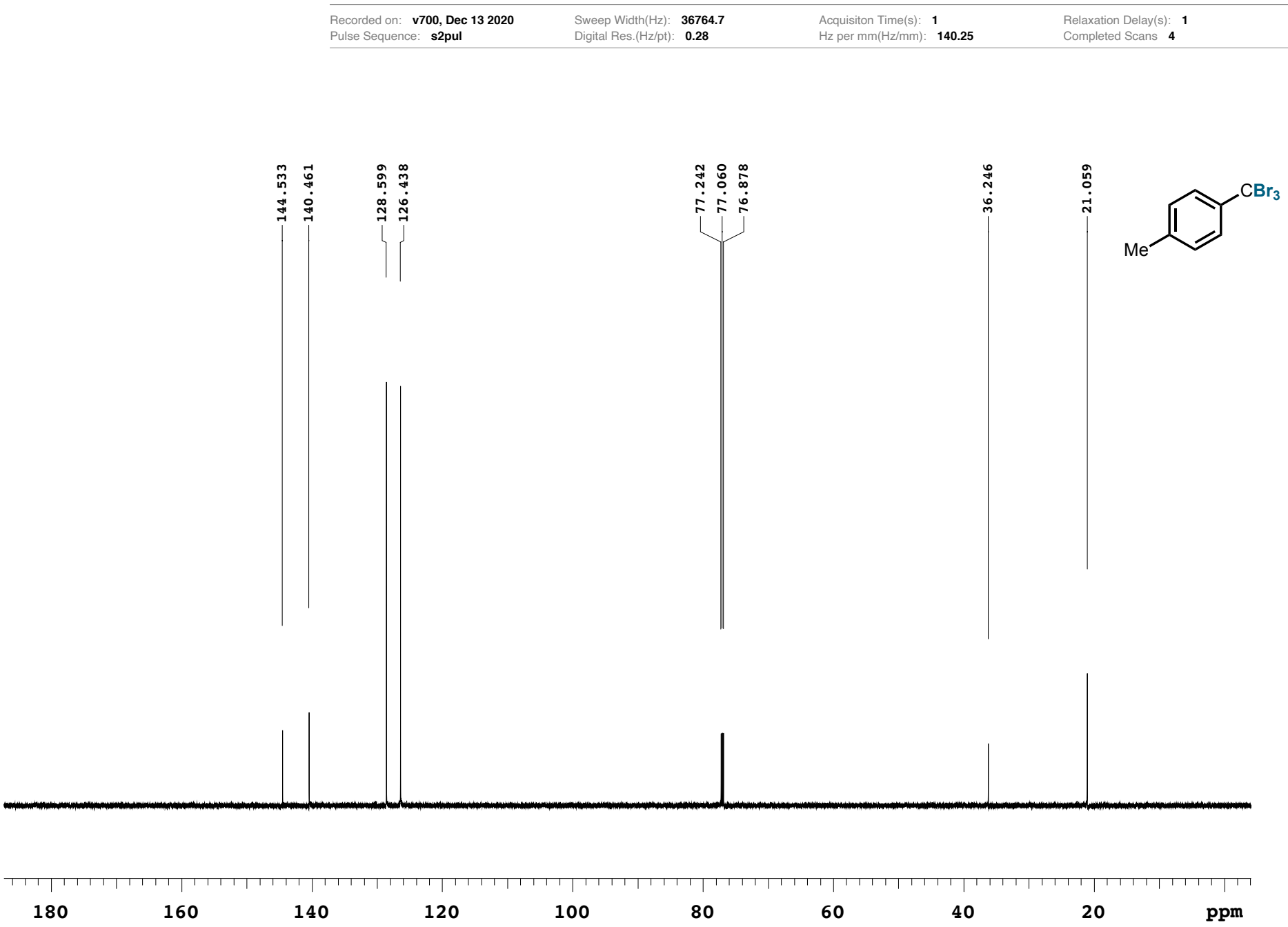

Figure S98: ^{1}H NMR spectrum of compound **5** ($CDCl_3$, 599.9 MHz)

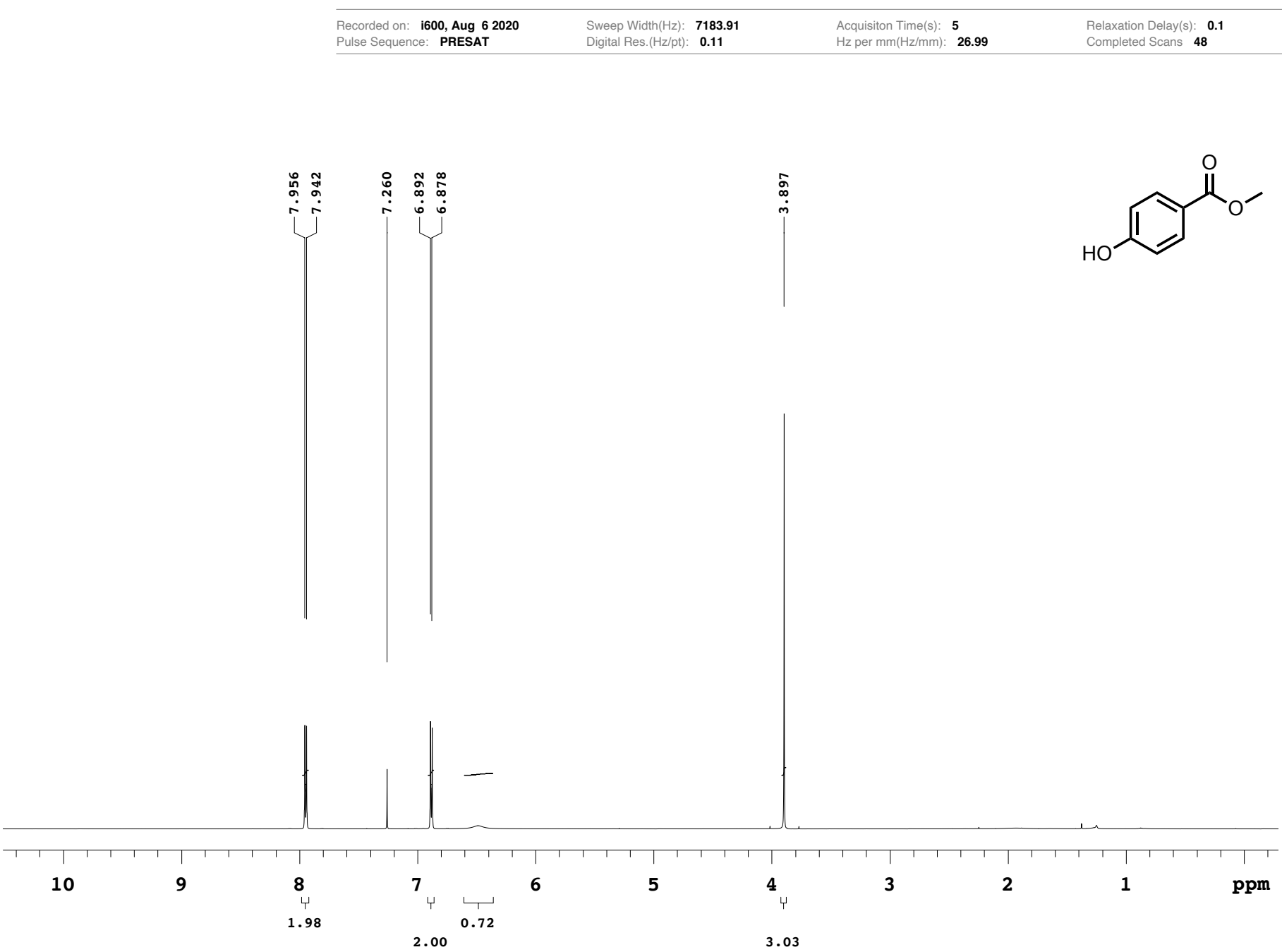

Figure S99: $^{13}C\{^{1}H\}$ NMR spectrum of compound **5** ($CDCl_3$, 150.9 MHz)